

AD-A057 660

TEXAS A AND M UNIV COLLEGE STATION DEPT OF OCEANOGRAPHY F/G 13/2
FLUME EXPERIMENTS ON SAND, SILT, AND CLAY MIXTURES FROM THE OFF--ETC(U)
JUN 78 A J MOHEREK DACW39-76-C-0115

UNCLASSIFIED

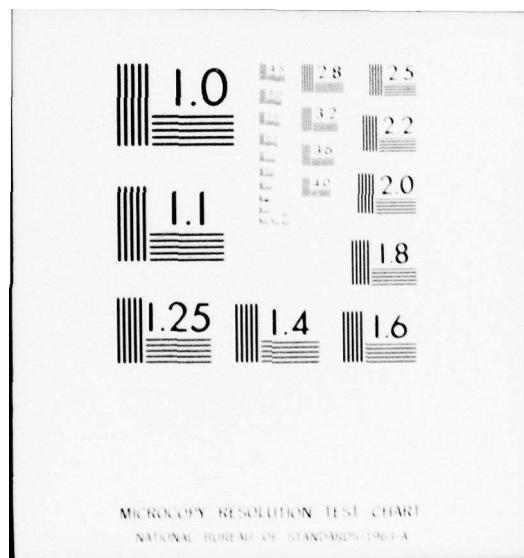
WEC-TD-D-78-34

NI

1 of 3

AD
A057 660

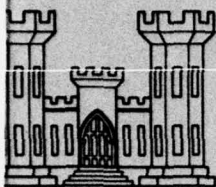




AD A057660

NO.

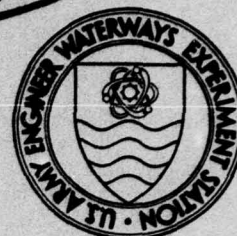
UDC FILE COPY



LEVEL II

12

DREDGED MATERIAL RESEARCH PROGRAM



TECHNICAL REPORT D-78-34

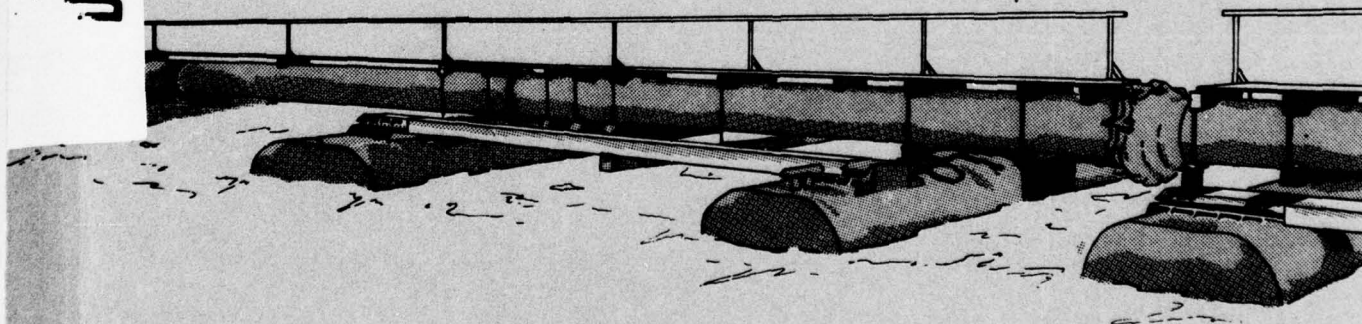
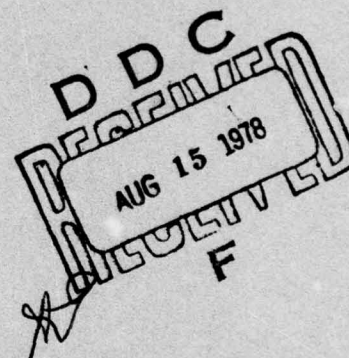
FLUME EXPERIMENTS ON SAND, SILT AND CLAY MIXTURES FROM THE OFFSHORE DREDGED MATERIAL DISPOSAL SITE GALVESTON, TEXAS

by

Anthony J. Moherek
Department of Oceanography
Texas A&M University
College Station, Tex. 77843

June 1978
Final Report

Approved For Public Release; Distribution Unlimited



Prepared for Office, Chief of Engineers, U. S. Army
Washington, D. C. 20314

Under Contract No. DACW39-76-C-0115
(DMRP Work Unit No. 1B08A)

Monitored by Environmental Laboratory
U. S. Army Engineer Waterways Experiment Station
P. O. Box 631, Vicksburg, Miss. 39180

78 14 08 179



DEPARTMENT OF THE ARMY
WATERWAYS EXPERIMENT STATION, CORPS OF ENGINEERS
P. O. BOX 631
VICKSBURG, MISSISSIPPI 39180

IN REPLY REFER TO: WESYV

31 July 1978

SUBJECT: Transmittal of Technical Report D-78-34

TO: All Report Recipients

1. The technical report transmitted herewith represents the results of Work Unit 1B08A of Task 1B, Movements of Dredged Material, of the Corps of Engineers' Dredged Material Research Program (DMRP). It was a part of the Environmental Impacts and Criteria Development Project (EICDP), which had a general objective of developing techniques for determining the spatial and temporal distribution of dredged material discharged into various hydrologic regimes. The study reported on herein was part of a series of research contracts developed to achieve the EICDP general objective.

2. Regardless of the location or character of a disposal site, an integral part of the problem of assessing the environmental impact of open-water disposal operations is an ability to determine the movement of dredged material. Dredged material at an aquatic disposal site is subject to dispersion by the tidal stream, estuarine circulation, waves, and disturbances of the hydraulic flow by storms. In shallow coastal waters, sediment may be transported periodically by tidal currents or episodically by storm-generated currents. A major objective of this investigation was to evaluate the susceptibility of submerged dredged material mounds to these disturbances.

3. This report describes investigations conducted in the Gulf of Mexico at the Galveston, Texas, dredged material disposal site in order to determine the critical erosion velocity, shear stress, and modes of sediment transport for four sediment mixtures. The four different sediments eroded similarly as evidenced by a similar critical bed shear. Laboratory results were compared with field data, indicating greatest bedload erosion on the northern portions of the site with movement of the sediment away from the Galveston Bay entrance channel.


4. The information and data published in this report are contributions to the further understanding of the complex nature of sediment transport and stability of submerged dredged material deposits and should help establish a baseline from which to develop meaningful evaluations for

WESYV

31 July 1978

SUBJECT: Transmittal of Technical Report D-78-34

the selection of an environmentally compatible disposal alternative. It is expected that the interpretation of the physical interactions will be of significant value to those persons concerned with CE dredged material permit programs.



JOHN L. CANNON

Colonel, Corps of Engineers
Commander and Director

Unclassified

SECURITY CLASSIFICATION OF THIS PAGE (When Data Entered)

| REPORT DOCUMENTATION PAGE | | READ INSTRUCTIONS BEFORE COMPLETING FORM |
|--|--|---|
| 1. REPORT NUMBER | 2. GOVT ACCESSION NO. | 3. RECIPIENT'S CATALOG NUMBER |
| Technical Report D-78-34 | | |
| 4. TITLE (and Subtitle) | 5. TYPE OF REPORT & PERIOD COVERED | |
| FLUME EXPERIMENTS ON SAND, SILT, AND CLAY MIXTURES FROM THE OFFSHORE DREDGED MATERIAL DISPOSAL SITE, GALVESTON, TEXAS. | Final report, Feb 75 - Jan 76, | |
| 6. AUTHOR(s) | 7. PERFORMING ORG. REPORT NUMBER | |
| Anthony J. Moherok | | |
| 8. CONTRACT OR GRANT NUMBER(s) | 9. PROGRAM ELEMENT, PROJECT, TASK AREA & WORK UNIT NUMBERS | |
| Contract No. DACW39-76-C-0115 | DMRP Work Unit No. 1B08A | |
| 10. PERFORMING ORGANIZATION NAME AND ADDRESS | 11. REPORT DATE | |
| Department of Oceanography Texas A&M University College Station, Tex. 77843 | June 1978 | |
| 12. CONTROLLING OFFICE NAME AND ADDRESS | 13. NUMBER OF PAGES | |
| Office, Chief of Engineers, U. S. Army Washington, D. C. 20314 | 204 | |
| 14. MONITORING AGENCY NAME & ADDRESS (if different from Controlling Office) | 15. SECURITY CLASS. (of this report) | |
| U. S. Army Engineer Waterways Experiment Station Environmental Laboratory P. O. Box 631, Vicksburg, Miss. 39180 | Unclassified | |
| 15a. DECLASSIFICATION/DOWNGRADING SCHEDULE | | |
| 16. DISTRIBUTION STATEMENT (of this Report) | | |
| Approved for public release; distribution unlimited. | | |
| 17. DISTRIBUTION STATEMENT (of the abstract entered in Block 20, if different from Report) | | |
| (18) WES (19) TR-D-78-34 | | |
| 18. SUPPLEMENTARY NOTES | | |
| 19. KEY WORDS (Continue on reverse side if necessary and identify by block number) | | |
| Dredged material Dredged material disposal Flumes Galveston Offshore Dredged Material Disposal Site Sediment transport Waste disposal sites | | |
| 20. ABSTRACT (Continue on reverse side if necessary and identify by block number) | | |
| Flume experiments were performed on four sediment mixtures sampled from the offshore Galveston dredged material disposal site in order to determine their critical erosion velocity, shear stress, and modes of sediment transport. Also, an analysis of the offshore Galveston hydrographic regime was performed using meteorologic and oceanographic data. The results of the flume experiments indicated that the four sediment (Continued) | | |

DD FORM 1 JAN 73 1473

EDITION OF 1 NOV 65 IS OBSOLETE

Unclassified

SECURITY CLASSIFICATION OF THIS PAGE (When Data Entered)

401 203 78 14 08 179 LB

Unclassified

SECURITY CLASSIFICATION OF THIS PAGE(When Data Entered)

ABSTRACT. (Continued)

✓ mixtures eroded similarly. Extrapolation of flume results to recorded off-shore bottom current speed measurements indicate that bedload erosion occurs much more frequently near the northern margin of the disposal site. Also, net bedload transport of disposal material is oriented down the coast or offshore from the disposal site, suggesting that material will not likely return to the channel proper as shoaling sediment. ↗

✓

| | | |
|---------------|----------------------------------|-------------------------------------|
| ACCESSION for | White Section | <input checked="" type="checkbox"/> |
| NTIS | Buff Section | <input type="checkbox"/> |
| DDC | | |
| UNANNOUNCED | | |
| JUSTIFICATION | | |
| BY | DISSEMINATION/AVAILABILITY CODES | |
| Dist. | INT. | SPECIAL |
| A | | |

Unclassified

SECURITY CLASSIFICATION OF THIS PAGE(When Data Entered)

THE CONTENTS OF THIS REPORT ARE NOT TO BE USED FOR
ADVERTISING, PUBLICATION, OR PROMOTIONAL PURPOSES.
CITATION OF TRADE NAMES DOES NOT CONSTITUTE AN OFFI-
CIAL ENDORSEMENT OR APPROVAL OF THE USE OF SUCH COM-
MERCIAL PRODUCTS.

SUMMARY

Flume experiments were performed using four sand, silt, and clay mixtures sampled from the offshore Galveston dredged material disposal site in order to determine the critical erosion velocity, shear stress, and modes of sediment transport for each mixture. Also, an analysis of the hydrographic regime for offshore Galveston was performed based on meteorologic and oceanographic data collected between February 1975 and June 1976. Results of the flume experiments and hydrographic analysis were extrapolated to sediment transport processes believed operative in the offshore disposal site.

The results of the flume experiments indicated that the four sediment mixtures erode similarly as evidenced by the same critical bed shear ($\tau_{ocr} \approx 1.0 \text{ dynes/cm}^2$) necessary to induce massive bedload transport and rapid suspended sediment increases. Significant deposition of suspended fine silt and clay occurred at low bed shears ($\tau_o \leq 0.2 \text{ dynes/cm}^2$). Extrapolation of these erosion and deposition bed shears to recorded offshore bottom current speed measurements over month-long periods suggests that bedload erosion occurs much more frequently near the northern margin of the disposal site than at the southern end. In addition, progressive vector diagrams indicate a net down-coast and/or offshore-directed bottom drift. These net drift directions presumably result from strong prevailing onshore winds that generate onshore-directed flow near the surface and down-coast to offshore flow at the bottom. Maximum bottom velocities occur during these wind-generated bottom flows.

This suggests that net bedload transport of disposal mound sediment is oriented away from the Galveston Bay entrance channel, and therefore material will not likely return as shoaling sediment.

PREFACE

The work described in this report was performed under Contract No. DACW39-76-C-0115, dated 30 June 1976, between the U. S. Army Engineer Waterways Experiment Station (WES), Vicksburg, Miss., and the Texas A&M University (TAMU) Research Foundation, College Station, Tex. The research was sponsored by the Office, Chief of Engineers, U. S. Army, as part of the Dredged Material Research Program (DMRP) managed by the Environmental Laboratory (EL), WES. The study constituted DMRP Work Unit No. IB08A.

The research and report writing were conducted by and under the supervision of Anthony J. Moherrek, Department of Oceanography, TAMU, College Station, Tex. Ms. Jo Ann Treat coordinated the contract for the TAMU Research Foundation. The hydrographic and meteorologic data incorporated in this report were acquired from work conducted under Contract No. DACW64-75-C-0069.

The contract was managed at WES by Mr. Barry Holliday under the general supervision of Dr. Robert M. Engler, Project Manager for the Environmental Impacts and Criteria Development Project, and Dr. John Harrison, Chief of EL.

Directors of WES during the study and preparation of this report were COL G. H. Hilt, CE, and COL J. L. Cannon, CE. Technical Director was Mr. F. R. Brown.

CONTENTS

| | <u>Page</u> |
|---|-------------|
| SUMMARY..... | 2 |
| PREFACE..... | 4 |
| LIST OF TABLES..... | 9 |
| LIST OF FIGURES..... | 10 |
| CONVERSION FACTORS, U. S. CUSTOMARY TO METRIC (SI) UNITS OF MEASUREMENT..... | 15 |
| PART I: INTRODUCTION..... | 16 |
| Objectives..... | 16 |
| Study Area..... | 17 |
| PART II: LITERATURE REVIEW..... | 25 |
| General..... | 25 |
| Bed Shear Stress..... | 28 |
| The Problem..... | 29 |
| Previous Flume Experiments..... | 29 |
| Offshore Sediment Transport..... | 31 |
| Flow Near the Bed..... | 34 |
| PART III: TECHNIQUES..... | 37 |
| Field Techniques..... | 37 |
| Geotechnical Properties of Bedload..... | 38 |
| Geotechnical Properties of Washload..... | 49 |
| Flume Experiments..... | 55 |
| PART IV: RESULTS..... | 65 |
| Geotechnical Properties of Bedload..... | 65 |
| Grain-size Distribution..... | 65 |
| Physical Properties..... | 71 |
| Flume Experiments..... | 74 |
| Bedload Introduction..... | 74 |
| Erosional Runs..... | 75 |
| Dense Bed--Sediment Transport..... | 77 |
| Dense Bed--Critical Shear Stress and Erosion Velocity..... | 81 |
| Floc Bed..... | 84 |
| Erosion Rates..... | 88 |

CONTENTS

| | <u>Page</u> |
|---|-------------|
| Depositional Runs..... | 90 |
| Geotechnical Properties of Washload..... | 92 |
| Grain-size Distribution..... | 92 |
| Composition..... | 98 |
| Summary..... | 101 |
| Hydrography of Offshore Galveston..... | 103 |
| Tide Regime..... | 103 |
| Current Data..... | 107 |
| Velocity Profiles..... | 107 |
| Offshore Tidal Current Circulation Pattern..... | 113 |
| Progressive Vector Diagrams..... | 118 |
| Oscillatory Bottom Velocities..... | 132 |
| Summary..... | 143 |
| Applicability of Flume Experimental Results to Offshore Sediment Transport at Galveston..... | 144 |
| Scaling Considerations..... | 144 |
| Critical Erosion and Deposition Velocities..... | 146 |
| Sediment Transport Processes in the Offshore | |
| Dredged Material Disposal Site..... | 147 |
| Effect of Climate..... | 147 |
| Persistent Winds..... | 147 |
| Tropical Storms..... | 149 |
| Modes of Sediment Transport..... | 150 |
| Offshore Disposal Mounds..... | 158 |
| PART V: CONCLUSIONS..... | 160 |
| Flume Experiments..... | 160 |
| Hydrography of Offshore Galveston..... | 161 |
| Offshore Sediment Transport..... | 162 |
| REFERENCES..... | 163 |
| APPENDIX A: TOTAL SUSPENDED MATTER CONCENTRATION, TIME AFTER VELOCITY CHANGE, MEAN FLOW SPEED, AND WATER SAMPLE LOCATIONS OBTAINED DURING EXPERIMENTAL RUNS..... | A1 |
| APPENDIX B: CURRENT VELOCITY PROFILES AND SHEAR STRESS CALCULATIONS FOR EXPERIMENTAL RUNS..... | B1 |

CONTENTS

| | <u>Page</u> |
|---|-------------|
| APPENDIX C: EXPERIMENTAL RUNS..... | C1 |
| APPENDIX D: WASHLOAD GRAIN-SIZE ANALYSES..... | D1 |
| APPENDIX E: REYNOLDS AND FROUDE NUMBER CALCULATIONS..... | E1 |
| APPENDIX F: NOTATION..... | F1 |

LIST OF TABLES

| <u>No.</u> | | <u>Page</u> |
|------------|--|-------------|
| 1 | Type, Location, Date, and Time of Current Meter Data Recovered | 39 |
| 2 | Physical Property Values Determined for Block 15, Buoy C, Block 27, and Buoy D Sediment | 72 |
| 3 | Rate of Change of TSM Concentration for Erosional Runs | 89 |
| 4 | Percent Frequency of Wind Speed and Direction Versus Sea Height | 134 |
| 5 | Wind Speed Versus Sea Height | 139 |
| 6 | Percent Frequency of Wave Height Versus Wave Period | 140 |

LIST OF FIGURES

| <u>No.</u> | <u>Page</u> |
|--|-------------|
| 1 Side view of laboratory flume..... | 16 |
| 2 Location map of offshore Galveston dredged material disposal site and sampling stations..... | 18 |
| 3 Locations of specific disposal sites at Buoys B, C, and D and control blocks in study area..... | 20 |
| 4 Predump bathymetry of disposal area (from Coulthard 1976)..... | 21 |
| 5 Bathymetric configuration of sediment mound at Buoy B (from Estes and Scrudato 1977)..... | 22 |
| 6 Bathymetric configuration of sediment mound at Buoy C (from Estes and Scrudato 1977)..... | 23 |
| 7 Bathymetric configuration of sediment mound at Buoy D (from Estes and Scrudato 1977) | 24 |
| 8 Erosion, transportation, and despoition criteria (after Hjulstrom 1935)..... | 26 |
| 9 Relationship between particle diameter, mean current speed, and consolidation characteristics (modified from Postma 1967)..... | 27 |
| 10 Relationship between generating forces and flow regions within the offshore water column (modified from Weggel 1972)..... | 33 |
| 11 Velocity distribution in the turbulent boundary layer (from Rouse 1961)..... | 36 |
| 12 Bottom current meter array positioned adjacent to both Buoy B and Buoy D..... | 40 |
| 13 Example of torque versus rotation angle plot..... | 44 |
| 14 Schematic diagram of suspended matter filtration system..... | 51 |
| 15 Example of washload grain-size analysis worksheet..... | 53 |

| <u>No.</u> | | <u>Page</u> |
|------------|--|-------------|
| 16 | Schematic illustration of rectangular circulating flume..... | 56 |
| 17 | Cross-sectional view of flume current propulsion system..... | 57 |
| 18 | Schematic illustration of washload sampling system..... | 60 |
| 19 | Location chart for current velocity profiles and water samples..... | 63 |
| 20 | Block 15 sediment dispersed grain-size distribution..... | 66 |
| 21 | Block 27 sediment dispersed grain-size distribution..... | 67 |
| 22 | Buoy C sediment dispersed grain-size distribution..... | 68 |
| 23 | Buoy D sediment dispersed grain-size distribution..... | 69 |
| 24 | Shear Strength (C_u) measurements..... | 73 |
| 25a | Turbidity plume generated 14 seconds after Buoy D sediment discharge..... | 76 |
| 25b | Turbidity plume generated 22 seconds after Buoy D sediment discharge..... | 76 |
| 25c | Turbidity plume generated 35 seconds after Buoy D sediment discharge..... | 76 |
| 25d | Turbidity plume generated 45 seconds after Buoy D sediment discharge..... | 76 |
| 26 | Selected dense bed erosional runs performed on Buoy C and Buoy D sediment..... | 78 |
| 27 | Selected dense bed erosional runs performed on Block 15 and Block 27 sediment..... | 79 |
| 28a | Sediment-water interface 16 hours after Buoy D sediment discharge..... | 83 |
| 28b | Sediment interfaces following two weeks of experimental runs on Buoy D sediment..... | 83 |

| <u>No.</u> | <u>Page</u> |
|------------|---|
| 29 | Relationship between average TSM concentration and bed shear for dense bed erosional runs....., 83 |
| 30 | Block 27 flocculated bed erosional runs....., 86 |
| 31 | Buoy D flocculated bed erosional runs....., 87 |
| 32 | Depositional runs performed on each of the four sediment mixtures....., 91 |
| 33 | Grain-size distributions of three washload samples collected during Block 15 erosion run....., 93 |
| 34 | Grain-size distributions of three washload samples collected during Buoy D erosion run....., 94 |
| 35 | Grain-size distributions of three washload samples collected during Block 27 dense bed erosional run....., 96 |
| 36 | Grain-size distributions of three washload samples collected during Block 27 floc bed erosional runs....., 97 |
| 37 | X-ray diffractograms of suspended matter collected during a 31-cm/sec, Buoy C erosional run....., 99 |
| 38 | X-ray diffractograms of suspended matter collected during a 23-cm/sec, Buoy C depositional run.....100 |
| 39 | Example of mixed tide cycle.....104 |
| 40 | Observed versus predicted tide cycle during sustained southeasterly winds.....105 |
| 41 | Observed versus predicted tide cycle during strong northwesterly winds.....106 |
| 42 | Two-hour interval vertical profiles obtained at Buoy C.....108 |
| 43 | Two-hour interval vertical profiles obtained at Buoy C.....109 |
| 44 | Two-hour interval vertical profiles obtained at Buoy C.....110 |
| 45 | Flow velocity at various depths versus time.....112 |

| <u>No.</u> | | <u>Page</u> |
|------------|---|-------------|
| 46 | Velocity profile obtained at Buoy B..... | 114 |
| 47 | Velocity profile obtained at Buoy D..... | 115 |
| 48 | Rotary offshore flow pattern developed during flood tide (from Hall, 1976)..... | 116 |
| 49 | Rotary offshore flow pattern developed during ebb tide (from Hall, 1976)..... | 117 |
| 50 | Progressive vector diagram for 9 October through 14 November 1975 at Buoy D..... | 119 |
| 51 | Progressive vector diagram for 17 March through 23 March 1976 at Buoy B..... | 120 |
| 52 | Progressive vector diagram for 17 March through 7 April 1976 at Buoy D..... | 121 |
| 53 | Progressive vector diagram for 8 April through April 30, 1976 at Buoy B..... | 122 |
| 54 | Progressive vector diagram for 8 April through 3 May 1976 at Buoy D..... | 123 |
| 55 | Stick diagrams of a) surface wind speed and direction and b) bottom current speed and direction for 4 May through 8 May 1976..... | 126 |
| 56 | Observed versus predicted tidal cycle for 3 May through 9 May 1976..... | 127 |
| 57 | Bottom current speed and direction for 9 April through 26 April 1976..... | 129 |
| 58 | Observed versus predicted tidal cycle in channel for 29 March through 3 April 1976..... | 130 |
| 59 | Stick diagram of wind speed and direction at Galveston for 29 March through 3 April 1976..... | 131 |
| 60 | Relationship between wave period and oscillatory bottom velocity (U_m) for an average 14-m water depth..... | 142 |
| 61 | Wind rose and net bottom drift vectors for offshore Galveston..... | 148 |

| <u>No.</u> | | <u>Page</u> |
|------------|--|-------------|
| 62 | Cumulative curve of the current velocity distribution for 9 October to 14 November 1975 at Buoy D (modified from Hall 1976)..... | 151 |
| 63 | Cumulative curve of the current velocity distribution for 17 March to 24 March 1976 at Buoy B..... | 152 |
| 64 | Cumulative curve of the current velocity distribution for 17 March to 7 April 1976 at Buoy D..... | 153 |
| 65 | Cumulative curve of the current velocity distribution for 8 April to 1 May 1976 at Buoy B..... | 154 |
| 66 | Cumulative curve of the current velocity distribution for 8 April to 3 May 1976 at Buoy D..... | 155 |

CONVERSION FACTORS, U. S. CUSTOMARY TO METRIC (SI)

UNITS OF MEASUREMENT

U. S. customary units of measurement used in this report can be converted to metric (SI) units as follows:

| <u>Multiply</u> | <u>By</u> | <u>To Obtain</u> |
|---------------------------|------------|------------------|
| feet | 0.3048 | metres |
| miles (U. S. statute) | 1.609344 | kilometres |
| miles (U. S. nautical) | 1.852 | kilometres |
| inch-ounces (force) | 0.0070615 | newton-metres |
| horsepower (550 ft-lbf/s) | 745.6999 | watts |
| gallons (U. S. liquid) | 3.785412 | cubic decimetres |
| degrees (angular) | 0.01745329 | radians |

PART I: INTRODUCTION

Objectives

1. A rectangular circulating flume (Figure 1) was designed and constructed to model the effects of unidirectional turbulent flow upon bedload and suspended sand, silt, and clay mixtures sampled from the Galveston dredged material disposal site.



Figure 1. Side view of laboratory flume

2. The objectives of this study were to determine:
 - a. The critical erosion velocity, in terms of bed shear and current speed, necessary to erode each sediment mixture.
 - b. The transport conditions during which this eroded material remained in suspension.

- c. The amount and composition of suspended matter that resulted from erosion under controlled velocity conditions.
- d. The relationships that describe the recorded events of sediment erosion and transport in order to predict the relative degree of erosion, transport, and deposition occurring in the off-shore dredged material disposal site.

In addition, this study included an evaluation of hydrographic data acquired within and immediately adjacent to the offshore disposal site. These data, obtained between February 1975 and June 1976, constituted part of a related study (Estes and Scrudato 1977) that attempted to determine the fate of dredged material discharged into the Galveston site.

Study Area

3. The location of the offshore disposal site is presented in Figure 2. The northern boundary is situated approximately 4.5 km southeast of the southern extremity of the Galveston Bay entrance channel south jetty. The site is near rectangular, extending 6.7 km in length and 3.8 km in width, and is oriented with the long axis trending in a northwest-southeast direction. Also shown in Figure 2 are the locations of three buoys (B, C, and D) that mark specific dredged material discharge sites and two reference areas (Block 15 and Block 27) that served as control sites for sediment sampling operations.

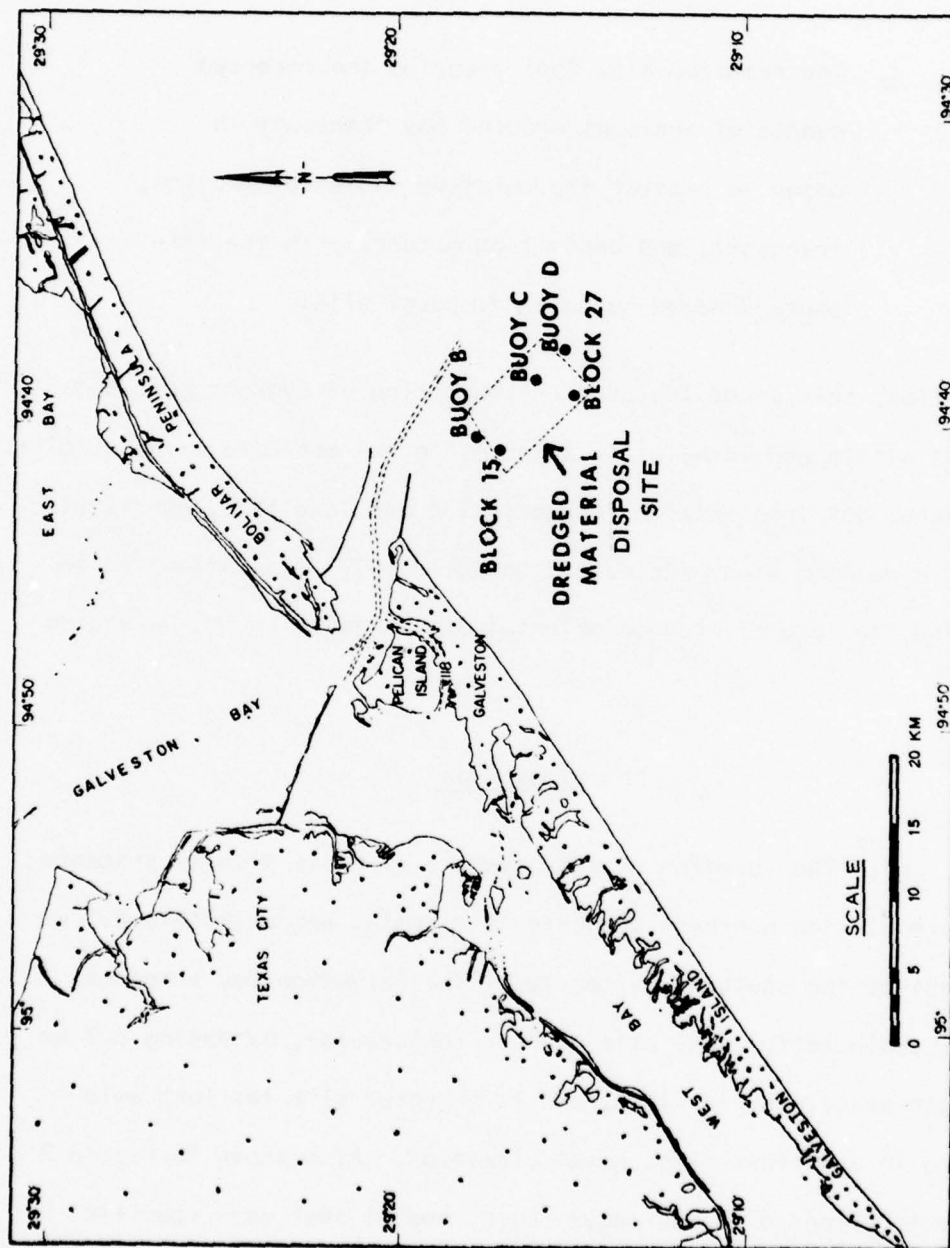


Figure 2. Location map of offshore Galveston dredged material disposal site and sampling stations

The disposal site was divided into 28 individual 1.3-km-square blocks in order to facilitate sample location designations (Figure 3).

4. Water depths within the disposal site ranged from 10 m at the northern extremity to a maximum of 16 m at the southern boundary. Prior to the start of discharge operations, a bathymetric survey (Figure 4) was performed in April 1975. This baseline study indicated that the seafloor of the disposal site is very smooth with a dip of approximately 1.5 m per mile* towards the southeast. Subsequent to this survey, dredged material discharge operations were carried out at each of the three designated discharge sites (Buoys B, C, and D). Two bathymetric surveys have been completed since disposal operations were initiated in order that changes in the disposal mound topographies over time due to sediment transport processes could be assessed (Estes and Scrudato 1977). The bathymetric configurations of the three individual disposal mounds, as determined by the June 1976 survey, are illustrated in Figures 5, 6, and 7.

*A table of factors for converting U. S. customary units of measurement to metric (SI) units is presented on page 15.

Figure 3. Locations of specific disposal sites at Buoys B, C, and D and control blocks in study area

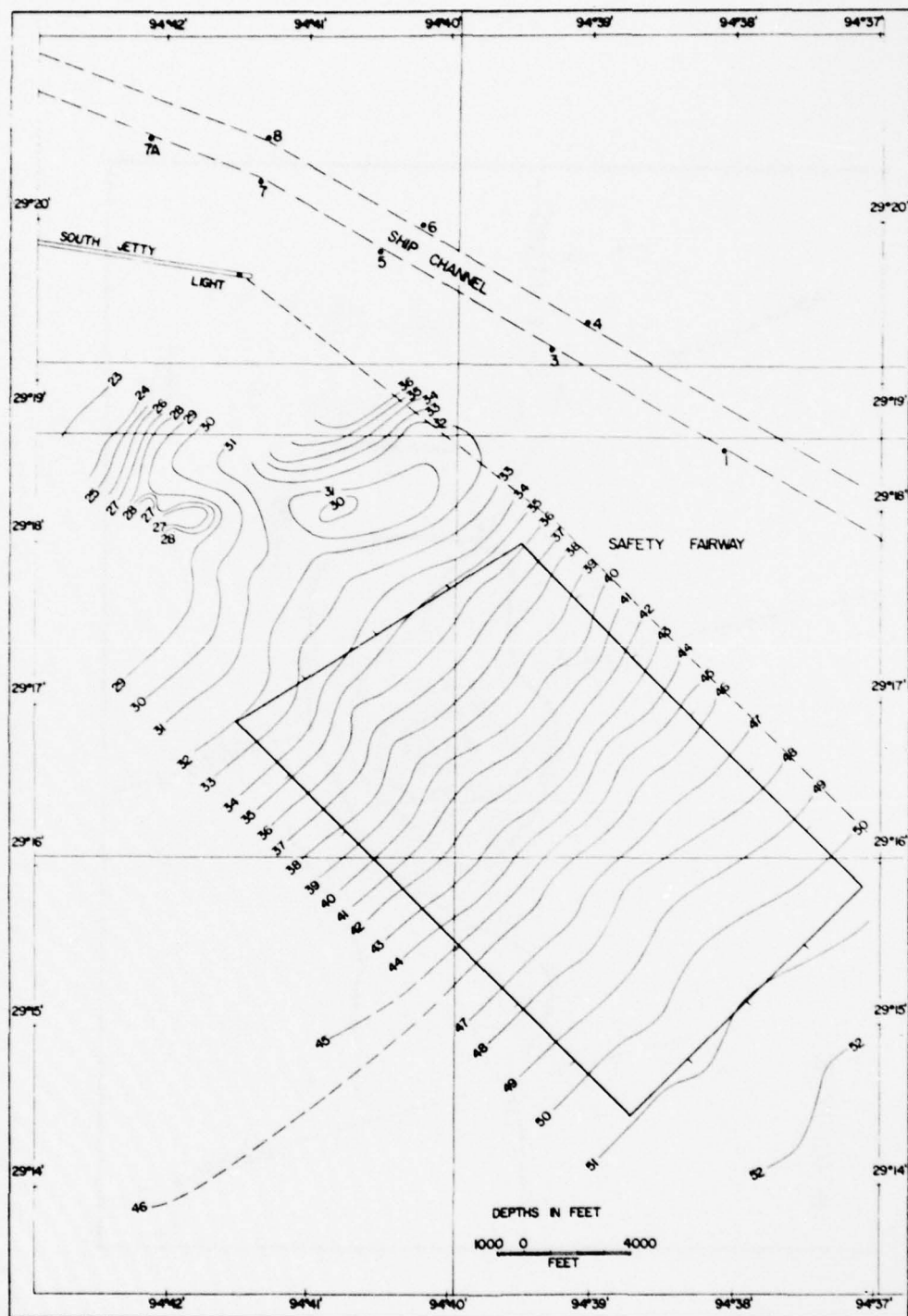


Figure 4. Predump bathymetry of disposal area (from Coulthard 1976)

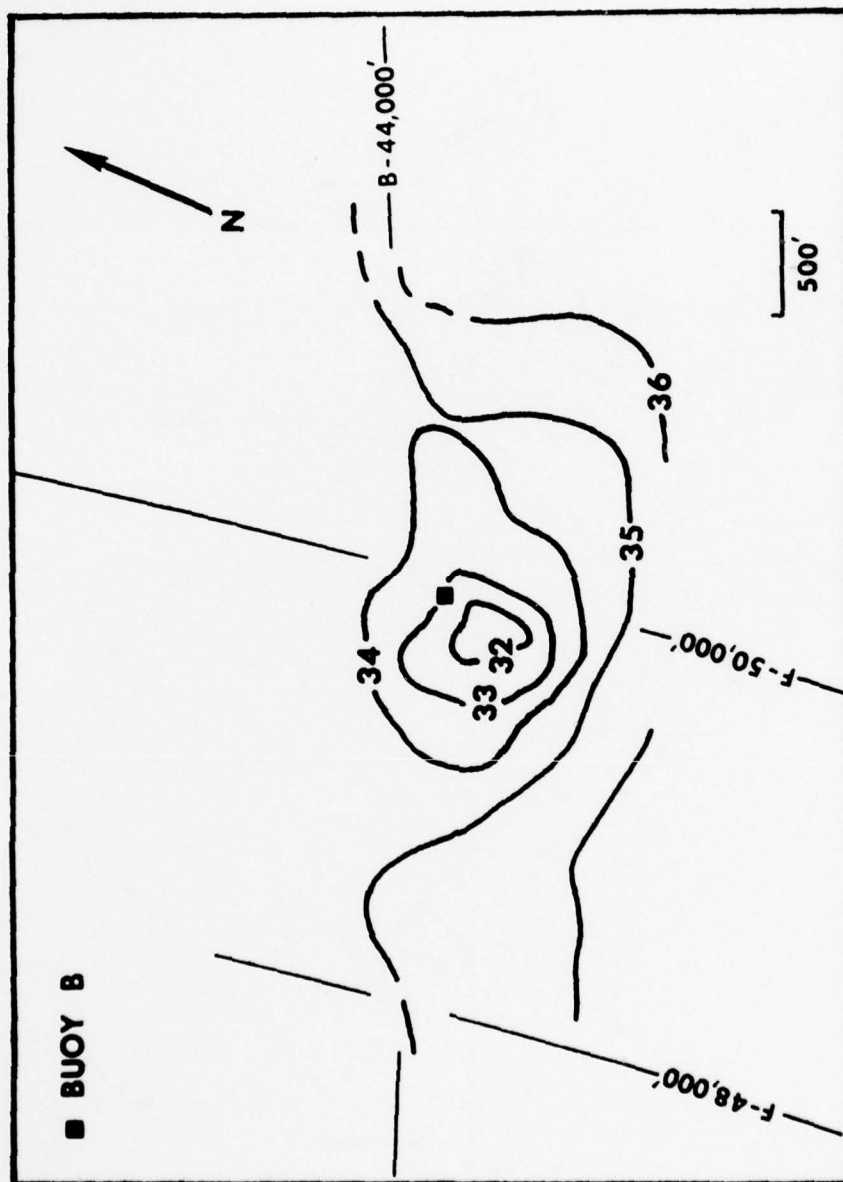


Figure 5. Bathymetric configuration of sediment mound at Buoy B, Contour interval: 1 ft
(from Estes and Scrudato 1977)

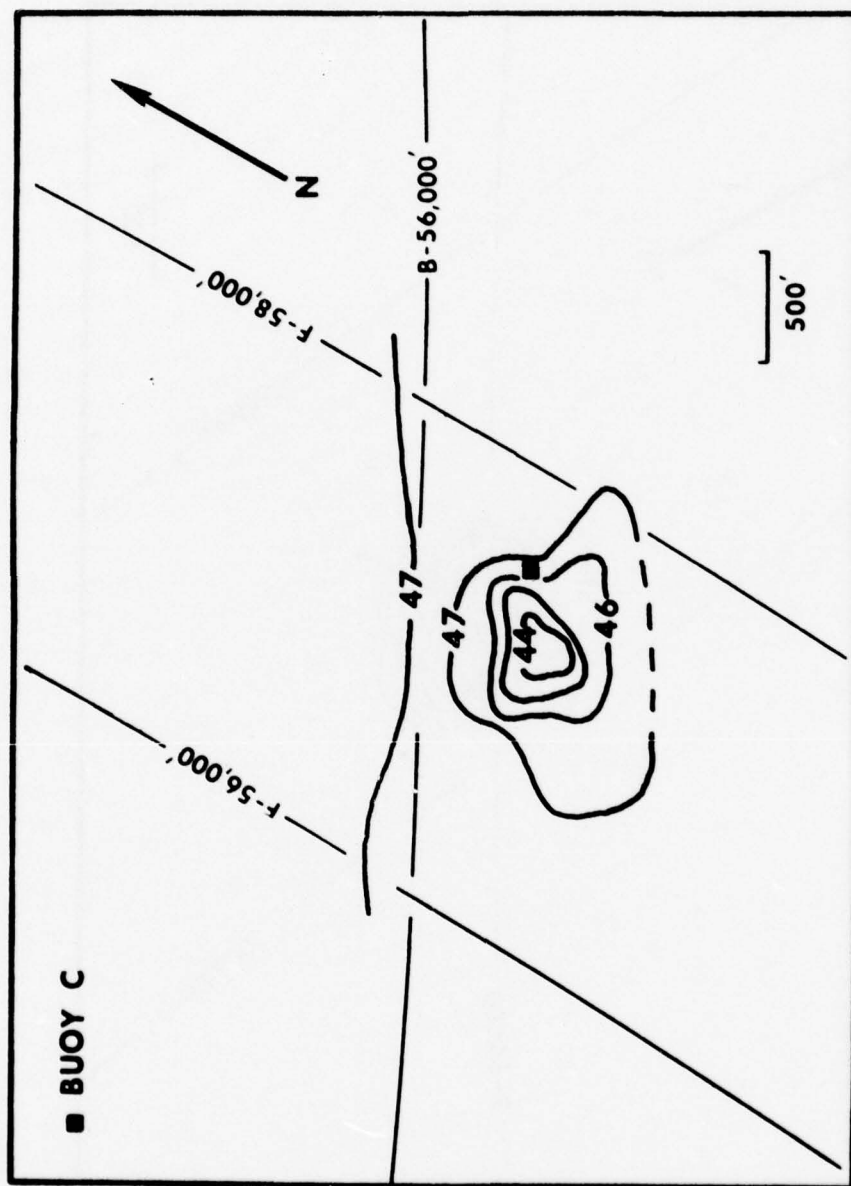


Figure 6. Bathymetric configuration of sediment mound at Buoy C, Contour interval: 1 ft
(from Estes and Scrudato 1977)

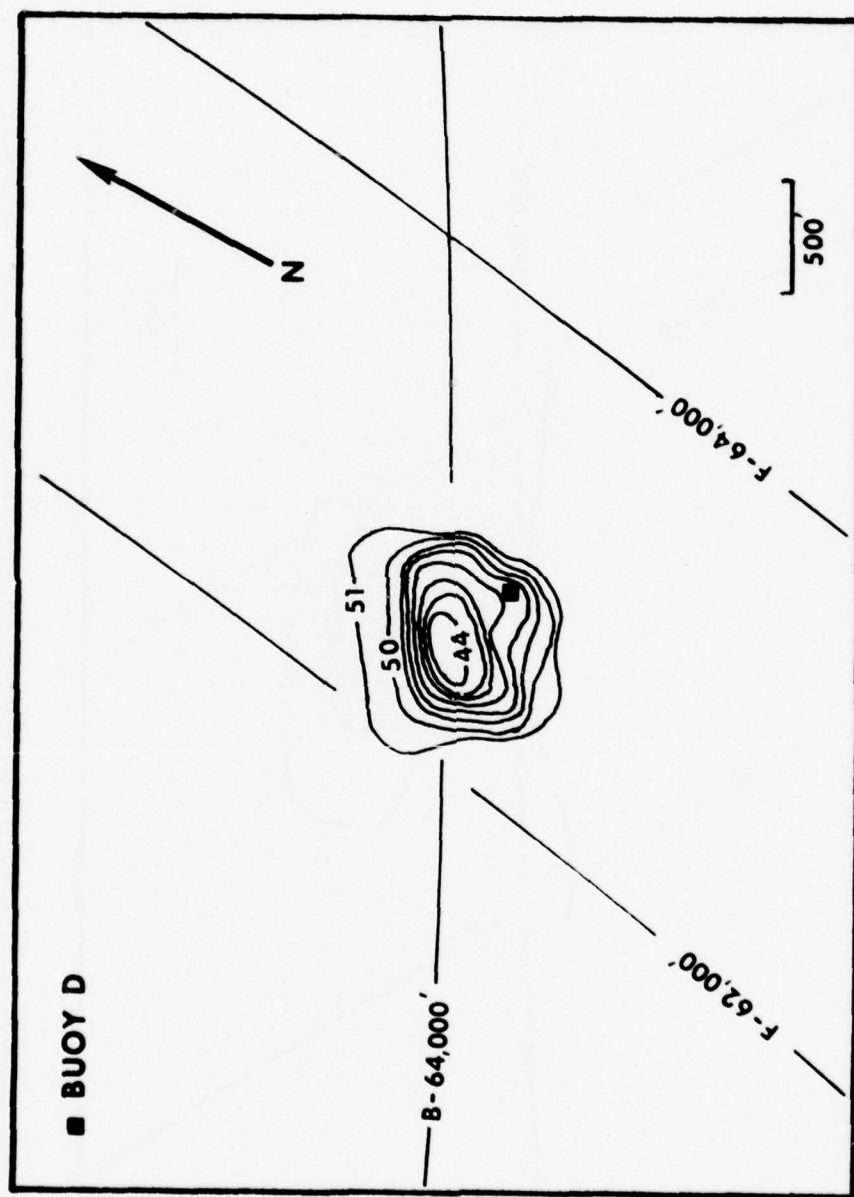


Figure 7. Bathymetric configuration of sediment mound at Buoy D, Contour interval: 1 ft
(from Estes and Scrudato 1977)

PART II: LITERATURE REVIEW

General

5. The physical parameters governing sediment transport processes of marine cohesive material are at best qualitatively understood. This is due to the fact that the focus of recent hydraulic research has centered on the erosion, transport, and deposition of primarily loose, noncohesive particles such as rounded quartz grains. To the author's knowledge, no studies have been reported dealing directly with sediment mixtures containing near equivalent amounts of sand, silt, and clay.

6. The first significant study establishing erosion-deposition criteria for sedimentary particles of uniform size was presented by Hjulstrom (1935). Figure 8 illustrates the well known "Hjulstorm diagram." The flow velocities given represent the average current speed that is presumably 40 percent greater than the bottom velocity for a flow depth exceeding 1 m. The diagram shows that erosion of loose, noncohesive fine sand occurs at significantly lower current velocities than for cohesive silts and clays. Alternately, fine particles are apt to remain in suspension at considerably lower flow speeds than coarse particles. Postma (1967) presented a refinement of Hjulstorm's diagram using data reported by Sundborg (1956). He related sediment transport criteria to varying degrees of cohesive sediment consolidation. The results depicted in Figure 9 are not likely to be representative of erosion-deposition criteria for discharged dredged material having highly variable consolidation characteristics.

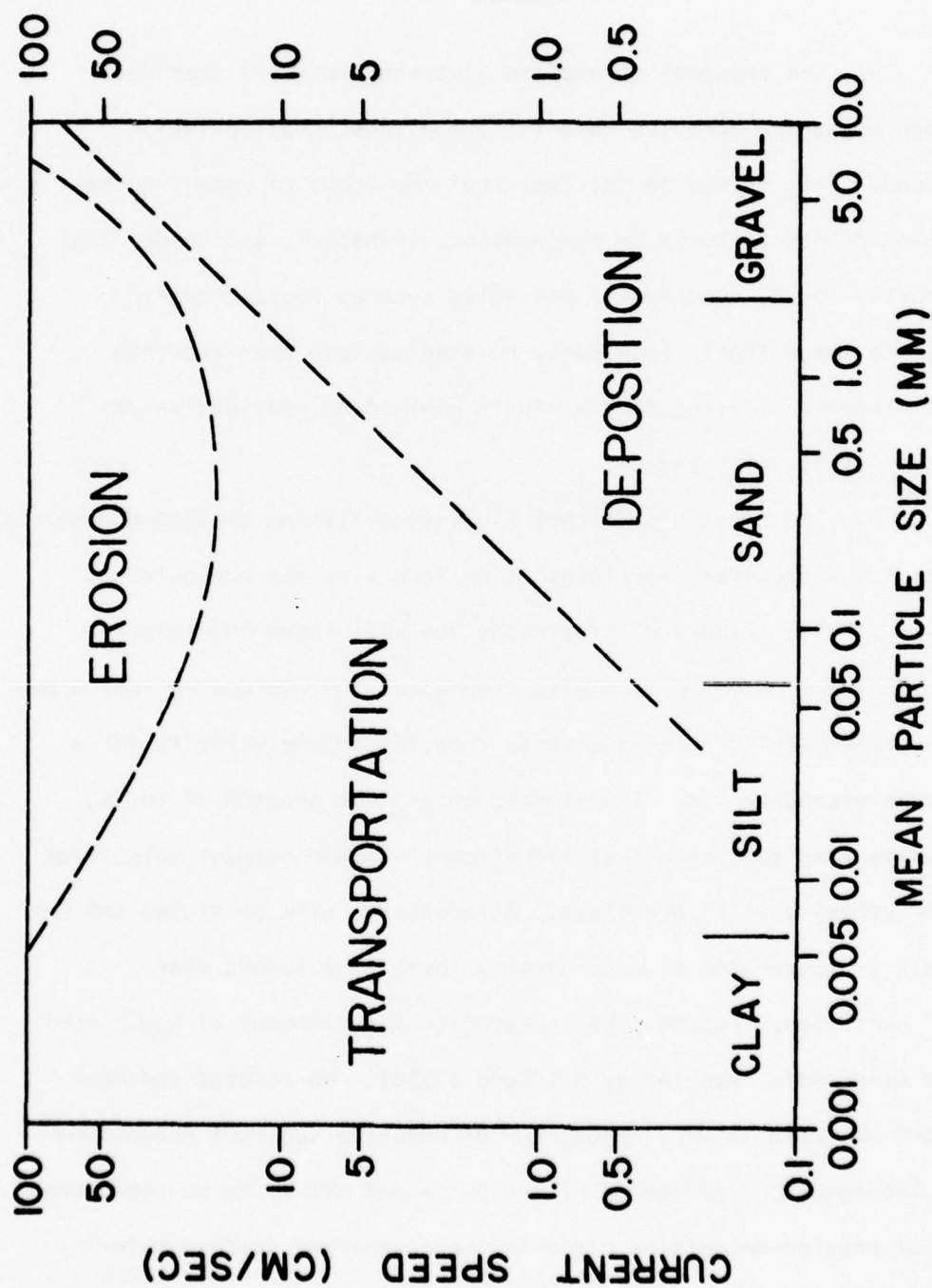


Figure 8. Erosion, transportation, and deposition criteria (after Hjulstorm 1935)

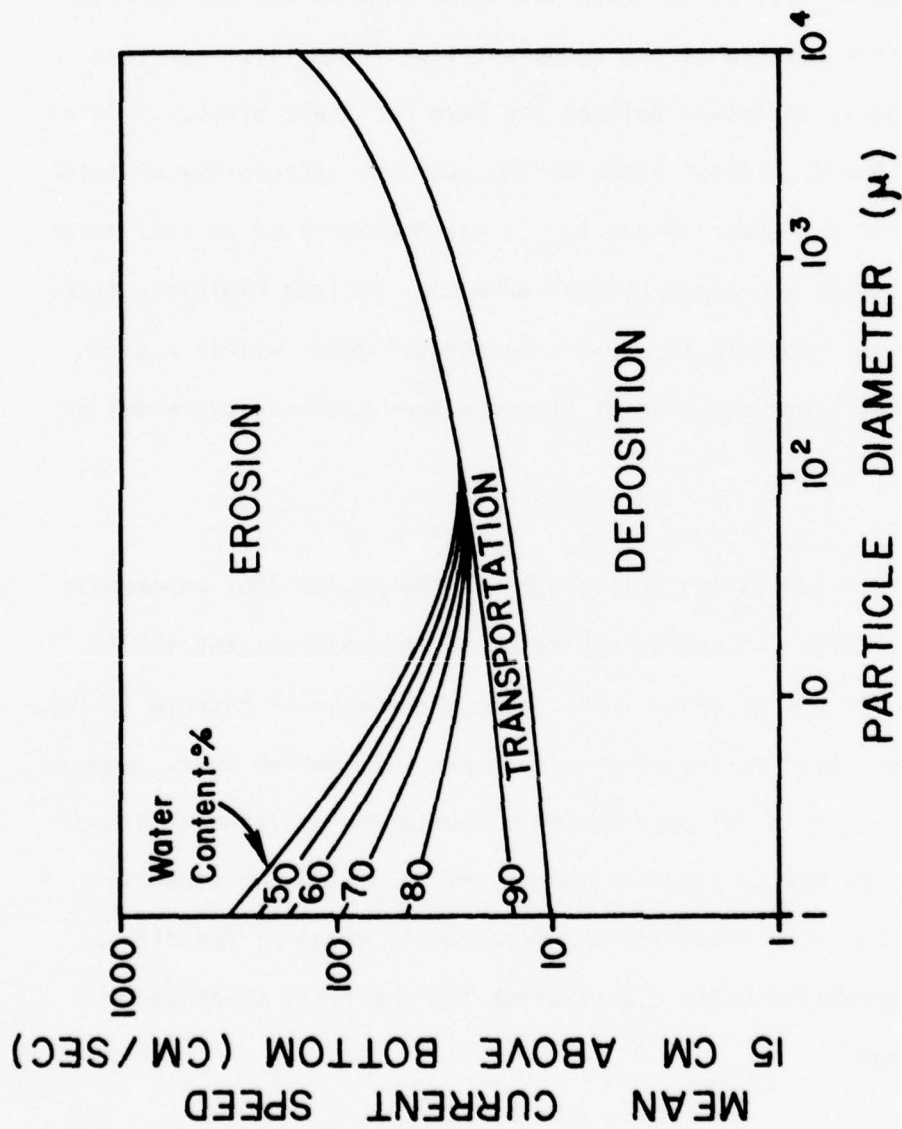


Figure 9. Relationship between particle diameter, mean current speed, and consolidation characteristics (modified from Postma 1967)

Bed Shear Stress

7. Workers realized early that description of the competency, or erosion capability, of currents acting on a given bedload depended upon an accurate measure of the turbulent flow intensity. For this reason, hydraulic engineers defined the term bed shear stress (τ_o)* as representing the frictional force acting upon the sediment-water interface. The critical shear stress (τ_{ocr}) was then defined as that force necessary to cause incipient bedload erosion. Various empirical techniques have been proposed for measuring the bed shear within a given flow. Bed shear for open channel flow has been commonly expressed as:

$$\tau_o = \gamma R_h S \quad (1)$$

where (γ) is defined as the unit weight of the fluid; (R_h) represents the hydraulic radius or wetted perimeter of the channel; and (S) is the slope of the energy grade line. This expression is representative of the average value of the shear stress per unit wetted area. However, the product ($\gamma R_h S$) is not applicable to the marine environment since the slope of the energy gradient cannot, at this time, be directly measured. Thus, most investigators resorted to usage of Prandtl-von Karman's universal velocity distribution law for fully developed turbulent flow:

$$\frac{U}{u^*} = 2.5 \ln Y/z_o \quad (2)$$

*For convenience, symbols and unusual abbreviations are listed and defined in the Notation (Appendix F).

where: U = the flow speed at elevation (Y) above the bed

Z_0 = the roughness element

$u_* = \sqrt{\tau_0 / \rho}$ = the friction element

ρ = water density

8. Simple regression methods can be employed to estimate (u_*) and (Z_0) in order to calculate (τ_0). The main restriction of this relationship is that current velocity measurements are required from at least two points immediately above the bed. Teleki (1972) related Von Karman's logarithmic law to the "velocity defect law" and "law of the wall" in turbulent boundary layers of incompressible steady flow.

The Problem

9. A universal relationship equating erosion and transport of cohesive sediment has yet to be formulated due to the complex adhesive and cohesive forces acting between sediment particles. Graf (1971) outlined the basic problem by defining the critical shear stress necessary to erode sediment as a function of sediment particle diameter (d) and a coefficient of cohesion (C_0), such that:

$$\tau_{ocr} = f(d, C_0)$$

(3)

Previous Flume Experiments

10. Flume experiments performed by Smerdon and Beasley (1969) using 11 different Missouri soils demonstrated that the critical shear

stress correlated best with the plasticity index (I_p) of the soil. This study used Equation 1 to calculate the bed shear, or unit tractive force, acting on the soil for a given flow rate, defining incipient bedload motion as corresponding to "general movement of the bed material." Similar experiments by Lyle and Smerdon (1965), testing seven different Texas soils, determined that (I_p) and the void ratio (e) correlated well with (τ_{ocr}). Determination of the critical shear stress was made by plots of the soil's erosion rates against the measured bed shear. The point at which the erosion rate increased sharply indicated initial bed failure. For both studies, results were based upon erosional current flow over a smooth plane bed. The applicability of their results to dredged material discharged into an open marine environment appears highly tenuous because of the hydrodynamically rough surface produced by material mounding on the sea floor.

11. Einstein and Krone (1962) correlated modes of sediment transport with suspended sediment concentration using San Francisco Bay mud containing nearly equal amounts of silt and clay. A recirculating flume, 1.0 m wide and 30.48 m long, was filled to a 30.5-cm water depth for monitoring of the suspended matter concentrations at uniform flow speeds. Depositional concentration changes indicated that below 300 ppm the suspended sediment concentration decreased logarithmically with time. Plots of deposition rates versus bed shear showed that at shears exceeding 0.60 dyne/cm^2 (kPa) deposition of suspended particles did not occur. For concentrations greater than 300 ppm, flocculation of the suspended clays became a dominant factor

in increasing deposition rates. This was attributed to "an increase in frequency of interparticle contacts forming large floc sizes over a short time period." Scour experiments, performed by Krone (1962) with the same bedload material, revealed a log-log relationship between the suspended sediment concentration and time, suggesting that exchange of suspended and deposited sediment occurred. No correlation was found between the critical shear stress and the shear strength of the bed as determined by in situ penetrometer measurements.

12. Partheniades and Mehta (1971) presented data on rates of deposition of fine cohesive sediments in turbulent flows. Using kaolinite clay suspensions in a rotating annular channel and ring apparatus, they demonstrated that the percentage of the total sediment within a given flow depends only on the bed shear stress (τ_0). Furthermore, the percentage (C') of the depositable sediment deposited at time (t) was found to vary with time according to the law:

$$C' = \alpha \log t + \beta \quad (4)$$

where α is a constant independent of the flow conditions and sediment concentration, and β is a constant dependent on shear stress only.

Offshore Sediment Transport

13. Understanding of the extent of sediment transport processes in the open marine environment requires knowledge of the fluid motions involved both in the entire water column and at the sediment-water

interface. Weggel (1972) outlined the fundamental fluid motions in the water column, as well as their respective generating forces. These forces include: meteorological, such as wind-driven surface stresses generating waves and storm surges; astronomical forces producing tides and associated tidal currents; and baroclinic forces induced by fluid density gradients that are, in turn, due to temperature and salinity differences. Figure 10 illustrates schematically the relationship between these forces and flow regions within the water column (\bar{U} is mean flow speed).

14. Teleki (1972) described the complexities in evaluating near-bottom oscillatory motion generated by surface waves. His study demonstrated that sediment motion is dependent upon the characteristic frequency and amplitude of oscillation as determined experimentally by shear stress measurements shoreward outside the zone of breaking waves. Komar and Miller (1973) derived an empirical relationship for determining the oscillatory bottom velocities needed to reach the threshold of sediment movement for grain diameters less than 0.05 cm (medium sand). Phillips (1969) pointed out that surface waves induce a mean forward velocity near the bottom in addition to strictly oscillatory motion. This phenomena, first observed by Caligny (1878), has been termed boundary layer streaming. During the literature survey, no studies were found that quantitatively assessed the effects of near-bottom oscillatory motions on heterogeneous sediment.

15. The theory of surface wind stresses generating nearshore

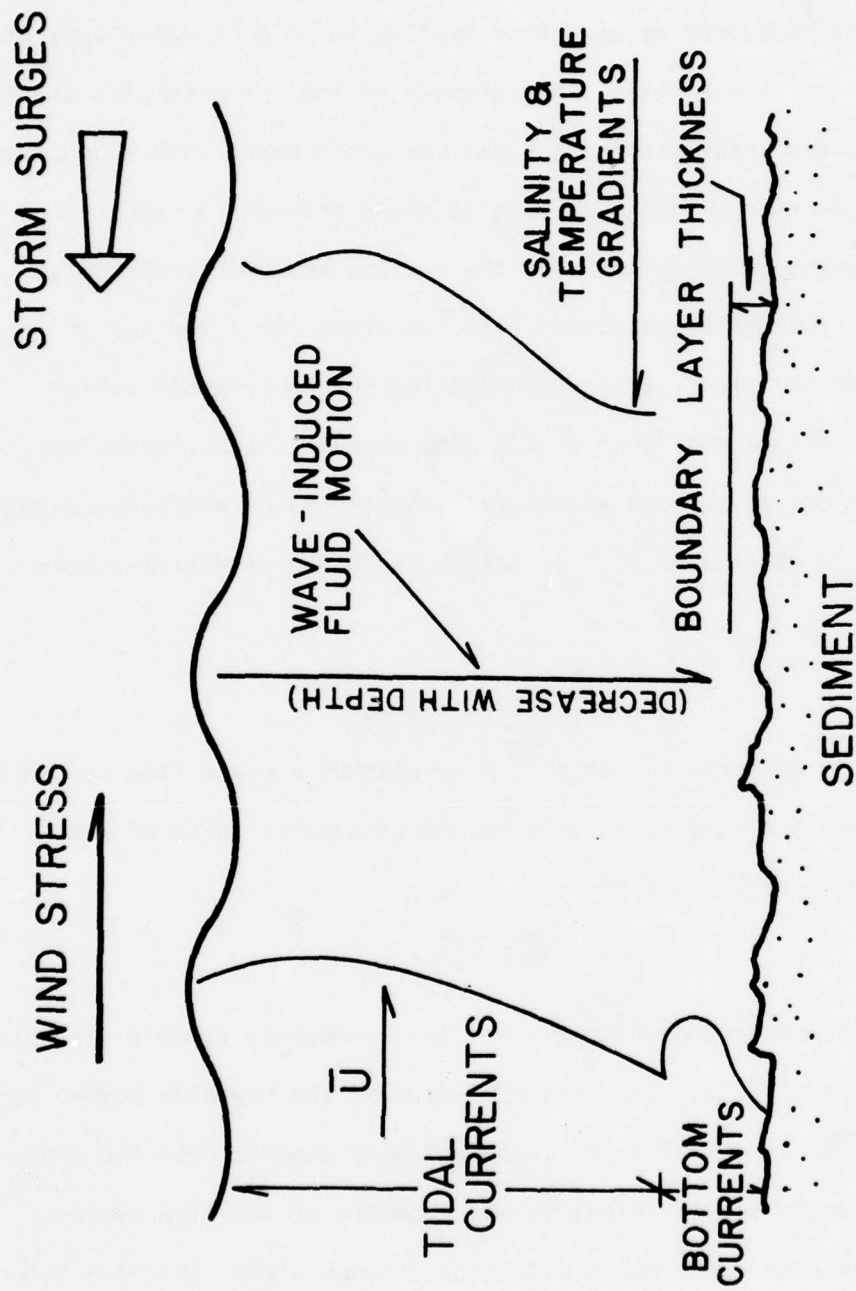


Figure 10. Relationship between generating forces and flow regions within the offshore water column (modified from Weggel 1972)

vertical circulation patterns has been discussed by Sverdrup et al., (1942). Murray (1972) presented results of current and water density observations recovered at an anchor station in 15 m of water east of the Mississippi River delta. Measurement of the currents plus salinity-induced density gradients for a 5-day period in March 1970 showed that southeasterly storm winds exceeding 13 m/sec produced a circulation pattern causing onshore flow near the surface and offshore flow at the bottom. Currents associated with the storm persisted for at least 3 days after the storm passage, generating stable offshore bottom currents. Longard and Banks (1952) also reported that wind-driven, shoreward-directed surface waters were coupled to offshore-moving bottom currents at a station in 91 m of water, southeast of Halifax, Nova Scotia.

Flow Near the Bed

16. Criteria for establishing whether a given flow is laminar or turbulent in nature is based upon the calculated value of its Reynolds number (R_e) such that:

$$R_e = \frac{UL\rho}{\mu} \quad (5)$$

where (L) is the reference length and (μ) represents dynamic viscosity (after Reynolds 1883). The critical value of the Reynolds number for the transition from laminar to turbulent flow depends upon the representative length scale, velocity, and geometry of the flow system. Based on numerous experiments with flow through pipes, Reynolds determined that flows with (R_e) <2000 are laminar, and those characterized

by (R_e) >2000 are turbulent. For oceanic currents, it is apparent that the representative length scale will be large resulting in Reynolds numbers greater than a few thousand for current speeds exceeding a few centimeters per second. Thus, such currents, on a macroscopic scale, can be considered as fully turbulent.

17. Prandtl and Tietzens (1934) demonstrated that the turbulent layer immediately above the bed consisted of a flow region where the horizontal component of the fluid velocity approaches zero. This zone has commonly been observed as being laminar (or streamline) and is referred to as the laminar (or viscous) sublayer. Figure 11 illustrates the velocity distribution in the turbulent boundary layer (modified from Rouse 1961).

18. Nikuradse (1933) demonstrated that hydraulically rough or turbulent flow occurs when the scale length of the bottom roughness (e.g., median grain-size diameter) exceeds the laminar sublayer thickness. Under such conditions, irregularities on the bed cause local variations in the bed shear stress and consequently reduce the average bottom shear stress needed to initiate grain movement. For inhomogeneous discharged dredged material on the sea floor, it seems appropriate to classify flow near the bed as hydrodynamically rough resulting in locally wide variations in the bed shear stress. The implication of this is that determination of the critical shear stress needed to cause incipient bedload erosion becomes difficult. Additionally, bottom sediment is likely to be entrained within a given flow above a rough bed at lesser current speeds than for a smooth bed.

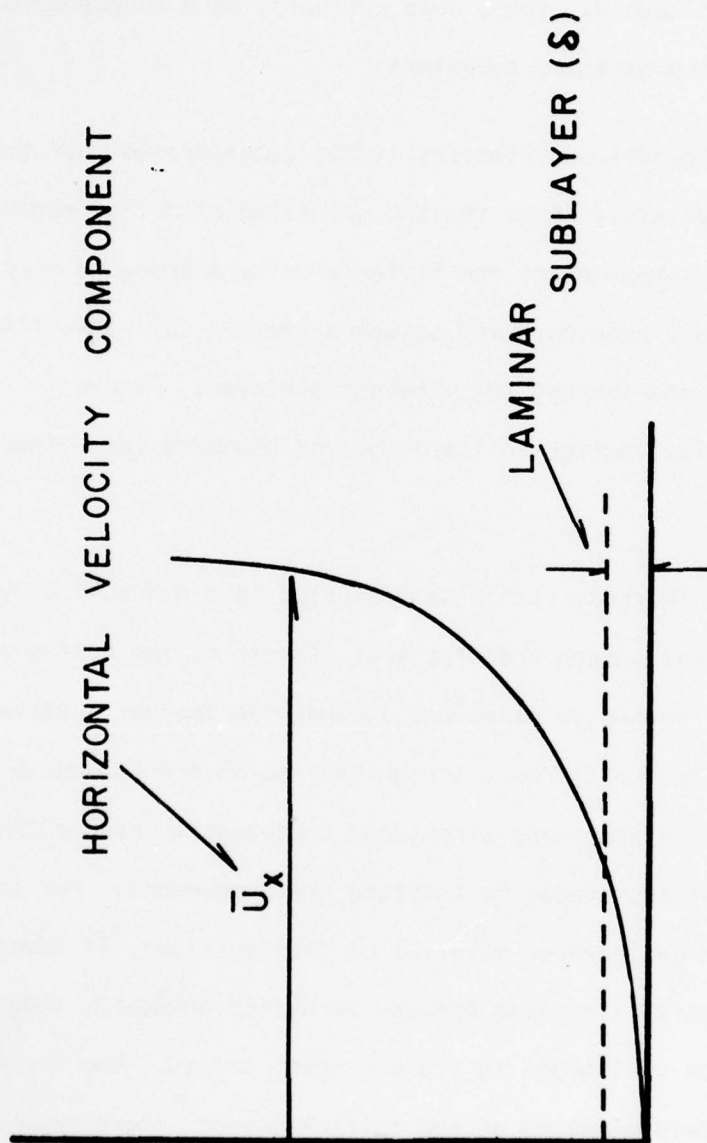


Figure 11. Velocity distribution in the turbulent boundary layer (modified from Rouse 1961)

PART III: TECHNIQUES

Field Techniques

Offshore sediment sampling

19. Offshore sediment sampling operations were carried out onboard the R/V TEXAS STAR.

20. A 0.3048-cu-m box core was used to recover approximately 100 kg of sediment from four localities within the field study area. These sampling stations were designated as Block 15, Block 27, Buoy C, and Buoy D. Sediment samples from Block 15 and Buoy C were obtained during November 1975; Block 27 and Buoy D sites were sampled in May 1976. Blocks 15 and 27 were selected as reference sites since they were believed to be uncontaminated by dredged material disposal operations being carried out at Buoys B, C, and D. Figure 3 depicts the locations of the sampling stations. An inoperative Del Norte navigation system on board the R/V TEXAS STAR prevented accurate location of the reference blocks. Thus, the Block 15 station was located by dead reckoning from Buoy B. Similarly, the position of the Block 27 station was ascertained by dead reckoning from Buoy D. Buoy C and D sampling stations were located approximately 30 m southwest of the respective buoys. Such positioning permitted sampling of previously deposited dredged material. All sediment samples were stored in sealed 55-gal drums until experiments could be performed.

Collection of current data

21. Two types of current meters were employed in the field operations: a hand-held Bendix Q-15 current meter and two Braincon

Savonius continuous-recording meters. Malfunctioning of the current meters did occur occasionally during scheduled periods of observations. Table I contains exact time, location, and type of current meter data recovered.

22. Vertical profiles were taken with the Q-15 meter at Buoy B, C, and D stations. The profiles were obtained by lowering the Q-15 meter from the surface in 1.5-m intervals to a position 1.5 m above the bottom. Then it was lowered in 0.3-m increments to the seabed. In this manner, point measurements of the ambient current speed and direction were recorded for the entire water column with emphasis on the lowermost 1.5 m where profiles of the bottom currents were desired.

23. Bottom current measurements, obtained with Savonius current meters, consisted of current speed and direction recorded at 15-min intervals, 1.0 m above the bottom. Bottom current speed and azimuth were recorded for month-long periods at Buoy B and D stations. Figure 12 schematically illustrates the bottom current meter arrays positioned approximately 50 m southwest of Buoys B and D. A submersible buoy above and approximately 175 kg of anchor weight below held this instrument stationary 1.0 m off the bottom.

Geotechnical Properties of Bedload

24. The geotechnical properties measured on the field samples obtained from the Galveston site include (1) grain-size distribution (dispersed and nondispersed analysis), (2) water content, (3) bulk density, (4) void ratio, (5) specific gravity, (6) remolded shear

Table 1
Type, Location, Date, and Time
of Current Meter Data Recovered

| <u>Type</u> | <u>Location</u> | <u>Date</u> | <u>Time (CST)</u> |
|-------------------------------|-----------------|----------------------------|---|
| Velocity Profiles | Buoy B | 8 April 1976 | 1000, 1120 hr |
| | | 9 April 1976 | 1055 hr |
| | | 1 May 1976 | 1150 hr |
| | Buoy C | 8 April 1976 | 1430 hr |
| | | 1-2 May 1976 | 1400, 1600, 1800, 2000, 2200, 2400, 0200, 0400, 0600, 0800, 1000, 1200, 1400 hr |
| | Buoy D | 8 April 1976 | 1245, 1330 hr |
| | | 3 May 1976 | 1200 hr |
| Bottom Current Readings | Buoy B | 17-24 March 1976 | 1100-1315 hr |
| | | 18 April - 1 May 1976 | 1200-0915 hr |
| | | 1 May - 11 May 1976 | 1345 to 1930 hr |
| | Buoy D | 9 Oct. - 14 Nov. 1975 | 1600 - 1020 hr (from Hall 1976) |
| | | 17 March - 8 April 1976 | 1230 - 1030 hr |
| | | 8 April - 3 May 1976 | 1415 - 0900 hr |
| | | 3 May - 11 May 1976 | 1345 - 0715 hr |

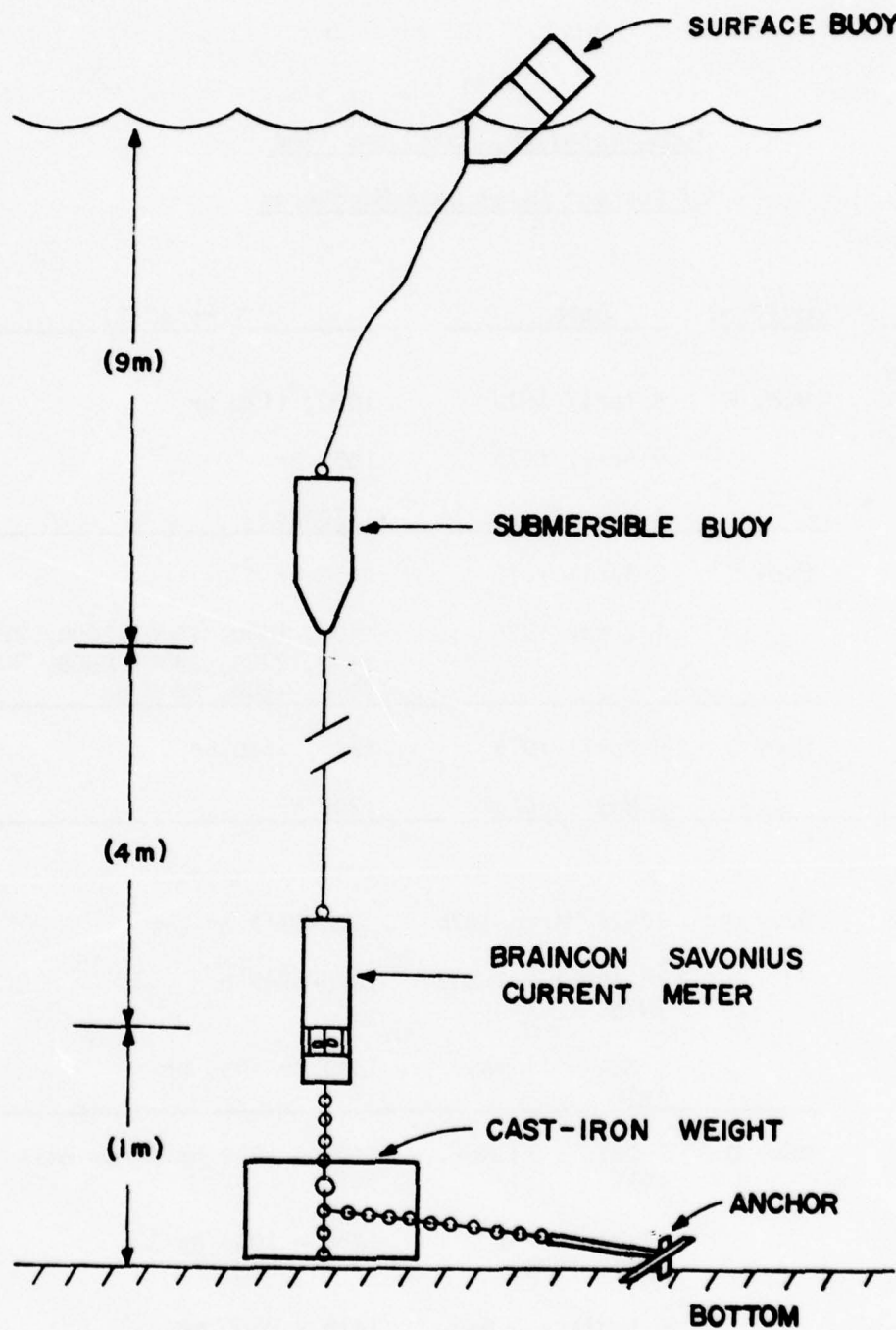


Figure 12. Bottom current meter array positioned adjacent to both Buoy B and Buoy D

strength, (7) organic content, and (8) Atterberg limits (liquid limit, plastic limit, and plasticity index). Each analysis was performed on homogenized sediment samples obtained just prior (within minutes) to their introduction into the flume. Homogenization entailed thorough mixing of the sample with a stirring rod until all clay lumps were dispersed. The following section describes the individual techniques that were employed for each geotechnical property analysis.

Textural analysis

25. The dispersed grain-size analysis performed on the homogenized field samples followed the procedure given by Folk (1974). A solution of Calgon and distilled water was added to approximately 10 g of dredged material. This mixture was then shaken to disassociate the clay particles before being sieved through a U.S. Standard No. 230 sieve (0.0625-mm openings) into a 1-l cylinder. The filtrate was pipetted according to Folk's method. The material retained on the 230 mesh sieve was then dried and sieved through sieve sizes of U.S. Standard No. 10 (2.0 mm), 18 (1.0 mm), 35 (0.50 mm), 60 (0.25 mm), 120 (0.125 mm), and 230. Finally, the sediment was weighed using a precision balance (accuracy 0.0005 g) in order to calculate the proportion of material per given grain-size (ϕ) size range. This proportion was recorded as percent dry weight.

26. The nondispersed grain-size analysis followed the procedure cited above except that distilled water was substituted for Calgon dispersing solution when called for. This physical condition

was desired in order to assess the grain-size distribution of the field samples in a manner that more closely approximated their in situ state.

27. Lastly, cumulative curves were plotted from the cumulative weight percent data for each phi size. Since the No. 10.2-phi size range was the highest phi size measurement (smallest grain size), that part of the cumulative curve was extrapolated to higher phi sizes (>10.2) by continuing the curve upward at approximately the equivalent rate of the slope change determined by the 9- and 10.2-phi-size data points. Each cumulative curve supplied the necessary information to calculate statistical parameters that described the grain-size distribution. The parameters calculated were graphic mean, inclusive graphic standard deviation, and inclusive graphic skewness. These parameters, from Folk (1974), are as follows:

$$\begin{aligned} M_z &= \text{Graphic Mean} \\ &= \frac{\phi_{16} + \phi_{50} + \phi_{84}}{3} \end{aligned} \quad (6)$$

$$\begin{aligned} \phi_I &= \text{Inclusive Graphic Standard Deviation} \\ &= \frac{\phi_{84} - \phi_{16}}{4} + \frac{\phi_{95} - \phi_5}{6.6} \end{aligned} \quad (7)$$

$$\begin{aligned} SK_I &= \text{Inclusive Graphic Skewness} \\ &= \frac{\phi_{16} + \phi_{84} - 2\phi_{50}}{2(\phi_{84} - \phi_{16})} + \frac{\phi_5 + \phi_{95} - 2\phi_{50}}{2(\phi_{95} - \phi_5)} \end{aligned} \quad (8)$$

Shear strength

28. The vane shear test consisted of immersing a vane shear

into a 50-g homogenous sample and measuring the torque required to shear the sediment around the vane's cylinder of rotation. The low shear strength of the field samples necessitated use of a visco-elastic vane shear for sample measurements. This instrument, developed by Stevenson (1973) for determination of the visco-elastic modulus of submarine sediments, consists of a four-bladed vane-shear coupled to a variable-speed motor via a step-function reducer.

29. Torque was measured by a strain-gaged torque transducer and was recorded on an oscillograph as a plot of torque versus rotation angle. Torque sensitivity of this instrument was measured to be 1.38×10^{-5} kg-m (0.001 in.-lb). Point of maximum torque, termed failure, was read from the torque versus rotation angle plot where torque values became constant with increasing rotation angle. Figure 13 represents an example of this plot. Conversion of the maximum torque to standard units of shear strength, kilopascals (kPa), was accomplished by simple multiplication of torque units (inch-ounces) by the factor 1.3434×10^{-2} .

Void ratio, water content,
bulk density, and specific gravity

30. Void ratio, water content, bulk density, and specific gravity were determined from a single sample. Determination of these geotechnical properties generally followed the methodology presented by Cernock (1967). Correction for salt content in the interstitial water of the sediment was excluded because (1) measurements of the

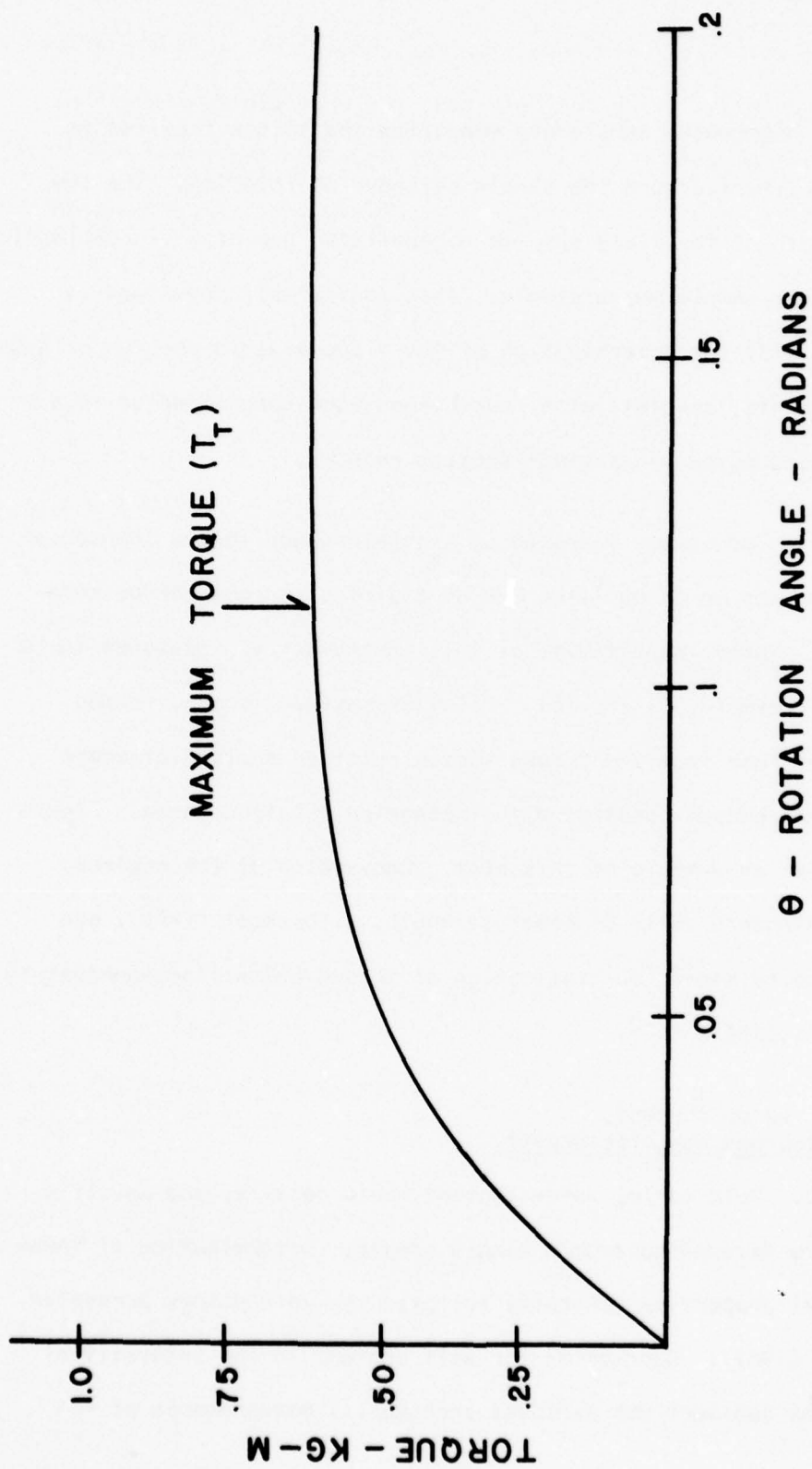


Figure 13. Example of torque versus rotation angle plot

interstitial water salinity were lacking, and (2) the weight contribution of the salts to the sediment mass was negligible, since the field area bottom water salinity was less than 28 ‰ (from Cool 1976). Prior to introduction into the flume, the test material was sampled twice in order that two values of each physical property could be ascertained. These two values were then averaged.

31. The laboratory procedure for this analysis required use of the following apparatus: (1) a Beckman Air Comparison Pycnometer utilizing helium gas for volumetric determinations of sediment samples (accuracy $\pm 0.02 \text{ cm}^3$), (2) a Sartorius Electra balance for weight measurements (accuracy $\pm 0.0001 \text{ g}$), and (3) a Thelco oven for sample dessication at 105°C .

32. The analytical procedure consisted of first placing approximately 40 g of homogenized sediment into a tared beaker for immediate wet volume and wet weight measurement. Next, the sample was oven-dried at 105°C for 24 hr and then allowed to equilibrate for 1 to 2 hr in a dessicator. The dry weight of the sample was obtained prior to mechanical crushing via mortar and pestle for volumetric determination of the solid mass. An additional 24-hr oven-drying period after crushing removed the interstitial moisture.

33. Final recording of the crushed dry volume and dry weight permitted computation of the four previously cited physical properties. The equations utilized for these calculations are as follows (modified after Cernock 1967):

a. Void ratio (e) is defined as the ratio of void volume

(V_v) to the volume of the solid particles (V_s) within a given sediment mass, such that

$$e = \frac{V_v}{V_s} \quad (9)$$

where (V_v) is defined as the total volume of the sediment (V_T) minus the volume of the particles (V_s).

b. Water content (W) is defined as the ratio in percent of the weight of seawater (W_{sw}) to the weight of the oven-dried sediment (W_s) such that

$$W = \frac{W_{sw}}{W_s} 100 \quad (10)$$

c. Bulk density (Y_d) is defined as the ratio of the total weight of the sediment mass (W_T) to the total volume of the sediment mass (V_T) such that

$$Y_d = \frac{W_T}{V_T} \quad (11)$$

d. Specific gravity (G) is defined as the ratio of weight in air of a given solid volume (W_s) to the weight in air of an equivalent volume of distilled water at 4°C ($V_s Y_w$) such that

$$G = \frac{W_s}{V_s Y_w} \quad (12)$$

where (Y_w) is defined as the specific gravity of distilled water at 4°C (1.000).

Atterberg limits

34. The procedure for the determination of the Atterberg limits (i.e., liquid limit, plastic limit, and plasticity Index) followed

that given by Lambe (1951). Due to the high sand content (≈ 10 percent) in each material type, all samples required wet-sieving using distilled water through a U.S. Standard No. 40 (0.42-mm) sieve in order to produce a test sample that was within the upper limit of grain sizes (1.25ϕ) used for Atterberg limit analysis.

35. Liquid limit. Liquid limit (W_L) is defined as the moisture content, percent dry weight, of the oven-dried sediment at which the material will flow to close a 2-mm-wide groove when jarred. Each material's liquid limit was determined by first subdividing the sieved fraction into four equal aliquots. Next, one aliquot at a time was homogenized into a uniform paste and placed into the cup of a liquid limit device. A special grooving tool of standard dimensions was drawn through the sample resulting in a groove 2-mm wide. The cup was calibrated 1.0 cm above a flat surface upon which it was mechanically jarred when operative. The number of blows required to close the groove approximately 1.25 cm along its length was recorded. A 10-g sample was immediately extracted from the closed groove. This sample was placed into a tared container and weighed with a Sartorius Electra balance for wet weight determination. This process was repeated for each aliquot. Finally all four tested aliquots, per given sediment type, were oven-dried for 24 hours and then weighed. Knowing the dry and wet weight of each aliquot permitted calculation of its moisture content. Then, a plot of the moisture content versus the log of the number of blows required to close each groove was drawn. Visual interpolation of a regression line through the four plotted points of measurement allowed

computation of the liquid limit. This value corresponded to the moisture content at log 25 blows (after Lambe 1951).

36. Plastic limit. The plastic limit (W_p) is defined as the lowest moisture content of the oven-dried sediment at which the material can be rolled into threads 0.318 cm in diameter without breaking into pieces. After homogenizing approximately 15 g of the material, the sample was hand-rolled on a smooth glass plate continuously until a thread 0.318 cm in diameter formed and crumbling appeared. This thread was placed in a tared container for water content determination according to the method described in the previous section. This moisture content was then recorded as the plastic limit.

37. Plasticity index. The plasticity index (I_p) is defined as the difference between the liquid and plastic limit. Hence, determination of the latter properties permitted simple computation of (I_p).

38. Organic content. Six dried samples analyzed for combustible organic content were placed in a Themco infrared oven and heated for 2 hr at 600°C. Measurement of the weight difference before and after combustion permitted computation of the combustible organic content as percent dry weight. This process was considered an approximation since inorganic particulate matter was partially oxidized in the process.*

*Personal communication, David B. Mathis, U. S. Army Engineer Waterways, Experiment Station, 3 May, 1976.

Geotechnical Properties of Washload

39. One-half-liter water samples were collected at specific time intervals (see Appendix A) from the flume during experimental runs in order to ascertain total suspended matter concentration, suspended sediment grain-size distribution, and washload composition. Emphasis was placed upon measuring the total suspended matter concentration of each sample obtained since changes in the washload concentration were expected to be a function of bedload erodibility or stream competency. The following sections describe the laboratory techniques employed to quantitatively assess the physical characteristics of the washload.

Total suspended matter concentration

40. The total suspended matter concentration (TSM) of the washload samples was determined by the gravimetric procedure outlined by Cool (1976). Individual 47-mm-diam Nucleopore GE-40 filters (pore size = $0.40\ \mu\text{m}$) were each preweighed twice using an Ainsworth Type 24 N balance (accuracy 0.0001 g). Expected static electricity was minimized during the weighing process by passing each filter over uranyl acetate crystals and then weighing each one beneath an α -emitting ionizing source (Polonium 210). Three control filters were each weighed five times during the weighing of each set of experimental filters. Thus, a correction factor was attained to compensate for changes due to humidity, temperature, etc., between the time the filters were preweighed, used, and dried. Control filter weight variations were found to be approximately 8 to 10 μg , which was considered negligible compared to the concentration levels measured during the experimental

runs.

41. Apparatus utilized for the suspended matter filtration was composed of five millipore in-line disc filter holders, 0.5-ℓ plastic sample containers, Tygon tubing, one Gast 760-mm mercury vacuum pump, and five 1.0-ℓ-volume vacuum flasks. Figure 14 illustrates schematically the filter system used.

42. Double-distilled deionized water was used to rinse and thus dissolve retained sea salts on the Nucleopore filters. The filtrate was tested with 0.1 N silver nitrate for evidence of salt contamination. Three to four thorough washings, approximately 25 ml each, removed all visual traces of salt precipitation if the filters were allowed to drain dry before the next wash. All filters were stored in a dessicator for at least 5 days prior to weighing to ensure thorough drying. The total suspended sediment concentration in mg per ℓ was calculated by dividing the weight difference of the dried filters by the volume of water filtered.

Grain-size distribution

43. A Model TA Coulter Counter was employed for determining the suspended sediment grain-size distribution of selected water samples taken during experimental runs with the flume. The laboratory procedure given by Shideler (1975) with certain modifications was followed. Sheldon and Parsons (1966), Shideler (1975), and others have established through repetitive experimentation that the size distribution of a particular sample can be determined using a Coulter Counter with a

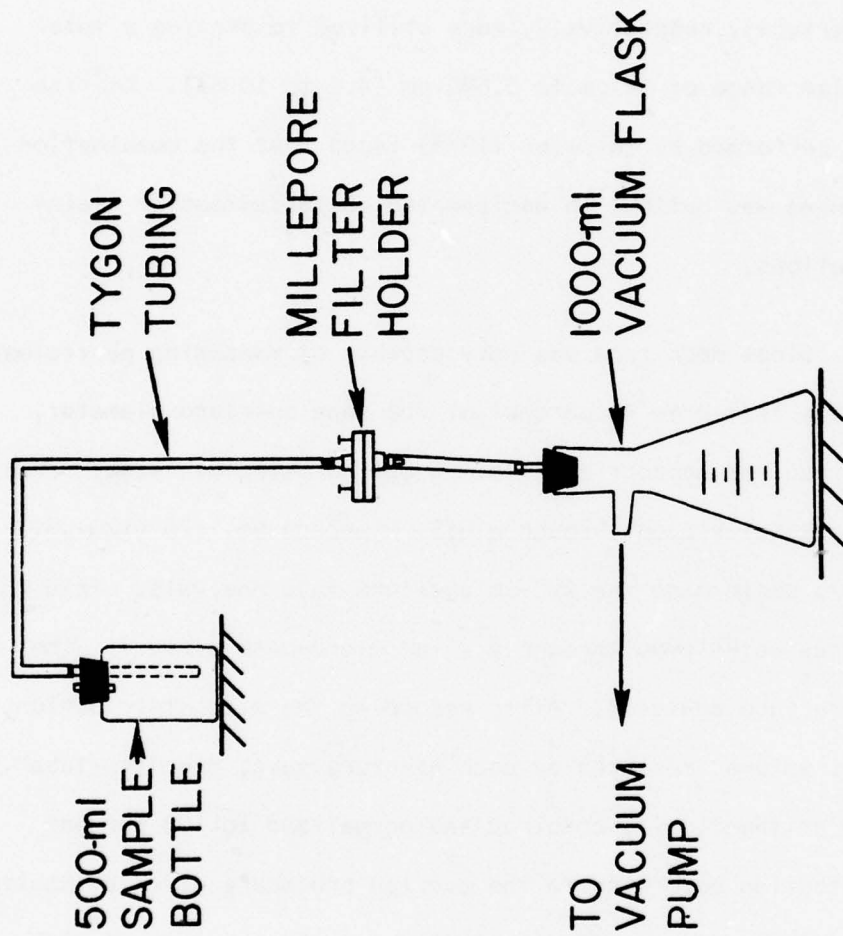


Figure 14. Schematic diagram of suspended matter filtration system

precision equivalent to or better than the standard time-consuming pipette analysis.

44. During each analysis, two aperture tubes with 200- μm and 30- μm apertures, respectively, were utilized to provide a total analytical size range of 64 μm to 0.630 μm (4.0 to 10.6 ϕ). Routine mud analysis performed by Shideler (1975) found that the combination of the two tubes was optimal in deciphering suspended matter grain-size distributions.

45. Since each tube was only capable of measuring particles in a size range from 2 to 40 percent of the tube aperture diameter, each sample required appropriate sieving before being analyzed. Thus, each sample was wet-sieved through a U.S. Standard No. 120 (125- μm) sieve prior to performing the 200- μm aperture tube analysis. This sample was then wet-sieved through a 20- μm micro-mesh sieve for the 30- μm aperture tube analysis. After recording the size distribution, percent total volume, measured by each aperture tube, the "two-tube" results were arithmetically combined and normalized to 100 percent volume distribution according to the overlap procedure given by Coulter Electronics (1975). Figure 15 illustrates a typical worksheet with recorded results of one analysis.

46. After data normalization, the resultant cumulative volume percent for each size range was plotted on probability scale graph paper to produce a cumulative curve. By assuming a constant density for the particles measured within the analytical size range (4.0 to 10.6 ϕ), the

200 μ)
30 μ)

11.29
10.95
10.62
10.29
9.96
9.62
9.29
8.96
8.62
8.29
7.96
7.62
7.29
6.96
6.62
6.29
5.96
5.62
5.29
4.96
4.63
4.29
3.96
3.63

200 μ)
30 μ)

| SAMPLE #16 | | DISPERANT | |
|--|--------------------|---|------------|
| ELECTROLYTE Sea Water | | | |
| EQUIPMENT Model TA II | SERIAL 1310-2361 | Apert. Dia. | Se. No. |
| ORGANIZATION Texas A&M University, College Station | DATE 9/4/76 | CALIBRATION DATA | Part. Dia. |
| OPERATOR JC | DATE 9/4/76 | W | $\pm 1A$ |
| Total Count- 539.6 | Total Time- 479526 | | |
| Total Count- 212.4 | Total Time- 200601 | | |
| $k = d \sqrt{\frac{2W}{A}}$ FOR MODEL T | | $\frac{A_1}{A_2} = \left(\frac{d_1}{d_2}\right)^2 \frac{W_2}{W_1}$ For Model T $\frac{A_1}{A_2} = \left(\frac{d_1}{d_2}\right)^3 \frac{W_2}{W_1}$ For Model T _A | |
| APERTURE DIA 200 30 | | SAMPLE DATA | |

| Geometric Mean μ | Volume μ^3 | Diameter μ | Channel (W) | | | | | | |
|----------------------|---------------------|----------------|-------------|------|------|-------|------|--|--|
| | | | 200 | 30 | % | % | | | |
| 00575 | .004001 | .198 | | | | | | | |
| 0115 | .008181 | .260 | | | | | | | |
| 0231 | .01636 | .318 | | | | | | | |
| 0462 | .03272 | .397 | | | | | | | |
| 0925 | .06545 | .500 | | | | | | | |
| 1851 | .1309 | .630 | 3 | | 5.3 | 141.7 | 100% | | |
| 3702 | .2618 | .794 | 4 | | 3.6 | 136.4 | 96.3 | | |
| 7406 | .5236 | 1.00 | 5 | | 2.5 | 132.8 | 93.7 | | |
| 1481 | 1.047 | 1.26 | 6 | | 2.4 | 130.3 | 92.0 | | |
| 2962 | 2.094 | 1.58 | 7 | | 2.0 | 127.9 | 90.3 | | |
| 5924 | 4.189 | 2.00 | 8 | | 3.3 | 125.1 | 88.3 | | |
| 1185 | 8.378 | 2.52 | 9 | 0 | 5.6 | 121.8 | 86.0 | | |
| 2370 | 16.76 | 3.17 | 10 | 0 | 10.3 | 116.2 | 82.0 | | |
| 4739 | 33.51 | 4.00 | 11 | 9.8 | 23.1 | 105.3 | 74.3 | | |
| 9478 | 67.02 | 5.04 | 12 | 17.1 | 27.0 | 82.3 | 58.1 | | |
| 1896 | 134.0 | 6.36 | 13 | 26.3 | 26.3 | 53.8 | 38.0 | | |
| 3791 | 268.1 | 8.00 | 14 | 26.1 | 7.7 | 27.5 | 19.4 | | |
| 7583 | 536.2 | 10.08 | 15 | 12.6 | 19.8 | | 14.0 | | |
| 1516 | 1072 | 12.7 | 16 | 2.6 | 7.3 | | 5.1 | | |
| 3033 | 2145 | 16.0 | 17 | 0.6 | 4.6 | | 3.2 | | |
| 6066 | 4289 | 20.2 | 18 | 0.4 | 4.0 | | 2.8 | | |
| 1213 $\times 10^3$ | 8579 | 25.4 | 19 | 0.8 | 3.6 | | 2.5 | | |
| 2427 $\times 10^3$ | 1716 $\times 10^3$ | 32.0 | 20 | 0.6 | 3.2 | | 2.6 | | |
| 4854 $\times 10^3$ | 3431 $\times 10^3$ | 40.3 | 21 | 1.2 | 2.6 | | 1.8 | | |
| 9718 $\times 10^3$ | 6863 $\times 10^3$ | 50.8 | 22 | 1.4 | 1.4 | | 0.1 | | |
| 1944 $\times 10^3$ | 1373 $\times 10^3$ | 64.0 | 23 | 0.7 | | | | | |
| 3887 $\times 10^3$ | 2745 $\times 10^3$ | 80.6 | 24 | 0.5 | | | | | |
| 7774 $\times 10^3$ | 5490 $\times 10^3$ | 101.6 | | | | | | | |
| 1555 $\times 10^6$ | 1.098 $\times 10^6$ | 128 | | | | | | | |
| 3109 $\times 10^6$ | 2.196 $\times 10^6$ | 161 | | | | | | | |
| 6219 $\times 10^6$ | 4.392 $\times 10^6$ | 203 | | | | | | | |
| 1244 $\times 10^6$ | 8.784 $\times 10^6$ | 256 | | | | | | | |
| 2488 $\times 10^6$ | 1757 $\times 10^6$ | 322 | | | | | | | |
| 4975 $\times 10^6$ | 3514 $\times 10^6$ | 406 | | | | | | | |
| 9950 $\times 10^6$ | 7027 $\times 10^6$ | 512 | | | | | | | |
| 1990 $\times 10^6$ | 1405 $\times 10^6$ | 645 | | | | | | | |
| 3980 $\times 10^6$ | 2811 $\times 10^6$ | 812 | | | | | | | |
| 7960 $\times 10^6$ | 5622 $\times 10^6$ | 1024 | | | | | | | |

Figure 15. Example of washload grain-size analysis worksheet

volume percent data could then be interpreted in terms of weight percent per given size range. Folk's (1974) statistical parameters for grain-size distribution were used in the final interpretation of these data (see p. 42 for specific equations used).

Washload composition

47. Suspended matter composition of the eroded bedload material was determined by binocular microscope (7X) examination of washload material retained on 0.40- μ m Nucleopore filters. One dried filter from each experimental run was observed for particle identification other than silt and clay. Also, a X-ray diffraction analysis was performed on two suspended sediment samples obtained at a 30.5-cm water depth during experimental runs using Buoy C type sediment.

48. Sample preparation of the suspended matter for X-ray diffraction analysis followed that of Jackson (1954), and X-ray diffractogram interpretation corresponded to that given by Scafe (1968). Removal of carbonates from the samples was accomplished by treatment with 5 N NaOAc (sodium acetate). Addition of 30 percent H_2O_2 (hydrogen peroxide) and heat removed organic matter and MnO_2 (manganese oxide).

49. Each sample was then centrifuged and split into two equivalent aliquots. One was saturated with magnesium (Mg^{2+}) and the other with potassium (K^+) prior to sedimentation onto Vycor (heat-resistant) glass slides. After treatment of half of the Mg-saturated samples with ethylene glycol, X-ray diffraction analysis was performed on glycolated and Mg-saturated samples at room temperature. The

K-saturated samples were analyzed at room temperature, after heating to 300°C, and also after heating to 500°C. The X-ray diffraction apparatus consisted of a Phillips X-ray diffractometer set at Cu K - alpha radiation 30 kV, 20 mA, and a scanning rate of 1°/min spanning 4° to 30° 2θ.

Flume Experiments

Flume description

50. A rectangular circulating flume (Figure 16) was designed and constructed to model the effects of unidirectional turbulent flow upon sand, silt, and clay bedload material sampled from the Galveston site. The flume's outermost dimensions measured 744.2 by 243.8 cm. The actual water-bearing channel measured 61.6-cm wide and 71.0-cm high. This width minimized current boundary effects caused by the walls, and this height permitted a water depth within which parametric vertical profiles could be obtained during experimental runs. A baffle system was incorporated within two radii (inner radius 30.5 cm, outer radius 91.5 cm) in order to minimize helical streamline patterns developed by unrestricted passage through channel turns. This system consisted of the placement of progressively larger radii sheet metal strips within the channel corners (Figure 16).

51. The flume was constructed of 16-gage sheet metal bent to the channel dimensions previously cited and then welded to rigid angle iron supports. The cross-sectional view shown in Figure 17 illustrates the trough shape and its containment by arc-welded angle iron supports. All metal was spray-painted with a red oxide chlorinated-

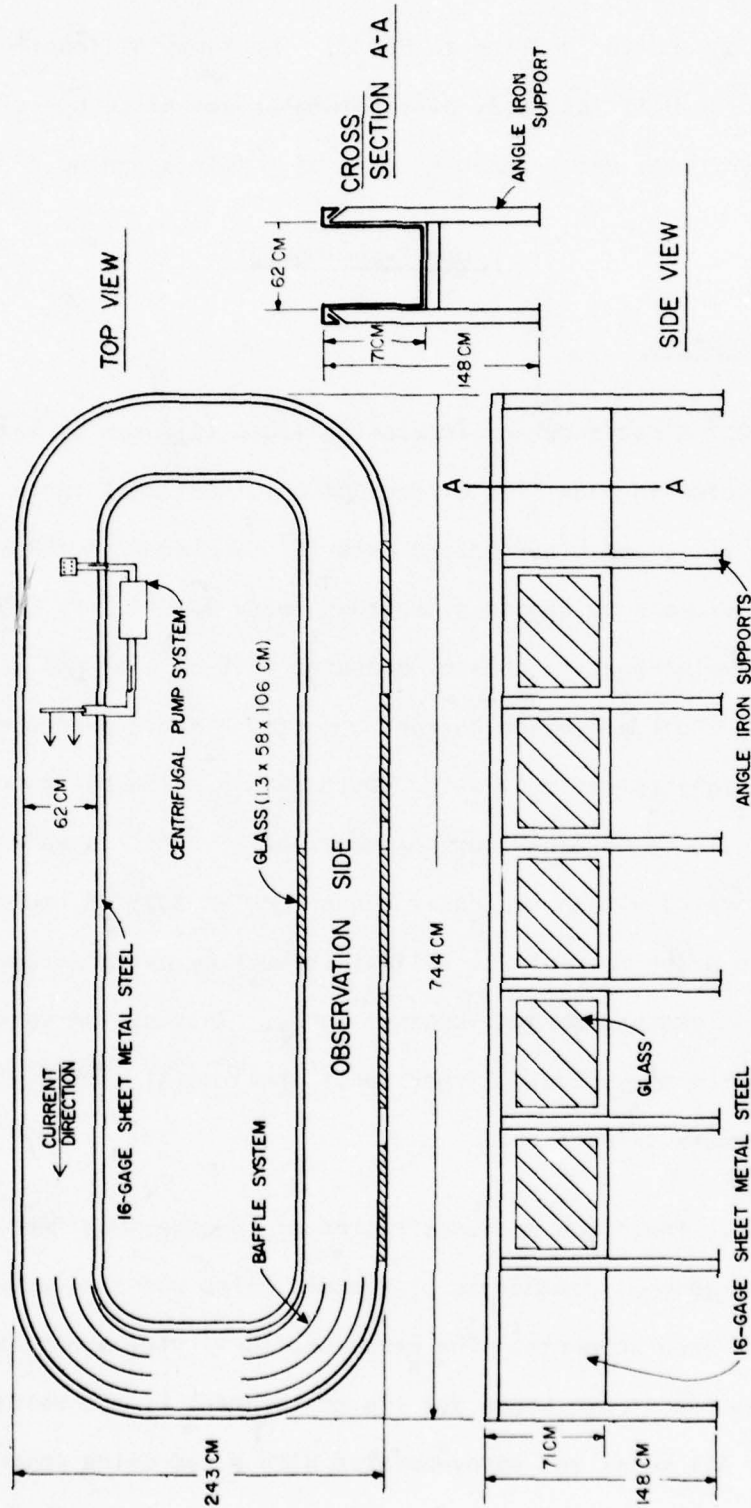


Figure 16. Schematic illustration of rectangular circulating flume

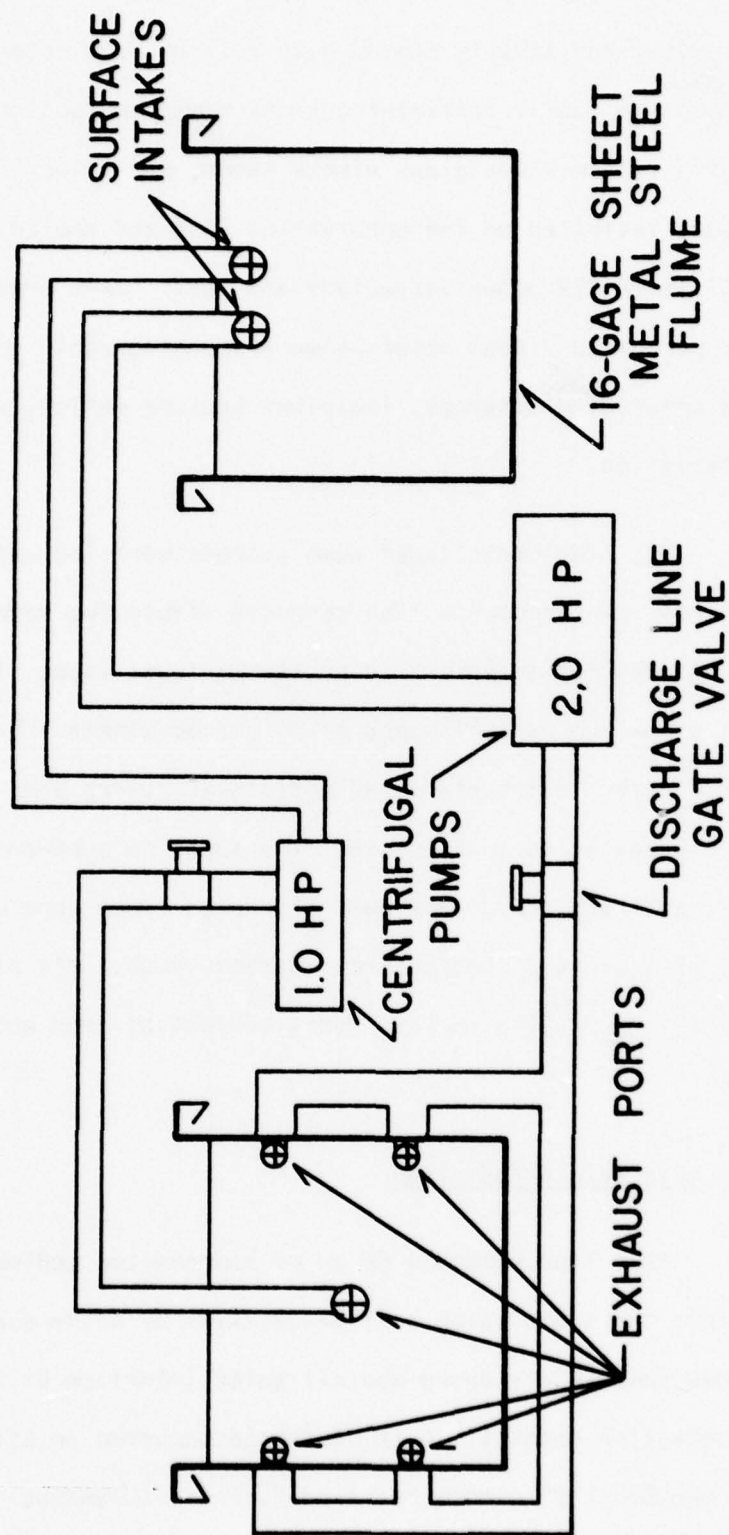


Figure 17. Cross-sectional view of flume current propulsion system

rubber primer and finally coated with a light blue chlorinated-rubber base enamel to resist saltwater corrosion and bedload material abrasion. Six 1.3-cm-thick glass window panes, measuring 58.4 by 106.7 cm each, were installed on the observation side and sealed into place using Silastic 732 adhesive/sealant and metal frame brackets. These windows permitted visual observation and photographic documentation of dredged material discharges, incipient bedload motion, and bedform characteristics.

52. Two centrifugal pump systems were installed to initiate and control low-turbulence flow currents within the water column. Figure 17 illustrates these systems in cross-sectional view. The 1.0-hp pump induced a maximum current speed of 31 cm/sec within the observation channel. Later in the study, an additional 2.0-hp pump and filter system was installed to boost the flow speed to a 60-cm/sec maximum. Gate valves installed on the pump discharge lines were used to regulate outflow pressure and thus control current speed. All piping was constructed of PVC tubing to keep metal corrosives from entering the system.

Bedload material introduction

53. Approximately 68 kg of homogenized sediment was introduced into the flume using a 27.9- by 27.9- by 45.7-cm release box suspended immediately above the air-water interface at the center of the observation channel. Each discharge occurred in still water except one Block 27 sample released during a 30-cm/sec current speed.

Photographs and stopwatch timing of several discharges documented turbidity plume travel speed along the bottom of the observation channel. The plume's suspended sediment concentration was monitored during one Buoy D sample release. Suspended sediment dispersed from each discharge was permitted to settle out for 24 to 36 hr prior to the initiation of unidirectional currents in the flume.

Suspended sediment sampling

54. Equipment used for collecting water samples during experimental runs consisted of 0.5-ℓ sampling bottles as shown in Figure 18. These bottles enabled point sampling of the ambient current with little disturbance to the flow. Sampling of turbidity plumes generated by sediment ejected into still water was accomplished by installation of plastic siphon tubing on a depth-calibrated ruler. Either method permitted withdrawal of 0.5-ℓ water samples in 60 sec or less. Each sample collected was stored in 0.5-ℓ Nalge plastic bottles for TSM and grain-size distribution analysis.

55. Sampling bottles were positioned at water depths of 15.2, 30.5 and 45.7 cm in the channel center at the downstream sections of the observation side. The 30.5-cm sampling depth was selected as the primary sampling point since mean flow conditions existed at this depth. Thus, plots of TSM concentration versus time were based upon samples collected here.

56. A total of 32 experimental runs were performed on the four sediment mixtures. Four of the runs had a duration of longer than 24 hr.

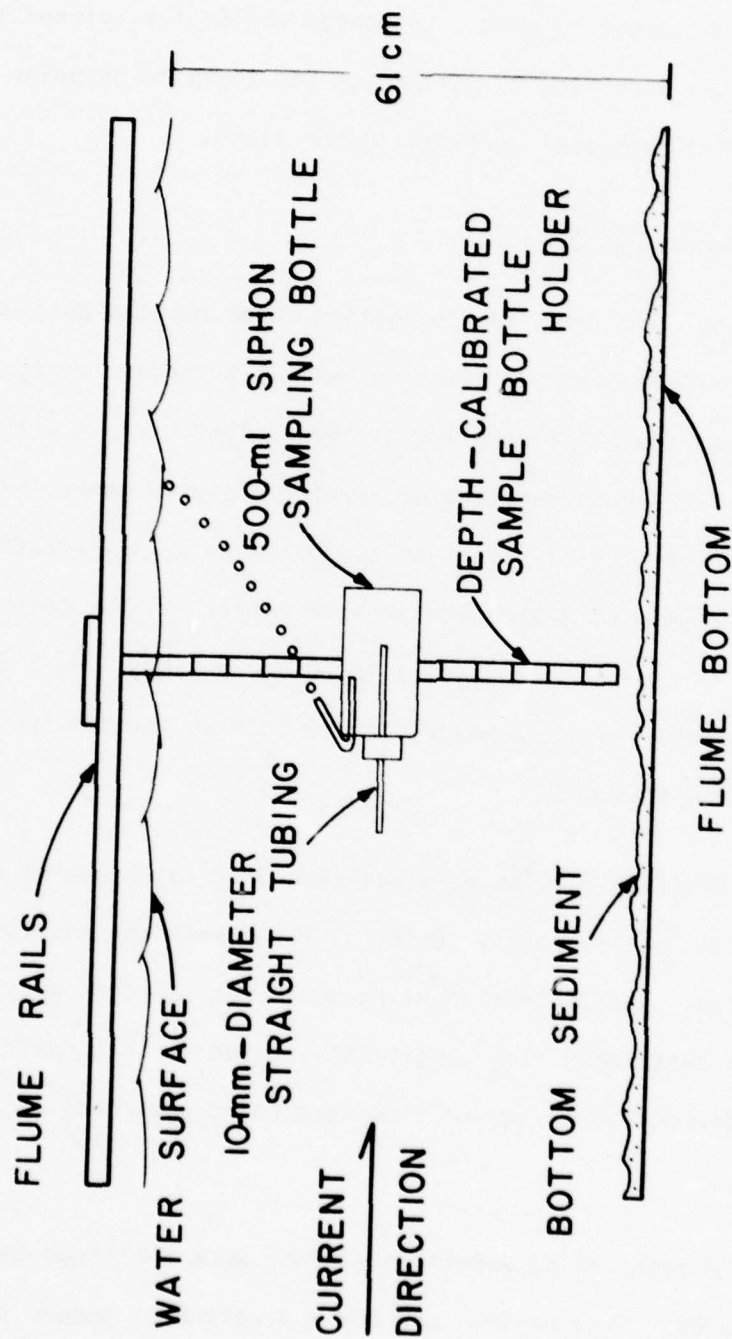


Figure 18. Schematic illustration of washload sampling system

Suspended sediment samples were taken intermittently during each run. The time in minutes since the previous current velocity increase or decrease was recorded for every water sample obtained in order to accurately assess the changes in suspended sediment concentration over time. Appendix A lists the TSM concentration, time after velocity change, and location of each water sample retrieved during experimental runs.

Current speed measurements

57. A Price-Pygmy water current meter was used for point measurements of the unidirectional current velocities for Buoy C and Block 15 experimental runs. Later in the study, a Model 631 Velmeter electromagnetic current meter replaced the Price-Pygmy meter for flow speed measurements during Block 27 and Buoy D experimental runs. The instrument's 0.1-sec response time and 1.0-mm/sec sensitivity permitted ample vertical measurements to be taken within the water column. The sensor consisted of a streamlined probe measuring 27.94 cm long with sensing electrodes located 7.62 cm from the bottom.

58. Vertical point measurements of the flow speed were obtained during each experimental run in order to calculate the approximate bed shear (shear stress acting upon the sediment-water interface) and mean current speed. Profiles taken with the Price-Pygmy current meter consisted of point measurements obtained at 6.1, 15.2, 30.5, 45.7, and 57.9 cm above the bed. Velocity profiles obtained with the electromagnetic current meter consisted of point readings measured at the

following elevations above the bed: 9.1, 12.2, 15.2, 18.3, 21.3, 24.8, 30.5, 42.7, and 54.9 cm. Profile locations in the observation channel were recorded at positions charted in Figure 19.

Bed shear stress

59. Determination of the shear stress acting upon the sediment-water interface was calculated using the Bedload Function for sediment transport in open channel flows (after Einstein 1950):

$$\frac{U}{u_*} = 5.75 \log_{10} \left(30.2 \frac{Y}{\Delta} \right) \quad (13)$$

where (Δ) is defined as the apparent bed roughness given by (k_s/x) where (k_s) is the roughness of the bed and (x) is a corrective parameter. The friction velocity (u_*) was determined by regression analysis such that:

$$u_* = m/5.75 \quad (14)$$

where (m) is defined as the slope of plot of $\log(Y)$ versus (U).

The bed shear was computed from the following equation:

$$\tau_o = \rho u_*^2 \quad (15)$$

where (τ_o) is measured in dynes per cm^2 and (u_*) is measured in cm per centimeter per second. Computed values of the bed shear stress for each vertical profile are listed in Appendix B.

Salinity control

60. Artificial seawater was made by adding 21 g sodium

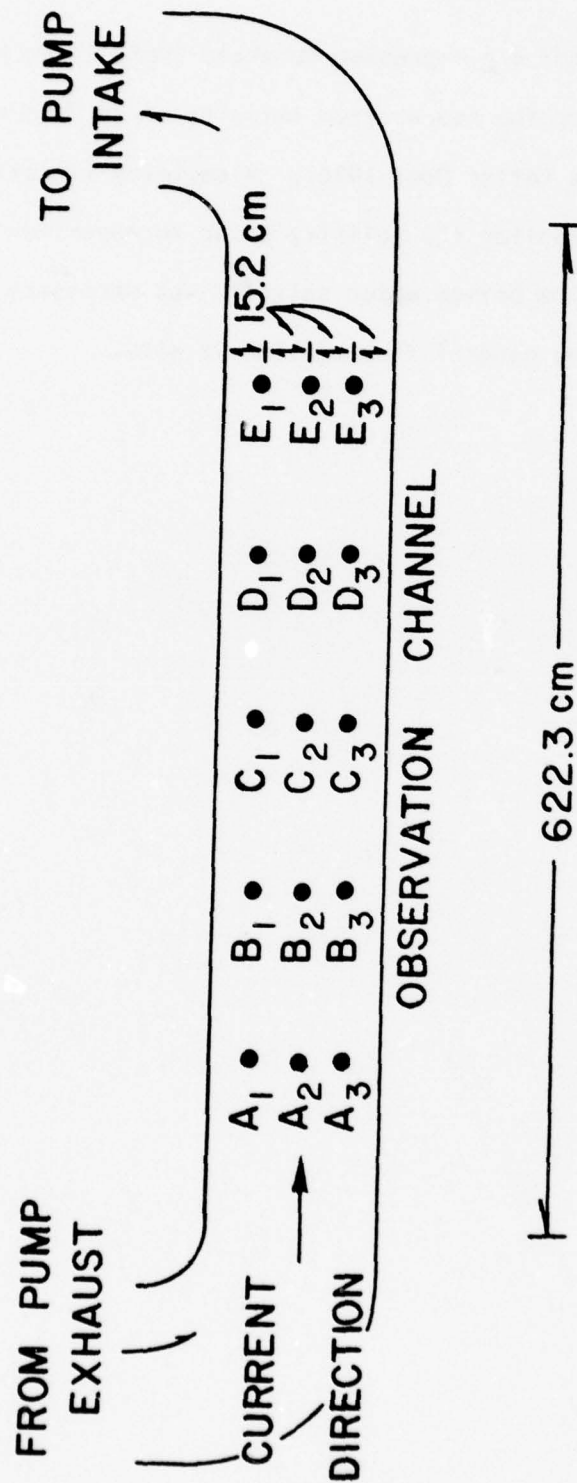


Figure 19. Location chart for current velocity profiles and water samples (observation side of flume)

chloride (NaCL) and 4 g magnesium sulphate (MgSO_4) per liter of tap water to reproduce the near-bottom salinity of 28 ‰ that exists in the study area (after Cool 1976). A salinity titration technique was employed to monitor the salinity prior to experimental runs. Reproduction of the bottom water salinity was necessary to duplicate the degree of clay mineral flocculation in situ.

PART IV: RESULTS

Geotechnical Properties of Bedload

Grain-size distribution

61. Dispersed grain-size analyses performed on sediment mixtures sampled from Buoy C, Buoy D, Block 27, and Block 15 stations (see Figure 3) indicate that all four types had a median grain size in the silt range, were very to extremely poorly sorted, and were near symmetrical to finely skewed. The statistical measures used to describe the grain-size distributions are given by Folk (1974). Cumulative curves showing the percentage distribution of particle sizes plotted on a probability axis and each phi size class plotted on an arithmetic axis served as the basis for these determinations. These curves are shown in Figures 20 through 23.

62. The two control areas, Block 15 and Block 27, exhibited textural distributions correlative with their proximity to the Galveston barrier island system. The 50.5 percent sand content of Block 15 material is attributable to the proximity of sampling areas (4.8 km) to the Galveston Bay entrance channel, where Coulthard (1976) documented the occurrence of a major sand source. This sand presumably is the result of high-energy tidal currents within and adjacent to the entrance channel. Hall (1976) suggested that this control block represents an upper shoreface sediment of a typical barrier island sequence. Block 27 material, obtained approximately 11 km southwest of the entrance channel, presumably represented a lower shoreface zone sediment where

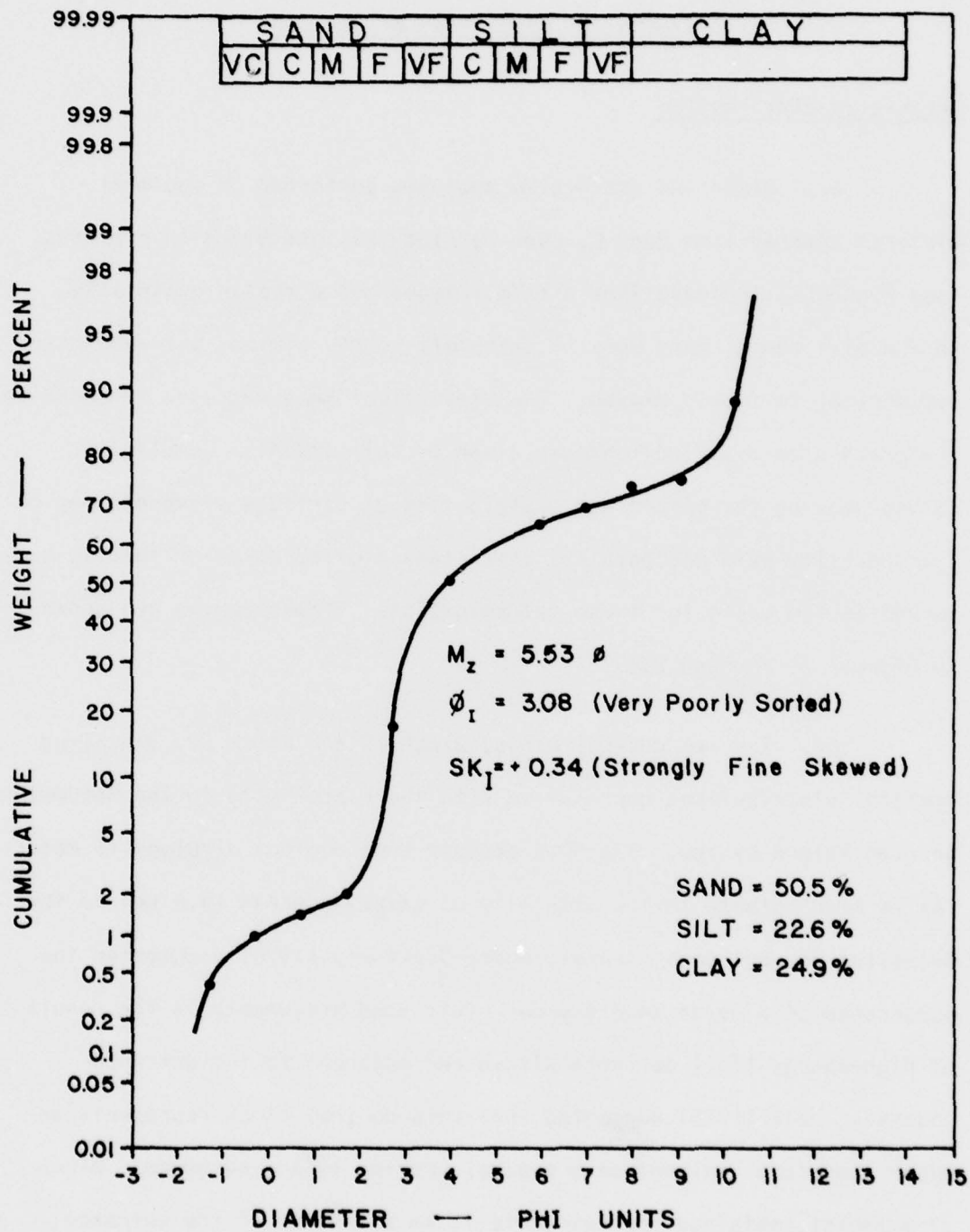


Figure 20. Block 15 sediment dispersed grain-size distribution

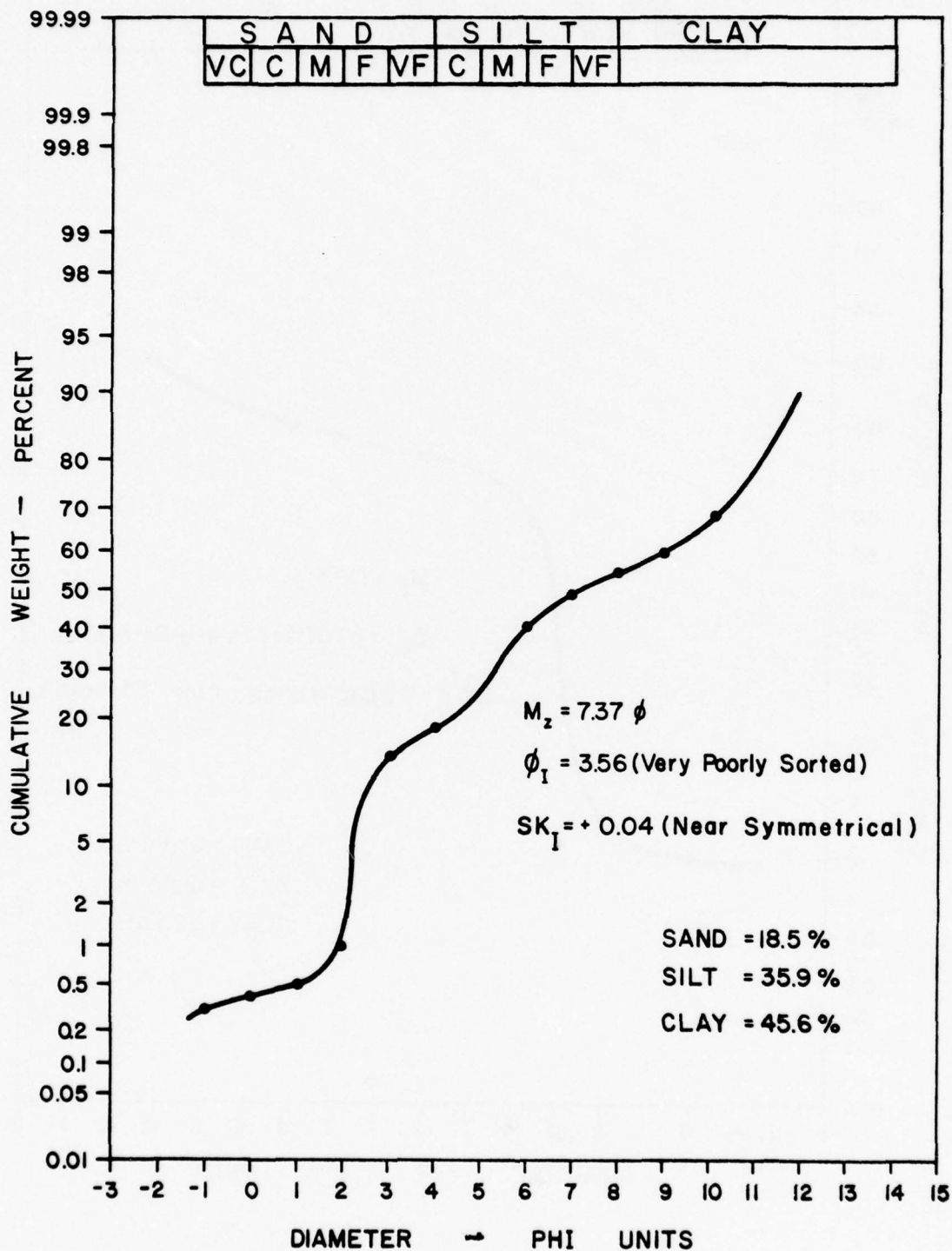


Figure 21. Block 27 sediment dispersed grain-size distribution

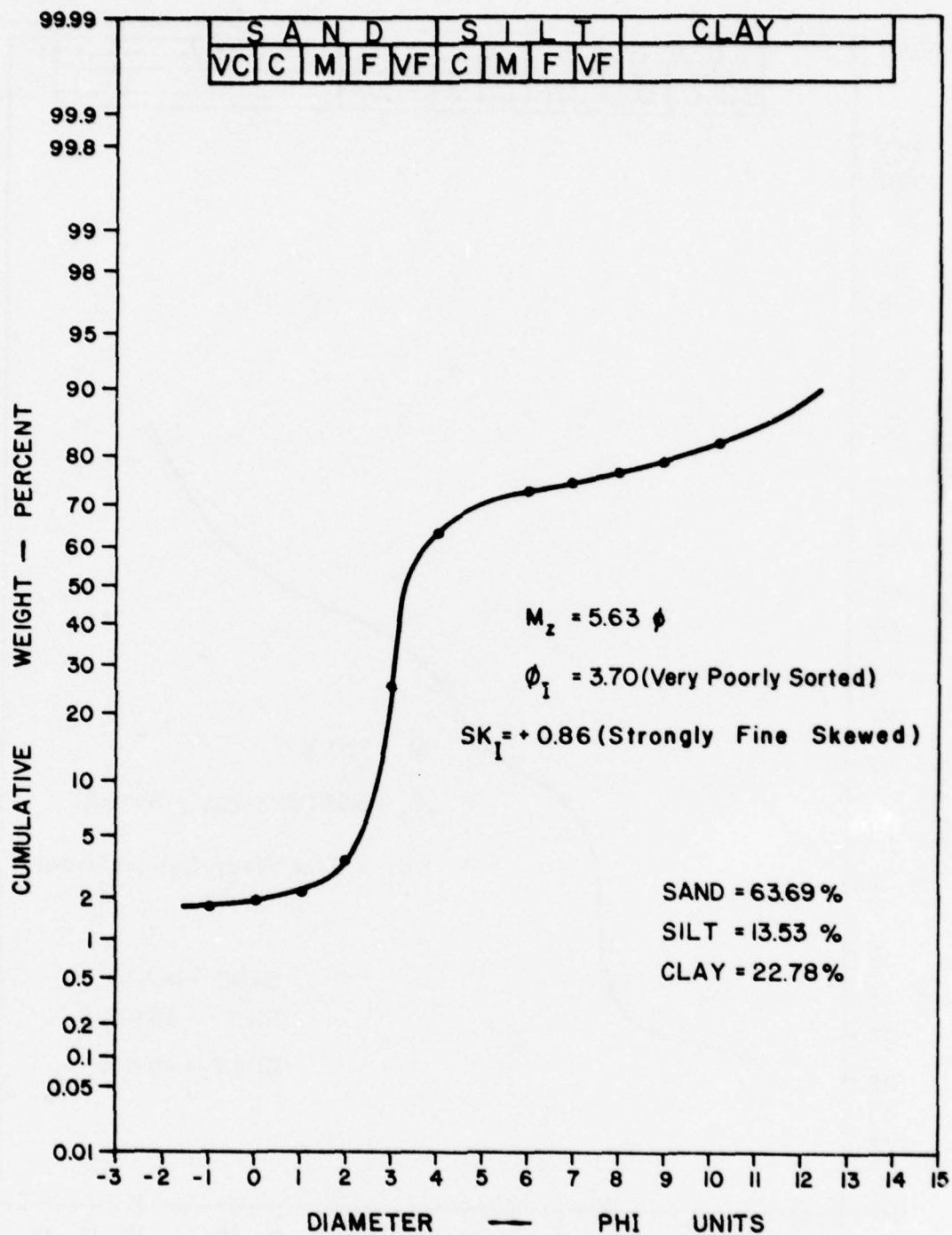


Figure 22. Buoy C sediment dispersed grain-size distribution

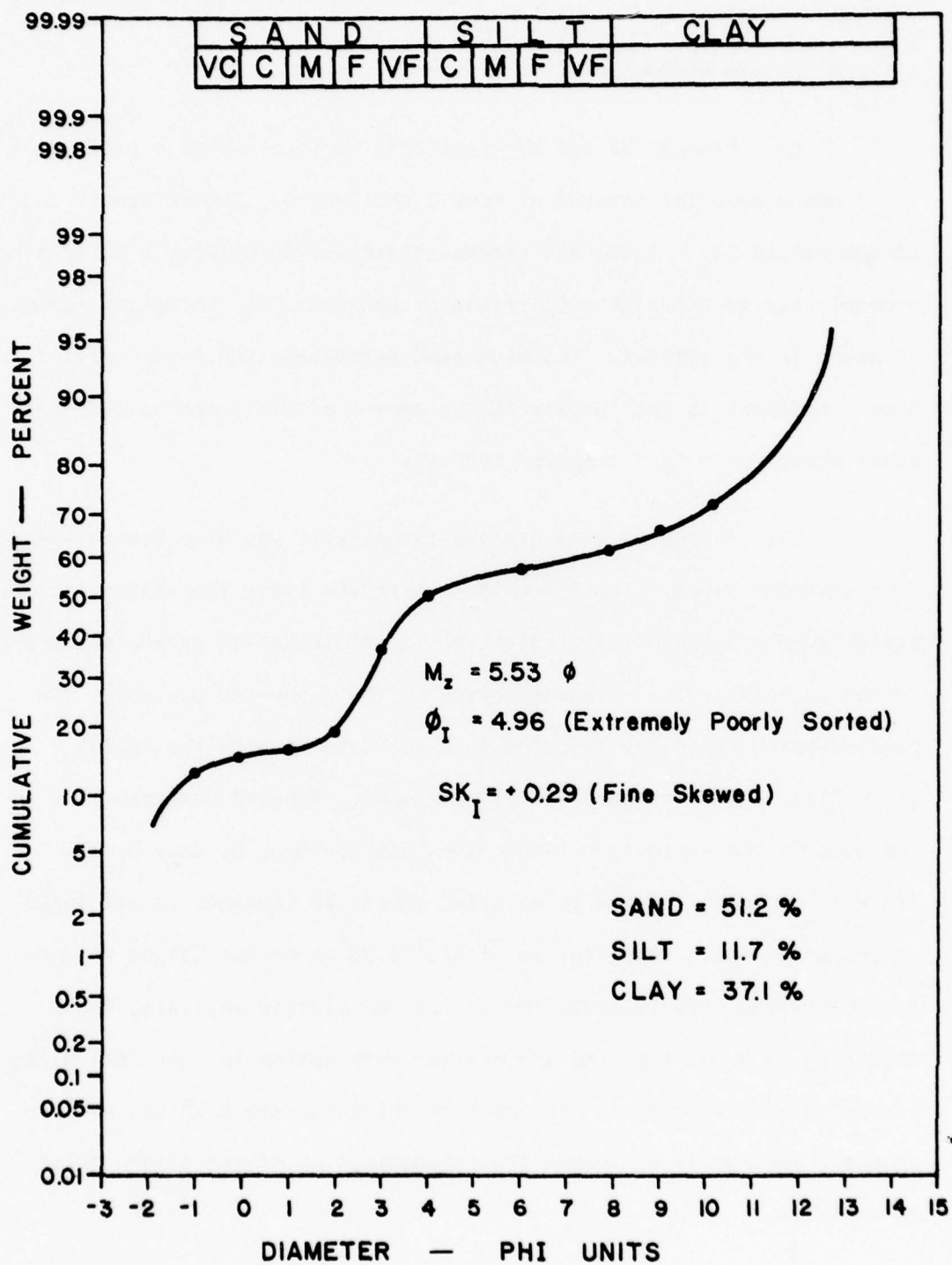


Figure 23. Buoy D sediment dispersed grain-size distribution

silts and clays predominate.

63. Figures 22 and 23 illustrate the grain-size distribution for dredged material sampled at Buoy C and Buoy D. The extremely poorly sorted nature ($\phi_1 = 4.96$) and bimodal distribution of Buoy D material are probably due to the high proportions of Beaumont Clay Formation sediment observed in the samples. The high sand percentage (63.7 percent) of Buoy C sediment is due largely to the amount of shell debris (≈ 20 percent) observed in sand fraction samples.

64. A nondispersed grain-size analysis was also run on the four sediment types. The following tabulation lists the sand:silt:clay percentages and the calculated grain-size distribution parameters presented by Folk (1974). In comparison to the dispersed analysis, the nondispersing technique resulted in a decrease in both the median grain size (ϕ units) and inclusive graphic standard deviation and an increase in the inclusive graphic skewness for Buoy C, Buoy D, and Block 27 sediment. Block 15 material showed an increase in all three parameter values. Substitution of distilled water for Calgon dispersant permitted clay flocculation during the pipette analysis, thus resulting in a shift of the grain-size distribution to lower ϕ sizes (larger grain diameters). An opposite shift for Block 15 sediment is probably the result of incomplete homogenization of the sample prior to analysis.

| | <u>Buoy C</u> | <u>Buoy D</u> | <u>Block 15</u> | <u>Block 27</u> |
|--------------|---------------|---------------|-----------------|-----------------|
| Sand, % | 64.9 | 64.3 | 36.7 | 13.6 |
| Silt, % | 16.5 | 11.9 | 30.4 | 55.1 |
| Clay, % | 18.6 | 23.7 | 32.9 | 31.3 |
| $M_z (\phi)$ | 4.80 | 3.77 | 6.83 | 6.53 |
| ϕ_I | 2.61 | 4.14 | 4.20 | 2.50 |
| SK_I | 0.78 | 0.21 | 0.60 | 0.31 |

Physical properties

65. The following physical properties were measured for sediment recovered from Buoy C, Buoy D, Block 15, and Block 27: (1) void ratio, (2) water content, (3) bulk density, (4) specific gravity, (5) remolded shear strength, (6) organic content, and (7) Atterberg limits. Values of these physical properties, along with sand:silt:clay percentages determined from dispersed grain-size analysis, are presented in Table 2.

66. As anticipated, an increase in void ratio and water content corresponded to a decrease in bulk density for the four sediment mixtures. With the exception of the remolded shear strength values, Buoy C and Buoy D dredged material exhibited similar physical property values. Figure 24 illustrates remolded shear strength (C_u) measurements via plots of torque versus rotation angle for the four mixtures. The high

Table 2

Physical Property Values Determined for Block 15, Buoy C, Block 27, and Buoy D Sediment

| | % SAND | % SILT | % CLAY | WATER CONTENT (W) (% dry weight) | BULK DENSITY (Y) (gm/cm ³) | VOID RATIO (e) | SPECIFIC GRAVITY (G) | REMOLED SHEAR STRENGTH (C) (kPa x 10 ³) | % ORGANIC CONTENT | LIQUID LIMIT (W) | PLASTIC LIMIT (W) | PLASTICITY INDEX (I _p) |
|----------|-------------------------------------|--------|--------|---------------------------------------|---|----------------|----------------------|--|----------------------|---------------------|----------------------|---------------------------------------|
| BLOCK 15 | 50.5 | 22.6 | 24.9 | 90.4 | 1.49 | 2.46 | 2.71 | 3.36 | 3.13 | 66.5 | 51.4 | 15.1 |
| BUOY C | 63.7 | 13.5 | 22.8 | 70.1 | 1.59 | 1.87 | 2.67 | 3.09 | 1.84 | 40.5 | 40.0 | 0.5 |
| BLOCK 27 | 18.5 | 35.9 | 45.6 | 117.6 | 1.41 | 3.13 | 2.67 | 6.72 | 4.14 | 101.5 | 63.5 | 38 |
| BUOY D | 51.2 | 11.7 | 37.1 | 61.9 | 1.64 | 1.67 | 2.70 | 11.08 | 2.91 | 56.0 | 48.2 | 7.80 |
| | DISPERSED GRAIN-SIZE ANALYSIS | | | VALID FOR >1.25-φ FRACTION ONLY | | | | | | | | |

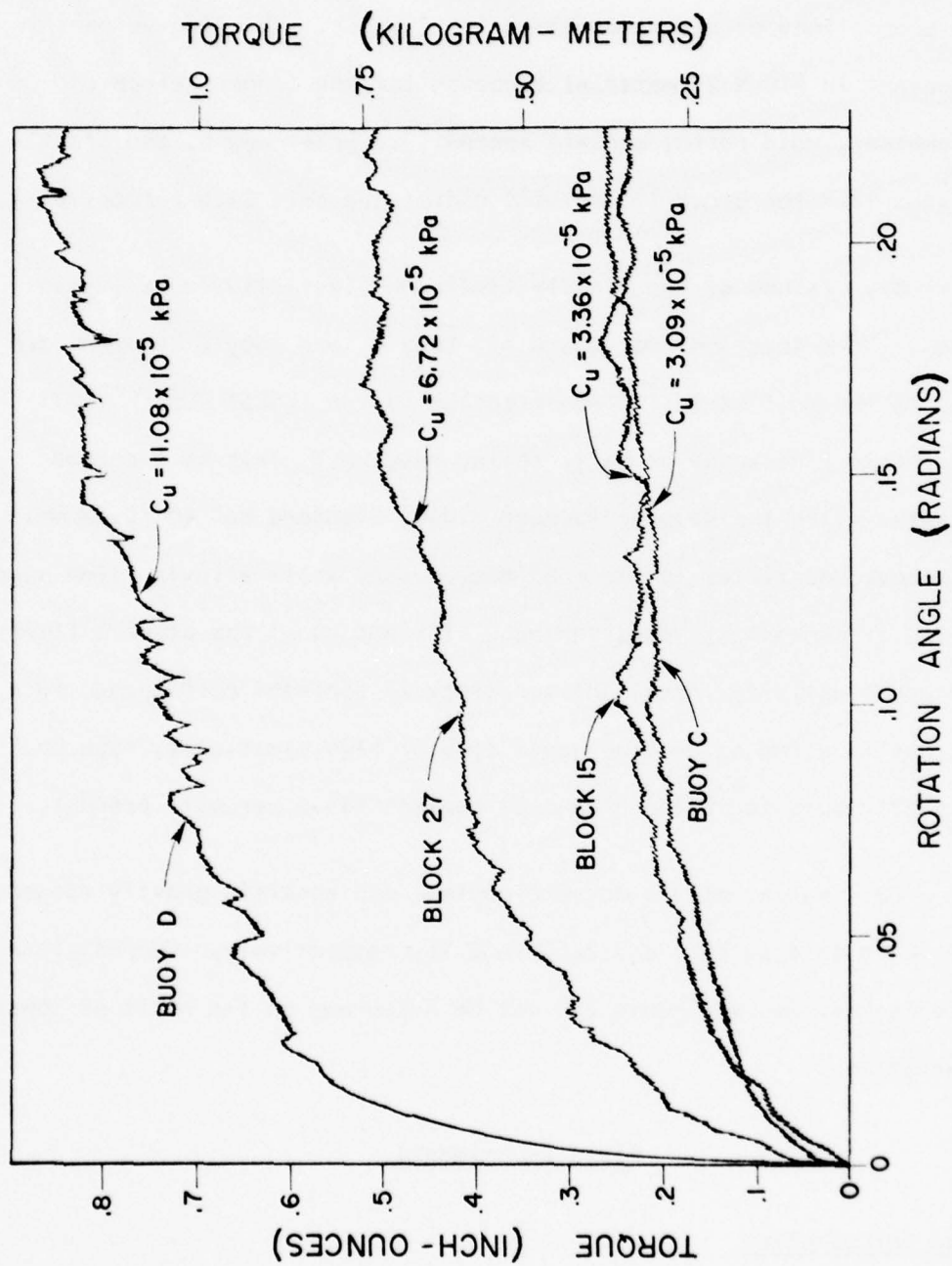


Figure 24. Shear strength (C_u) measurements determined by torque versus rotation angle plots

shear strength of Buoy D sediment is probably attributable to the highly consolidated Beaumont Clay Formation present. The variations in the physical properties between Block 15 and Block 27 material are due to the proportions of clay present in the samples. The 45.6-percent clay content in Block 27 material accounts for the larger values of water content, void ratio, organic content, shear strength, and plasticity index than for Block 15 sediment containing only 24.9 percent clay.

67. Values of the plastic limit and plasticity index (valid for the 1.25- ϕ fraction) for Block 15, Buoy C, and Buoy D sediment are defined by the Unified Soil Classification System (USCS) (USWES 1953) as "inorganic fine sandy or silty soils, type MH." This is expected since wet-sieving the samples through a U.S. Standard No. 40 (0.42-mm) sieve removed particles larger than medium sand while allowing fine sand and silt, if present, to pass through. The values of the plastic limit (63.5) and plasticity index (38) for Block 27 sediment correspond to a USCS classification as an "inorganic clay of high plasticity, type CH." This is attributable to the high clay content (45.6 percent) present.

68. Values of the organic content and specific gravity ranged from 1.84 to 4.14 percent and 2.67 to 2.71, respectively. Compositional differences between sediments can not be discerned on the basis of these low variations.

Flume Experiments

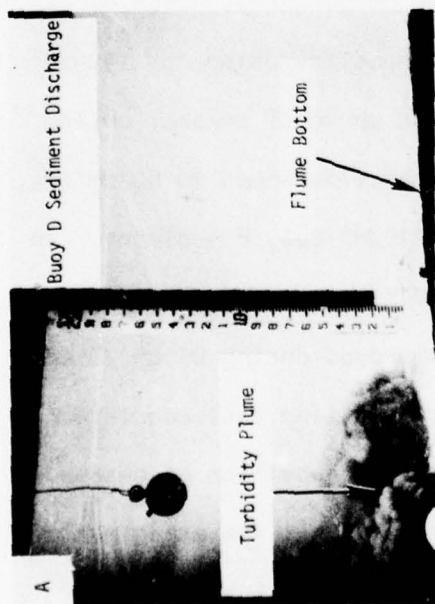
Bedload Introduction

69. The discharge of each test sediment into the water column

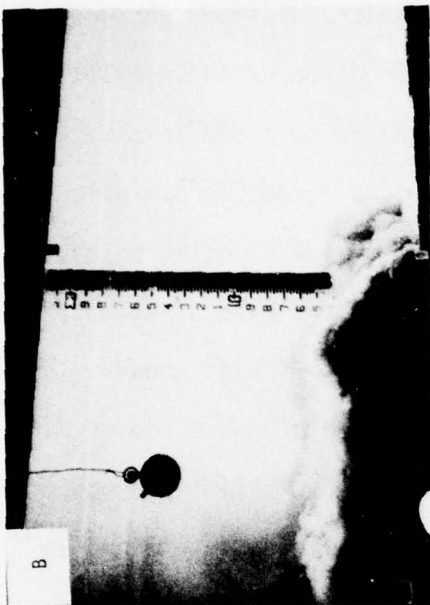
resulted in simultaneous turbidity plume generation and mounding of sediment on the flume bottom. The mounds exhibited a hummocky relief up to 20 cm high and were spread about 1.5 meters upstream and downstream from the discharge point. All discharges occurred in still water except for one Block 27 material discharge released into a 30-cm/sec flow. The resultant (Block 27) mound formed an elliptical configuration approximately 1.2 m downstream of the ejection point. Figure 25 illustrates the turbidity plume generated by a 34-kg Buoy D sediment discharge. Stopwatch timing of the plume travel speed immediately after ejection indicated an approximate head speed of 7.0 cm/sec. Also, two water samples, taken during the initial passage of the plume 1.2 m downstream of the discharge site, were determined to have an average TSM concentration of 50 mg/l at a 45-cm water depth.

Erosional runs

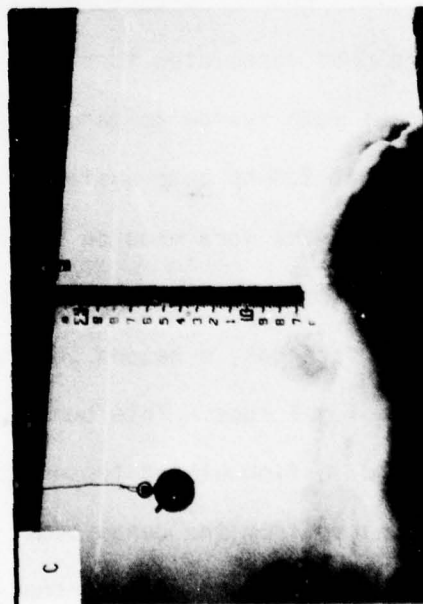
70. Four erosional runs were made on both Buoy C and Block 15 mounds (and associated turbidity plume deposits) using the 1.0-hp centrifugal pump system to generate currents up to 31 cm/sec. Using an additional 2.0-hp pump system to boost the flow speed to 60 cm/sec, nine erosion runs were made on both Block 27 and Buoy D sediment. In addition to scouring the bed (herein termed dense bed) that resulted from the discharges, a second bed type was eroded during Block 27 and Buoy D erosional runs. This bed (herein called floc bed) consisted primarily of a flocculated loose bed formed by deposition of suspended matter scoured from the dense bed. A listing of all the experimental runs in their sequence of occurrence is contained in Appendix A.



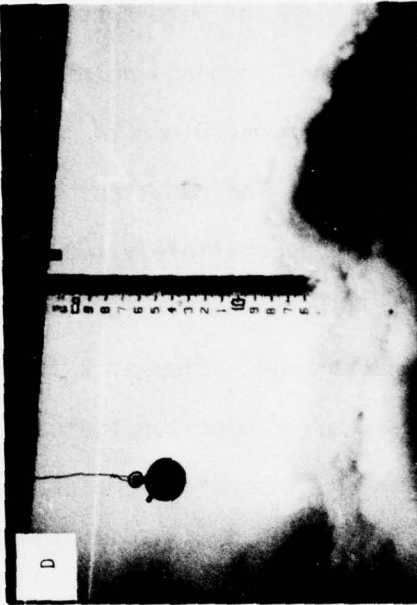
a. 14 sec after discharge



b. 22 sec after discharge



c. 35 sec after discharge



d. 45 sec after discharge

Figure 25. Turbidity plume generated by Buoy D sediment discharge (vertical scale is numbered in tenths of a foot)

71. Dense bed--sediment transport. Determination of the mode of sediment transport for each of the four sediment types was made on the basis of monitoring the TSM concentration over time per given flow rate. Plots of the log of the TSM concentration versus time per given flow rate for each experimental run are shown in Appendix C. For the purpose of comparing the erodibility of the four sediment mixtures, selected log TSM versus time curves were combined. Figure 26 illustrates such a graph for Buoy C and Buoy D dredged sediment erosional runs. As shown, the TSM concentrations increased logarithmically during the initial few hours following each current speed increase and then assumed a linear slope for the duration of the experimental run until the next current speed change was implemented. The initial rapid increase in the TSM concentrations may be attributable to resuspension of previously deposited turbidity plume sediment in the flume channel, in addition to scouring of material from the mound. The TSM concentration decrease exhibited by the 16-cm/sec Buoy D run indicates that some deposition of suspended matter occurred. Comparison of Buoy C and Buoy D erosional runs (Figure 26) illustrates the similarity between the average TSM concentration held in suspension by a given flow rate. This result is not surprising since the two dredged material sediments exhibited similar geotechnical properties (Table 2).

72. Figure 27 illustrates a comparison of Block 15 and Block 27 dense bed erosional runs. The log TSM versus time curves display a pattern similar to that of the Buoy C and Buoy D scour run curves (Figure 26). Variations in the TSM concentration values for near-

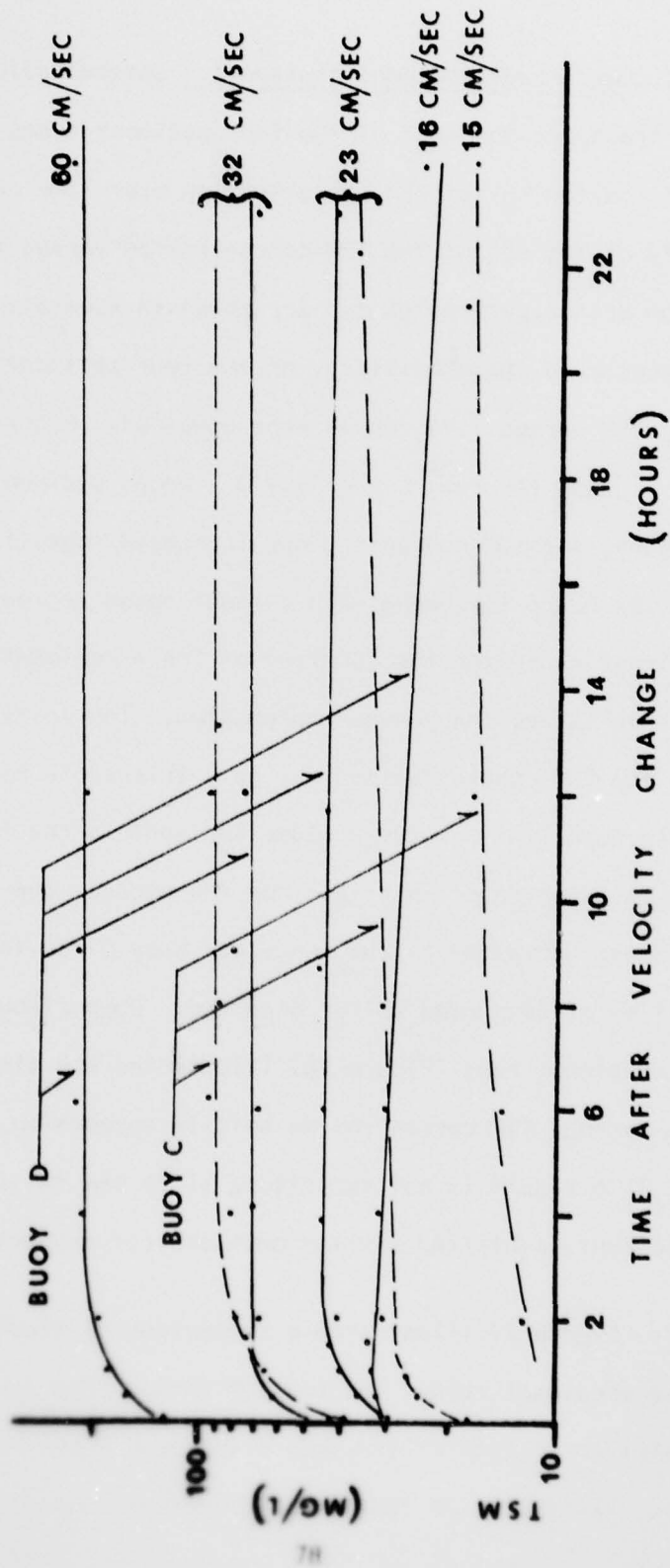


Figure 26. Selected dense bed erosional runs performed on Buoy C and Buoy D sediment

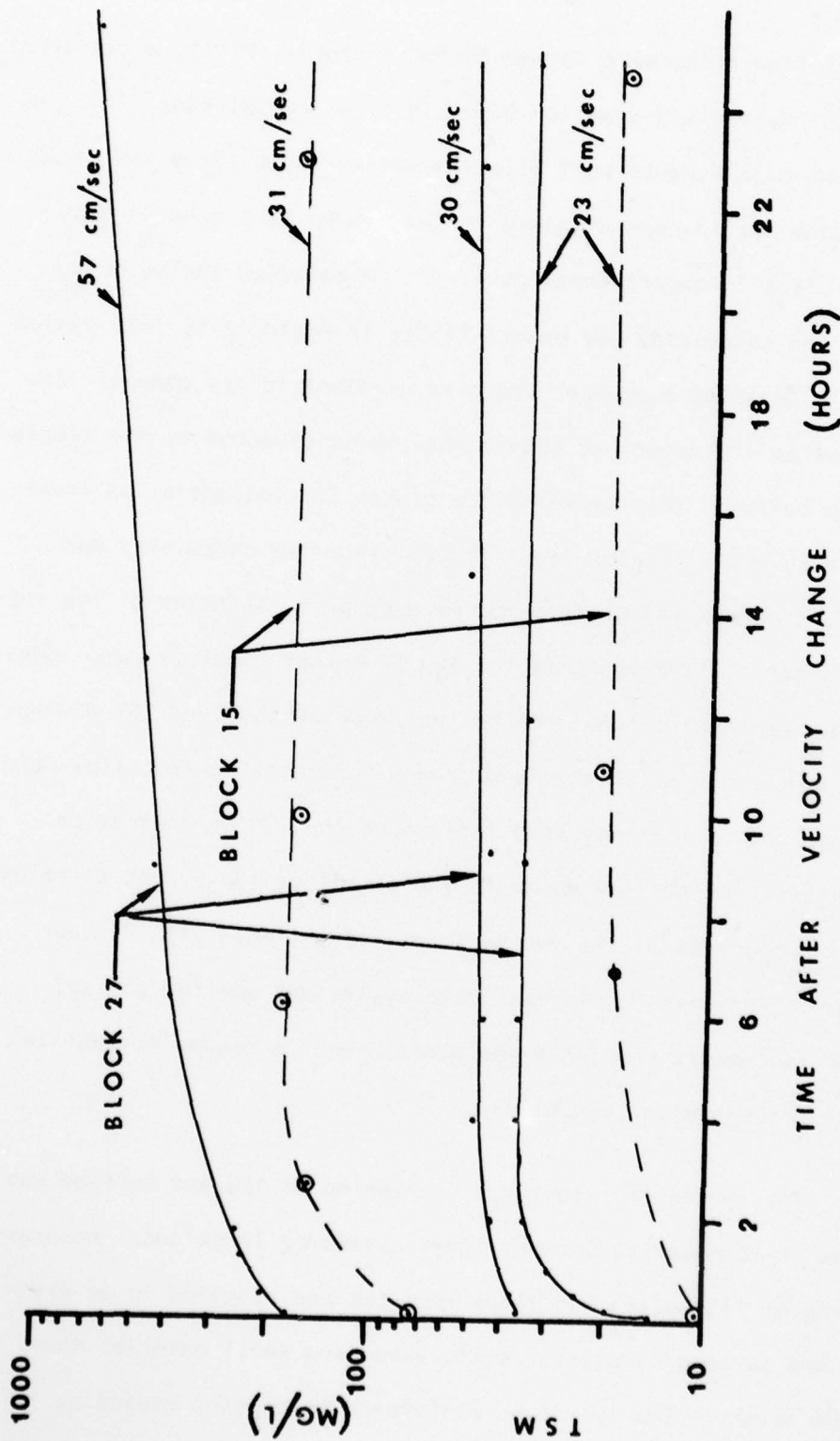


Figure 27. Selected dense bed erosional runs performed on Block 15 and Block 27 sediment

equivalent flow rates were caused by two factors. First, a different pump outlet system was used for Block 15 experimental runs. In lieu of the open-pipe exhaust port illustrated in Figure 17, a set of 12 0.32-cm-diam nozzles was attached to the 1.0-hp pump exhaust pipe prior to Block 15 experimental runs. As revealed by the velocity profiles and calculated bed shears listed in Appendix B, this system apparently imparted a steeper velocity gradient to the channel flow that resulted in larger bed shears than those produced by the simple open-pipe outlet. This explains the higher TSM concentration level exhibited by the 31-cm/sec Block 15 run since the calculated bed shear (2.53 dynes/cm^2) of this run is greater by a factor of two than the bed shear (1.12 dynes/cm^2) for the 30-cm/sec Block 27 run. However, this explanation does not account for the observed TSM concentration levels and calculated bed shears for the 23-cm/sec flow rate. The second factor that may have influenced the TSM concentration variations per given flow speed is the effect caused by the different physical properties of the two sediment types (Table 2). Further experimentation using a singular pump system and smaller current velocity increments between experimental runs is needed to explain such TSM concentration variations.

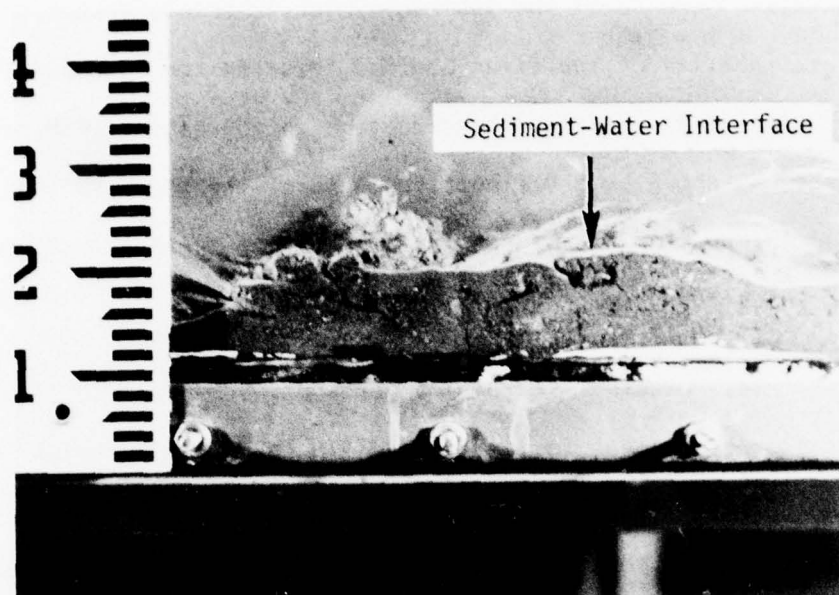
73. A distinct textural coarsening of the bed surface was observed to form during current flows exceeding 16 cm/sec. Apparently, winnowing of fine silts and clays from the bed resulted in an armoring of the bed surface by coarser silt, sand, and shell material that remained intact. The increased resistance to erosion caused by this

grain-size increase at the sediment-water interface probably reduced the availability of the finer bedload fraction for resuspension. This may partially account for the reduction in the rate of TSM concentration increase as shown by the linear segments of the scour curves. Quantitative information on physical changes of the surface texture during scour is needed to verify this hypothesis.

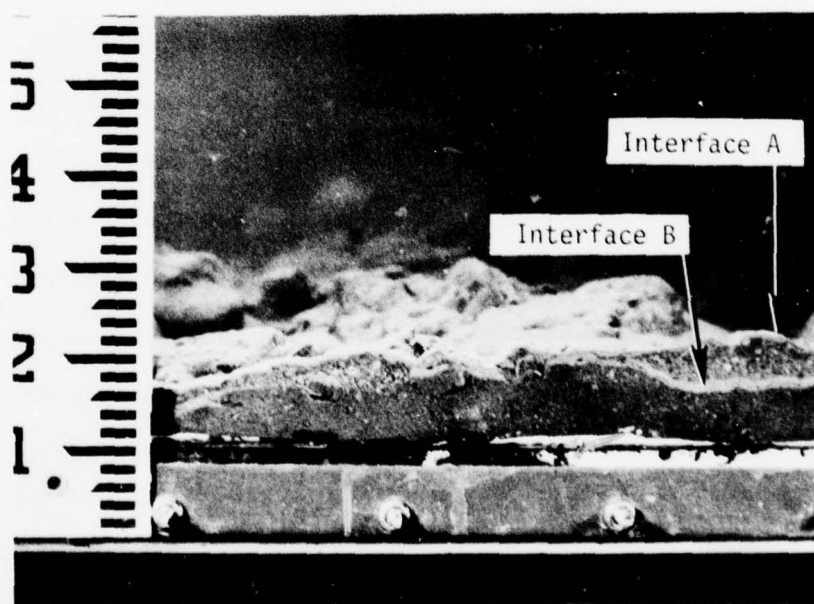
74. Distinct textural interfaces were observed to form against the center glass pane in the flume. Figure 28a illustrates the sediment-water interface 16 hr after discharge of Buoy D sediment. The light-gray sediment on the bed surface represents an oxidized layer composed of flocculated clays deposited from turbidity plume suspensions. Figure 28b illustrates the same bed surface after 2 weeks of experimental runs. The thin layer depicted as interface A formed as a result of flocculant clays deposited at the conclusion of the last erosion run. Interface B was the remnant oxidized layer shown in Figure 28a. A lag deposit comprised mostly of coarse silt, sand, and shell hash was exhibited between these two interfaces. This deposit formed during erosional runs exceeding about 23 cm/sec. The nonuniformity of this deposit illustrates the large textural variations that can form within the sediment column as a result of scour over a hydrodynamically rough surface.

75. Dense bed--critical shear stress and erosion velocity.

A plot of the bed shear stress in dynes per cm^2 versus the average TSM concentration in mg per l for dense bed erosional runs is illustrated in Figure 29. The average TSM concentration per erosion run was ascertained by calculating the mean TSM concentration of the linear slope of



a. Sediment-water interface 16 hr after discharge



b. Sediment interfaces following 2 weeks of experimental runs

Figure 28. Sediment-water and sediment interfaces following discharge of and experiments with Buoy D sediment (vertical scale is numbered in tenths of a foot)

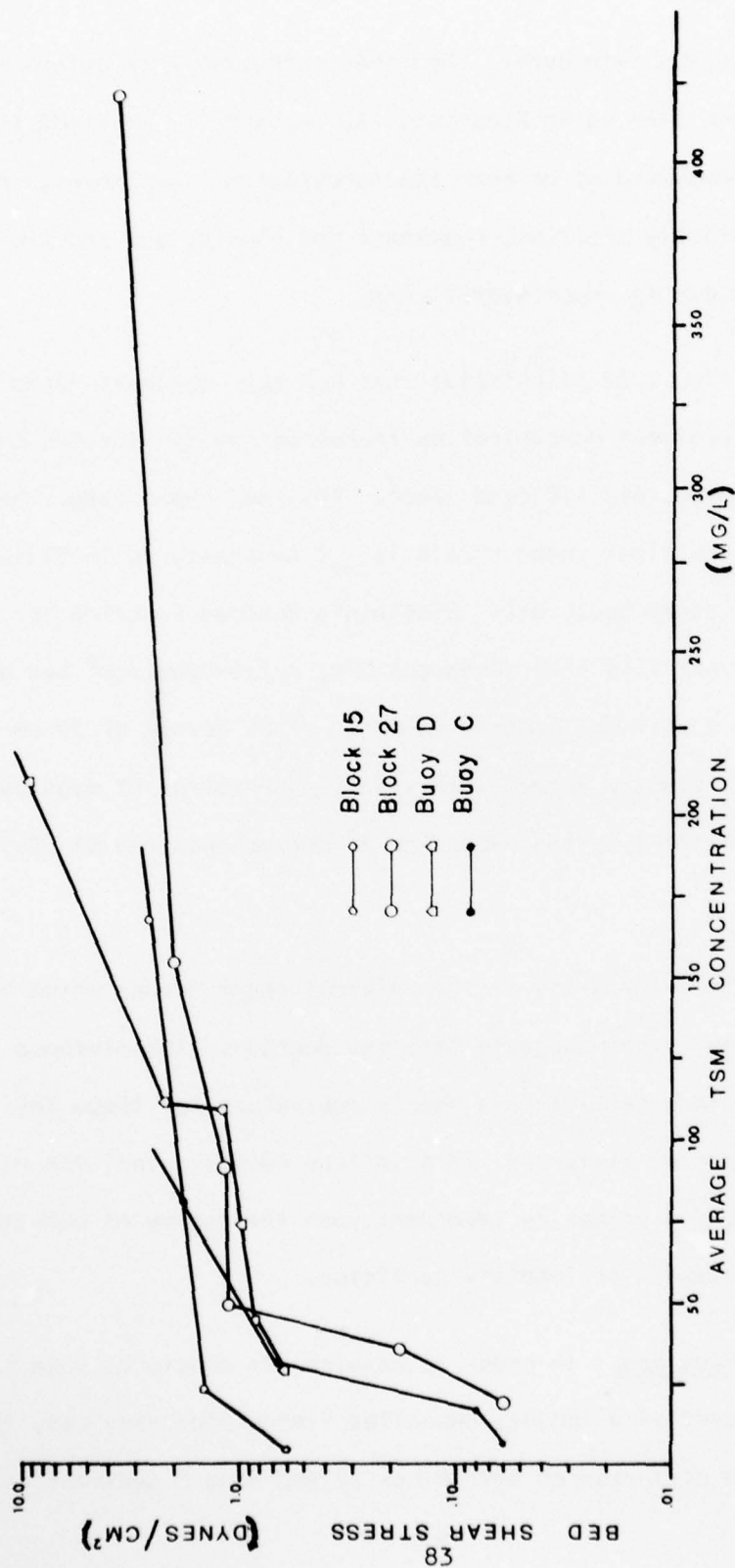


Figure 29. Relationship between average TSM concentration and bed shear for dense bed erosional runs

each log TSM versus time curve. Bed shear stresses were determined from the velocity profiles using Equations 13, 14, and 15. Most of these profiles were measured at or near the foreslope of each mound. Appendix B lists the velocity profiles, resultant bed shears, and profile locations obtained during experimental runs.

76. Figure 29 illustrates that for the sediment types tested the suspended sediment concentration increased rapidly for bed shears exceeding approximately 1.0 dyne /cm^2 . This bed shear value then represents the critical shear stress (τ_{ocr}) necessary to initiate rapid erosion of the dense bed. Using Einstein's Bedload Function for open channel flow conditions (see paragraph 59), a 1.0-dyne /cm^2 bed shear corresponds to a critical erosion velocity of 24 cm/sec at 30 cm above the bed. This velocity agrees with visual observation of mass bedload transport for current speeds exceeding 23 cm/sec measured at 30.5 cm above the bed.

77. The similarity of the critical shear stress value for the four sediment types suggests that the degree of cohesiveness between sedimentary particles is nearly equivalent for these four sand, silt, and clay mixtures. This is true assuming that the resistance to erosion is primarily dependent upon the degree of cohesive force acting between sedimentary particles.

78. Floc bed. In order to examine the erosional mode of sediment transport on a loosely deposited flocculated clay bed, three scour runs were performed on both Block 27 and Buoy D sediment deposited

from suspension. The first of these runs was initiated after a settling period that followed the last deposition run. The 14-cm/sec Block 27 floc bed erosion run was initiated after a 36-hr settling period, whereas the 16-cm/sec Buoy D floc bed erosion run began following a 48-hr settling period. In both cases, the channel bottom and sediment mound were uniformly blanketed with a thin (0.32-cm-thick) layer composed of flocculant clays and very fine silts.

79. The scour curves for these erosional runs are exhibited in Figures 30 and 31. As shown, the TSM concentration tended to increase rapidly to some asymptotic level. A slight decrease in the TSM concentration with time was evident for Block 27 Run No. 9 and Buoy D Run Nos. 9 and 10, which indicated that deposition occurred. Much of the material that was resuspended probably originated as a floc bed in the return channel of the flume. Since the current propulsion system was located here, much higher bed shears were produced than in the observation channel. This was substantiated by the higher TSM concentration levels attained by the floc bed runs than for the dense bed runs made at similar flow rates. Unfortunately, the lack of point velocity measurements within the return channel prevented an accurate estimation of the critical bed shear required to induce floc bedload erosion. However, the data collected suggest that the pattern of floc bed erosion was similar to that exhibited by the dense bed erosion runs; that is, the TSM concentration of the fluid appears to be directly dependent upon the magnitude of the bed shear stress acting on the sediment-water interface.

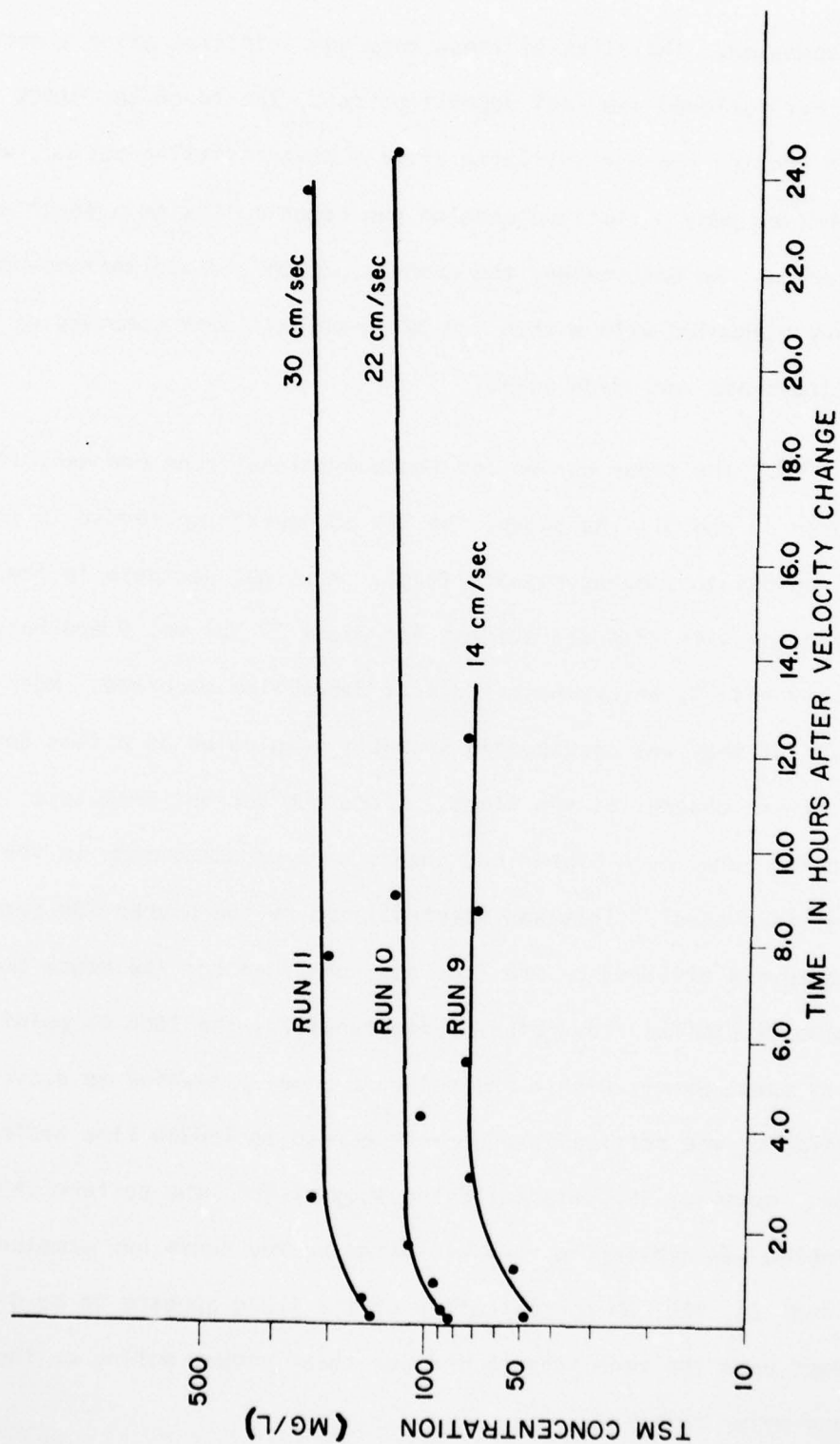


Figure 30. Block 27 flocculated bed erosional runs

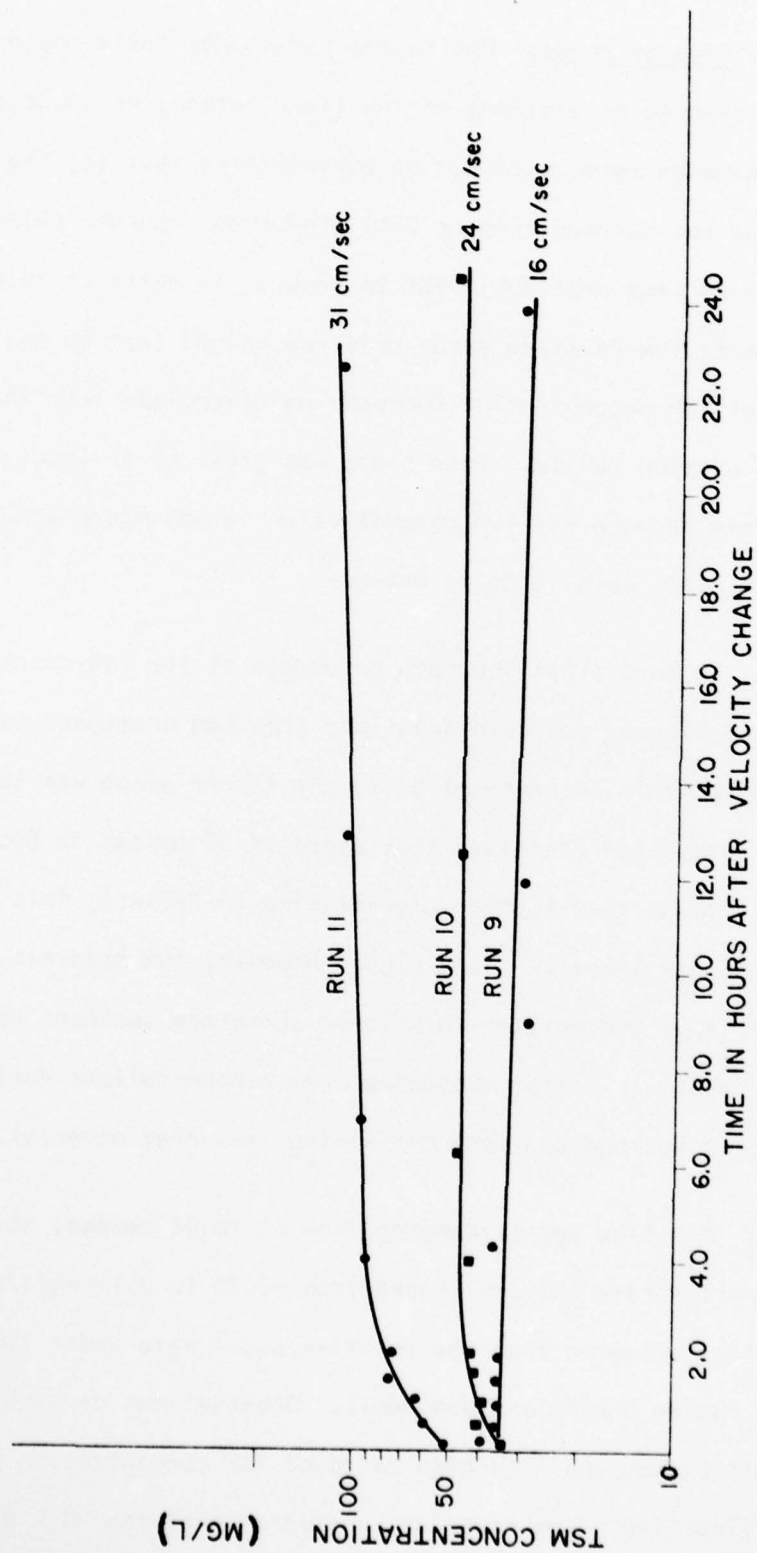


Figure 31. Buoy D flocculated bed erosional runs

80. Erosion rates. Due to the hydrodynamically rough surface produced by mounding of sediment on the flume bottom, an accurate estimate of the erosion rate could not be ascertained; that is, the nonuniformity of the bed surface (Figure 28b) prevented accurate determination of the actual surface area subjected to scour. In spite of this, an approximation of the relative scour rate was gained from an evaluation of the rate of TSM concentration increase as determined from the linear slope of the erosion curves. This slope was given by a visual regression line drawn through the TSM concentration values measured between 4 to 24 hours after each velocity change.

81. Table 3 lists the rate of change of the TSM concentration per average flow speed for both dense and floc bed erosional runs. The maximum observed rate increase given by the linear slope was 16.47 mg/l/hr for an average sustained flow speed of 57 cm/sec on Block 27 sediment. In comparison to the values listed in Table 3, this TSM concentration rate increase seems high. However, the naturally high clay content (45.6 percent) of this lower shoreface sediment would be expected to result in higher suspended clay concentrations during erosion than for a bedload sediment containing less clay material.

82. For flow speeds ranging from 10 to 44 cm/sec, observed TSM concentration rate changes ranged from -0.36 to 2.17 mg/l/hr. Such low rates indicated that the relative scour rate under low to medium flow regime conditions was small. Observations of turbidity plume formation, coupled with high rates of TSM concentration increase during the first few hours of scour, indicated that the bulk of clay

Table 3

Rate of Change of TSM Concentration For Erosional Runs

| <u>Buoy</u> | <u>Type Of Bed</u> | <u>Run No.</u> | <u>Average Current Velocity (cm/sec)</u> | <u>Rate of Change of TSM Concentration mg/l/hr</u> |
|-------------|------------------------|----------------|--|--|
| Buoy C | Dense | 1 | 10 | 0.09 |
| | | 2 | 15 | 0.25 |
| | | 3 | 23 | 0.51 |
| | | 4 | 32 | 1.02 |
| Buoy D | Dense | 1 | 16 | -0.36 |
| | | 2 | 23 | 0.01 |
| | | 3 | 32 | 0.24 |
| | | 4 | 39 | 0.40 |
| | | 5 | 44 | 0.50 |
| | | 6 | 60 | 1.42 |
| | Floc | 9 | 16 | -0.23 |
| | | 10 | 24 | 0.23 |
| | | 11 | 31 | 1.80 |
| Block 15 | Dense | 2 | 16 | 0.02 |
| | | 3 | 23 | -0.04 |
| | | 4 | 31 | 0.74 |
| | Dense | 1 | 12 | -0.10 |
| | | 2 | 23 | 0.11 |
| | | 3 | 30 | 0.14 |
| | | 4 | 38 | 1.06 |
| | | 5 | 44 | 2.17 |
| | | 6 | 57 | 16.47 |
| | Floc | 9 | 14 | -0.06 |
| | | 10 | 22 | 1.10 |
| | | 11 | 30 | 1.73 |

and silt resuspension occurred during the first few hours immediately following a dredged material discharge. Then scour rates were reduced to small values as textural coarsening of the bed surface occurred and perhaps also as the sediment consolidated under the effect of gravity.

Depositional runs

83. Experiments were performed to determine the approximate current velocity and associated bed shear at which significant deposition of the suspended sediment occurred. Figure 32 illustrates the depositional runs made using each of the four sediment mixtures. The deposition runs for Block 15 and Buoy C sediments were initiated at the conclusion of the 32-cm/sec erosional runs, whereas Block 27 and Buoy D deposition runs began immediately following the 57- and 60-cm/sec erosion runs, respectively. In this manner, the suspended sediment concentration that resulted from scour of the dense bed was monitored over time at a 30.5-cm depth.

84. As shown in Figure 32, significant deposition of the suspended sediment occurred during sustained flow speeds less than about 10 cm/sec and initial flow concentrations exceeding approximately 100 mg/l. Deposition curves for the 6-cm/sec Block 27 run and 4-cm/sec Buoy D run indicate that the suspended sediment concentration decreased logarithmically for the 24-hr period of observation. For current velocities exceeding 10 cm/sec, the TSM concentration remained stable indicating that suspended silts and clays are apt to remain in suspension indefinitely. An average flow speed of 10 cm/sec, 30 cm above the

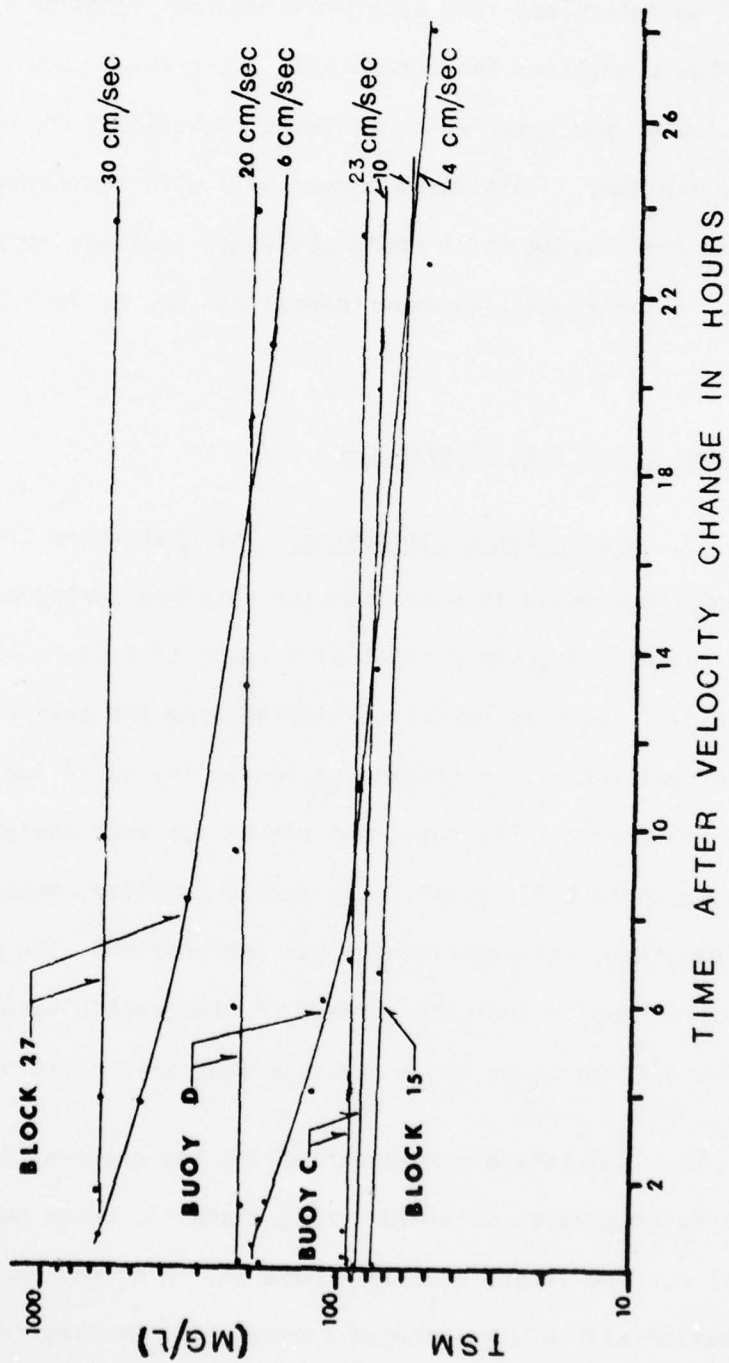


Figure 32. Depositional runs performed on each of the four sediment mixtures

AD-A057 660

TEXAS A AND M UNIV COLLEGE STATION DEPT OF OCEANOGRAPHY F/G 13/2
FLUME EXPERIMENTS ON SAND, SILT, AND CLAY MIXTURES FROM THE OFF--ETC(U)
JUN 78 A J MOHEREK

DACW39-76-C-0115

UNCLASSIFIED

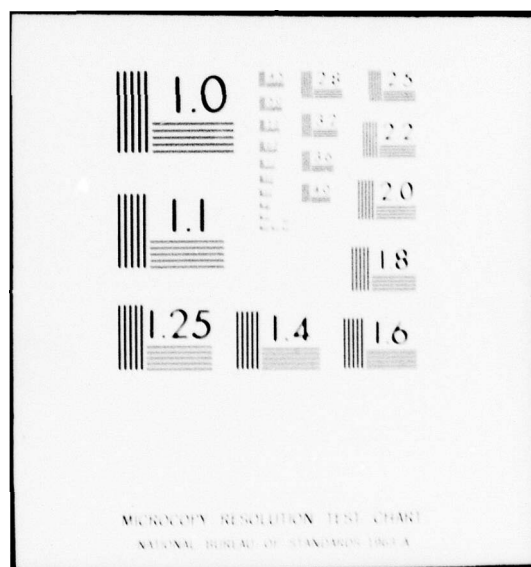
WEC-TD-D-7A-34

ALL

2 of 3

AD
A057 660





bed, corresponds to a calculated bed shear of approximately 0.20 dyne /cm² as determined from Einstein's Bedload function for open channel flow conditions (paragraph 59). This value should then represent the lowest bed shear which inhibits significant deposition of suspended sediment. This value agrees well with the lowest bed shear (0.23 dyne /cm²) above which rapid suspended sediment deposition did not occur in the flume (see experimental run No. 6, Buoy C, in Appendix B).

Geotechnical properties of washload

85. Grain-size distribution. The grain-size distributions of the sediment suspended in water samples obtained during experimental runs were determined over a total size range of 4.0 ϕ to 10.6 ϕ (coarse silt to clay). Cumulative curves plotted from the measured cumulative weight percent per size increment served as the basis for determination of the graphic mean. The resultant values for each analysis are tabulated in Appendix D, in addition to sample location, mean flow speed, time of sampling, and experimental run designation. The grain-size distribution results indicate a range of the graphic means from 6.5 to 9.7 ϕ (fine silt to clay) and an average clay:silt ratio of 3.9:1.

86. Cumulative curves exhibiting the grain-size distribution of three water samples obtained during Block 15, dense bed 31-cm/sec erosional run are illustrated in Figure 33. A slight decrease in the silt fraction with a simultaneous increase in the clay fraction is indicated for samples obtained during increasing time after velocity change. A similar pattern is depicted in Figure 34 for three samples

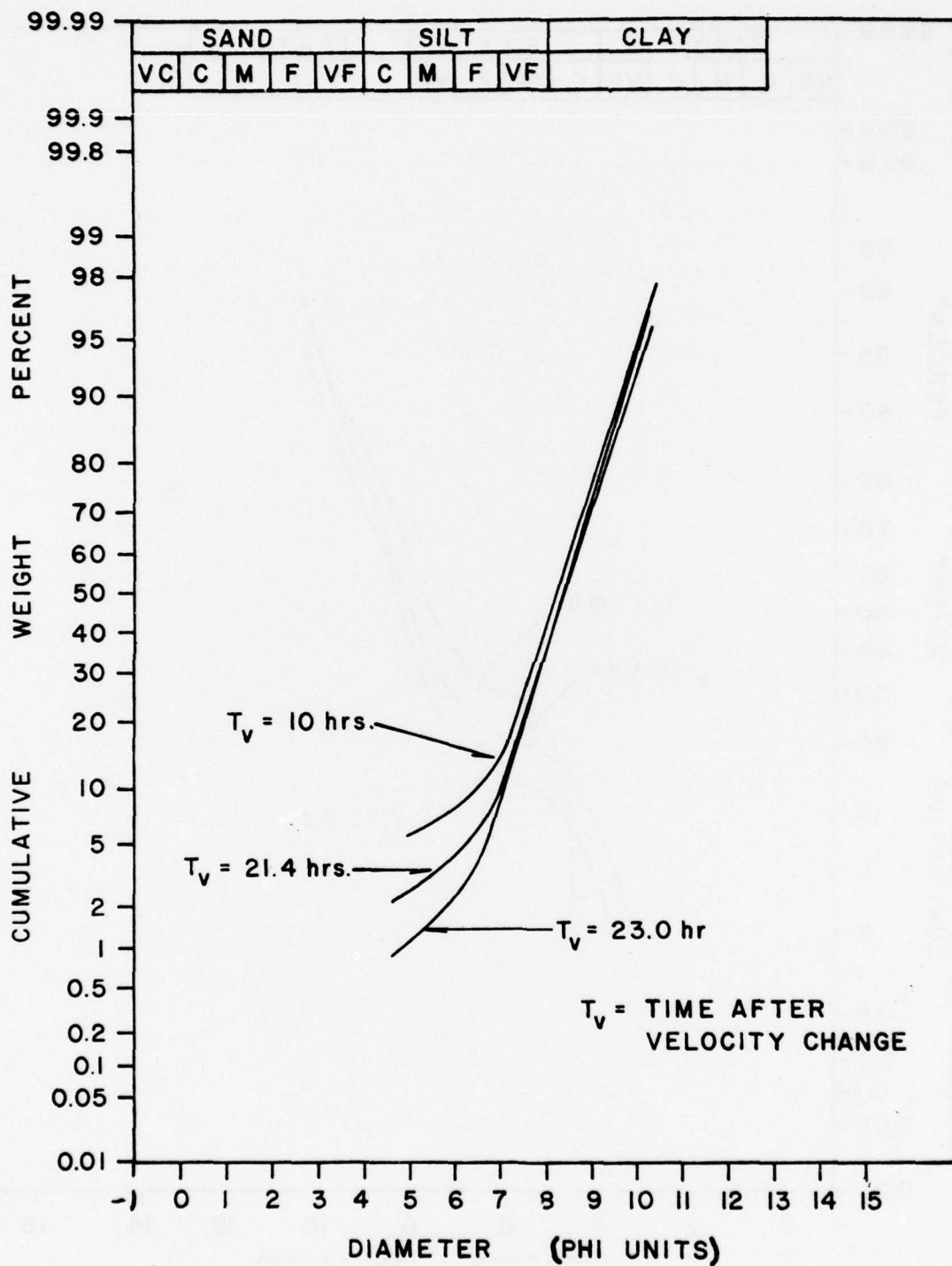


Figure 33. Grain-size distributions of three washload samples collected during Block 15, dense bed 31-cm/sec erosion run

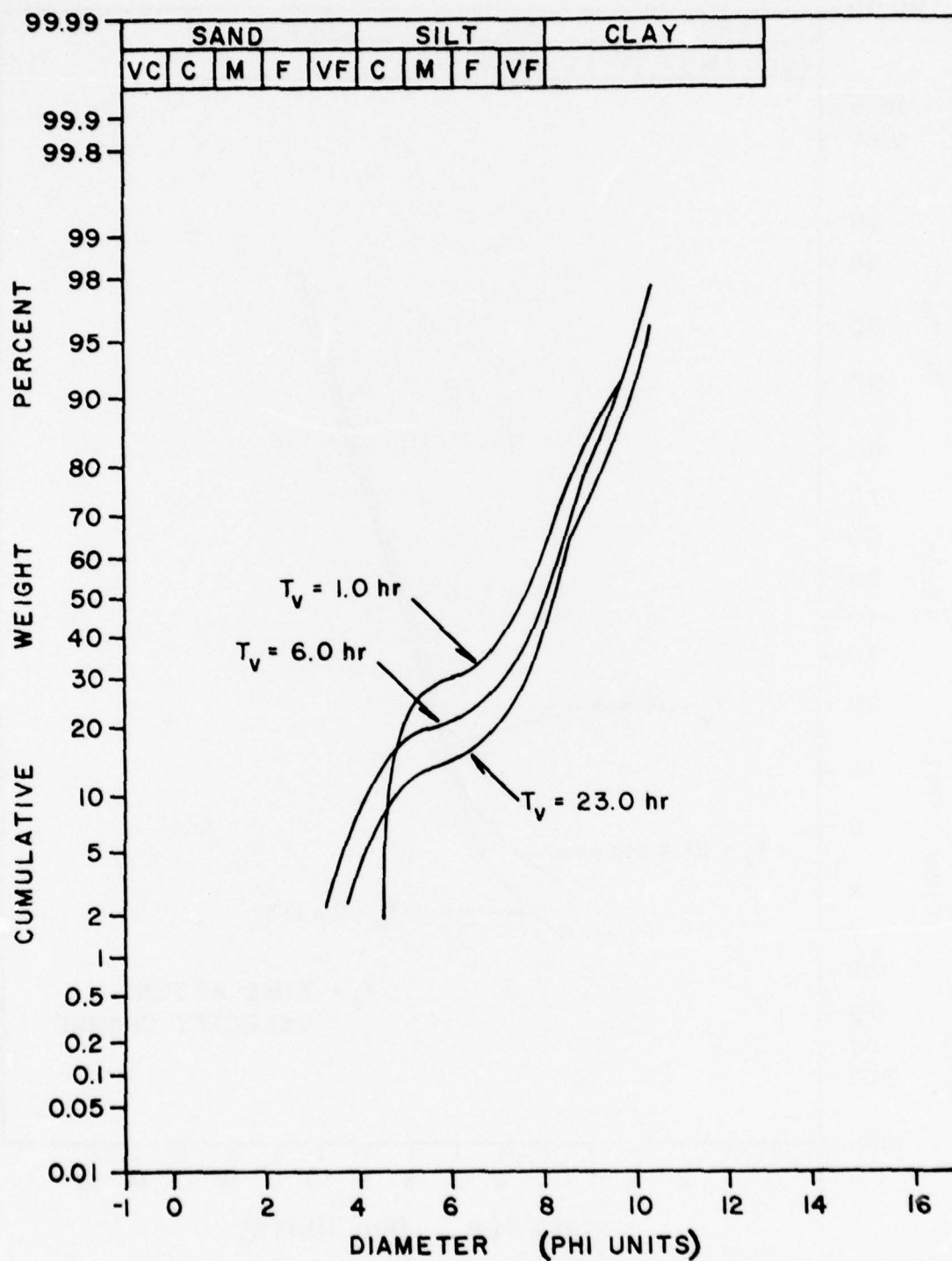


Figure 34. Grain-size distributions of three washload samples collected during Buoy D, dense bed 23-cm/sec erosion run

collected during Buoy D, dense bed 23-cm/sec erosional run. Both sets of samples were recovered 30 cm above the bed. The decrease in the silt content for these sustained flow rates may have resulted from the deposition of silt that originated as resuspended turbidity plume deposits in the return channel. The higher shearing rates produced within the return channel by the current propulsion system probably caused rapid resuspension of the silt and clay fraction plume material during each initial current speed increase. Then, lower bed shears in the observation channel, which resulted from frictional drag along the channel surfaces, allowed deposition of those silt-size fractions that exceeded the stream competency. However, further experimentation is desired to determine the magnitude of the shearing rate in the return channel per given flow speed, and the correspondent grain size of the *resuspended* material.

87. Large variations in the washload grain-size distribution were noted for water samples collected at different flow rates. Figure 35 illustrates the textural and compositional differences between samples obtained during Block 27, dense bed 44-, 57-, and 30-cm/sec experimental runs. These samples were also collected 30 cm above the bottom. As revealed, a 30 to 77 percent increase in the silt content occurred after the mean flow speed was increased from 44 to 57 cm/sec. Next, a 77 to 21 percent silt content decrease took place as the flow rate was reduced to 30 cm/sec. Another example displaying an increase in the silt content with increasing current speed is shown in Figure 36 for Block 27, floc bed erosion runs. These silt-content variations illustrate the dependence of the washload grain-size distribution upon the competency of a

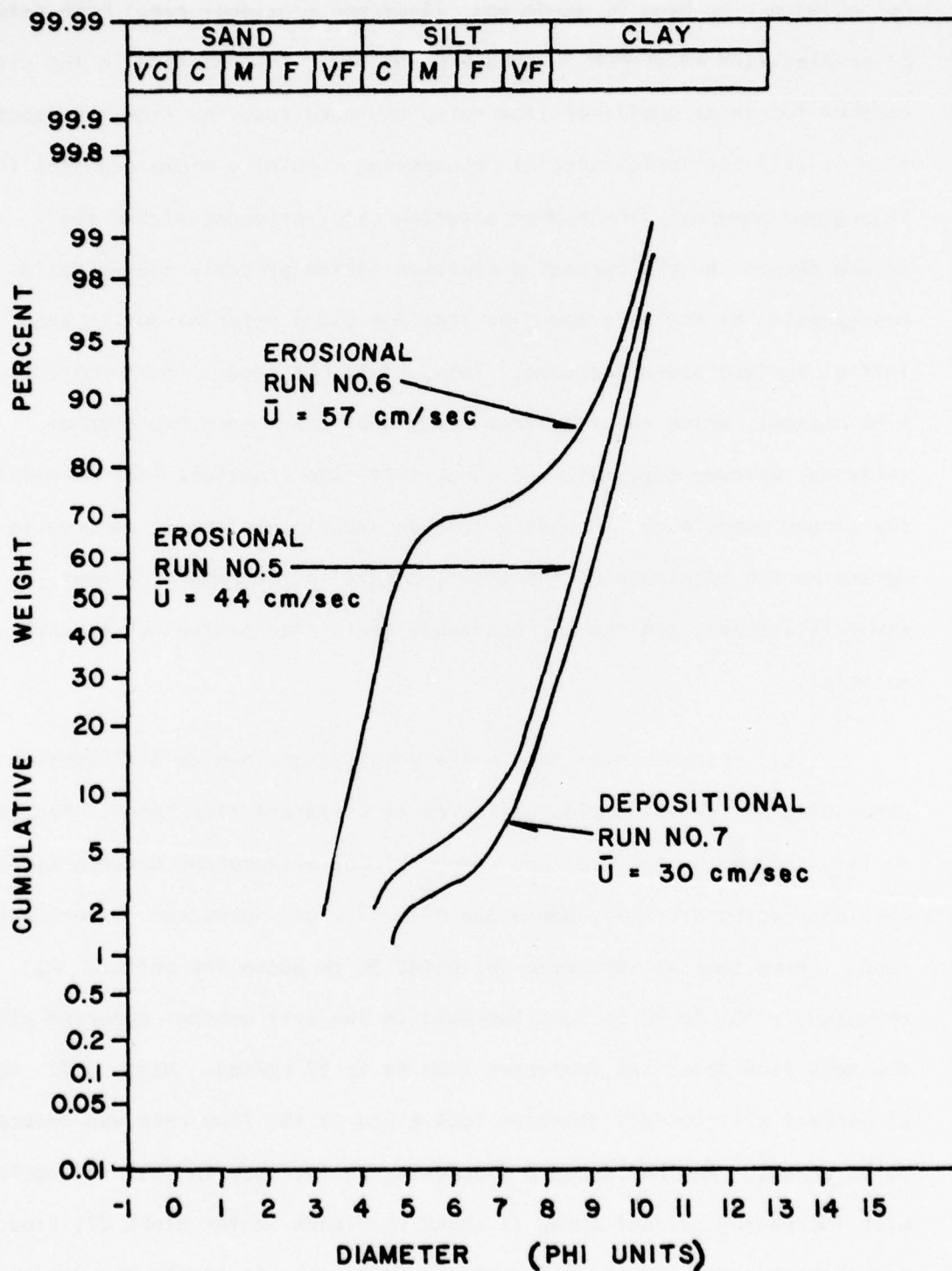


Figure 35. Grain-size distributions of three washload samples collected during Block 27, dense bed 44-, 57-, and 30-cm/sec erosional runs

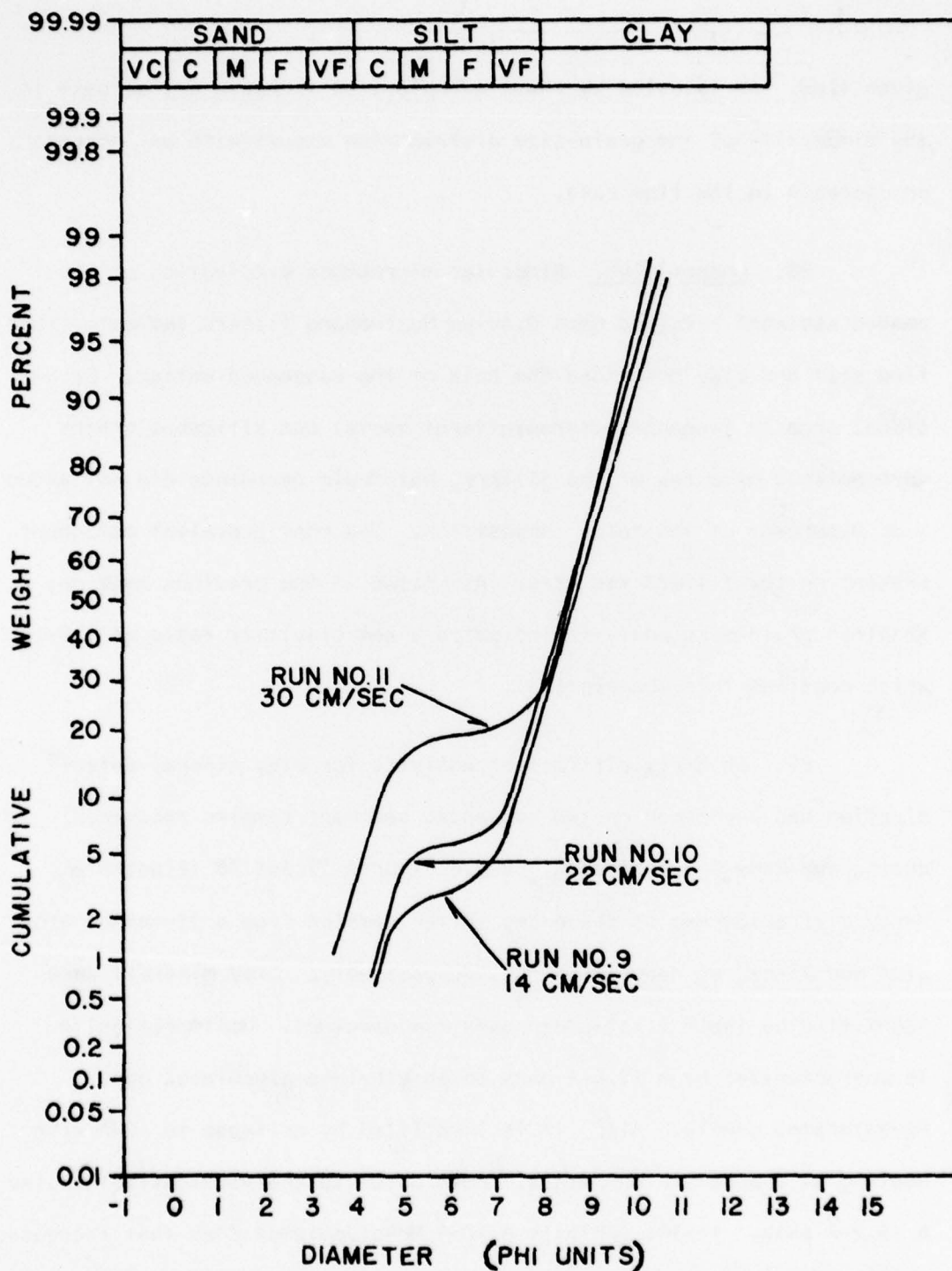


Figure 36. Grain-size distributions of three washload samples collected during Block 27, floc bed 14-, 22-, and 30-cm/sec erosional runs

given flow. As revealed by these examples, an increase or decrease in the bimodality of the grain-size distribution occurs with an increase or decrease in the flow rate.

88. Composition. Binocular microscope examination of suspended sediment retained upon 0.40- μ m Nucleopore filters indicated that fine silt and clay comprised the bulk of the suspended matter. Occasional organic fragments (foraminiferal tests) and siliceous grains were noticed on a few of the filters, but their abundance did not exceed 1 or 2 percent of the total composition. The most prevalent component present on the filters was clay. As stated in the previous section, washload grain-size analyses indicated a net clay:silt ratio of 3.9:1, which confirms this observation.

89. An X-ray diffraction analysis for clay mineral determination was performed on two suspended sediment samples recovered during two Buoy C experimental runs. Figures 37 and 38 illustrate X-ray diffractograms of suspended matter sampled from a 31-cm/sec erosion and 23-cm/sec deposition run, respectively. Clay minerals were identified by their first-order angstrom spacings. Montmorillonite is characterized by a $17.6\text{-}\overset{\circ}{\text{A}}$ peak on an ethylene-glycolated and Mg-saturated sample. Also, it is identified by collapse to $10\text{-}\overset{\circ}{\text{A}}$ with heating of a K-saturated sample. Both chlorite and vermiculite display a $14.2\text{-}\overset{\circ}{\text{A}}$ peak. Illite exhibits a $10\text{-}\overset{\circ}{\text{A}}$ Mg-glycolated peak that increases in height with K-saturation plus heat. A chlorite-kaolinite peak occurs at $7.2\text{-}\overset{\circ}{\text{A}}$ on the Mg-saturated and glycolated diffractogram.

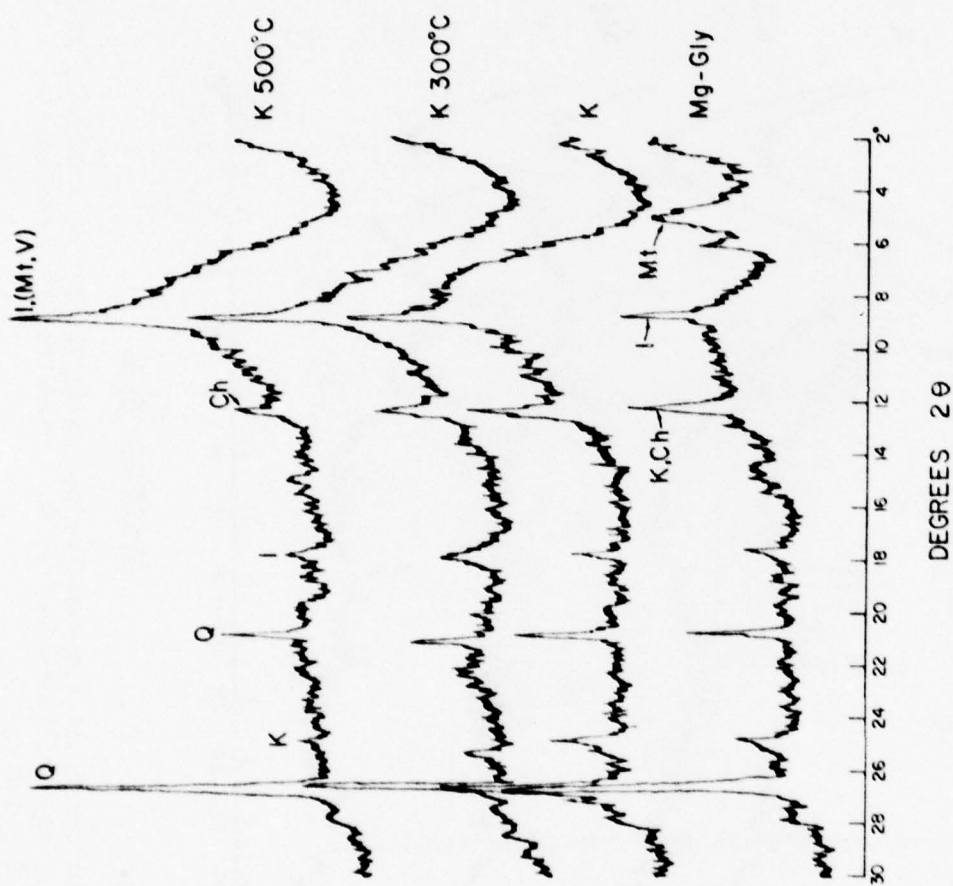


Figure 37. X-ray diffractograms of suspended matter collected during a Buoy C, 31-cm/sec erosional run
 (Legend: Mt = montmorillonite, Ch = chlorite, V = vermiculite, K = kaolinite, I = illite,
 Q = quartz)

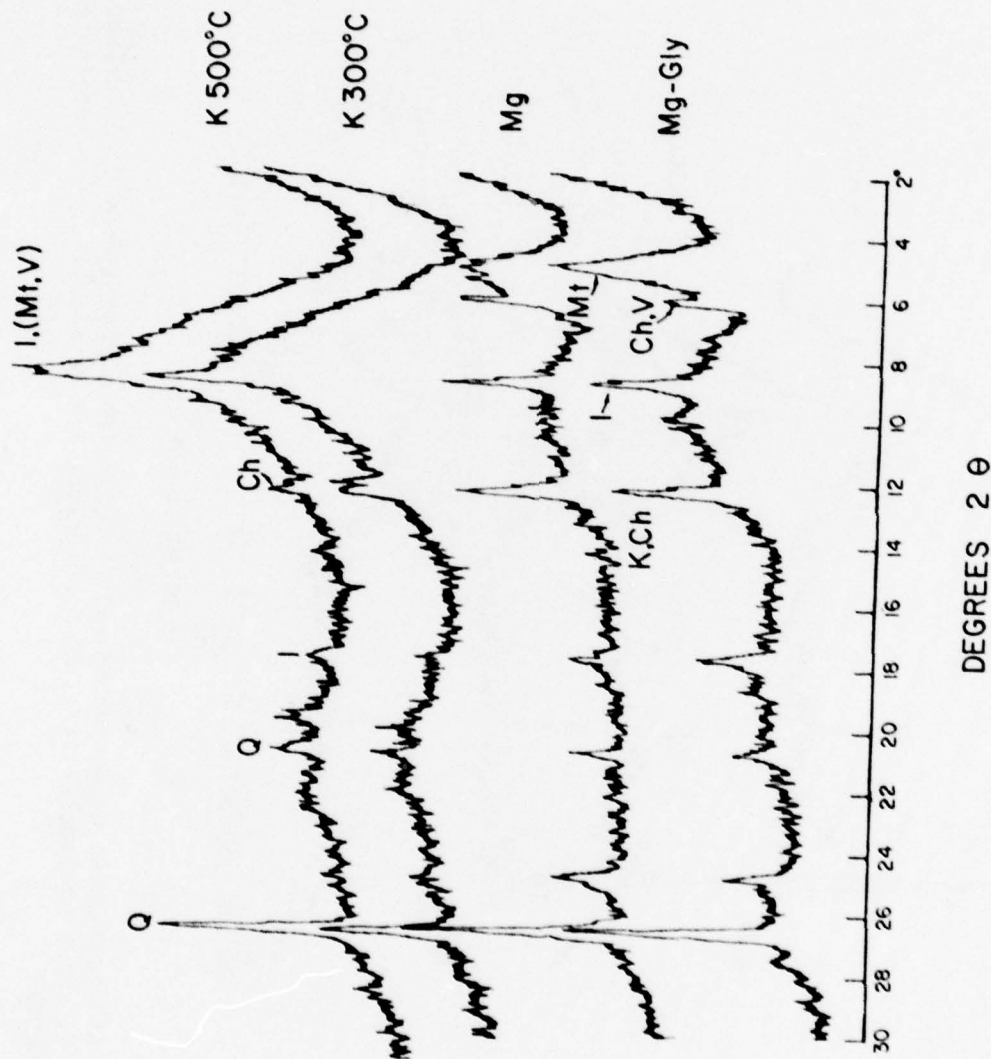


Figure 38. X-ray diffractograms of suspended matter collected during a Buoy C, 23-cm/sec depositional run (Legend: Mt = montmorillonite, Ch = chlorite, V = vermiculite, K = kaolinite, I = illite, Q = quartz)

90. Estimates of the relative percentages of the clay minerals were calculated using the peak height method described by Scafe (1968). The illite peak (10 \AA) was utilized as the internal standard in the computations. The relative percentage of the clay minerals for the less than 2- μm fraction of the two samples are presented in the following tabulation:

| Run No. | Composition % | | | |
|------------|---------------|------------------------|-----------------|--------------------------|
| | Illite | Kaolinite- Chlorite | Montmorillonite | Chlorite- Vermiculite |
| 4 | 59 | 23 | 15 | 3 |
| 5 | 58 | 21 | 17 | 4 |

As shown, illite exhibited the highest percent composition in the samples followed by kaolinite-chlorite, montmorillonite, and chlorite-vermiculite in decreasing order of abundance. Cool (1976) reported high illite percentages in both suspended matter and bottom sediment samples collected from the offshore disposal site. He suggested that the source of this illite was the Pleistocene Beaumont Clay Formation that is subaerially exposed along portions of the Galveston Ship Channel. Thus, scour of Buoy C sediment, which presumably was dredged from the entrance channel, resulted in an expected high illite content in the two washload samples.

Summary

91. Laboratory flume experiments performed on the four sediment mixtures indicated:

- a. Each of the four sediment mixtures eroded similarly as evidenced by the similar shape of the scour curves and a similar critical shear stress value (≈ 1.0 dyne /cm²) necessary to cause both massive bedload transport and rapid TSM concentration increases.
- b. Primary silt and clay resuspension occurred during the discharge process and the initial 2 to 3 hr immediately following each current speed increase.
- c. The winnowing of silts and clays from the bed by erosion resulted in a textural coarsening of the bed surface. Continuous scour over a hydrodynamically rough bed produced texturally diverse sediment interfaces within the sediment column.
- d. Rapid deposition of suspended fine silts and clays occurred at bed shears less than approximately 0.2 dyne /cm² for initial TSM concentrations exceeding about 100 mg/l.
- e. Fine silt and clay comprised the bulk of suspension produced by scour. The washload grain-size distribution depended primarily upon the competency of a given flow. An increase or decrease in the silt mode of the distribution occurred with an increase or decrease in the flow rate.
- f. Illite was the primary clay component produced by scour of Buoy C dredged material.

Hydrography of Offshore Galveston

Tide regime

92. Tide readings obtained from the U.S. Army Engineer District, Galveston, were recorded at the south jetty lighthouse of the Galveston Bay entrance channel. These readings consisted of continuous strip chart records taken from February 1975 through 1 May 1976. Normal tides ranged from 0.3 to 0.6 m in height, and were mixed (i.e., diurnal and semidiurnal in frequency). Figure 39 illustrates a typical mixed tide cycle for the period 7 through 21 July 1975.

93. Adverse meteorological conditions were found to alter tide heights. Hourly wind speed and direction data for the time period February 1975 through May 1976 were obtained from the Galveston Weather Bureau. Examination of both tide and meteorologic data revealed that primary storm wind azimuths affecting tide heights include (1) strong persistent east, southeast, or south winds blowing across the Gulf of Mexico for several days and (2) strong persistent north to northwest winds following the passage of a cold front. In the first instance, tides up to 0.9 m above normal were observed, while in the second case, tides up to 0.6 m below normal were recorded. Figures 40 and 41 illustrate occurrences of these two phenomena. It is presumed that strong, long-duration southerly winds pile surface water onto the coast resulting in a measureable sea level increase, whereas strong northerly winds push water seaward causing a sea level decrease.

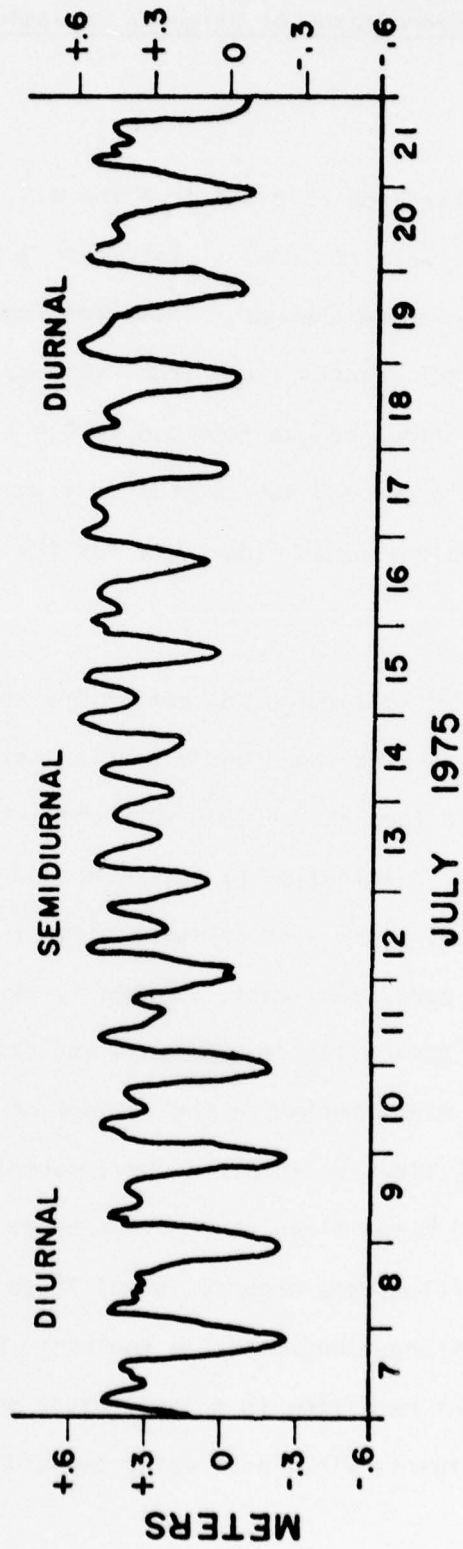


Figure 39. Example of mixed tide cycle for 7 through 21 July 1975



Figure 40. Observed versus predicted tide cycle during sustained southeasterly winds for the period 14 through 20 April 1976. (Predicted times of high and low tide were obtained from U.S. Dept. of Commerce 1976)

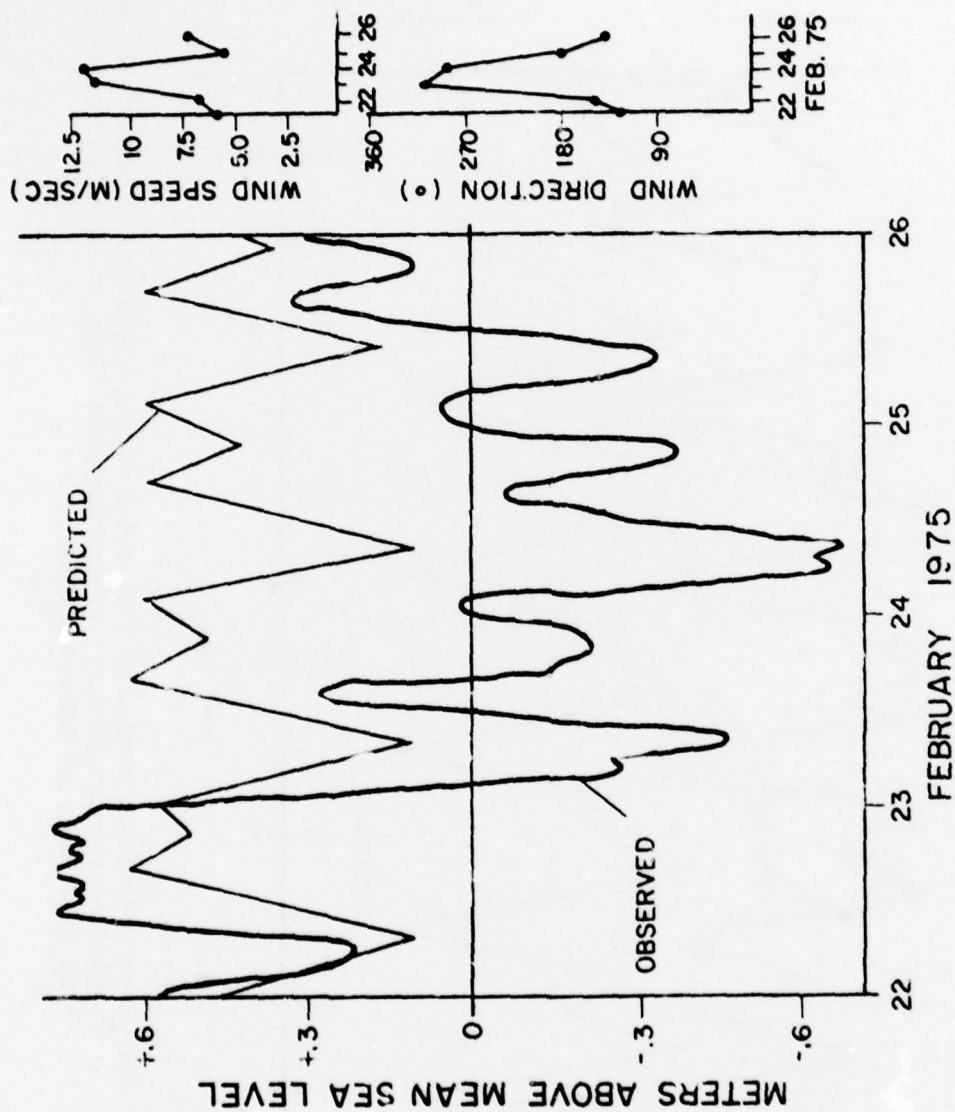


Figure 41. Observed versus predicted tide cycle during strong northwesterly winds for the period 22 through 25 February 1975

Current data

94. Numerous velocity profiles and bottom current measurements were recorded to ascertain the circulation pattern within the study area. Table 1 lists the type, location, date, and time period of the current meter data recovered. Data on the tidal currents passing through the entrance channel were discussed by Hall (1976).

Velocity profiles

95. Velocity profiles obtained by Hall (1976) at Buoy B, located within the entrance channel, indicated that current speed and direction are controlled by the cyclic passage of tidal currents through the inlet. Measured flood and ebb tide current velocities in excess of 100 cm/sec were recorded during normal tide cycles within the entrance channel. In contrast, velocity profiles taken near Buoys B, C, and D indicate maximum current velocities of only 75 cm/sec.

96. Vertical profiles were made at 2-hr intervals during a 24-hr anchor station at Buoy C on 1 - 2 May 1976 (during a diurnal tide). Figures 42 through 44 illustrate a succession of six profiles recorded at 2000, 2200, and 2400 hr 1 May and 0200, 0400, and 0600 hr 2 May. Three important results were gained from an evaluation of these profiles. First, the speed and direction of the currents in the upper half of the water column are coincident with entrance channel tidal currents. Second, a northeasterly-directed bottom flow persisted throughout the observation period. Third, the near-bottom sampling points in each profile suggest either a shear zone between the near-bottom and upper water column currents or a flow reversal near the bed.

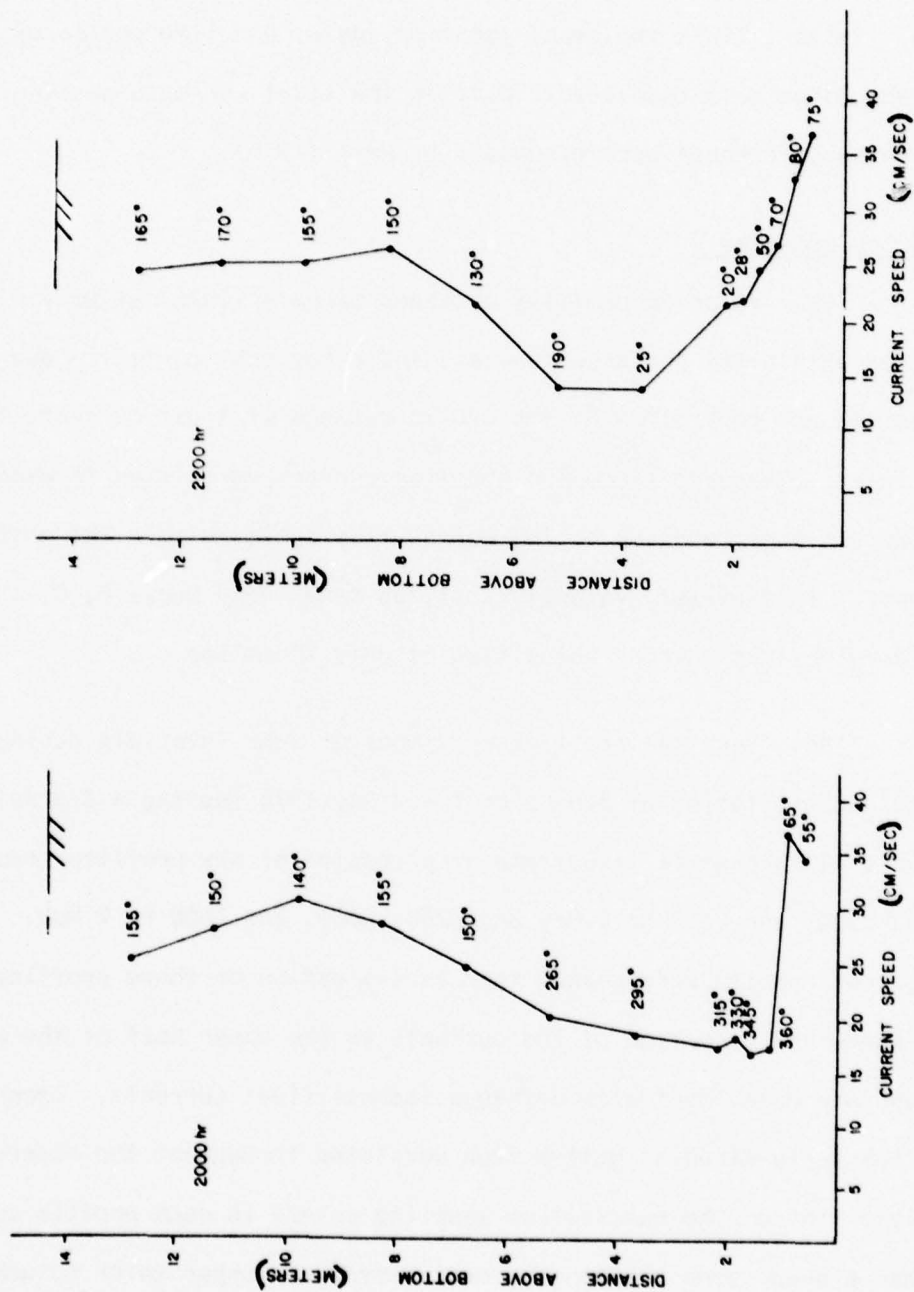


Figure 42. Vertical profiles taken at 2-hr intervals obtained at Buoy C, 1 May 1976 (current direction is in degrees magnetic north)

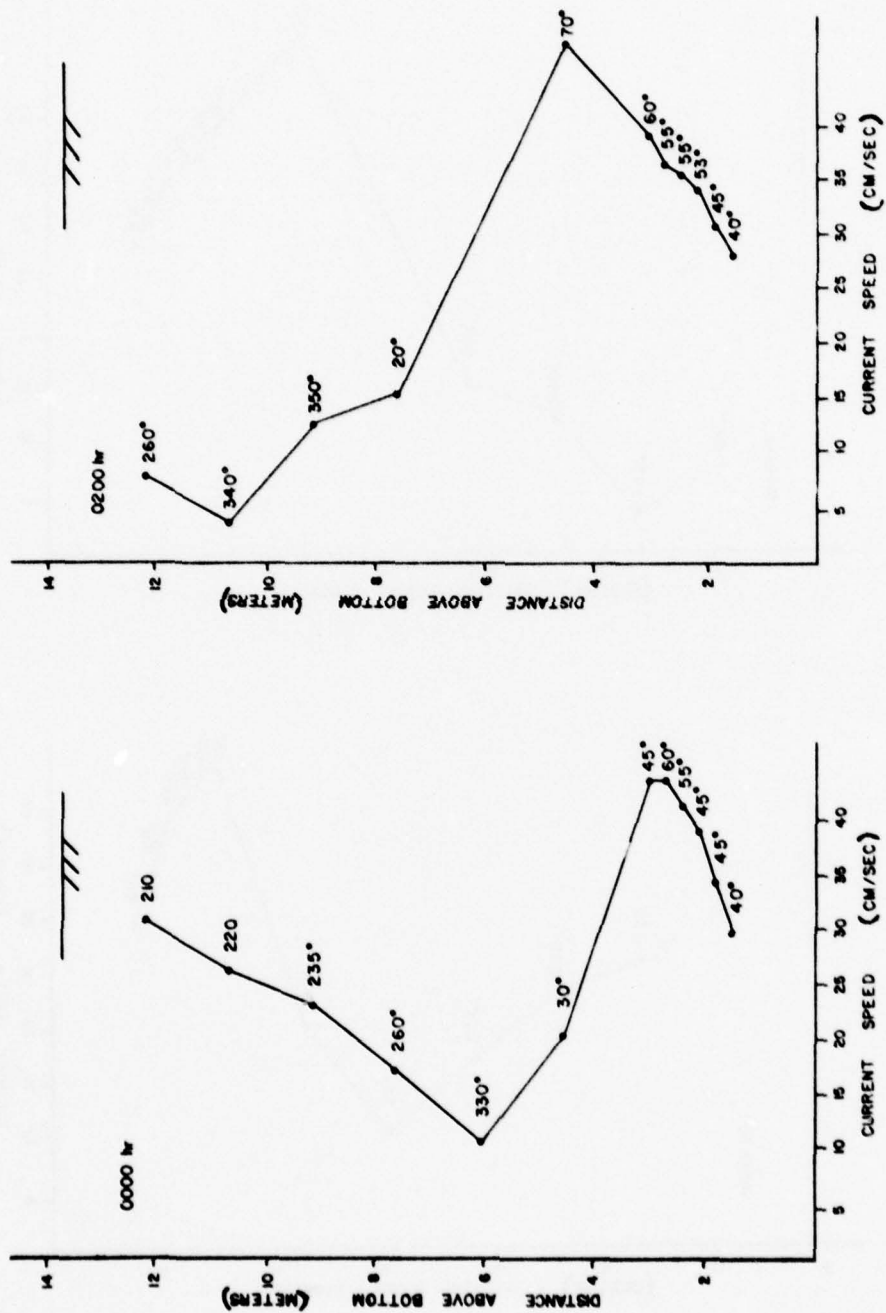


Figure 43. Vertical profiles taken at 2-hr intervals obtained at Buoy C, 1 and 2 May 1976 (current direction is in degrees magnetic north)

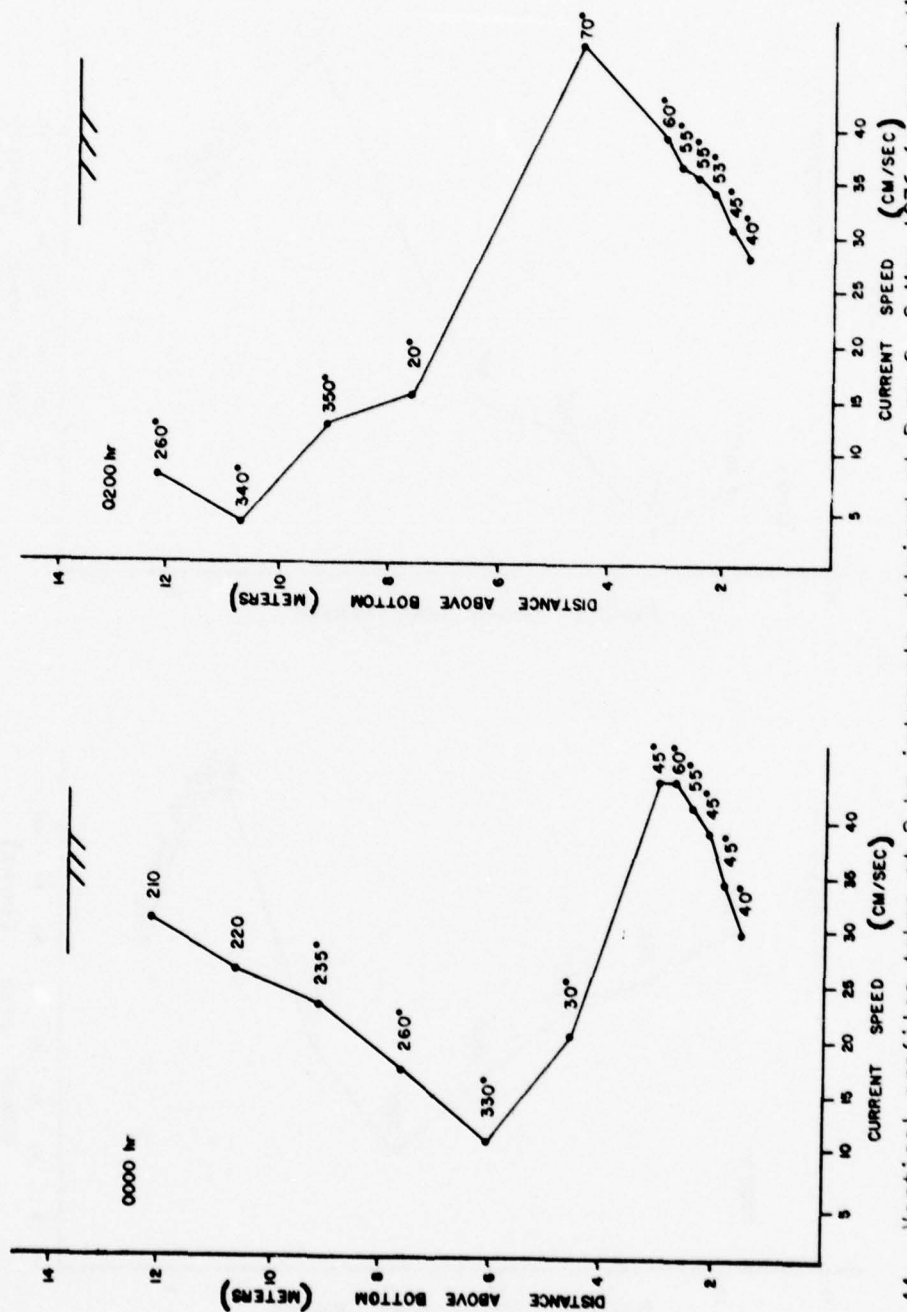


Figure 44. Vertical profiles taken at 2-hr intervals obtained at Buoy C, 2 May 1976 (current direction is in degrees magnetic north)

97. The time of slack water at the south jetty lighthouse (on the entrance channel) occurred at 0200 hr, 2 May 1976, with ebb tide preceding and flood tide following. Figures 42 and 43 show the southerly directed, near-surface ebb flows prior to slack water development. Between 2400 hr and 0200 hr, a sharp decrease (from 30 to 7 cm/sec) in near-surface flow speed occurred which corresponded to slack water during mean low tide (Figure 43). Later, a north-northeasterly flood-directed surface current was initiated as illustrated in Figure 44. Maximum and minimum near-surface flow speeds varied with the entrance channel tidal range, as did the surface current direction. Also, during this 24-hr observation period, sustained 5-m/sec southeasterly winds occurred. Such onshore-directed winds account for the clockwise deflection of the near-surface current direction with depth due to Ekman drift (from Ekman 1905).

98. In order to compare current speed fluctuations during a tidal cycle, a plot of flow velocity at various depths versus time was made using the profiles collected from 1400 hr 1 May to 1400 hr 2 May 1976 at Buoy C. This graph is depicted in Figure 45. Vertical lines of demarcation indicate predicted times of slack water for the entrance channel as listed in U.S. Dept. of Commerce, "Tidal Current Tables 1976." As shown, high-speed surface ebb currents are coupled with low-speed ebb flows lower in the water column. Conversely, flood-directed currents exhibit greater velocities near the bottom than at the surface. Also, the time of flood current commencement near the seabed precedes that in the upper water column. This suggests that a flood-tide underflow occurred near the bottom. Ludwick (1974) also observed such underflows within the tidal entrance to

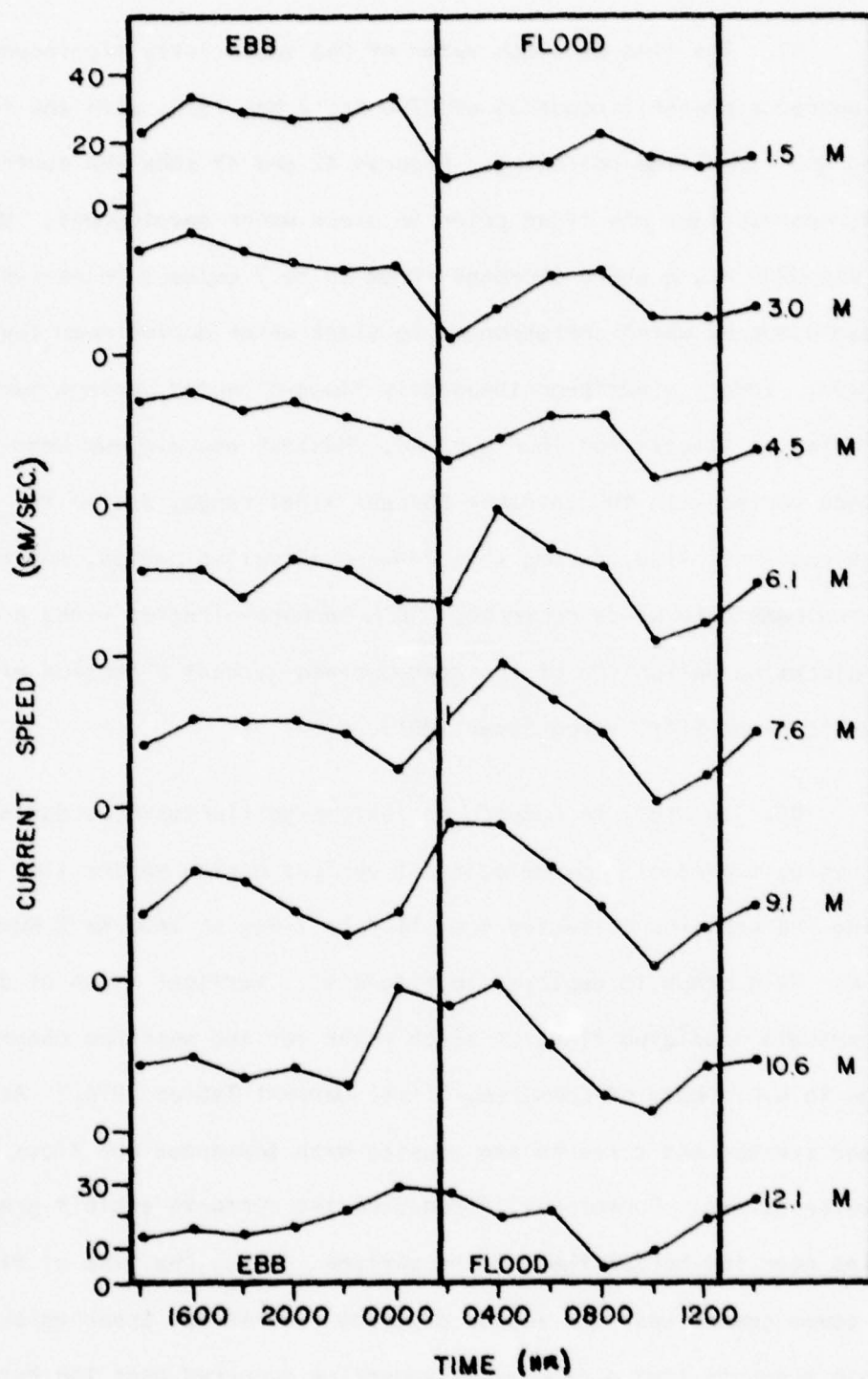


Figure 45. Flow velocity at various depths versus time for the period 1400 hr 1 May to 1400 hr 2 May 1976 at Buoy C

Chesapeake Bay, Virginia.

99. Typical velocity profiles obtained near Buoy B and Buoy D are shown in Figures 46 and 47. The profile recorded at Buoy B at 1055 hr 9 April 1976 exhibits current velocities and directions that are concurrent with an ebb flow from Galveston Bay. The Buoy D profile illustrated in Figure 47 indicates an ebb-directed surface flow and a flood-directed bottom flow. This apparent flow reversal demonstrates the spatial and temporal dissimilarity between upper and lower water column currents near the southern margin of the study area. In contrast, profiles taken near Buoy B (northern margin) suggest uniformity between upper and lower flows. This may be explained by the close proximity (3.2 km) of the Buoy B station to the entrance channel, where tide currents may regulate the entire water column.

Offshore tidal current circulation pattern

100. The tidal current regime exhibited by the Buoy B, C, and D velocity profiles is consistent with the general circulation pattern described by Hall (1976). Figure 48 illustrates the flow pattern developed during flood tide at the entrance channel. The greatest current speeds and subsequent water transport occur within the entrance channel. Flood tide currents in the study area are typically oriented east-northeast. Figure 49 illustrates the ebb-flow circulation pattern. In this case, seaward-moving waters are deflected toward the southwest by prevailing southeasterly winds and the Coriolis force (Hall 1976). Thus, near-surface ebb tidal flows travel southwest or down coast parallel to Galveston Island.

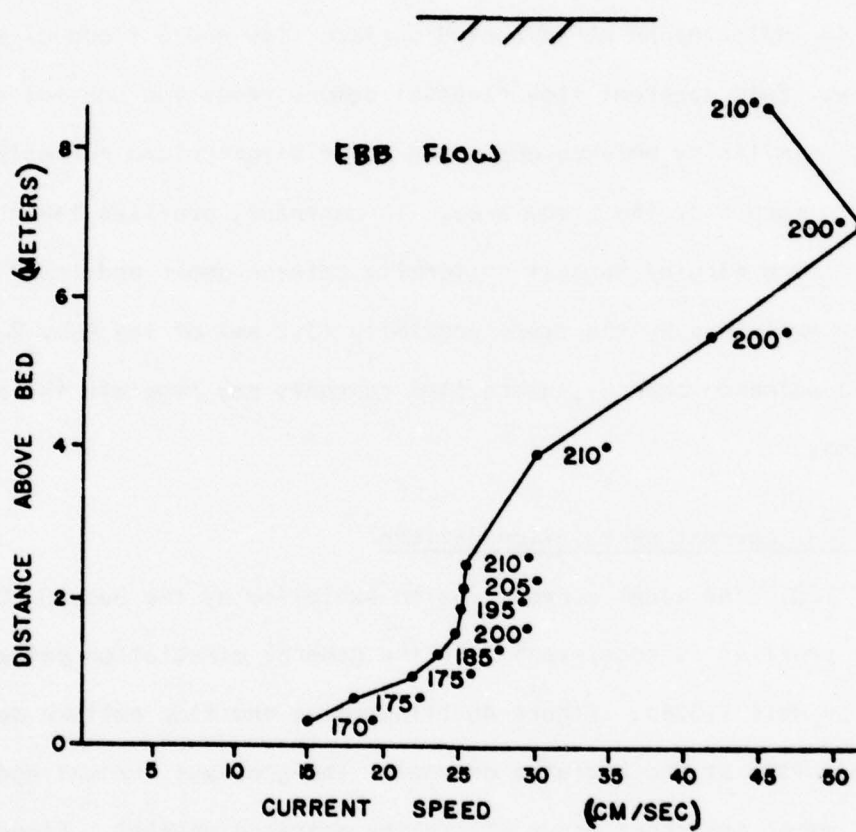


Figure 46. Velocity profile obtained at Buoy B, 1055 hr, 9 April 1976 (current direction is in degrees magnetic north)

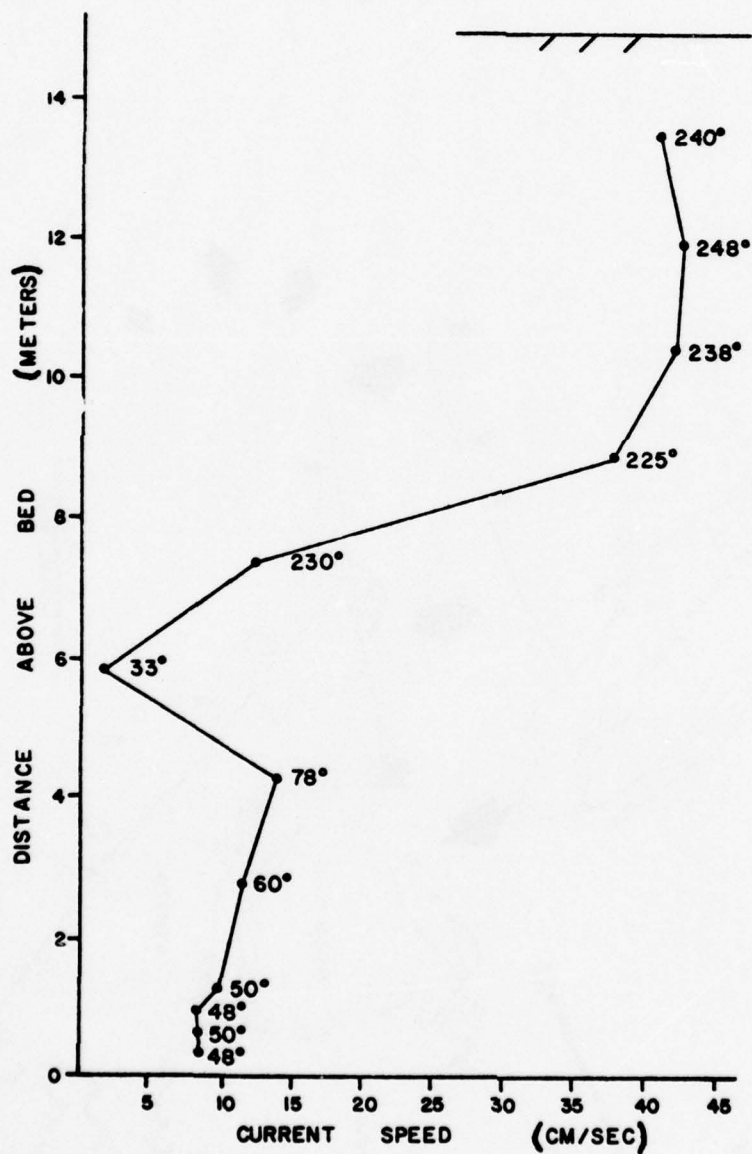


Figure 47. Velocity profile obtained at Buoy D, 1245 hr, 8 April 1976 (current direction is in degrees magnetic north)

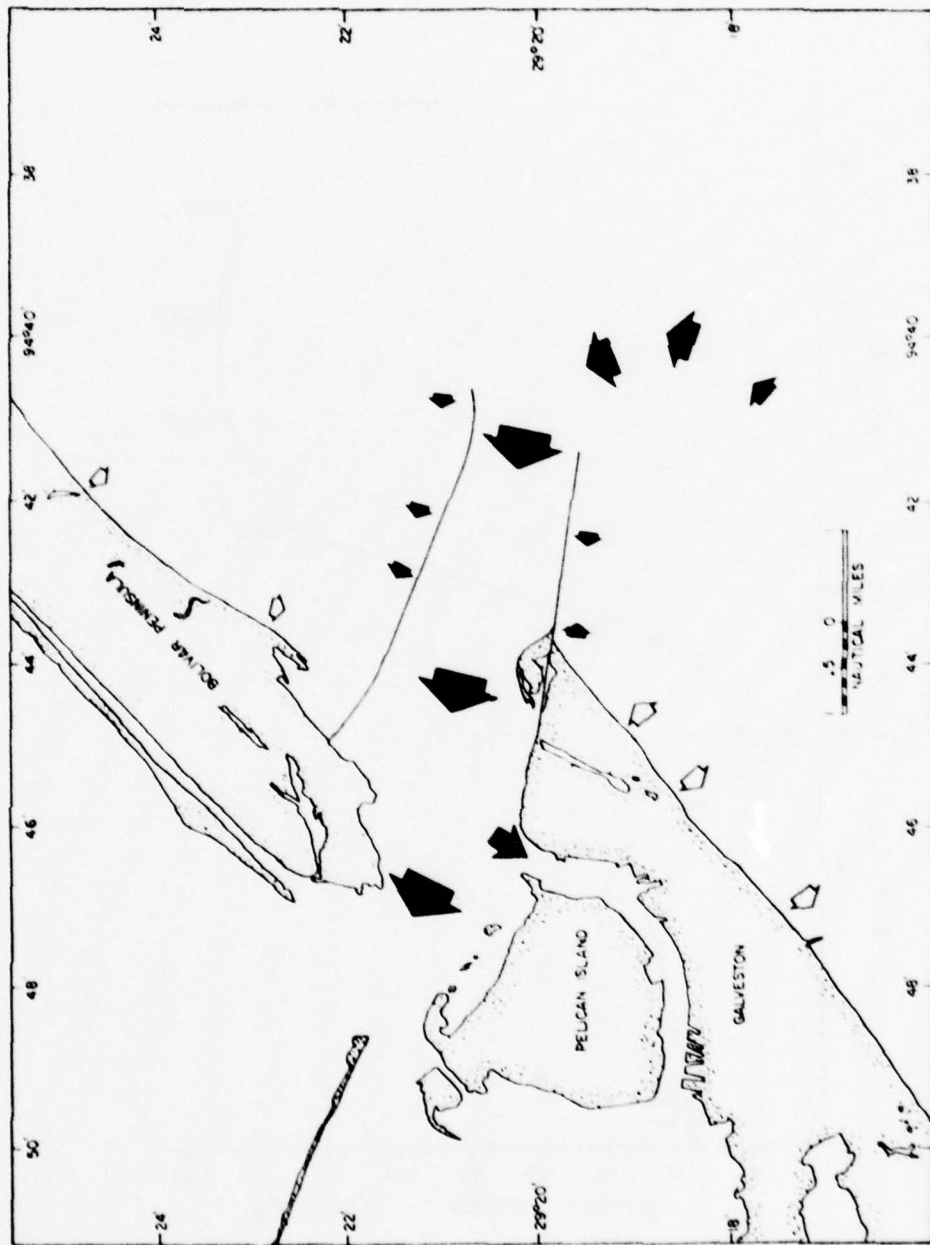


Figure 48. Rotary offshore flow pattern developed during flood tide at Galveston Bay entrance channel (from Hall 1976)

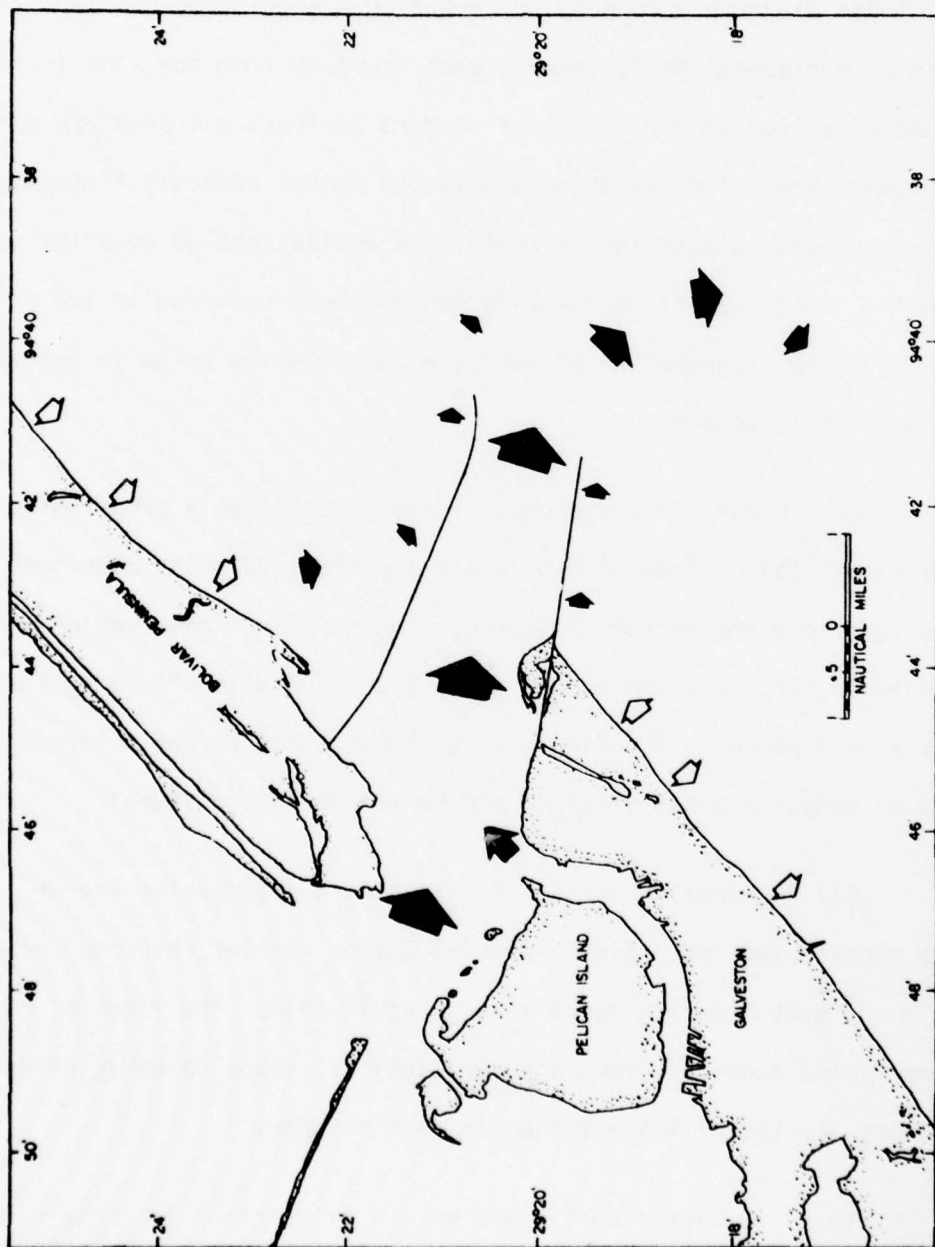


Figure 49. Rotary offshore flow pattern developed during ebb tide at the Galveston Bay entrance channel (from Hall 1976)

Progressive vector diagrams

101. To evaluate the bottom current circulation pattern operative in the field area, progressive vector diagrams were prepared from the continuous bottom current measurements recorded at Buoy B and Buoy D. These diagrams were made by computing a succession of time integrals of horizontal measurements, each starting from the same initial time. Hence, a plot of the resultant vectors portrays a trajectory with spatial dimensions. True water mass movement is not actually illustrated by the vector path, unless the currents lack spatial change over the scale of the path. Such spatial homogeneity has not been observed in the field area; thus, these diagrams are primarily of qualitative value in assessing net bottom water movement.

102. Figure 50 (after Hall 1976) illustrates a progressive vector diagram plotted from 15-min interval current velocity measurements recorded 1.0 m off the bottom at Buoy D. The period of observation extends from 9 October through 14 November 1975. Each plus sign (+) marks the start of a 6-hr period. Assuming spatial homogeneity of the bottom currents, Hall (1976) computed a net drift of 260 km toward the southwest.

103. Figures 51 through 54 illustrate progressive vector diagrams constructed from 15-min interval bottom current readings recorded at Buoy B and Buoy D during March through April 1976. The times of observation for these plots are tabulated in Table 1. Also, calendar dates are marked along the vector trajectories in each diagram.

104. Two significant features are illustrated in these diagrams:

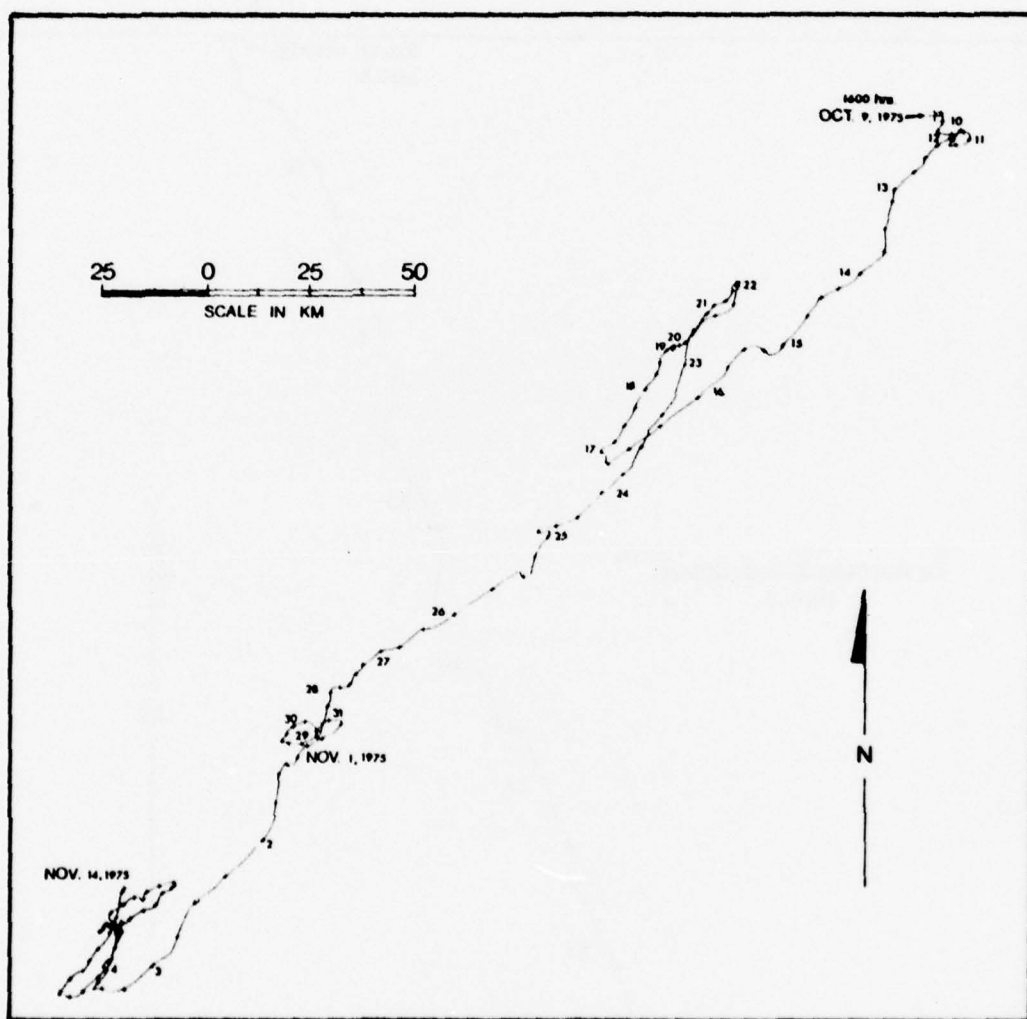


Figure 50. Progressive vector diagram for 9 October through 14 November 1975 at Buoy D

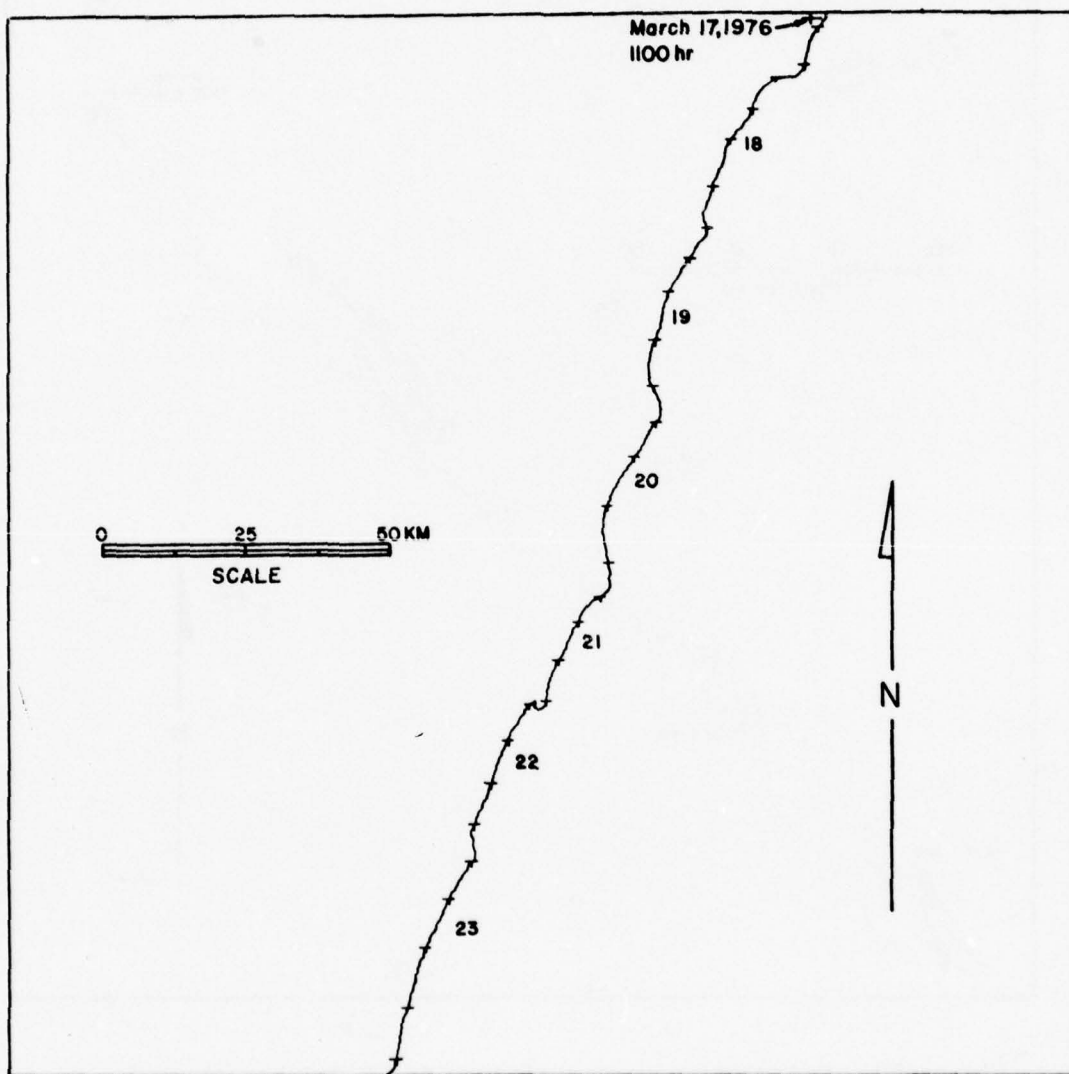


Figure 51. Progressive vector diagram for 17 March through 23 March 1976 at Buoy B

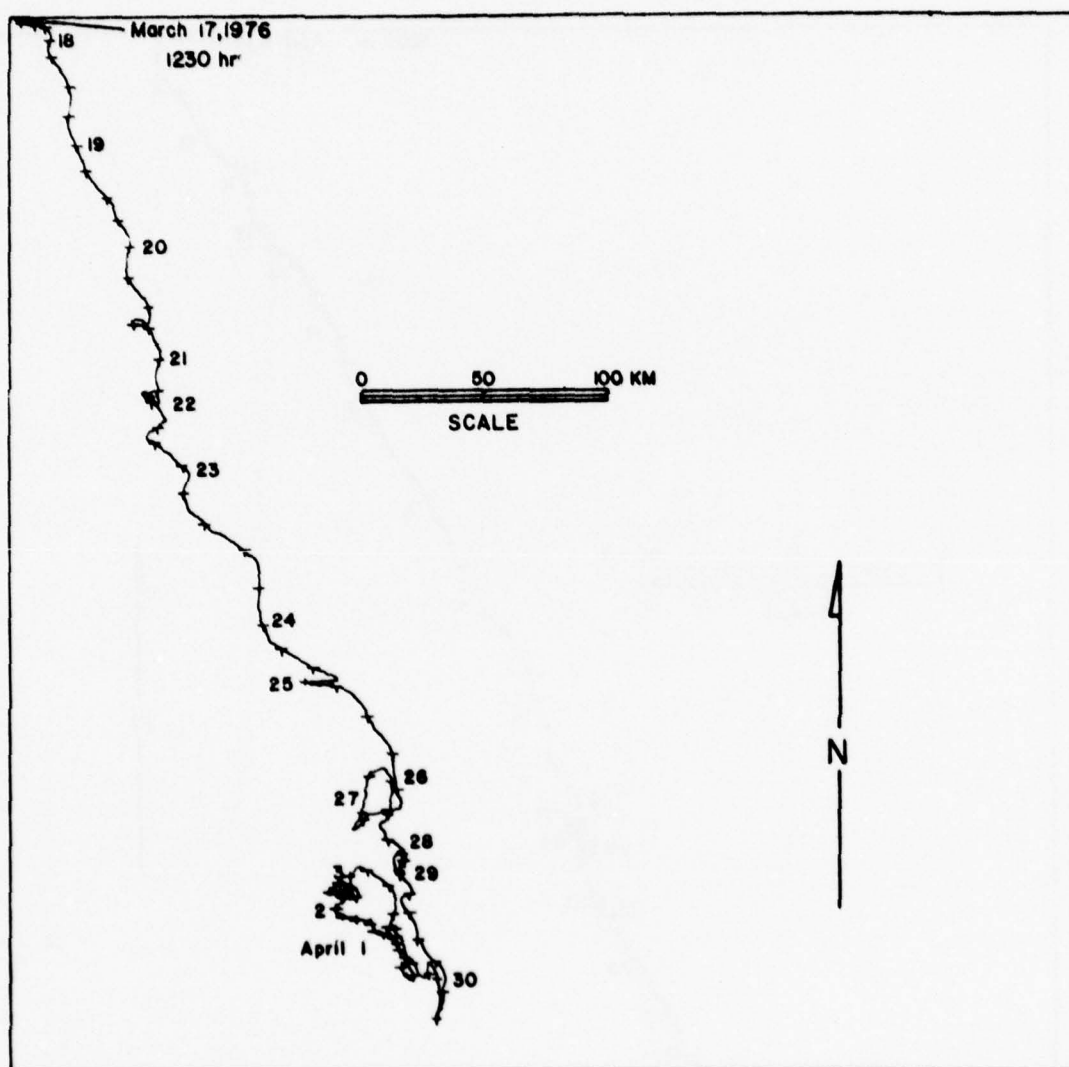


Figure 52. Progressive vector diagram for 17 March through 7 April 1976 at Buoy D

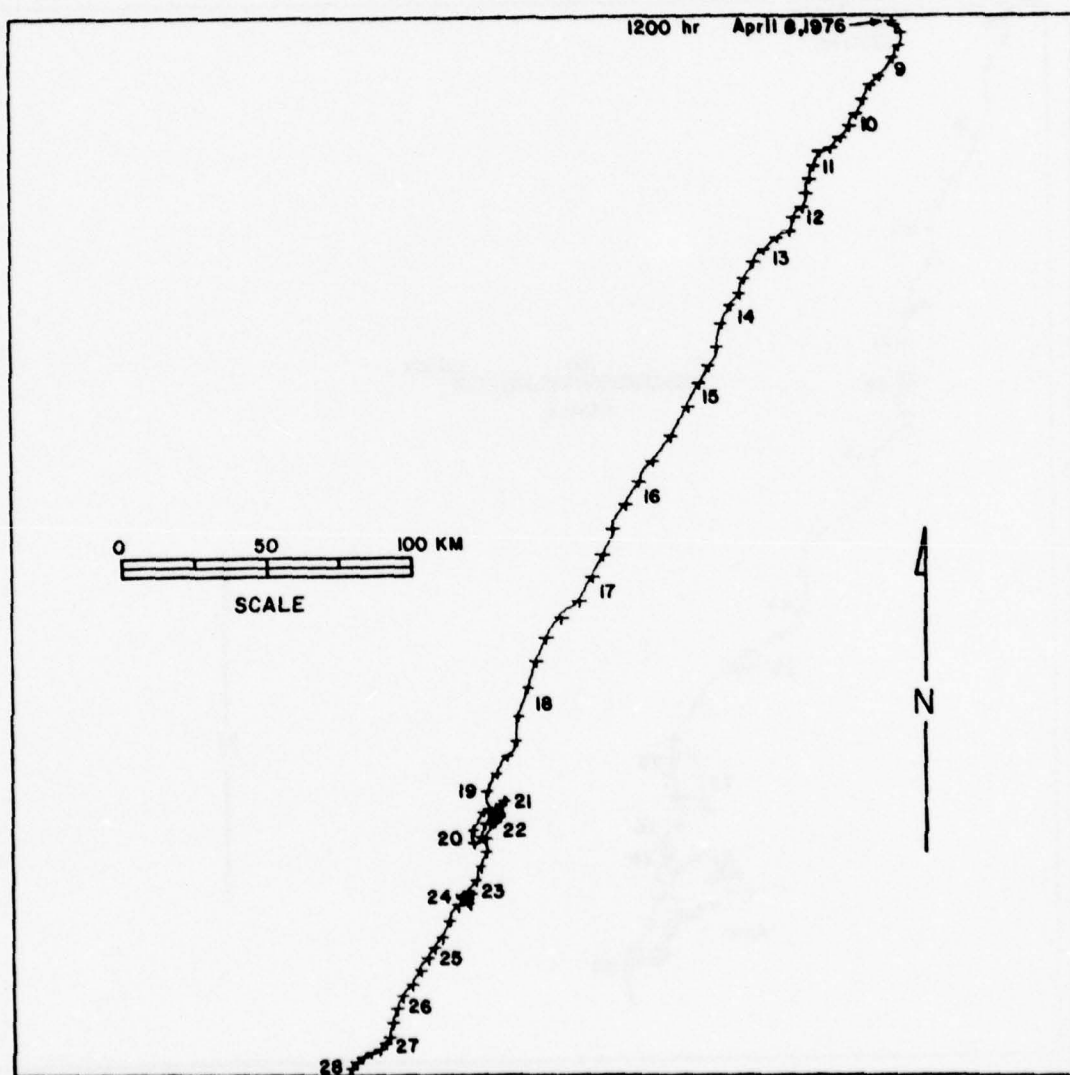


Figure 53. Progressive vector diagram for 8 April through
30 April 1976 at Buoy B
122

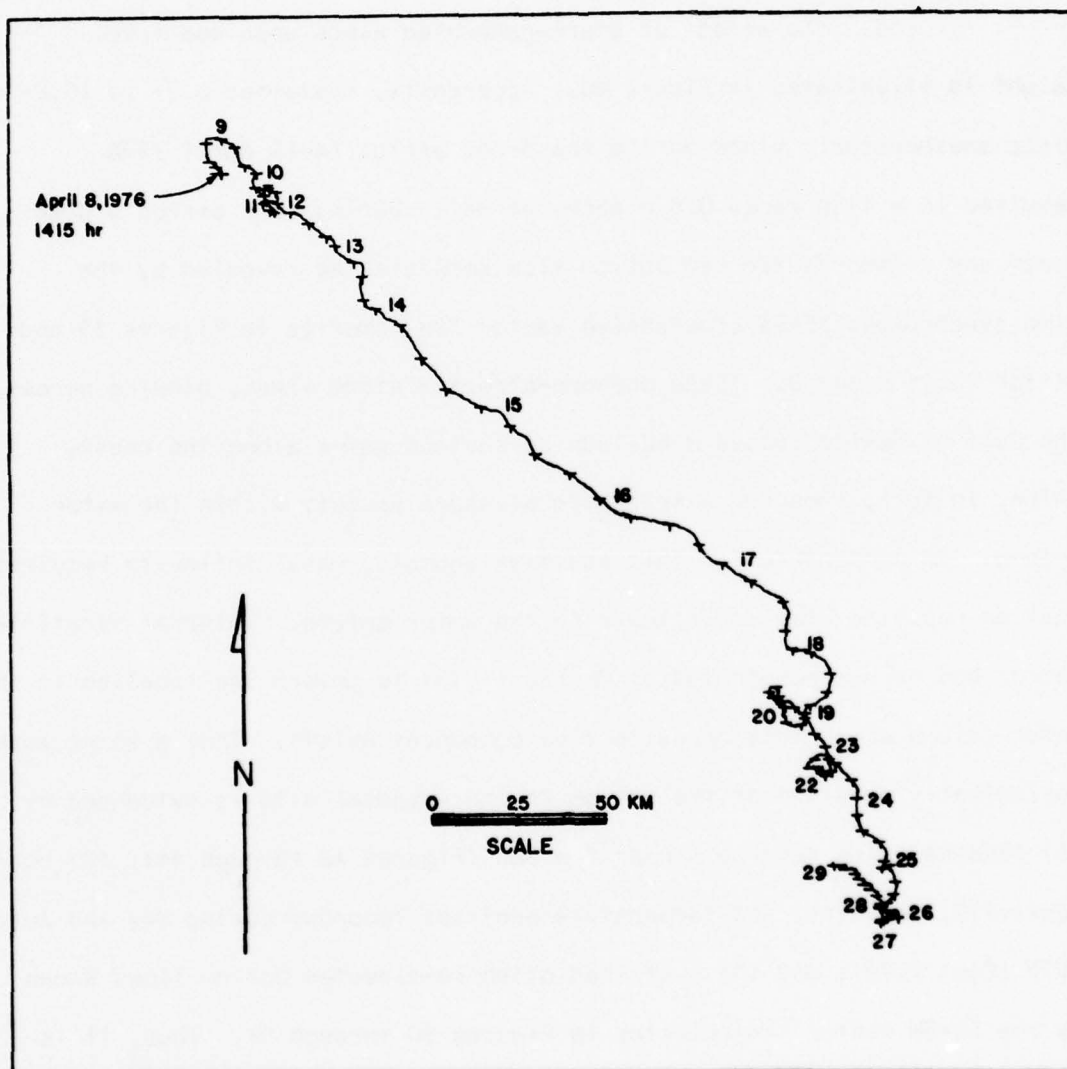


Figure 54. Progressive vector diagram for 8 April through 3 May 1976 at Buoy D

(1) persistent down-coast or offshore-directed (SW or SE) vector trajectories and (2) intermittent loops. The latter may represent the flow reversals influenced by flood and/or ebb tidal currents, while the former signify the occurrence of onshore-directed storm winds. Examples of these two phenomena follow.

105. The effect of storm-generated winds upon sea level height is illustrated in Figure 40. Apparently, sustained 6.0- to 10.0-m/sec southeasterly winds during the 5-day period 14-19 April 1976 resulted in a tide range 0.6 m above normal. During this period a down-coast and offshore-directed bottom flow persisted as revealed by the time synchronous SE-SW progressive vector trajectories in Figures 53 and 54 for Buoys B and D. These onshore-directed storm winds, blowing across the Gulf of Mexico caused a buildup of surface water along the coast, which, in turn, produced a nearshore pressure anomaly within the water column. To compensate for this positive anomaly, mass continuity requires that an opposing flow occur lower in the water column. Internal stratification has been demonstrated by Murray (1975) to govern the location in the water column where this opposite flow component exists. That a shear zone periodically exists near the bottom in the disposal site is evidenced by (1) observed flow reversals near the bed (Figures 42 through 44); (2) conductivity, salinity, and temperature profiles recorded during May and July 1975 (Cool 1976); and (3) sustained offshore-directed bottom flows shown by the SE-SW vector trajectories in Figures 50 through 54. Thus, it is hypothesized on the basis of these data that a two-layer nearshore circulation pattern forms during the passage of onshore-directed storm winds;

that is, persistent southeasterly winds exceeding about 5 m/sec cause onshore flow at the surface and stable down-coast to offshore currents near the bottom.

106. Another example of this phenomena is illustrated by the time-synchronous wind and bottom current vectors plotted as stick diagrams in Figure 55. The period of observation extended from 4 May through 8 May 1976. Both wind and current azimuths are oriented toward the direction of traverse. The bottom current vectors represent discrete 2-hr interval current speed and direction (true north) measurements recorded at Buoy B and Buoy D 1 m above the bottom. Note that a N-NE to S-SW bottom current reversal occurred at both stations during 5 May. On this same day, a 0.2-m positive tide anomaly was initiated as shown by the observed versus predicted tide cycle diagram in Figure 56. Sustained 5- to 10-m/sec southeasterly winds that occurred during 5 May (see wind vector plot, Fig. 55) probably induced this anomaly via the mechanism previously cited. In addition, note that the tide anomaly continued for the duration of the observation period as did the offshore-directed bottom currents. The 50° to 90° offset between the simultaneous bottom current directions displayed at Buoys B and D may be attributable to topographic effects created by dredged material mounding adjacent to the buoys or perhaps to a rotary bottom flow pattern indigenous to the area. Further hydrographic reconnaissance is required to explain such variations. The important point is that positive tide anomalies produced by onshore-directed storm winds in excess of about 5 m/sec generate relatively steady down-coast to offshore-directed bottom flows.

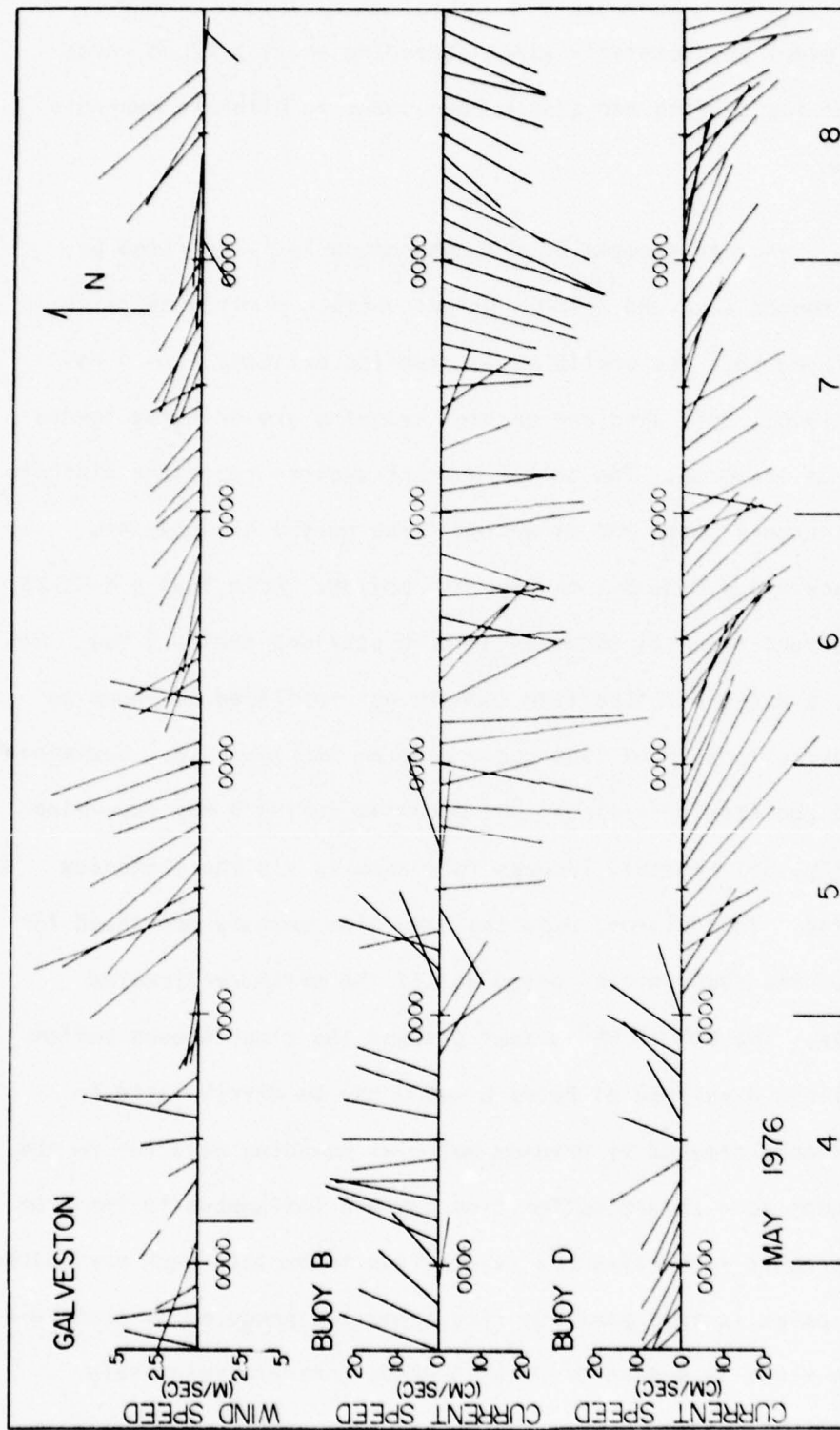


Figure 55. Stick diagrams of (a) surface wind speed and direction and (b) bottom current speed and direction for 4 through 8 May 1976

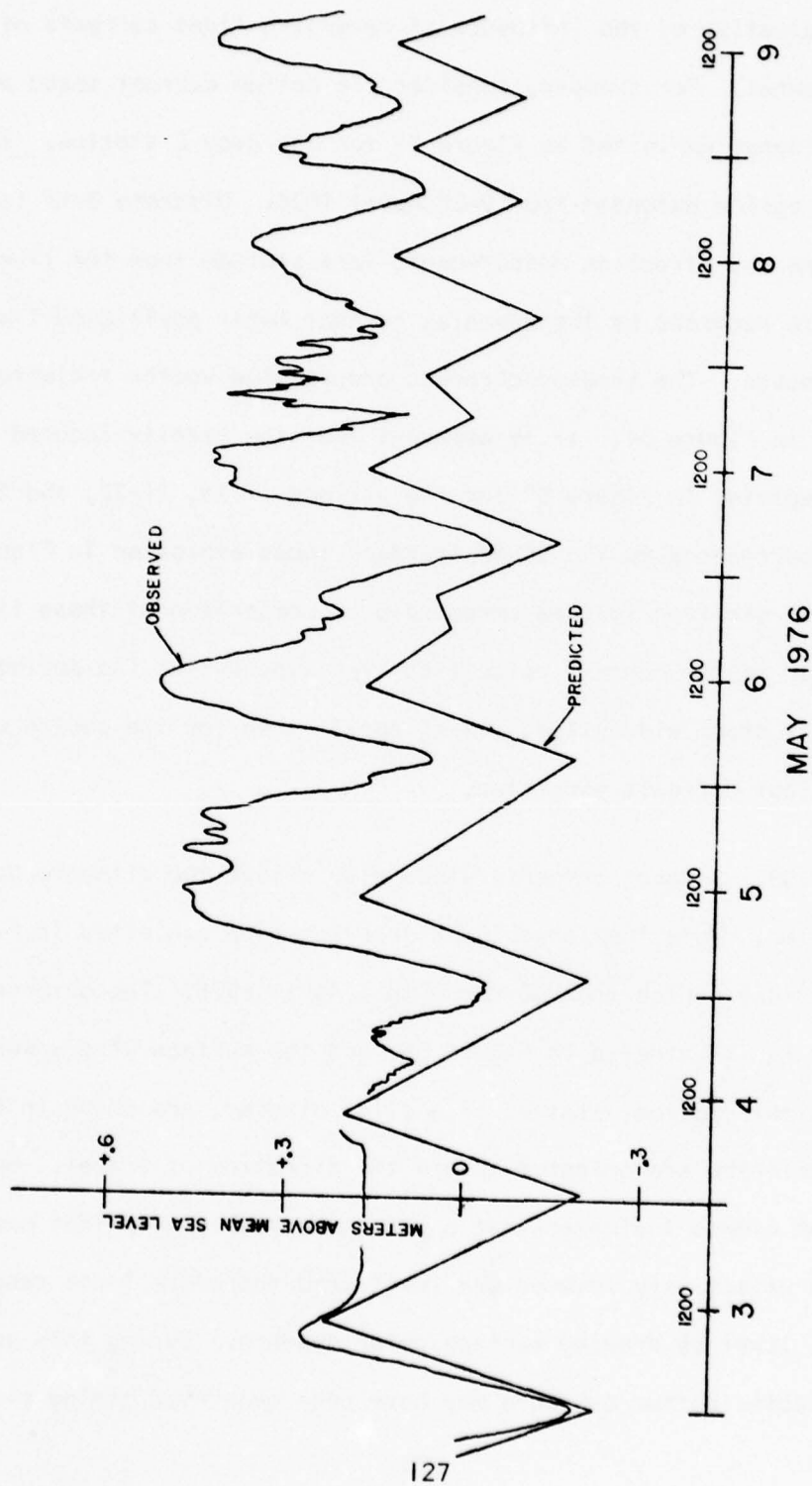


Figure 56. Observed versus predicted tidal cycle for 3 through 9 May 1976

107. The loops displayed in the vector trajectories are presumed indicative of the influence of reversing tidal currents of the entrance channel. For example, consider the bottom current speed and direction diagram exhibited in Figure 57 for the Buoy D station. The observation period extended from 9-26 April 1976. Discrete 3-hr interval current speed and direction measurements were plotted from the 15-min interval data recorded by the Savonius current meter positioned 1 m above the seabed. The time-synchronous progressive vector trajectory is illustrated in Figure 54. It is apparent that the tidally induced current reversals depicted in Figure 57 for the periods 11-13, 21-22, and 25 April 1976 correspond to the SE-SW trending loops exhibited in Figure 54. An additional striking feature revealed by a comparison of these figures is the higher bottom current velocities displayed during the period of southeasterly storm winds (i.e., 14-19 April) than for the period where reversing tidal currents persisted.

108. Strong northerly winds also affect the offshore bottom current regime. Note the large SE-NW trending loop exhibited in Figure 52 for the 5-day period from 30 March to 3 April 1976. The observed tidal cycle is illustrated in Figure 58, and the surface wind speed and azimuth for this period, plotted as a stick diagram, are shown in Figure 59. Wind azimuths are oriented toward the direction of travel. Reconstruction of events indicates that a strong northerly wind that occurred 30-31 March effectively lowered sea level (and therefore tidal range) to a normal level by drawing surface water seaward. During this process onshore-directed bottom currents may have been generated giving rise to

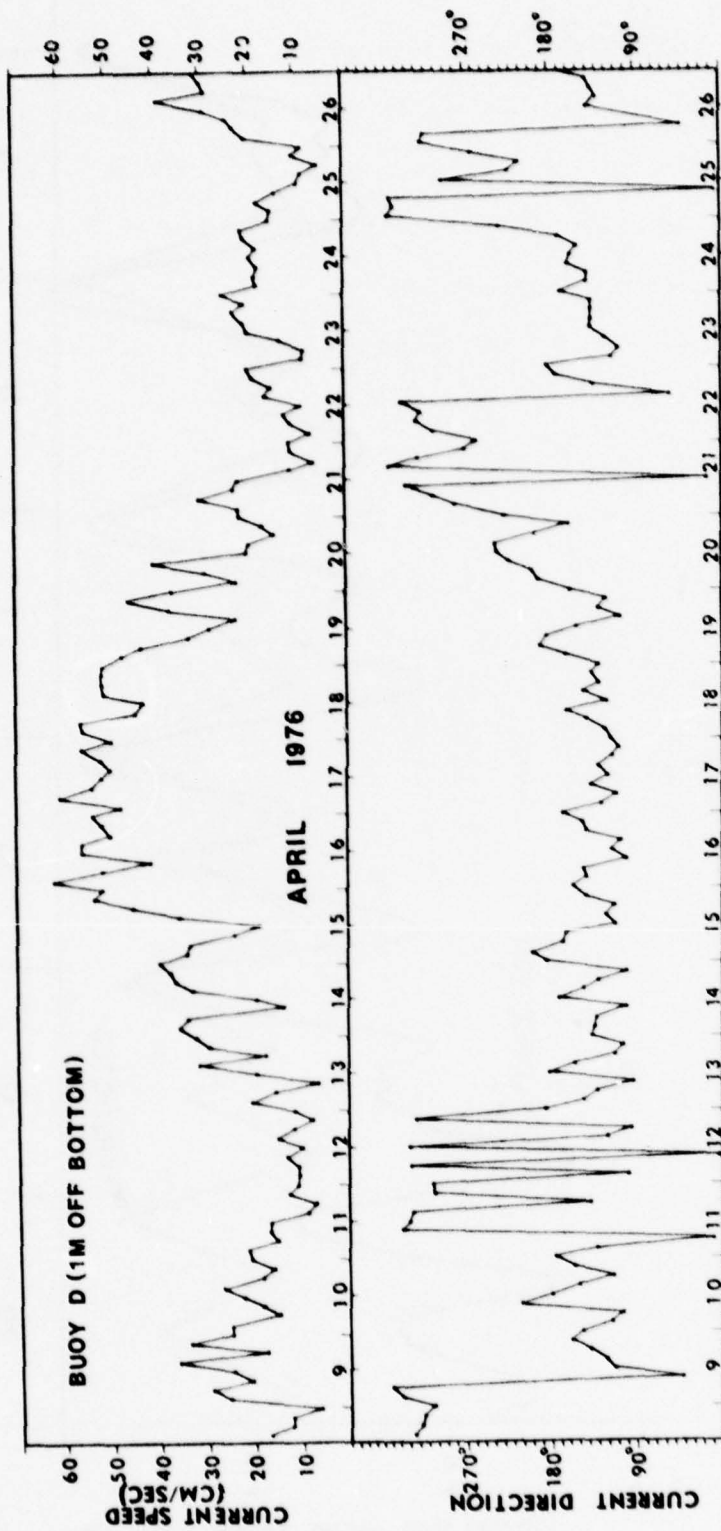


Figure 57. Bottom current speed and direction at Buoy D for 9 through 26 April 1976

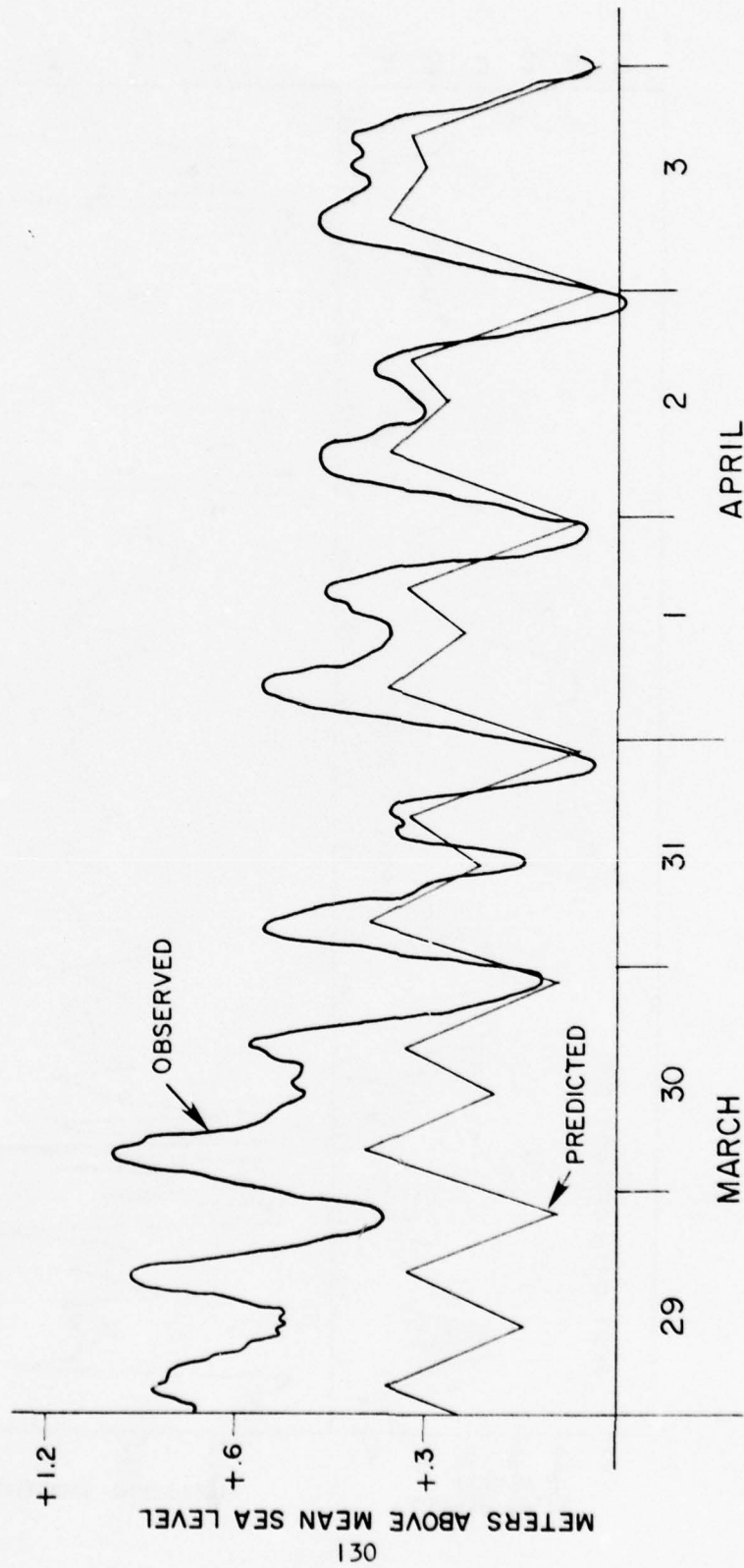


Figure 58. Observed versus predicted tidal cycle in the entrance channel for 29 March through 3 April 1976

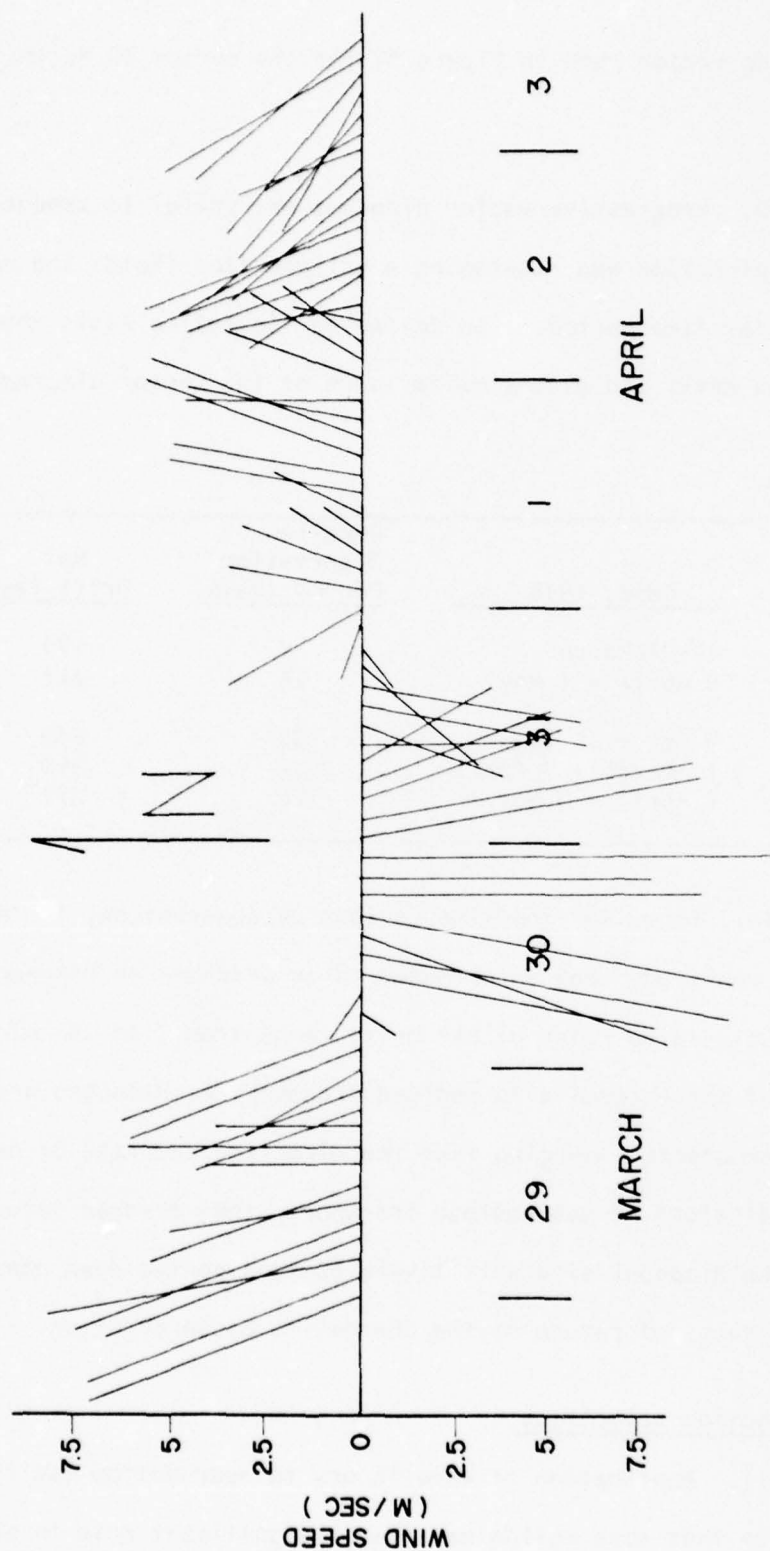


Figure 59. Stick diagram of wind speed and azimuth at Galveston for 29 March through 3 April 1976

the NW-trending vector path in Figure 52 for the period 30 March to 3 April.

109. Progressive vector diagrams are useful in assessing both the net flow direction and (assuming a uniform flow field) the net drift for a particular time period. The following tabulation lists the calculated net flow drift and direction for each of the vector diagrams illustrated:

| <u>Location</u> | <u>Date, 1976</u> | <u>Duration of Observation Period (Days)</u> | <u>Net Drift (km)</u> | <u>Net Direction</u> |
|-----------------|--------------------|--|---------------------------|--------------------------|
| Buoy B | 17-24 March | 7 | 195 | SW |
| | 8 April - 1 May | 24 | 417 | SW |
| Buoy D | 9 Oct - 14 Nov | 37 | 260 | SW |
| | 17 March - 7 April | 22 | 390 | SE |
| | 8 April - 3 May | 26 | 277 | SE |

110. Thus, for the time periods of observation, the net flow direction in the study area is oriented in an offshore or down-coast direction. Calculated rates of net drift range from 7 to 28 km/day. The implication of these results to bedload transport of disposed dredged material is apparent. Assuming that the direction and rate of net drift are valid indicators of net bedload transport, then dredged material located in the disposal site will likely be transported down coast or offshore and thus not return to the channel to cause shoaling.

Oscillatory bottom velocities

111. Application of wave theory to near-bottom oscillatory flow indicates that such motion may play a significant role in sediment

transport processes within the offshore dredged material disposal site. Surface waves produce an oscillatory motion which, near the bottom, reduce to a back-and-forth horizontal motion, the orbital diameter (d_o) such that:

$$d_o = H/\sin h(kh) \quad (16)$$

where (H) is the wave height, (h) is the water depth and (k) is the wave number that is equal to 2 divided by the wavelength (L_w). Wavelength is obtained by:

$$L_w = L_D \tanh(2h/L_D) \quad (17)$$

where (L_D), the deepwater wavelength, is equal to 1.56 multiplied by the square of the period in seconds. The maximum oscillatory bottom velocity (U_m) attained by this horizontal bottom motion is then:

$$U_m = d_o/T \quad (18)$$

where (T) is the wave period. The oscillatory bottom velocity can be predicted as a function of the depth of water and the wave height and period.

112. Unfortunately, wave height and period measurements in the study area were not logged during field operations. However, annual sea surface data were acquired from Tables 18-19 of "Summary of Synoptic Meteorological Observations," U.S. Naval Weather Command (1976). This information was compiled from marine surface observations made by ships in passage near Galveston. Tables 4-6 are based on a total of 12,139 observations made during the period 1963-1971. Table 4 shows the percentage of frequency of surface wind speed and direction versus sea height.

Table 4
Percent Frequency of Wind Speed
and Direction Versus Sea Height

| | Wind Speed, m/sec - % | | | | |
|------------------|-----------------------|----------------|-----------------|------------------|--------------|
| <u>Height, m</u> | <u>0.5-1.5</u> | <u>1.5-5.0</u> | <u>5.0-10.8</u> | <u>10.8-17.0</u> | <u>Total</u> |
| <u>North</u> | | | | | |
| .25 | 0.2 | 0.5 | | 0 | 0.7 |
| .25-.75 | 0.1 | 1.5 | 0.7 | 0 | 2.3 |
| .75-1.25 | | 0.9 | 2.0 | 0.2 | 3.1 |
| 1.25-1.75 | | 0.2 | 1.6 | 0.6 | 2.3 |
| 1.75-2.25 | 0 | | 0.8 | 0.6 | 1.5 |
| 2.25-2.75 | 0 | 0 | 0.3 | 0.4 | 0.7 |
| 2.75-3.25 | 0 | 0 | | 0.2 | 0.3 |
| 3.25-3.75 | 0 | 0 | 0 | 0.1 | 0.1 |
| 3.75-4.75 | 0 | 0 | | 0.1 | 0.1 |
| Total Percent | .3 | 3.1 | 5.4 | 2.2 | 11.2 |
| <u>Northeast</u> | | | | | |
| .25 | .2 | .7 | | .0 | .9 |
| .25-.75 | | 2.4 | .9 | .0 | 3.4 |
| .75-1.25 | | 1.3 | 3.0 | .1 | 4.4 |
| 1.25-1.75 | | .3 | 2.0 | .3 | 2.7 |
| 1.75-2.25 | .0 | | .6 | .4 | 1.0 |
| 2.25-2.75 | .0 | | .2 | .3 | .5 |
| 2.75-3.25 | .0 | .0 | | .1 | .2 |

Table 4 (continued)

| | Wind Speed, m/sec - % | | | | |
|------------------|-----------------------|---------|----------|-----------|-------|
| Height, m | 0.5-1.5 | 1.5-5.0 | 5.0-10.8 | 10.8-17.0 | Total |
| <u>Northeast</u> | | | | | |
| 3.25-3.75 | .0 | .0 | | .1 | .1 |
| 3.75-4.75 | .0 | .0 | .0 | | .1 |
| Total Percent | .2 | 4.8 | 6.8 | 1.4 | 13.3 |
| <u>East</u> | | | | | |
| .25 | .2 | 1.1 | | .0 | 1.3 |
| .25-.75 | .2 | 3.9 | 1.7 | .0 | 5.8 |
| .75-1.25 | | 2.4 | 4.0 | .2 | 6.5 |
| 1.25-1.75 | | .5 | 2.4 | .3 | 3.2 |
| 1.75-2.25 | .0 | .1 | .8 | .3 | 1.1 |
| 2.25-2.75 | .0 | | .2 | .2 | .4 |
| 2.75-3.25 | .0 | .0 | | .1 | .1 |
| 3.25-3.75 | .0 | .0 | | .1 | .1 |
| 3.75-4.75 | .0 | .0 | .0 | | |
| Total Percent | .4 | 7.9 | 9.1 | 1.0 | 18.5 |
| <u>Southeast</u> | | | | | |
| .25 | .3 | 1.5 | | .0 | 1.8 |
| .25-.75 | .1 | 4.8 | 2.4 | .0 | 7.4 |
| .75-1.25 | .1 | 3.0 | 5.7 | .2 | 9.0 |
| 1.25-1.75 | | .6 | 3.4 | .3 | 4.4 |

Table 4 (continued)

| | <u>Wind Speed, m/sec - %</u> | | | | |
|------------------|------------------------------|----------------|-----------------|------------------|--------------|
| <u>Height, m</u> | <u>0.5-1.5</u> | <u>1.5-5.0</u> | <u>5.0-10.8</u> | <u>10.8-17.0</u> | <u>Total</u> |
| <u>Southeast</u> | | | | | |
| 1.75-2.25 | | .1 | 1.1 | .3 | 4.4 |
| 2.25-2.75 | | | .3 | .1 | .3 |
| 2.75-3.25 | .0 | .0 | .1 | .1 | .2 |
| 3.25-3.75 | .0 | .0 | | | |
| 3.75-4.75 | .0 | .0 | | | |
| Total Percent | .9 | 10.1 | 13.1 | 1.1 | 24.8 |
| <u>South</u> | | | | | |
| .25 | .4 | 1.3 | .1 | .0 | 1.7 |
| .25-.75 | .2 | 3.6 | 1.6 | .0 | 5.3 |
| .75-1.25 | | 1.9 | 3.5 | .1 | 5.5 |
| 1.25-1.75 | .0 | .3 | 1.9 | .3 | 2.5 |
| 1.75-2.25 | .0 | .1 | .6 | .2 | .9 |
| 2.25-2.75 | .0 | | .1 | .2 | .4 |
| 2.75-3.25 | .0 | | | .1 | .1 |
| 3.25-3.75 | .0 | | | .0 | |
| 3.75-4.75 | .0 | .0 | .0 | | |
| Total Percent | .5 | 7.2 | 7.8 | .9 | 16.9 |
| <u>Southwest</u> | | | | | |
| .25 | .1 | .5 | | .0 | .7 |

Table 4 (continued)

| | <u>Wind Speed, m/sec - %</u> | | | | |
|------------------|------------------------------|----------------|-----------------|------------------|--------------|
| <u>Height, m</u> | <u>0.5-1.5</u> | <u>1.5-5.0</u> | <u>5.0-10.8</u> | <u>10.8-17.0</u> | <u>Total</u> |
| <u>Southwest</u> | | | | | |
| .25-.75 | .1 | 1.4 | .9 | .0 | 1.9 |
| .75-1.25 | | .6 | .7 | | 1.6 |
| 1.25-1.75 | .0 | .1 | .4 | | .5 |
| 1.75-2.75 | .0 | | .1 | | .1 |
| 2.25-2.75 | .0 | | .1 | | .1 |
| 2.75-3.25 | .0 | .0 | .0 | | |
| 3.25-3.75 | .0 | .0 | .0 | | |
| 3.75-4.75 | .0 | .0 | .0 | | |
| Total Percent | .2 | 2.6 | 1.7 | .2 | 4.7 |
| <u>West</u> | | | | | |
| .25 | .1 | .5 | | .0 | .6 |
| .25-.75 | .1 | .9 | .3 | .0 | 1.3 |
| .75-1.25 | .0 | .3 | .4 | | .7 |
| 1.25-1.75 | | .1 | .3 | | .4 |
| 1.75-2.25 | .0 | | .1 | .1 | .2 |
| 2.25-2.75 | .0 | | | | |
| 2.75-3.25 | .0 | .0 | | | |
| 3.25-3.75 | .0 | .0 | .0 | | |
| 3.75-4.75 | .0 | .0 | .0 | .0 | .0 |
| Total Percent | .2 | 1.7 | 1.2 | .2 | 3.3 |

Table 4 (Concluded)

| <u>Height, m</u> | <u>Wind Speed, m/sec - %</u> | | | | <u>Total</u> |
|--------------------------------|------------------------------|----------------|-----------------|------------------|--------------|
| | <u>0.5-1.5</u> | <u>1.5-5.0</u> | <u>5.0-10.8</u> | <u>10.8-17.0</u> | |
| | <u>Northwest</u> | | | | |
| .25 | .1 | .4 | | .0 | .5 |
| .25-.75 | .1 | .9 | .3 | .0 | 1.2 |
| .75-1.25 | | .4 | .7 | .1 | 1.2 |
| 1.25-1.75 | | .1 | .5 | .2 | .9 |
| 1.75-2.25 | .0 | | .3 | .3 | .7 |
| 2.25-2.75 | .0 | .0 | | .2 | .2 |
| 2.75-3.25 | .0 | .0 | | .1 | .1 |
| 3.25-3.75 | .0 | .0 | | .1 | .1 |
| 3.75-4.75 | .0 | .0 | | .1 | .1 |
| <u>Total</u> <u>Percent</u> | .2 | 1.8 | 2.0 | 1.0 | 5.0 |

TOTAL PERCENT = 97.6

Table 5

Wind Speed Versus Sea Height

| <u>Height, m</u> | <u>Wind Speed, m/sec</u> | | | | | <u>Total</u> |
|------------------|--------------------------|----------------|-----------------|------------------|------------------|--------------|
| | <u>0.5-1.5</u> | <u>1.5-5.0</u> | <u>5.0-10.8</u> | <u>10.8-17.0</u> | <u>17.0-24.2</u> | |
| .25 | 4.1 | 6.6 | 0.3 | 0 | 0 | 10.9 |
| .25-.75 | 1.0 | 19.3 | 8.4 | 0 | 0 | 28.7 |
| .75-1.25 | 0.2 | 10.8 | 19.9 | 0.9 | 0 | 31.9 |
| 1.25-1.75 | | 2.0 | 12.5 | 2.1 | 0.1 | 16.8 |
| 1.75-2.25 | | 0.3 | 4.3 | 2.2 | 0.1 | 6.9 |
| 2.25-2.75 | | 0.1 | 1.2 | 1.4 | 0.1 | 2.9 |
| 2.75-3.25 | 0 | | 0.3 | 0.7 | 0.1 | 1.1 |
| 3.25-3.75 | 0 | | 0.1 | 0.3 | | 0.5 |
| 3.75-4.75 | 0 | 0 | 0.1 | 0.2 | 0 | 0.3 |
| Total Percent | 5.3 | 39.1 | 47.0 | 7.8 | 0.4 | 100.0 |

Table 6

Percent Frequency of Wave Height
Versus Wave Period

| | | <u>Wave Height, m</u> | | | | | | | | | |
|-------------------------------|------------|-----------------------|-----------------|------------------|------------------|------------------|------------------|------------------|------------------|--|--|
| <u>Period</u> <u>(sec)</u> | <u>.25</u> | <u>.25-1.25</u> | <u>.75-1.25</u> | <u>1.25-1.75</u> | <u>1.75-2.25</u> | <u>2.25-2.75</u> | <u>2.75-3.25</u> | <u>3.25-3.75</u> | <u>3.75-4.75</u> | | |
| 6 | 8.5 | 22.1 | 21.1 | 7.2 | 1.7 | .7 | .2 | .1 | | | |
| 6-7 | .4 | 2.3 | 7.0 | 7.4 | 3.0 | 1.3 | .4 | .2 | .1 | | |
| 8-9 | .1 | .4 | .9 | 1.6 | 1.3 | .8 | .4 | .2 | .1 | | |
| 10-11 | .0 | .4 | .3 | .3 | .4 | .3 | .2 | .1 | .1 | | |
| 12-13 | .0 | .0 | .2 | .1 | .1 | .1 | .1 | | | | |
| 13 | .0 | .0 | .0 | .1 | | .1 | | .1 | .1 | | |
| Total | 13.9 | 26.1 | 30.4 | 17.1 | 6.7 | 3.3 | 1.2 | .6 | .5 | | |
| Per- cent | | | | | | | | | | | |

Table 5 contains wind speed versus sea height. Table 6 lists the percent frequency of wave height versus wave period. Important findings gained from an examination of these tables are:

- a. Prevailing wind azimuths for offshore Galveston in decreasing order of frequency are southeast, east, and south.
- b. Common wind speeds ranging from 1.5 to 10.8 m/sec generate sea waves 0.25 to 1.75 m in height.
- c. Surface waves ranging in height from 0.25 to 1.75 m usually have wave periods less than 6.0 sec. However, swells exceeding 1.25 m in amplitude have occasionally been recorded with periods ranging from 6.0 to 9.0 sec in duration.

113. The significance of these results in assessing the effect of oscillatory motion on bottom sediment is revealed by a plot of the oscillatory bottom velocity versus the wave period for an average 14.0-m water depth (Figure 60). This graph was plotted using Equations 16, 17, and 18. As shown here, wave periods in excess of 5.0 sec in duration coupled with wave heights greater than 0.75 m theoretically induce oscillatory bottom speeds exceeding 10 cm/sec. The percent frequency of wave height versus wave period data in Table 6 suggest that such wave amplitudes and periods can occur up to 30 percent of the time. If these oscillatory bottom velocities are superimposed upon an existent 10- to 20-cm/sec bottom current, then the threshold of silt and clay movement

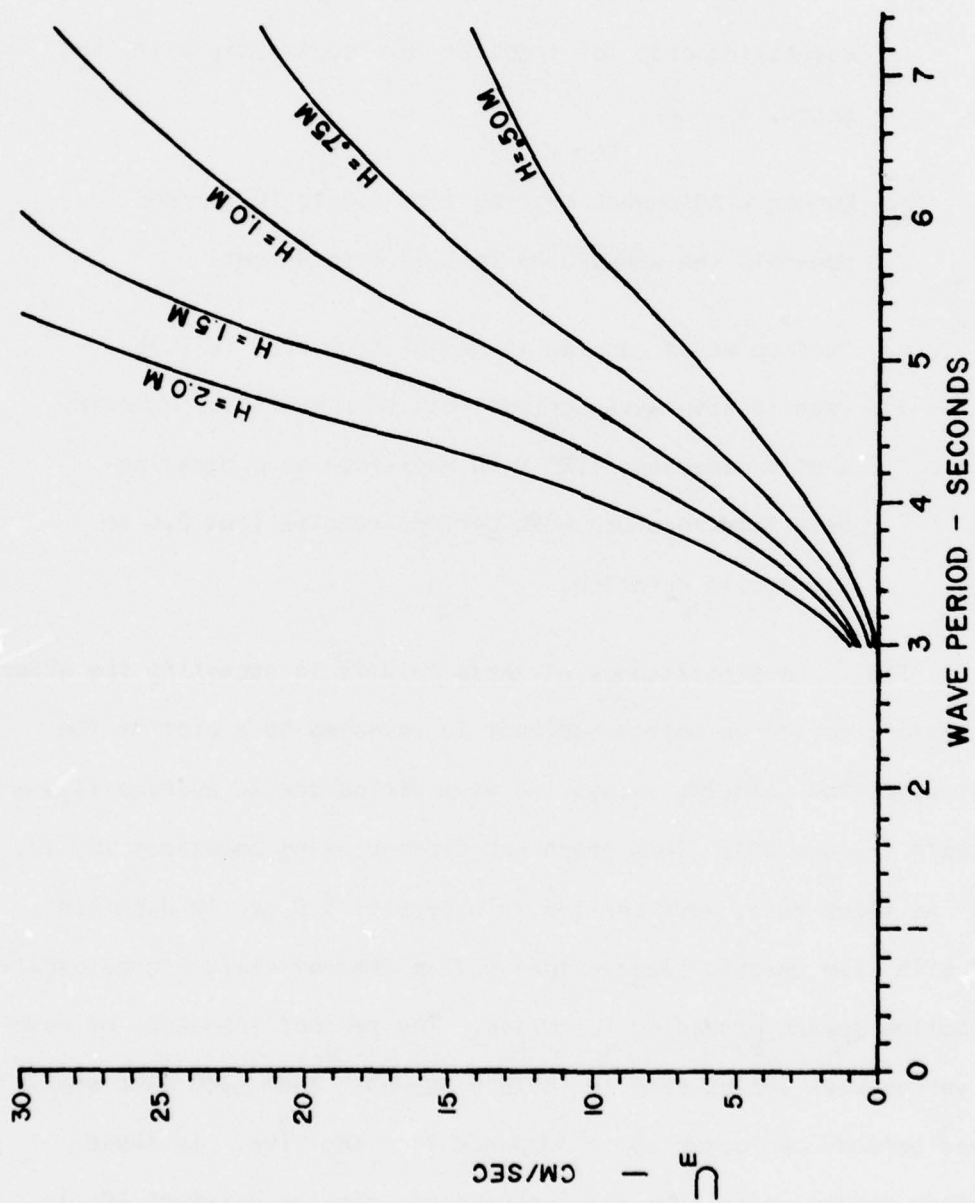


Figure 60. Relationship between wave period and oscillatory bottom velocity (U_m) for an average 14-m water depth

($\tau_{ocr} = 1.0 \text{ dyne /cm}^2$) will probably be exceeded. Such movement may then allow particles to be entrained within a given flow. Continuous near-bottom oscillatory motion may also prevent deposition of suspended particles if the resultant bed shear exceeds the threshold shear stress ($\approx 0.2 \text{ dyne /cm}^2$) permitting deposition. Hence, sea-state conditions in the dredged material disposal site can have a significant effect upon local near-bottom sediment transport processes.

Summary

114. The physical oceanographic and meteorologic data acquired during the period February 1975 through May 1976 for offshore Galveston and vicinity indicate that:

- a. Tides in the entrance channel are mixed in nature and typically range from 0.3 to 0.6 m in height.
- b. Tidal currents originating from cyclic passage through the entrance channel induce reversing rotary circulation patterns over the offshore dredged material disposal site. In particular, ebb tide flows generate S-SW directed currents, whereas flood tide currents produce E-NE directed flows during maximum current development.
- c. A shear zone periodically exists near the bottom of the water column in the offshore disposal area. This layer appears to form in response to either reversing tidal currents or near-bottom circulation patterns set up by

prevailing storm-wind azimuths.

- d. Adverse meteorological conditions affect both the nearshore sea level datum and the near-bottom circulation pattern. In particular, primary storm-wind azimuths affecting the hydrographic regime include: (1) strong persistent E, SE, or S winds traversing the Gulf of Mexico and (2) strong N to NW winds following the passage of a cold front
- e. Maximum bottom current velocities and net offshore-directed to down-coast bottom flows appear to be generated by strong prevailing southeasterly winds in excess of about 5 m/sec.
- f. Theoretical consideration of near-bottom oscillatory flows induced by surface waves suggests that such motion may play a significant role in governing near-bottom sediment transport processes, particularly during adverse meteorological conditions.

Applicability of Flume Experimental Results
to Offshore Sediment Transport at Galveston

Scaling considerations

115. The applicability of the results obtained from these flume experiments to offshore sediment transport can be partially realized if consideration is given to scaling effects between the prototype and the

natural environment. Dynamic similitude between the open channel flow and the offshore currents requires reproduction of primarily the gravity, inertial, and viscous forces that characterize these ocean currents. Unfortunately, there does not exist a single relationship that combines, as ratios, all three of these forces. However, scaling on the basis of the Reynolds number for both full and scaled conditions preserves a constant ratio between the viscous and inertial forces. Similarly, Froude number (F_r) scaling is based upon a constant ratio between gravity and inertial forces. Thus, these two scaling parameters were used to ascertain those open channel flow conditions that displayed dynamic similarity to the ocean environment.

116. Appropriate values of the Reynolds number, as previously discussed (refer to paragraph 16), establish whether a given flow is turbulent or laminar in nature. Due to the inherently large length scale needed to characterize ocean currents, the Reynolds number will result in values exceeding several thousand for current speeds greater than a few centimeters per second (see Equation 5). Such currents are typically considered as fully turbulent in nature. Reynolds number calculation for open channel flow in the flume (see Appendix E) indicated that turbulent flow ($R_e > 2000$) theoretically occurred at current velocities in excess of about 0.3 cm/sec. In addition, observation of fluorescent dye injected into the observation channel water column during flow rates ranging from 5 to 10 cm/sec showed full turbulent eddy development with time downstream from the injection point. Thus, the existence of fully developed turbulent flow during experimental runs was confirmed.

117. The Froude number describes the relationship between the inertial and gravity forces for a particular flow such that:

$$F_r = \frac{U}{gL} \quad (19)$$

where (L) represents the reference length and (g) is the acceleration due to gravity. Calculation of equivalent Froude and Reynolds numbers between the prototype and observed bottom currents (Appendix E) established that dynamic similarity in the vertical existed in the open channel flow for current speeds up to about 35 cm/sec. This similarity exists for uniform flow conditions that are characterized by fully developed turbulent eddies.

Critical erosion and deposition velocities

118. Application of the experimentally determined critical erosion and deposition velocities as measures of the critical velocities occurring within the offshore disposal site is valid under certain assumptions. These assumptions include the following: (1) bottom currents in the offshore dredged material site are characterized by uniform, fully developed turbulent flow; (2) the effect of wave-induced oscillatory motion on the threshold of cohesive sediment movement is negligibly small; and (3) the hydrodynamical roughness exhibited by the dredged material placed into the flume is similar to the roughness existent on the offshore disposal mounds. Establishment of the validity and/or variability of these three assumptions requires the development of new field monitoring techniques to measure the in situ bottom current and sediment conditions over long time periods. Until such techniques are developed, extrapolation of the "critical velocity" results to field conditions should be viewed as a best

estimate based upon state-of-the-art methods.

Sediment Transport Processes in the Offshore
Dredged Material Disposal Site

Effect of climate

119. Persistent winds. Examination of both meteorologic and hydrographic data for offshore Galveston during the period February 1975 through May 1976 indicates the importance of local climate on sedimentologic processes operative in the marine environment. In particular, the intensity and duration of persistent winds influence the nature and direction of offshore bottom currents that erode, transport, and deposit bottom sediments.

120. The principal wind azimuths affecting the Galveston vicinity are illustrated as a surface wind rose in Figure 61. These wind directions represent the relative percent frequency of prevailing wind directions as listed in Table 4 for the period 1963-1971. Also shown in Figure 61 are net bottom drift vectors. The longshore-directed vectors located adjacent to the Galveston Island shoreline and those within the entrance channel are based upon the sediment transport data presented by Hall (1976). The net bottom drift vectors illustrated at Buoy B and Buoy D are positioned according to the net drift directions given by the progressive vector trajectories illustrated in Figures 50 - 54.

121. The net drift azimuths shown at Buoys B and D presumably resulted from strong prevailing southeasterly winds. It should be realized that these bottom drift indicators are representative only of the

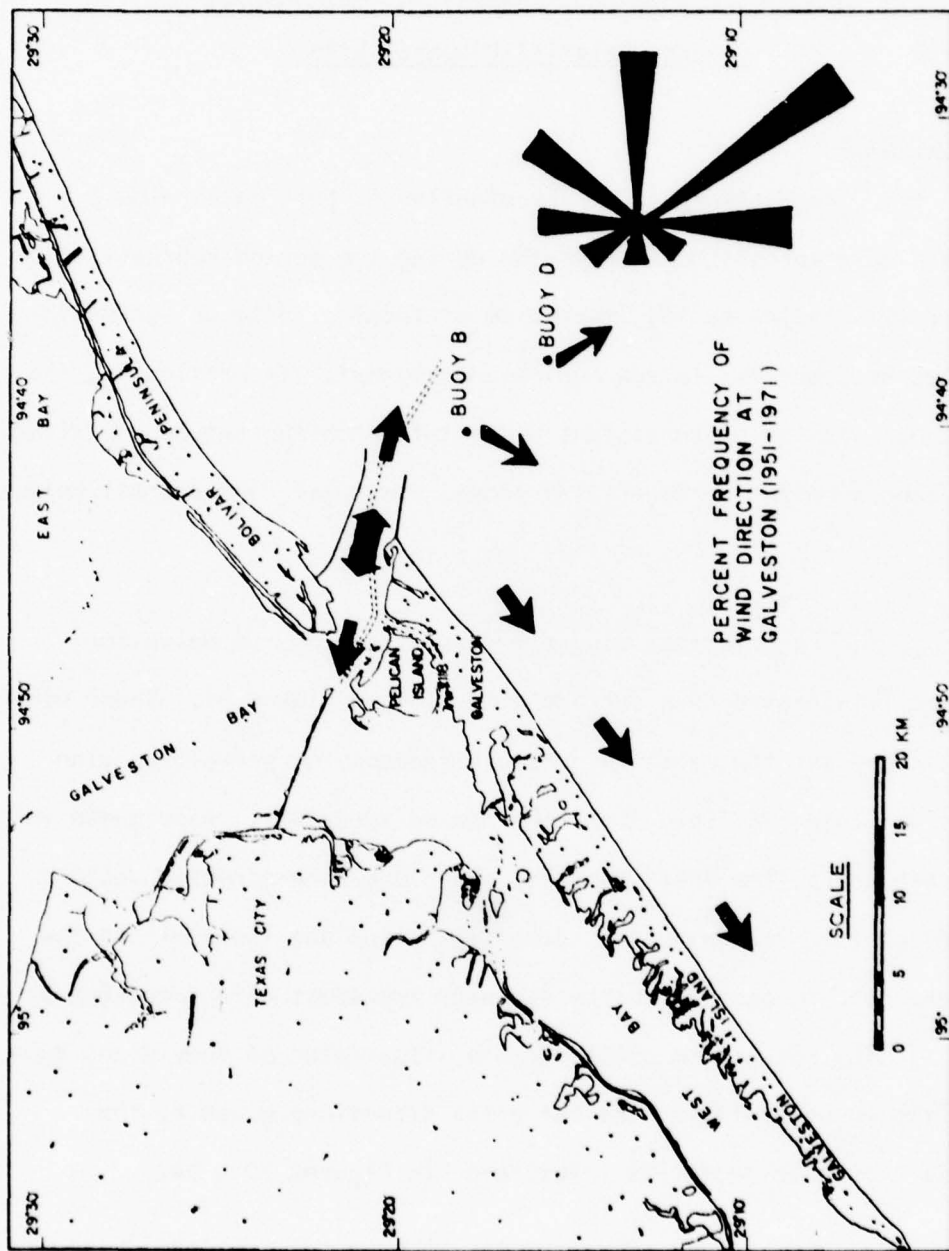


Figure 61. Wind rose and net bottom drift vectors for offshore Galveston

periods during which the bottom current meters were operative. This observation period, which totaled 31 days at Buoy B and 85 days at Buoy D, is not extensive enough in duration to establish annual net drift directions with statistical confidence. However, based upon the correlation found between the persistent southeasterly winds and net longshore to offshore bottom flow azimuths, it appears reasonable to speculate that annual net drift directions are oriented similarly. This speculation is based upon the fact that southeasterly winds occur most frequently on a yearly basis as evidenced by the 8-yr averaged prevailing wind data in Table 4.

122. Tropical storms. A discussion of climatic effects upon sediment transport processes for offshore Galveston would not be complete without consideration of severe tropical storms. Although no hurricanes seriously affected the Galveston vicinity during the period of this study, destructive storms such as hurricane Audrey (1957) and Carla (1961) have produced extreme storm tides. During the passage of Audrey, a positive tide anomaly of 3.1 m was recorded at Galveston. Similarly, Carla caused a 2.3-m tidal height rise. Hayes and Scott (1964) documented the effects of the storm surge and associated currents generated by hurricane Carla along the central Texas coast. After passage of the storm inland, seaward-flowing density currents deposited a fresh sand layer (up to 3 cm thick) over a sandy mud bottom in depths of 15 to 20 m. In addition, a graded bed (up to 10 cm thick) comprised of very fine sand, silt, and clay was traced over the homogenous mud bottom to depths exceeding 60 m. Such sedimentologic features point out the major role that a tropical storm can have in modifying an offshore geologic environment over a very short time

period.

Modes of sediment transport

123. Information on the various modes of sediment transport for offshore Galveston was obtained by combining the results of the flume experiments with those obtained from the hydrographic data in this study. The most valuable field data used to assess the relative degrees of erosion, transport, and deposition occurring in the disposal site were the current speed and direction measurements recovered from current meters positioned at Buoy B and Buoy D 1 m above the bottom. Discrete 15-min interval current vector readings were analyzed for the relative frequency of occurrence of cumulative 5.0-cm/sec current speed increments over the total range of values recorded at each station. The flow velocity distribution of each observation period for both stations was then determined. Cumulative curves showing the percentage distribution of flow speed increments (plotted on a probability axis) versus the logarithm to the base ten of the measured current speeds (plotted on an arithmetic axis) served as the basis for these determinations. These curves are illustrated in Figures 62 through 66. The velocity distribution shown in Figure 62 was plotted from cumulative speed data given by Hall (1976).

124. Examination of these velocity distributions indicates that the median velocities displayed by the curves for Buoy B ranged from 22 to 35 cm/sec, while those for Buoy D were slightly lower, ranging from 18 to 22 cm/sec. However, another purpose of presenting the current speed data for a specific time period in the form of a cumulative curve was to ascertain the relative frequency during which erosion, transportation, and

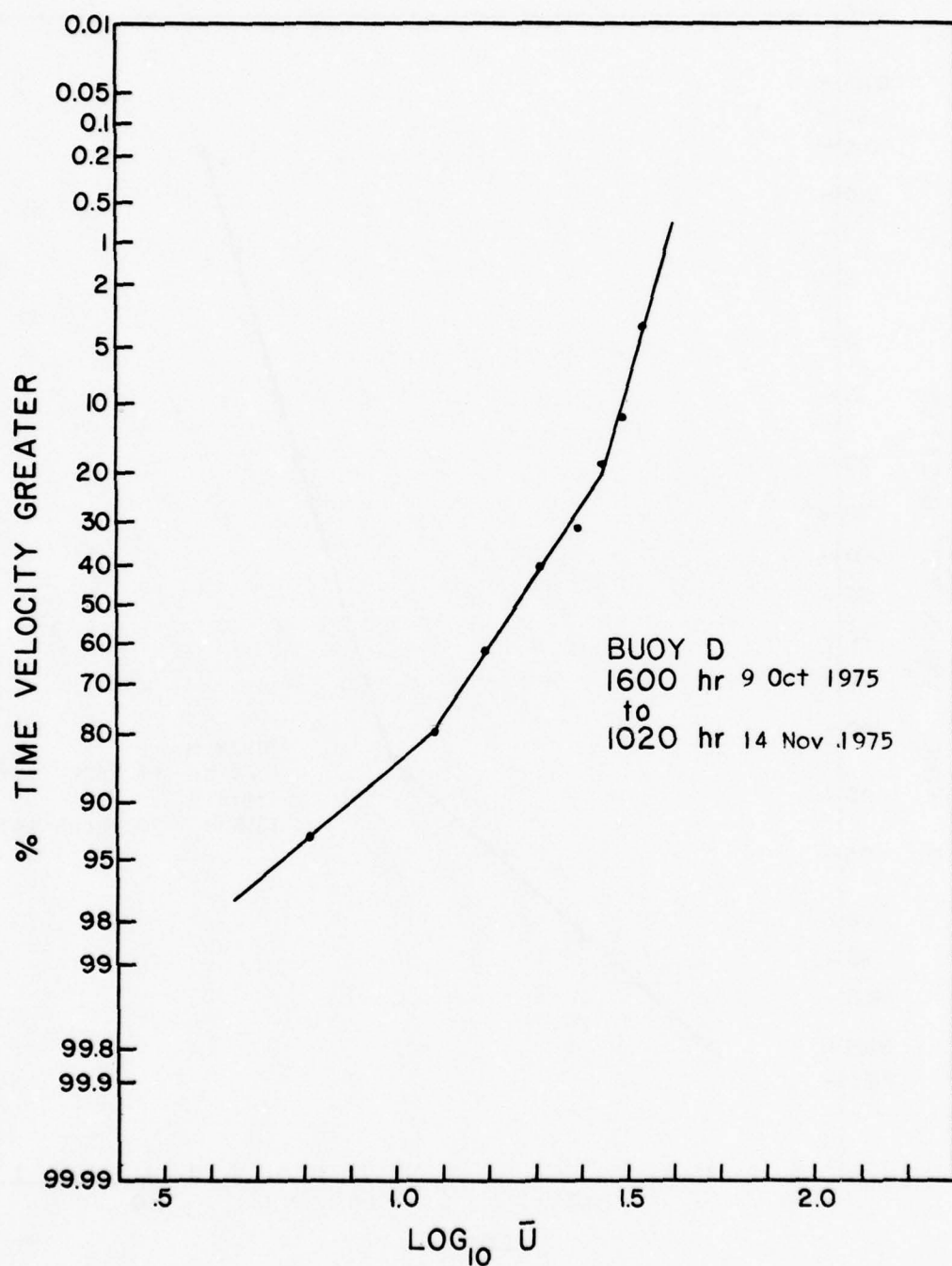


Figure 62. Cumulative curve of the current velocity distribution for 9 October to 14 November 1975 at Buoy D modified from Hall (1976) (\bar{U} = average current speed measured 1 m above bed)

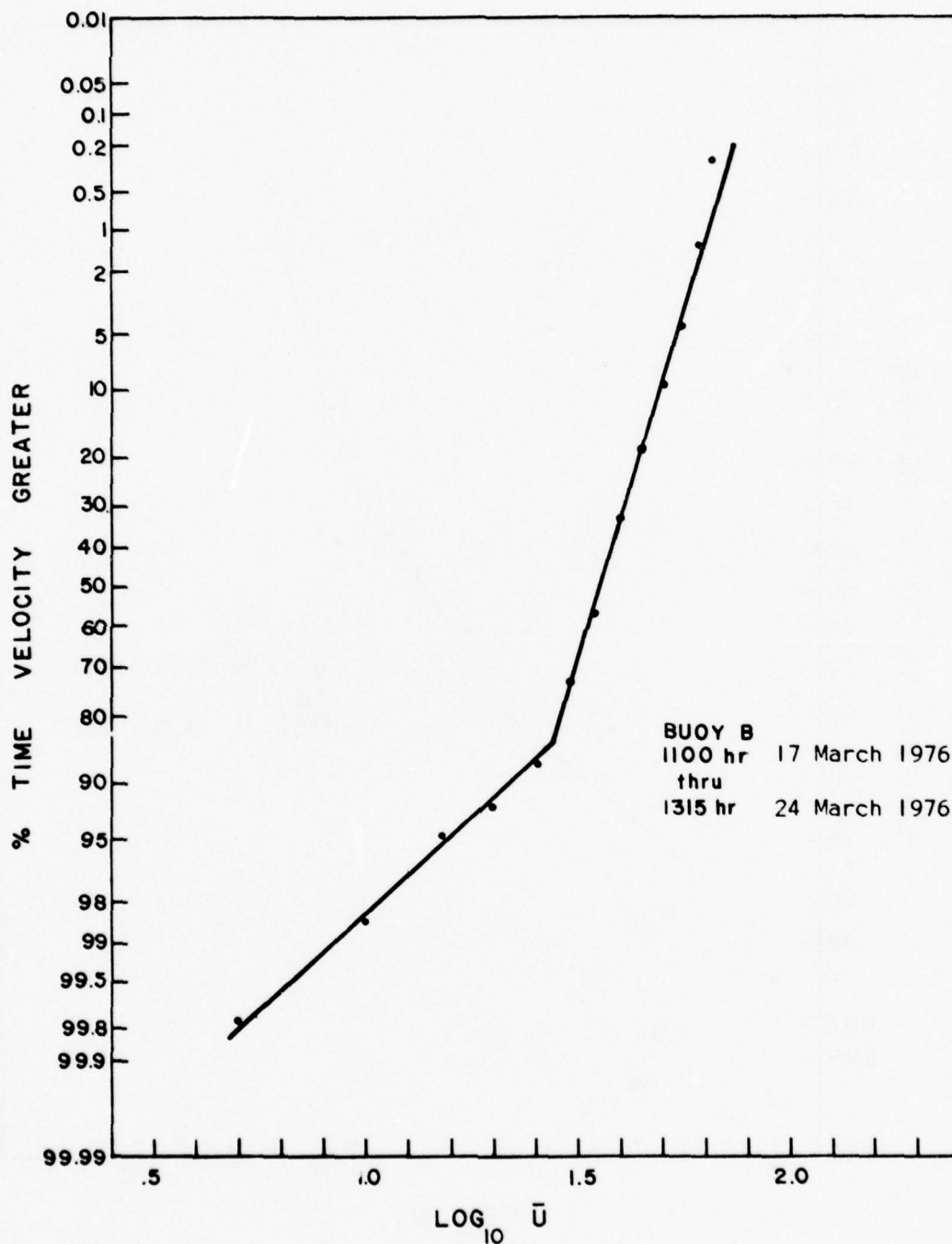


Figure 63. Cumulative curve of the current velocity distribution for 17 to 24 March 1976 at Buoy D (\bar{U} = average current speed measured 1 m above bed)

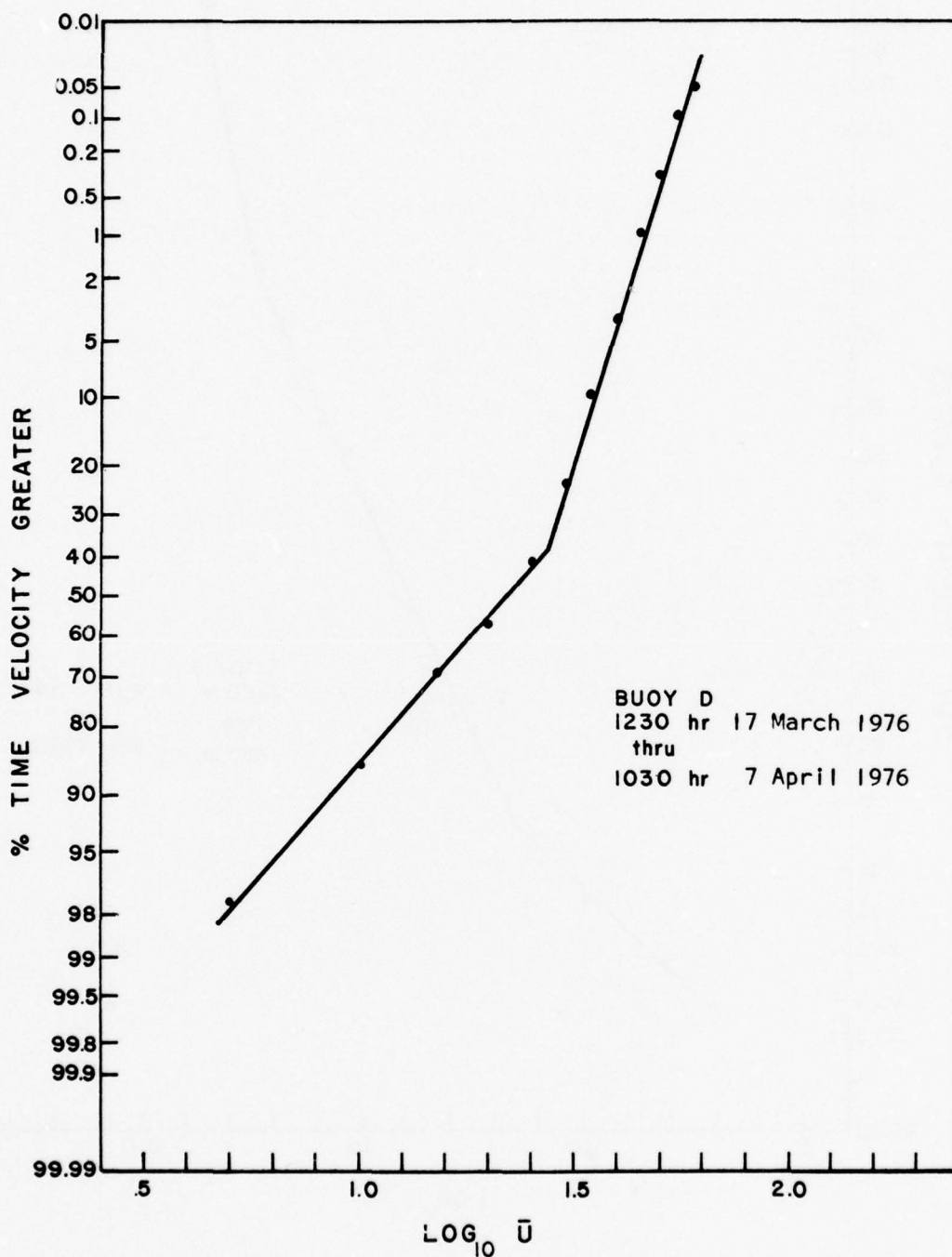


Figure 54. Cumulative curve of the current velocity distribution for 17 March to 7 April 1976 at Buoy D (\bar{U} = average current speed measured 1 m above bed)

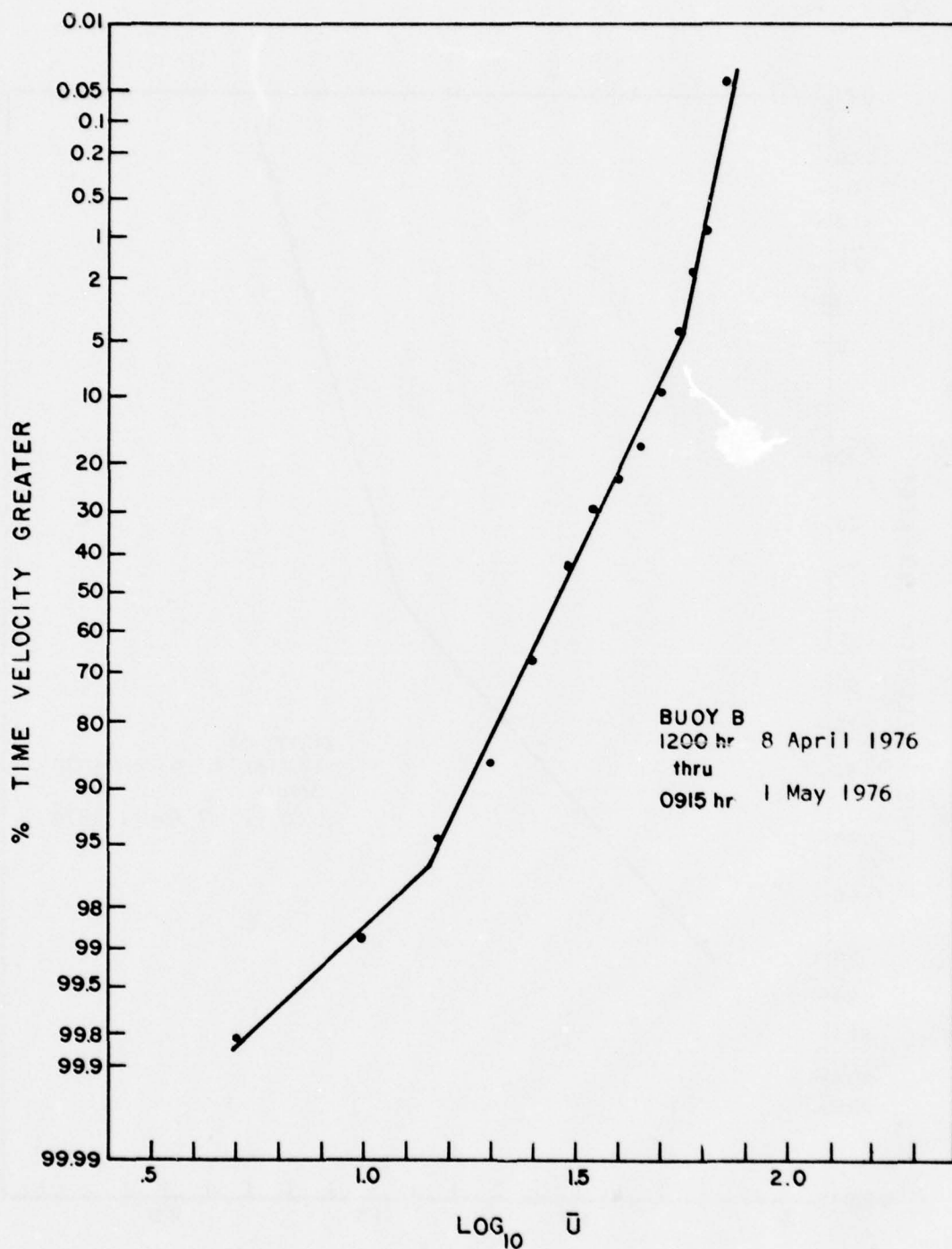


Figure 65. Cumulative curve of the current velocity distribution for 8 April to 1 May 1976 at Buoy B (\bar{U} = average current speed measured 1 m above bed)

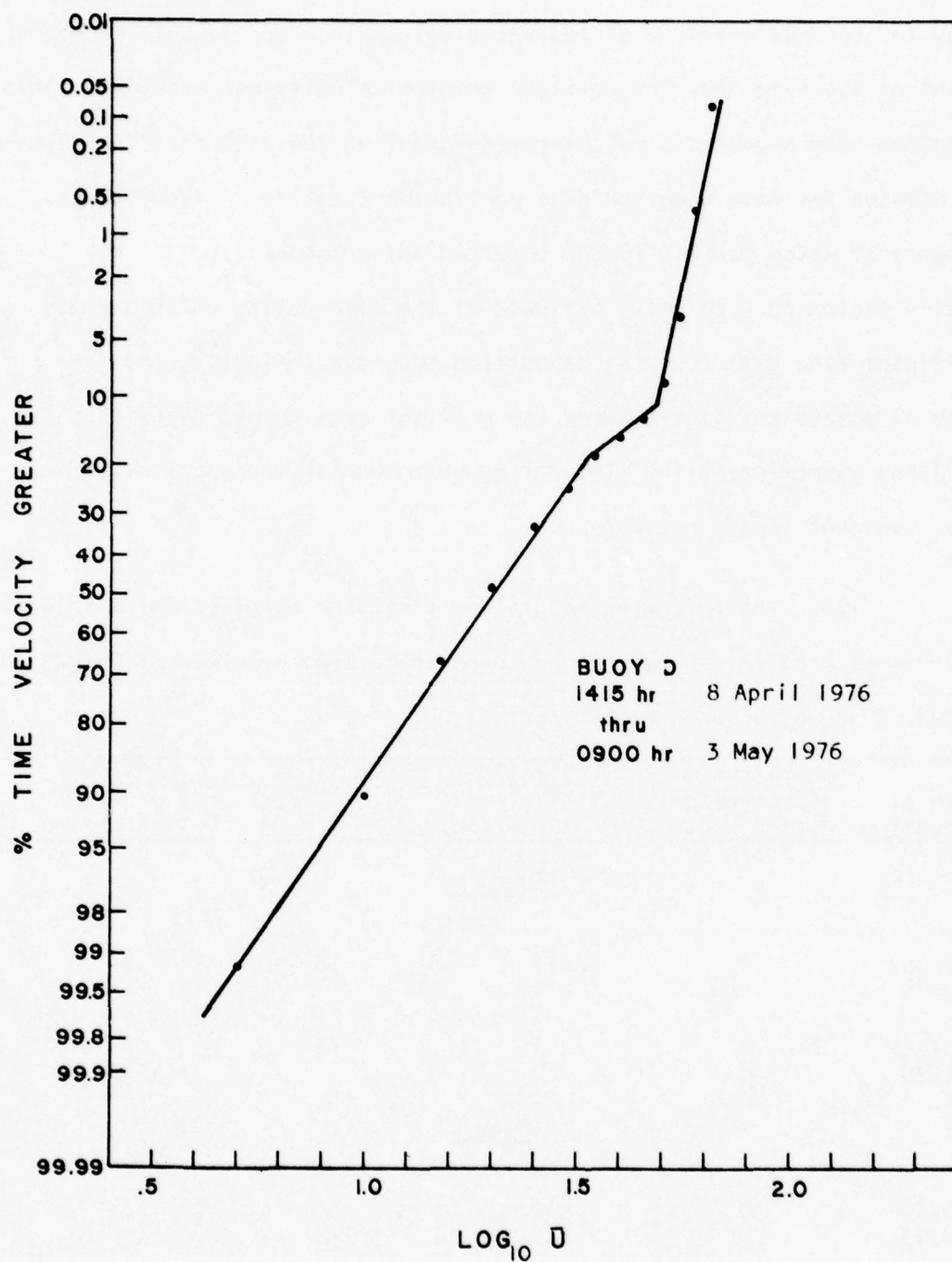


Figure 66. Cumulative curve of the current velocity distribution for 8 April to 3 May 1976 at Buoy D (\bar{U} = average current speed measured 1 m above bed)

deposition occurred at a specific locality. The frequency of the current speeds for each observation period was examined in order to determine the percent of the time that the critical erosion velocity was exceeded. This percentage then provided a relative assessment of the time that rapid bed-load erosion may have occurred at a particular locality. Likewise, the frequency at which current speeds occurred below the critical deposition velocity indicated a relative estimate of the time during which perhaps significant fine silt and clay deposition occurred. Finally, the frequency of speeds existent between the critical erosion and deposition velocities approximated the time during which mostly transport of suspended sediment likely occurred.

125. The following tabulation lists the relative percentage frequency of erosion, transport, and deposition that occurred at Buoy B and Buoy D per given observation period:

| <u>Date of Observation</u> | <u>Duration of Observation Period, days</u> | <u>DEPOSITION</u> | <u>TRANSPORT</u> | <u>EROSION</u> |
|--------------------------------|---|--|---|--|
| | | <u>% of Time</u> <u>$\bar{U} < 12 \text{ cm/sec}$</u> | <u>% of Time</u> <u>$12 \leq \bar{U} \leq 28$</u> | <u>% of Time</u> <u>$\bar{U} > 28 \text{ cm/sec}$</u> |
| <u>Buoy B</u> | | | | |
| 3/17/76- 3/24/76 | 7 | 3 | 16 | 81 |
| 4/ 8/76- 5/ 1/76 | 24 | 3 | 44 | 53 |
| <u>Buoy D</u> | | | | |
| 10/ 9/75- 11/14/75 | 37 | 19 | 59 | 22 |
| 3/17/76- 4/ 7/76 | 22 | 20 | 49 | 31 |
| 4/ 8/76- 5/ 3/76 | 26 | 18 | 56 | 26 |

The values of the critical erosion and deposition velocities ($\bar{U} = 28$ and 12 cm/sec, respectively) shown in the tabulation were ascertained from Einstein's Bedload Function for open channel flow over smooth boundaries using the experimentally determined critical erosion and deposition bed shears ($\tau_{ocr} = 1.0$ and 0.2 dyne /cm², respectively) to calculate values of the friction velocity. Examining the values in the tabulation, it is apparent that rapid cohesive bedload erosion probably occurred much more frequently at Buoy B than at D. Similarly, current speeds permitting significant silt and clay deposition likely occurred more often at Buoy D than at Buoy B. The relative percentage of time that transport conditions ($12 \leq \bar{U} \leq 28$ cm/sec) occurred at these sites does not necessarily indicate the total time during which a sedimentary particle remained in suspension. For instance, if a silt or clay particle was deposited from suspension on a cohesive bed during a decreasing flow rate, such as during slack water development during a tide cycle, that particle would probably adhere to the bed until the bottom velocity again increased to the critical erosion velocity needed to resuspend it. The bottom current may not resume erosional competency until maximum ebb or flood tidal current development is reinstated several hours later. In addition, both erosion and deposition of fine silt and clay can occur during the range of these so-called "transport" velocities as evidenced by (1) the negative and positive slopes of the scour curves for the dense and floc bed erosional runs and (2) the observed decrease in the silt content (increase in the clay content) of the washload during sustained flow rates. Thus, these critical erosion and deposition velocities are nonunique and delineate only the relative degree of erosion, transport, or deposition that

occurred at a given locality.

Offshore disposal mounds

126. The relative degrees of erosion and deposition occurring at each of the disposal mounds (see Figure 2) should be indicated indirectly by the texture of the surficial sediments, and also by general changes in the bathymetric configuration of the mounds. For instance, surficial dredged material at Buoy B would be expected to display a coarser sediment texture than at Buoy D due to the greater frequency of erosional bottom current velocities occurring at Buoy B. Conversely, the silt and clay content of surficial sediment at Buoy D should be higher than Buoy B due to the greater frequency of depositional current velocities occurring at Buoy D.

127. Expected variations in the bathymetric configuration over time include a lower topographic relief at Buoy B than at Buoy D (or Buoy C) and general changes in the mound orientation. The lower topographic relief expected at the Buoy B mound is again predicated on the evidence that a higher frequency of erosive bottom currents occurs at Buoy B than at D. Thus, local bedload erosion would result in the removal of more material at B than at C or D.

128. Finally, a southwest- and/or southeast-trending mound configuration might be expected to form at these disposal mounds if the net bottom drift directions shown in Figure 61 are valid indicators of net bedload movement. The analysis of variations in the bottom sediment textural distributions and bathymetric mound configurations as a function

of time by Estes and Scrudato (1977) may indicate such general trends.

PART V: CONCLUSIONS

Flume Experiments

129. As a result of the flume experiments performed on the four sand, silt, and clay mixtures, it was concluded that:

- a. Each of the four sediments eroded similarly as evidenced by the similar critical bed shear value ($\tau_{ocr} \approx 1.0 \text{ dyne /cm}^2$) necessary to initiate massive bedload transport and rapid TSM concentration increases.
- b. Rapid deposition of suspended fine silt and clay occurred at very low bed shear values ($\tau_o < 0.2 \text{ dyne /cm}^2$).
- c. Primary silt and clay resuspension occurred during the initial 2 to 4 hr following each current velocity increase. Thereafter, for sustained flow rates, the scour rate decreased to a near constant level.
- d. Continuous erosion on a hydrodynamically rough bed resulted in texturally diverse sediment interfaces within the sediment column.
- e. Washload composition consisted primarily of fine silt and clay at a 30-cm elevation above the bed. Significant variations in the washload grain-size distribution occurred with increasing or decreasing flow rates.

Hydrography of Offshore Galveston

130. It is concluded from an analysis of the hydrographic data obtained for offshore Galveston that:

- a. Tidal currents produced by cyclic passage through the Galveston Bay entrance channel induce reversing rotary circulation patterns over the offshore dredged material disposal site. In particular, ebb tide flows generate S-SW directed currents, whereas flood tide flows generate E-NE directed currents.
- b. A shear zone periodically exists near the bottom of the water column in the offshore disposal area. This zone appears to form in response to either reversing tidal currents or near-bottom circulation patterns set up by prevailing storm wind azimuths.
- c. Adverse meteorological conditions affect both the coastal sea level datum and the near-bottom circulation pattern. Primary storm wind azimuths affecting the hydrographic regime include: (1) strong persistent southeast, east, or south winds traversing across the Gulf of Mexico and (2) strong north to northwest winds following the passage of a cold front.
- d. Maximum bottom current velocities and net down-coast to offshore-directed bottom flows appear to be generated by southeasterly storm winds exceeding

about 5 m/sec.

Offshore Sediment Transport

131. Based on the evaluation of both the offshore hydrographic and laboratory experimental results, it appears that:

- a. Erosion is occurring more frequently near the northern margin (near Buoy B) of the offshore disposal site than at the southern margin (near Buoy D). Conversely, deposition of suspended silt and clay occurred more frequently near the southern boundary than at the northern end.
- b. Net bedload transport of dredged material moves down coast or offshore from the Galveston Bay entrance channel. Thus, the probability of significant quantities of dredged material returning to the entrance channel as shoaling sediment is small.

REFERENCES

- Caligny, A. F. H., "Experiences sur les Mouvements des Molecules Liquid des Ondes Courant, Considerees dans leur Mode D'actions sur la Marche des Navires," Vol. 87, C.R. Acad. Sci., Paris, 1878, pp. 1019-1023.
- Cernock, P. J., "Consolidation Characteristics and Related Physical Properties of Selected Sediments from the Gulf of Mexico", Unpub. M.S. Thesis, Texas A&M Univ., College Station, Texas, 1967, 137 p.
- Cool, T., "Dredged-Material Disposal and Total Suspended Matter Off-shore From Galveston, Texas", Unpub. M.S. Thesis, Texas A&M Univ., College Station, Texas, 1976, 160 p.
- Coulter Electronics, "Operators Manual for Coulter Counter Model TALL", Coulter Electronics, Inc., Hialeah, Florida, 1975, 88 p.
- Coulthard, D., "Nearshore Sediments Off Galveston Island and Jetty System, Texas", Unpub. M.S. Thesis, Texas A&M Univ., College Station, Texas, 1976, 117 p.
- Einstein, H. A., and Krone, R. B., "Experiments to Determine Modes of Cohesive Sediment Transport in Salt Water", Vol. 67, Journ. Geophy. Res., 1962, pp. 1451-1461.
- Ekman, V. W., "On the Influence of the Earth's Rotation on Ocean Currents", Vol. 2, No. 11, Ark. f. Mat. Astr. Ocn. Fysik. K. Sv. Vet. Ak., Stockholm, 1905.
- Estes, E. L., and Scrudato, R. J., "Aquatic Disposal Field Investigations, Galveston, Texas, Offshore Disposal Site; Appendix A: Investigation of the Hydraulic Regime and Physical Nature of Sedimentation," Technical Report D-77-20, Dec 1977, U. S. Army Engineer Waterways Experiment Station, CE, Vicksburg, Miss.
- Folk, R. L., Petrology of Sedimentary Rocks, Hemphill, Texas, 1974, 182 p.
- Graft, W. H., Hydraulics of Sediment Transport, McGraw-Hill, New York, 1971, 513 p.
- Hall, G., "Sediment Transport Processes in the Nearshore Waters Adjacent to Galveston Island and Bolivar Peninsula", Unpub. Ph.D. dissert., Texas A&M Univ., College Station, Texas, 1976 325 p.
- Hayes, M. O., and Scott, A. J., "Environmental Complexes South Texas Coast", Trans. Gulf Coast Assoc. Geol. Soc., Vol. 14, 1964, pp. 237-240.

- Hjulstorm, F., "The Morphological Activity of Rivers as illustrated by River Fyris", Vol. 25, Gull. Geol. Inst., Uppsala, 1935, Chap. II.
- Jackson, M. L., Soil Chemical Analysis-Advanced Course, Prentice, New Jersey, 1954, 498 p.
- Komar, P. D. and Miller, M. C., "The Threshold of Sediment Movement Under Oscillatory Water Waves", Vol. 43, No. 4, Jour. Sed. Pet., 1973, pp. 1101-1110.
- Krone, R. B., "Flume Studies of the Transport of Sediment in Estuarial Shoaling Processes", Contract No. DA-04-203, CIVENG-59-2, Corps of Engineers, U.S. Army, 1962, 108 p.
- Lambe, T. W., Soil Testing for Engineers, John Wiley and Sons, New York, 1951, 165 p.
- Longard, J. R., and Banks, R. E., "Wind-Induced Vertical Movement of the Water on an Open Coast", Vol. 33, No. 3, Trans. Am. Geophys. Union, 1952, pp. 377-380.
- Ludwick, J. D., "Tidal Currents and Zig-Zag Sand Shoals in a Wide Estuary Entrance", Vol. 85, Geol. Soc. Am. Bull., 1974, pp. 717-726.
- Lyle, W. M., and Smerdon, E. T., "Relation of Compaction and Other Soil Properties to Erosion and Resistance of Soils", Vol. 8, Am. Soc. Agric. Eng., 1965, pp. 419-421.
- Murray, S. P., "Trajectories and Speeds of Wind-Driven Currents Near the Coast", Vol. 5, J. Phys. Oceanogr., 1975, pp. 347-360.
- _____, "Observations on Wind, Tidal, and Density-Driven Currents in the Vicinity of the Mississippi River Delta", in Shelf Sediment Transport, Dowden, Stroudsburg, Penn., 1972, pp. 127-142.
- Nikuradse, J., "Laws of Flow in Rough Pipes", Vol. 1292, Nat. Adv. Comm. Aeronautics Tech. Memo, 1933, pp. 1-62.
- Partheniades, E., and Mehta, A. J., "Rates of Deposition of Fine Cohesive Sediments in Turbulent Flows", Proceedings of the 14th Conference of the International Association for Hydraulic Research, Paris, Vol. 4, 1971, pp. 17-26.
- Phillips, O. M., The Dynamics of the Upper Ocean, Cambridge, New York, 1969, 261 p.

- Postma, H., "Sediment Transport and Sedimentation in the Estuarine Environment", in Estuaries, (ed. G. H. Lauff), Amer. Assoc. Advmt. Sci., No. 83, 1967, pp. 158-179.
- Prandtl, L., and Tietzens, O. G., Fundamentals of Hydro and Aeromechanics, McGraw-Hill, New York, 1934, 270 p.
- Reynolds, O., "An Experimental Investigation of the Circumstances Which Determine Whether the Motion of Water Shall be Direct or Sinuous and the Law of Resistance in Parallel Channels", Vol. 174, Phil. Trans. Am., 1883, pp. 935-982.
- Rouse, H., Fluid Mechanics for Hydraulic Engineers, Dover, New York, 1961, 422 p.
- Scafe, D. W., "A Clay Mineral Investigation of Six Cores From the Gulf of Mexico", Unpub. Ph.D. dissert., Texas A&M Univ., College Station, Texas, 1968, 67 p.
- Sheldon, R. W., and Parsons, T. R., "On Some Applications of the Coulter Counter to Marine Research", Man. Rept. Series, No. 214, Fish. Res. Bd., Canada, 1966, 36 p.
- Shideler, G. L., "A Comparison of Electronic Particle Counting and Pipette Techniques in Routine Mud Analysis", U.S. Geol. Survey, Open File Report No. 76-269, 1975, 20 p.
- Smerdon, E. T., and Beasley, R. P., "The Tractive Force Theory Applied to Stability of Open Channels in Cohesive Soils", Univ. Missouri, Agric. Exp. Stat. Res. Bull. No. 715, 1969, 89 p.
- Stevenson, H. S., "Vane Shear Determination of the Viscoelastic Shear Modulus of Submarine Sediments", Unpub. M. S. Thesis, Texas A&M Univ., College Station, Texas 1973, 124 p.
- Sundborg, F. A., "The River Kloralven, A Study of Fluvial Processes", Geogr. Amer. Agr., Vol. 37, 1956, pp. 125-316.
- Sverdrup, H. U., Johnson, M. W., and Fleming, R. H., The Oceans, Prentice-Hall, New Jersey, 1942, 1087 p.
- Teleki, P. G., "Wave Boundary Layers and Their Relation to Sediment Transport", in Shelf Sediment Transport, Dowden, Stroudsburg, Penn., 1972, pp. 21-59.
- U. S. Army Engineer Waterways Experiment Station, CE, "The Unified Soil Classification System", Technical Memorandum No. 3-357, 1953, Vol. 1, 3.

U. S. Department of Commerce, East Coast of North and South America, "Tide Tables 1976", Table 1, 1976, pp. 136-139.

_____, Atlantic Coast of North America, "Tidal Current Tables 1976", Table 1, 1976, pp. 118-123.

U. S. Naval Weather Command, "Summary of Synoptic Meteorological Observations", Vol. 4, Tables 18-19, 1976, pp. 540-591.

Weggel, J. R., "Water Motion and Process of Sediment Entrainment" in Shelf Sediment Transport, Dowden, Stroudsburg, Penn., 1972, pp. 1-20.

APPENDIX A: TOTAL SUSPENDED MATTER CONCENTRATION, TIME
AFTER VELOCITY CHANGE, MEAN FLOW SPEED, AND WATER
LOCATIONS OBTAINED DURING EXPERIMENTAL RUNS

Table A1

Total Suspended Matter Concentration, Time After
Velocity Change, Mean Flow Speed, and Water Sample
Locations Obtained During Experimental Runs

| Set | Run | Sample # | L_s^* | Z^{**} (cm) | \bar{U}^\dagger (cm/sec) | $T_v^{\dagger\dagger}$ (hr) | TSM ‡ (mg/l) |
|--------|-----|----------|----------------|------------------|-------------------------------|--------------------------------|---------------------------|
| Buoy C | 1 | 1 | D ₂ | 30.5 | 10 | 0.1 | 0.95 |
| | | 2 | D ₂ | | | 0.5 | 1.42 |
| | | 3 | E ₂ | | | 0.5 | 1.64 |
| | | 4 | D ₂ | | | 1.0 | 2.07 |
| | | 5 | E ₂ | | | 1.0 | 3.00 |
| | | 6 | C ₂ | | | 2.0 | 4.97 |
| | | 7 | D ₂ | | | 2.0 | 5.28 |
| | | 8 | D ₂ | | | 4.0 | 7.12 |
| | | 12 | D ₂ | | | 16.0 | 7.97 |
| Buoy C | 2 | 14 | D ₂ | 30.5 | 15 | 24.0 | 7.86 |
| | | 15 | D ₂ | | | 0.1 | 8.17 |
| | | 17 | D ₂ | | | 1.0 | 9.56 |
| | | 18 | D ₂ | | | 2.0 | 12.25 |
| | | 20 | D ₂ | | | 6.0 | 14.38 |
| | | 22 | D ₂ | | | 12.0 | 17.51 |
| | | 23 | D ₂ | | | 22.3 | 18.67 |
| | | 25 | D ₂ | | | 24.0 | 17.60 |
| Buoy C | 3 | 26 | D ₂ | 30.5 | 23 | 0.1 | 17.98 |
| | | 27 | | | | 0.5 | 24.55 |
| | | 28 | | | | 0.9 | 26.13 |
| | | 32 | | | | 8.0 | 31.05 |

* L_s = Sample location, see Figure 19.

** Z = Water depth of sample.

$^\dagger \bar{U}$ = Mean flow speed.

$^\dagger \dagger T_v$ = Time after velocity change.

‡ TSM = Total suspended matter concentration.

Table A1 (continued)

| Set | Run | Sample # | L _s | Z (cm) | \bar{U} (cm/sec) | T _v (hr) | TSM (mg/l) |
|------------|-----|----------|----------------|-----------|-----------------------|------------------------|---------------|
| Buoy C | 3 | 34 | D ₂ | 30.5 | 23 | 22.3 | 37.34 |
| Buoy C | 4 | 37 | D ₂ | 30.5 | 31 | 0.1 | 29.14 |
| | | 38 | | | | 0.5 | 59.75 |
| | | 39 | | | | 1.0 | 67.00 |
| | | 40 | | | | 2.0 | 80.19 |
| | | 41 | | | | 4.0 | 83.75 |
| | | 42 | | | | 6.2 | 95.36 |
| | | 43 | | | | 8.0 | 90.59 |
| | | 44 | | | | 12.0 | 95.99 |
| | | 45 | | | | 13.3 | 90.71 |
| | | 48 | | | | 35.4 | 95.05 |
| | | 49 | | | | 47.4 | 89.53 |
| | | 50 | | | | 59.0 | 96.75 |
| | | 51 | | | | 71.6 | 94.82 |
| | | 52 | | | | 82.3 | 99.49 |
| | | 53 | | | | 98.4 | 98.73 |
| Buoy C | 5 | 54 | D ₂ | 30.5 | 23 | 0.1 | 91.54 |
| | | 55 | E ₂ | | | 0.2 | 94.14 |
| | | 56 | D ₂ | | | 0.3 | 98.08 |
| | | 57 | D ₂ | | | 7.0 | 93.09 |
| | | 58 | D ₂ | | | 8.4 | 84.18 |
| | | 60 | D ₂ | | | 23.4 | 88.48 |
| Buoy C | 6 | 61 | D ₂ | 30.5 | 10 | 0.1 | 89.56 |
| | | 62 | | | | 0.7 | 93.18 |
| | | 63 | | | | 8.5 | 81.63 |
| | | 64 | | | | 10.3 | 80.00 |
| | | 65 | | | | 19.9 | 78.45 |
| Block 15 2 | | 74 | D ₂ | 30.5 | 16 | 0.1 | 3.06 |
| | | 75 | | | | 1.9 | 2.52 |
| | | 77 | | | | 8.3 | 4.26 |
| | | 79 | | | | 15.3 | 5.58 |
| | | 80 | | | | 25.5 | 4.76 |
| Block 15 3 | | 81 | D ₂ | 30.5 | 23 | 0.1 | 9.46 |
| | | 82 | | | | 0.7 | 6.62 |
| | | 83 | | | | 7.0 | 19.57 |
| | | 87 | | | | 11.0 | 21.85 |
| | | 89 | | | | 24.8 | 19.62 |

Table A1 (continued)

| Set | Run | Sample # | L _s | Z (cm) | U (cm/sec) | T _v (hr) | TSM (mg/l) |
|------------|-----|----------|----------------|-----------|---------------|------------------------|---------------|
| Block 14 4 | | 90 | D ₂ | 30.5 | 31 | .1 | 73.54 |
| | | 91 | | | | 2.75 | 150.12 |
| | | 92 | | | | 6.25 | 182.52 |
| | | 95 | | | | 10.0 | 163.67 |
| | | 97 | | | | 23.0 | 175.66 |
| Block 15 5 | | 98 | D ₂ | 30.5 | 10 | .1 | 75.52 |
| | | 101 | | | | 6.8 | 72.02 |
| | | 102 | | | | 11.0 | 88.18 |
| | | 103 | | | | 22.8 | 63.38 |
| Block 27 1 | | 105 | C ₂ | 30.5 | 12 | .3 | 15.63 |
| | | 106 | E ₂ | | | 1.7 | 20.28 |
| | | 107 | E ₂ | | | 2.8 | 19.83 |
| | | 108 | E ₂ | | | 8.4 | 20.79 |
| | | 109 | E ₂ | | | 46.5 | 15.88 |
| | | 110 | E ₂ | | | 51.0 | 15.65 |
| Block 27 2 | | 111 | E ₂ | 30.5 | 23 | .1 | 14.47 |
| | | 112 | | | | .2 | 19.63 |
| | | 113 | | | | .5 | 24.49 |
| | | 114 | | | | 1.0 | 29.91 |
| | | 115 | | | | 1.5 | |
| | | 116 | | | | 2.0 | 34.88 |
| | | 117 | | | | 4.0 | 36.45 |
| | | 118 | | | | 6.0 | 36.66 |
| | | 119 | | | | 9.1 | 35.74 |
| | | 120 | | | | 11.9 | 34.81 |
| | | 121 | | | | 24.9 | 33.57 |
| Block 27 3 | | 122 | E ₂ | 30.5 | 30 | .2 | 36.57 |
| | | 123 | | | | .5 | 37.50 |
| | | 124 | | | | 1.0 | 43.58 |
| | | 125 | | | | 1.5 | 46.53 |
| | | 126 | | | | 2.0 | 48.57 |
| | | 127 | | | | 4.0 | 49.28 |
| | | 128 | | | | 6.0 | 45.90 |
| | | 129 | | | | 9.3 | 45.66 |
| | | 130 | | | | 14.8 | 52.17 |
| | | 131 | | | | 22.9 | 59.78 |

Table A1 (continued)

| Set | Run | Sample # | L _s | Z (cm) | \bar{U} (cm/sec) | T _v (hr) | TSM (mg/l) |
|----------|-----|----------|----------------|-----------|-----------------------|------------------------|---------------|
| Block 27 | 4 | 132 | E ₂ | 30.5 | 38 | .1 | 56.94 |
| | | 133 | | | | .4 | 57.20 |
| | | 134 | | | | 1.4 | 66.91 |
| | | 135 | | | | 1.8 | 65.45 |
| | | 136 | | | | 2.0 | 73.97 |
| | | 137 | | | | 4.0 | 81.07 |
| | | 138 | | | | 6.6 | 89.37 |
| | | 139 | | | | 9.0 | 90.13 |
| | | 140 | | | | 12.0 | 92.39 |
| | | 141 | | | | 23.9 | 102.27 |
| | | 142 | | | | 28.2 | 106.04 |
| | | 143 | | | | 37.8 | 108.00 |
| | | 144 | | | | 48.0 | 109.58 |
| Block 27 | 5 | 145 | E ₂ | 30.5 | 44 | .1 | 115.43 |
| | | 146 | | | | .5 | 117.99 |
| | | 147 | | | | 1.0 | 116.65 |
| | | 148 | | | | 1.8 | 128.00 |
| | | 149 | | | | 4.0 | 128.25 |
| | | 150 | | | | 5.5 | 149.11 |
| | | 151 | | | | 5.5 | 146.18 |
| | | 152 | | | | 5.5 | 142.34 |
| | | 153 | | | | 9.8 | 155.70 |
| | | 154 | | | | 12.1 | 158.04 |
| | | 155 | | | | 23.6 | 179.10 |
| | | 156 | | | | 24.0 | 179.88 |
| Block 27 | 6 | 157 | E ₂ | 30.5 | 57 | .1 | 173.70 |
| | | 158 | | | | .5 | 207.89 |
| | | 159 | | | | 1.3 | 237.82 |
| | | 160 | | | | 1.8 | 248.56 |
| | | 161 | | | | 6.4 | 398.66 |
| | | 162 | | | | 9.0 | 435.62 |
| | | 163 | | | | 13.1 | 471.00 |
| | | 164 | | | | 25.6 | 670.68 |
| Block 27 | 7 | 165 | E ₂ | 30.5 | 30 | 1.6 | 646.23 |
| | | 166 | | | | 3.8 | 643.43 |
| | | 167 | | | | 9.7 | 645.74 |
| | | 168 | | | | 23.6 | 614.30 |

Table A1 (continued)

| Set | Run | Sample # | L _s | Z (cm) | U (cm/sec) | T _v (hr) | TSM (mg/l) |
|----------|-----|----------|----------------|-----------|---------------|------------------------|---------------|
| Block 27 | 8 | 169 | E ₂ | 30.5 | 6 | .7 | 648.33 |
| | | 170 | | | | 3.7 | 461.53 |
| | | 171 | | | | 8.3 | 328.13 |
| | | 172 | | | | 20.9 | 180.00 |
| | | 174 | | | | 31.6 | 141.27 |
| Block 27 | 9 | 176 | E ₂ | 30.5 | 14 | .2 | 48.07 |
| | | 177 | | | | 1.2 | 54.65 |
| | | 178 | | | | 3.1 | 74.32 |
| | | 179 | | | | 5.5 | 74.51 |
| | | 180 | | | | 8.7 | 70.17 |
| | | 181 | | | | 12.3 | 74.93 |
| Block 27 | 10 | 183 | E ₂ | 30.5 | 22 | .1 | 84.34 |
| | | 184 | | | | .2 | 87.14 |
| | | 185 | | | | .6 | 96.85 |
| | | 186 | | | | 1.6 | 111.45 |
| | | 1 | | | | 4.3 | 105.08 |
| | | 3 | | | | 8.9 | 126.22 |
| | | 4 | | | | 24.4 | 133.42 |
| Block 27 | 11 | 5 | E ₂ | 30.5 | 30 | .1 | 150.75 |
| | | 6 | | | | .4 | 159.21 |
| | | 8 | | | | 2.6 | 228.21 |
| | | 10 | | | | 7.7 | 209.53 |
| | | 12 | | | | 23.7 | 256.51 |
| Buoy D | 1 | 14 | D ₂ | 30.5 | 16 | .1 | 31.82 |
| | | 15 | D ₂ | 30.5 | | .5 | 31.84 |
| | | 17 | D ₂ | 15.2 | | 1.0 | 33.60 |
| | | 21 | D ₂ | 30.5 | | 1.0 | 33.09 |
| | | 22 | D ₂ | 45.7 | | 1.0 | 34.56 |
| | | 23 | D ₂ | 30.5 | | 1.5 | 33.31 |
| | | 25 | D ₂ | 30.5 | | 2.0 | 30.41 |
| | | 26 | D ₂ | 15.2 | | 4.0 | 31.96 |
| | | 27 | D ₂ | 30.5 | | 4.0 | 31.96 |
| | | 37 | D ₂ | 45.7 | | 4.0 | 32.04 |
| | | 38 | D ₂ | 30.5 | | 6.0 | 30.38 |
| | | 39 | D ₂ | 30.5 | | 13.5 | 23.57 |
| | | 40 | D ₂ | 15.2 | | 23.9 | 24.00 |
| | | 41 | D ₂ | 30.5 | | 23.9 | 24.60 |
| | | 68 | D ₂ | 45.7 | | 23.9 | 28.24 |

Table A1 (continued)

| Set | Run | Sample # | L _s | Z (cm) | U (cm/sec) | T _v (hr) | TSM (mg/l) |
|--------|-----|----------|----------------|-----------|---------------|------------------------|---------------|
| Buoy D | 2 | 69 | D ₂ | 30.5 | 23 | .1 | 29.89 |
| | | 70 | D ₂ | 30.5 | | .5 | 36.09 |
| | | 71 | D ₂ | 15.2 | | 1.0 | 39.24 |
| | | 72 | D ₂ | 30.5 | | 1.0 | 40.35 |
| | | 73 | D ₂ | 45.7 | | 1.0 | 40.00 |
| | | 74 | D ₂ | 30.5 | | 1.5 | 42.75 |
| | | 75 | D ₂ | 30.5 | | 2.0 | 40.32 |
| | | 76 | D ₂ | 30.5 | | 3.9 | 45.60 |
| | | 77 | D ₂ | 15.2 | | 6.0 | 68.11 |
| | | 78 | D ₂ | 30.5 | | 6.0 | 45.97 |
| | | 79 | D ₂ | 45.7 | | 6.0 | 47.00 |
| | | 80 | D ₂ | 30.5 | | 8.8 | 46.81 |
| | | 81 | D ₂ | 30.5 | | 11.7 | 44.69 |
| | | 82 | D ₂ | 15.2 | | 23.0 | 41.36 |
| | | 83 | D ₂ | 30.5 | | 23.0 | 43.43 |
| | | 87 | D ₂ | 45.7 | | 23.0 | 43.37 |
| Buoy D | 3 | 88 | D ₂ | 30.5 | 32 | .1 | 42.93 |
| | | 89 | D ₂ | 30.5 | | .5 | 61.43 |
| | | 98 | D ₂ | 30.5 | | 1.3 | 71.47 |
| | | 99 | D ₂ | 15.2 | | 1.6 | 74.36 |
| | | 100 | D ₂ | 30.5 | | 1.6 | 74.11 |
| | | 101 | D ₂ | 45.7 | | 1.6 | 72.76 |
| | | 102 | D ₂ | 30.5 | | 2.0 | 69.04 |
| | | 103 | D ₂ | 30.5 | | 4.1 | 70.92 |
| | | 104 | D ₂ | 15.2 | | 6.0 | 71.32 |
| | | 106 | D ₂ | 30.5 | | 6.0 | 69.57 |
| | | 107 | D ₂ | 45.7 | | 6.0 | 81.75 |
| | | 109 | D ₂ | 30.5 | | 9.1 | 80.13 |
| | | 110 | D ₂ | 30.5 | | 12.0 | 77.03 |
| | | 111 | D ₂ | 15.2 | | 23.9 | 75.33 |
| | | 112 | D ₂ | 30.5 | | 23.9 | 77.96 |
| | | 113 | D ₂ | 45.7 | | 23.9 | 77.63 |
| Buoy D | 4 | 114 | D ₂ | 30.5 | 39 | .2 | 78.82 |
| | | 116 | D ₁ | 15.2 | | .6 | 81.65 |
| | | 117 | D ₂ | 30.5 | | .6 | 83.88 |
| | | 118 | D ₃ | 45.7 | | .6 | 77.87 |
| | | 119 | D ₂ | 30.5 | | 1.0 | 88.02 |
| | | 120 | D ₂ | 30.5 | | 1.6 | 93.78 |
| | | 121 | D ₂ | 30.5 | | 2.0 | 91.17 |
| | | 122 | D ₂ | 30.5 | | 4.0 | 99.60 |

Table A1 (continued)

| Set | Run | Sample # | L _s | Z (cm) | U (cm/sec) | T _v (hr) | TSM (mg/l) |
|--------|-----|----------|----------------|-----------|---------------|------------------------|---------------|
| Buoy D | 4 | 123 | D ₁ | 15.2 | 39 | 6.3 | 100.95 |
| | | 124 | D ₂ | 30.5 | | 6.3 | 100.24 |
| | | 125 | D ₃ | 45.7 | | 6.3 | 103.14 |
| | | 126 | D ₂ | 30.5 | | 9.0 | 103.27 |
| | | 127 | D ₂ | 30.5 | | 12.9 | 104.79 |
| | | 219 | D ₁ | 15.2 | | 23.7 | 105.52 |
| | | 130 | D ₂ | 30.5 | | 23.7 | 102.90 |
| | | 131 | D ₃ | 45.7 | | 23.7 | 104.93 |
| Buoy D | 5 | 132 | D ₂ | 30.5 | 44 | .1 | 105.53 |
| | | 133 | D ₁ | 15.2 | | .5 | 107.42 |
| | | 134 | D ₂ | 30.5 | | .5 | 104.19 |
| | | 135 | D ₃ | 45.7 | | .5 | 103.46 |
| | | 136 | D ₂ | 30.5 | | 1.0 | 110.97 |
| | | 137 | D ₂ | 30.5 | | 1.5 | 107.50 |
| | | 138 | D ₂ | 30.5 | | 2.0 | 106.24 |
| | | 140 | D ₂ | 30.5 | | 4.0 | 105.11 |
| | | 141 | D ₂ | 30.5 | | 6.0 | 111.22 |
| | | 142 | D ₁ | 15.2 | | 9.0 | 113.35 |
| | | 143 | D ₂ | 30.5 | | 9.0 | 114.59 |
| | | 144 | D ₃ | 45.7 | | 9.0 | 116.33 |
| | | 145 | D ₂ | 30.5 | | 12.0 | 117.17 |
| | | 146 | D ₁ | 15.2 | | 23.0 | 119.22 |
| | | 147 | D ₂ | 30.5 | | 23.0 | 115.55 |
| | | 148 | D ₃ | 45.7 | | 23.0 | 117.55 |
| Buoy D | 6 | 149 | D ₂ | 30.5 | 60 | .1 | 125.73 |
| | | 150 | D ₁ | 15.2 | | .5 | 164.15 |
| | | 152 | D ₂ | 30.5 | | .5 | 164.59 |
| | | 153 | D ₃ | 45.7 | | .5 | 166.74 |
| | | 154 | D ₂ | 30.5 | | 1.0 | 185.14 |
| | | 155 | D ₂ | 30.5 | | 1.5 | 192.35 |
| | | 156 | D ₂ | 30.5 | | 2.0 | 193.60 |
| | | 157 | D ₂ | 30.5 | | 4.0 | 217.70 |
| | | 158 | D ₁ | 15.2 | | 6.1 | 227.85 |
| | | 159 | D ₂ | 0.5 | | 6.1 | 226.77 |
| | | 160 | D ₃ | 45.7 | | 6.1 | 227.86 |
| | | 161 | D ₂ | 30.5 | | 9.0 | 224.45 |
| | | 163 | D ₂ | 30.5 | | 12.0 | 212.11 |
| | | 164 | D ₁ | 15.2 | | 24.0 | 241.10 |
| | | 165 | D ₂ | 30.5 | | 24.0 | 239.37 |
| | | 166 | D ₃ | 45.7 | | 24.0 | 223.00 |

Table A1 (continued)

| Set | Run | Sample # | L _s | Z (cm) | U (cm/sec) | T _v (hr) | TSM (mg/l) |
|--------|-----|----------|----------------|-----------|---------------|------------------------|---------------|
| Buoy D | 7 | 168 | D ₂ | 30.5 | 20 | .1 | 214.42 |
| | | 169 | D ₁ | 15.2 | | 1.4 | 211.72 |
| | | 170 | D ₂ | 30.5 | | 1.4 | 213.03 |
| | | 172 | D ₃ | 45.7 | | 1.4 | 221.77 |
| | | 176 | D ₂ | 30.5 | | 5.9 | 231.10 |
| | | 177 | D ₂ | 30.5 | | 9.4 | 230.00 |
| | | 179 | D ₂ | 30.5 | | 13.2 | 217.41 |
| | | 180 | D ₂ | 30.5 | | 23.9 | 206.90 |
| Buoy D | 8 | 181 | D ₂ | 30.5 | 4 | .1 | 183.89 |
| | | 183 | | | | .5 | 199.36 |
| | | 184 | | | | 1.1 | 186.64 |
| | | 186 | | | | 1.5 | 176.32 |
| | | 1 | | | | 4.0 | 121.13 |
| | | 2 | | | | 6.1 | 117.88 |
| | | 3 | | | | 10.9 | 89.87 |
| | | 4 | | | | 13.6 | 79.38 |
| Buoy D | 9 | 5 | | | | 26.0 | 53.61 |
| | | 6 | D ₂ | 30.5 | 16 | .2 | 39.31 |
| | | 7 | | | | .6 | 35.61 |
| | | 9 | | | | 1.0 | 34.97 |
| | | 10 | | | | 1.5 | 35.44 |
| | | 11 | | | | 2.0 | 34.97 |
| | | 187 | | | | 4.4 | 36.63 |
| | | 188 | | | | 9.0 | 29.12 |
| | | 189 | | | | 12.0 | 30.92 |
| Buoy D | 10 | 190 | | | | 24.0 | 30.78 |
| | | 191 | D ₂ | 30.5 | 24 | .1 | 34.71 |
| | | 192 | | | | .5 | 40.00 |
| | | 193 | | | | 1.0 | 39.58 |
| | | 194 | | | | 1.6 | 42.10 |
| | | 195 | | | | 2.0 | 43.62 |
| | | 196 | | | | 4.0 | 43.77 |
| | | 197 | | | | 6.2 | 46.58 |
| | | 198 | | | | 12.5 | 47.10 |
| Buoy D | 11 | 199 | | | | 24.5 | 48.93 |
| | | 200 | D ₂ | 30.5 | 34 | .1 | 51.66 |
| | | 201 | D ₂ | 30.5 | | .5 | 59.03 |
| | | 202 | D ₁ | 15.2 | | 1.0 | 68.83 |

Table A1 (concluded)

| Set | Run | Sample # | L _s | Z (cm) | U (cm/sec) | T _v (hr) | TSM (mg/l) |
|--------|-----|----------|----------------|-----------|---------------|------------------------|---------------|
| Buoy D | 11 | 203 | D ₂ | 30.5 | 31 | 1.0 | 66.34 |
| | | 204 | D ₃ | 45.7 | | 1.0 | 73.64 |
| | | 205 | D ₂ | 30.5 | | 1.5 | 75.97 |
| | | 206 | D ₂ | 30.5 | | 2.0 | 77.24 |
| | | 207 | D ₂ | 30.5 | | 4.0 | 90.95 |
| | | 208 | D ₁ | 15.2 | | 7.0 | 96.03 |
| | | 211 | D ₂ | 30.5 | | 12.9 | 107.36 |
| | | 212 | D ₁ | 15.2 | | 22.7 | 118.20 |
| | | 213 | D ₂ | 30.5 | | 22.7 | 118.50 |
| | | 214 | D ₃ | 45.7 | | 22.7 | 116.93 |

APPENDIX B: CURRENT VELOCITY PROFILES AND SHEAR STRESS
CALCULATIONS FOR EXPERIMENTAL RUNS

Table B1
Current Velocity Profiles and Shear Stress
Calculations for Experimental Runs

| Set | Run | L_p^* | Y^{**} (cm) | U^\dagger (cm/sec) | $u_*^{\dagger\dagger}$ (cm/sec) | τ_o^\ddagger (dynes/cm ²) |
|--------|-----|----------------|------------------|-------------------------|------------------------------------|---|
| Buoy C | 1 | B ₂ | 57.9 | 9.74 | | |
| | | | 45.7 | 10.36 | | |
| | | | 30.5 | 10.06 | | |
| | | | 15.2 | 9.75 | | |
| | | | 6.1 | 9.14 | 0.24 | 0.06 |
| Buoy C | 2 | B ₂ | 57.9 | 17.43 | | |
| | | | 45.7 | 18.20 | | |
| | | | 30.5 | 15.18 | | |
| | | | 15.2 | 14.33 | | |
| | | | 6.1 | 14.23 | 0.27 | 0.08 |
| Buoy C | 3 | C ₂ | 57.9 | 20.70 | | |
| | | | 45.7 | 24.44 | | |
| | | | 30.5 | 23.01 | | |
| | | | 15.2 | 20.63 | | |
| | | | 6.1 | 19.39 | 0.83 | 0.68 |
| Buoy C | 4 | C ₂ | 57.9 | 31.91 | | |
| | | | 45.7 | 34.41 | | |
| | | | 30.5 | 32.10 | | |
| | | | 15.2 | 28.96 | | |
| | | | 6.1 | 25.27 | 1.33 | 1.75 |

* L_p = Vertical profile location, see Figure 19.

** Y = Elevation above bed.

† U = Horizontal velocity.

†† u_* = Friction or shear velocity.

‡ τ_o = Bed shear stress.

Table B1 (continued)

| Set | Run | L_p | Y (cm) | U (cm/sec) | u_* (cm/sec) | τ_o (dynes/cm ²) |
|----------|-----|-------|-----------|---------------|-------------------|--------------------------------------|
| Buoy C | 5 | E_2 | 57.9 | 21.12 | 1.17 | 1.36 |
| | | | 45.7 | 23.74 | | |
| | | | 30.5 | 23.93 | | |
| | | | 15.2 | 21.61 | | |
| | | | 6.1 | 19.02 | | |
| Buoy C | 6 | E_2 | 57.9 | 9.72 | 0.48 | 0.23 |
| | | | 45.7 | 10.29 | | |
| | | | 30.5 | 10.10 | | |
| | | | 15.2 | 9.70 | | |
| | | | 6.1 | 9.08 | | |
| Block 15 | 1 | C_2 | 57.9 | 10.67 | 0.14 | 0.37 |
| | | | 45.7 | 10.36 | | |
| | | | 30.5 | 10.06 | | |
| | | | 15.2 | 9.67 | | |
| | | | 6.1 | 6.10 | | |
| Block 15 | 2 | C_2 | 57.9 | 15.82 | 0.78 | 0.61 |
| | | | 45.7 | 16.58 | | |
| | | | 30.5 | 16.58 | | |
| | | | 15.2 | | | |
| | | | 7.1 | 11.37 | | |
| Block 15 | 3 | E_2 | 57.9 | 21.12 | 1.22 | 1.49 |
| | | | 45.7 | 23.74 | | |
| | | | 30.5 | 23.93 | | |
| | | | 15.2 | 21.61 | | |
| | | | 6.1 | 19.57 | | |
| Block 15 | 4 | E_2 | 57.9 | 30.48 | 1.59 | 2.53 |
| | | | 45.7 | 32.58 | | |
| | | | 30.5 | 32.61 | | |
| | | | 15.2 | 30.08 | | |
| | | | 6.1 | 26.58 | | |
| Block 15 | 5 | C_2 | 57.9 | 9.75 | 0.91 | 0.83 |
| | | | 45.7 | 10.36 | | |
| | | | 30.5 | 10.06 | | |
| | | | 15.2 | 10.67 | | |
| | | | 6.1 | 6.17 | | |

Table B1 (continued)

| Set | Run | Lp | Y (cm) | U (cm/sec) | u_* (cm/sec) | τ_o (dynes/cm ²) |
|----------|-----|----------------|-----------|---------------|-------------------|--------------------------------------|
| Block 27 | 1 | B ₂ | 54.9 | 13.11 | | |
| | | | 42.7 | 14.02 | | |
| | | | 30.5 | 13.41 | | |
| | | | 24.8 | 12.19 | | |
| | | | 21.3 | 11.58 | | |
| | | | 18.3 | 11.28 | | |
| | | | 15.2 | 11.57 | | |
| | | | 12.2 | 10.06 | | |
| | | | 9.1 | 9.75 | 0.24 | 0.06 |
| Block 27 | 2 | B ₂ | 54.9 | 22.86 | | |
| | | | 42.7 | 23.77 | | |
| | | | 30.5 | 22.86 | | |
| | | | 24.8 | 22.56 | | |
| | | | 21.3 | 22.25 | | |
| | | | 18.3 | 21.95 | | |
| | | | 15.2 | 21.03 | | |
| | | | 12.2 | 20.12 | | |
| | | | 9.1 | 19.20 | 0.42 | 0.18 |
| Block 27 | 3 | A ₂ | 54.9 | 27.43 | | |
| | | | 42.7 | 30.48 | | |
| | | | 30.5 | 30.48 | | |
| | | | 24.8 | 30.17 | | |
| | | | 21.3 | 29.57 | | |
| | | | 18.3 | 29.26 | | |
| | | | 15.2 | 28.65 | | |
| | | | 12.2 | 29.87 | | |
| | | | 9.1 | 27.74 | 1.06 | 1.12 |
| Block 27 | 4 | B ₂ | 54.9 | 38.10 | | |
| | | | 42.7 | 39.01 | | |
| | | | 30.5 | 38.71 | | |
| | | | 24.8 | 38.10 | | |
| | | | 21.3 | 37.80 | | |
| | | | 18.3 | 37.49 | | |
| | | | 15.2 | 36.88 | | |
| | | | 12.2 | 36.27 | | |
| | | | 9.1 | 34.75 | 1.27 | 1.61 |
| Block 27 | 5 | B ₂ | 54.9 | 42.67 | | |
| | | | 52.7 | 45.72 | | |
| | | | 30.5 | 44.20 | | |

Table B1 (continued)

| Set | Run | L _p | Y (cm) | U (cm/sec) | u* (cm/sec) | τ _o (dynes/cm ²) |
|----------|-----|----------------|-----------|---------------|----------------|--|
| Block 27 | 5 | B ₂ | 24.8 | 43.89 | | |
| | | | 21.3 | 43.59 | | |
| | | | 18.3 | 43.28 | | |
| | | | 15.2 | 42.98 | | |
| | | | 12.2 | 42.06 | | |
| | | | 9.1 | 40.23 | 1.44 | 2.07 |
| Block 27 | 6 | B ₂ | 54.9 | 52.43 | | |
| | | | 42.7 | 56.39 | | |
| | | | 30.5 | 57.61 | | |
| | | | 24.8 | 55.78 | | |
| | | | 21.3 | 55.47 | | |
| | | | 18.3 | 54.56 | | |
| | | | 15.2 | 53.95 | | |
| | | | 12.2 | 53.34 | | |
| | | | 9.1 | 49.07 | 1.90 | 3.63 |
| Block 27 | 7 | B ₂ | 54.9 | 29.87 | | |
| | | | 52.7 | 32.00 | | |
| | | | 30.5 | 30.78 | | |
| | | | 24.8 | 30.18 | | |
| | | | 21.3 | 29.87 | | |
| | | | 18.3 | 30.48 | | |
| | | | 15.2 | 29.87 | | |
| | | | 12.2 | 29.57 | | |
| | | | 9.1 | 27.74 | 0.84 | 0.71 |
| Block 27 | 8 | B ₂ | 54.9 | 5.79 | | |
| | | | 42.7 | 6.10 | | |
| | | | 30.5 | 6.10 | | |
| | | | 24.8 | 5.79 | | |
| | | | 21.3 | 6.10 | | |
| | | | 18.3 | 5.79 | | |
| | | | 15.2 | 5.79 | | |
| | | | 12.2 | 5.49 | | |
| | | | 9.1 | 5.18 | 0.26 | 0.07 |
| Block 27 | 9 | B ₂ | 54.9 | 13.11 | | |
| | | | 42.7 | 14.33 | | |
| | | | 30.5 | 14.94 | | |
| | | | 24.8 | 14.02 | | |
| | | | 21.3 | 13.72 | | |
| | | | 18.3 | 13.72 | | |

Table B1 (continued)

| Set | Run | L _p | Y (cm) | U (cm/sec) | u _* (cm/sec) | τ _o (dynes/cm ²) |
|----------|-----|----------------|-----------|---------------|----------------------------|--|
| Block 27 | 9 | B ₂ | 15.2 | 13.11 | 0.67 | 0.46 |
| | | | 12.2 | 12.80 | | |
| | | | 9.1 | 11.89 | | |
| Block 27 | 10 | B ₂ | 54.9 | 20.42 | 0.84 | 0.71 |
| | | | 42.7 | 22.25 | | |
| | | | 30.5 | 22.25 | | |
| | | | 24.8 | 21.64 | | |
| | | | 21.3 | 21.03 | | |
| | | | 18.3 | 20.73 | | |
| | | | 15.2 | 20.42 | | |
| | | | 12.2 | 20.12 | | |
| Block 27 | 11 | B ₂ | 9.1 | 19.20 | | |
| | | | 54.9 | 28.96 | 1.16 | 1.36 |
| | | | 42.7 | 30.48 | | |
| | | | 30.5 | 33.53 | | |
| | | | 24.8 | 30.18 | | |
| | | | 21.3 | 29.57 | | |
| | | | 18.3 | 29.26 | | |
| | | | 15.2 | 28.65 | | |
| | | | 12.2 | 27.74 | | |
| Buoy D | 1 | B ₂ | 9.1 | 26.82 | | |
| | | | 54.9 | 15.54 | 0.79 | 0.63 |
| | | | 42.7 | 15.85 | | |
| | | | 30.5 | 16.15 | | |
| | | | 24.8 | 15.85 | | |
| | | | 21.3 | 15.54 | | |
| | | | 18.3 | 15.24 | | |
| | | | 15.2 | 14.94 | | |
| | | | 12.2 | 14.02 | | |
| Buoy D | 2 | B ₂ | 9.1 | 13.72 | | |
| | | | 54.9 | 21.34 | 0.91 | 0.83 |
| | | | 42.7 | 22.86 | | |
| | | | 30.5 | 23.16 | | |
| | | | 24.8 | 22.86 | | |
| | | | 21.3 | 22.86 | | |
| | | | 18.3 | 22.56 | | |
| | | | 15.2 | 22.25 | | |
| | | | 12.2 | 21.34 | | |
| | | | 9.1 | 19.81 | | |

Table B1 (continued)

| Set | Run | L _p | Y (cm) | U (cm/sec) | u _* (cm/sec) | τ _o (dynes/cm ²) |
|---------|-----|----------------|-----------|---------------|----------------------------|--|
| Block D | 3 | B ₂ | 54.9 | 30.18 | | |
| | | | 42.7 | 35.05 | | |
| | | | 30.5 | 33.53 | | |
| | | | 24.8 | 32.00 | | |
| | | | 21.3 | 30.48 | | |
| | | | 18.3 | 30.48 | | |
| | | | 15.2 | 30.18 | | |
| | | | 12.2 | 29.87 | | |
| | | | 9.1 | 29.57 | 0.98 | 0.96 |
| Buoy D | 4 | B ₂ | 54.9 | 36.88 | | |
| | | | 42.7 | 39.62 | | |
| | | | 30.5 | 38.10 | | |
| | | | 24.8 | 38.71 | | |
| | | | 21.3 | 38.10 | | |
| | | | 18.3 | 37.49 | | |
| | | | 15.2 | 36.88 | | |
| | | | 12.2 | 36.58 | | |
| | | | 9.1 | 34.44 | 1.09 | 1.20 |
| Buoy D | 5 | B ₂ | 54.9 | 42.37 | | |
| | | | 42.7 | 43.89 | | |
| | | | 30.5 | 44.50 | | |
| | | | 24.8 | 43.59 | | |
| | | | 21.3 | 42.98 | | |
| | | | 18.3 | 42.37 | | |
| | | | 15.2 | 42.06 | | |
| | | | 12.2 | 41.45 | | |
| | | | 9.1 | 37.19 | 1.48 | 2.20 |
| Buoy D | 6 | B ₂ | 54.9 | 54.86 | | |
| | | | 42.7 | 60.96 | | |
| | | | 30.5 | 61.26 | | |
| | | | 24.8 | 60.35 | | |
| | | | 41.3 | 59.74 | | |
| | | | 18.3 | 59.13 | | |
| | | | 15.2 | 57.91 | | |
| | | | 12.2 | 57.30 | | |
| | | | 9.1 | 54.25 | 3.0 | 9.53 |

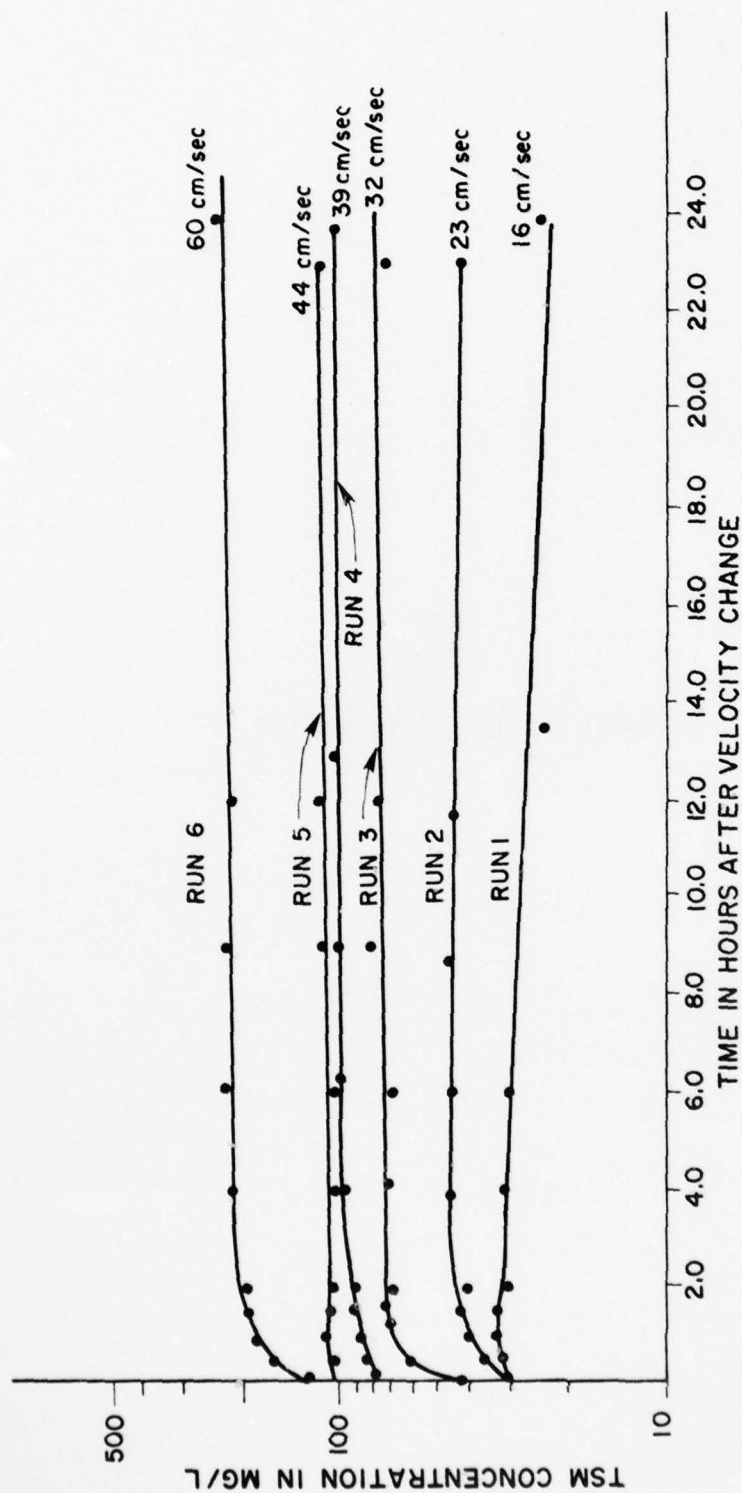
Table B1 (continued)

| Set | Run | L _p | Y (cm) | U (cm/sec) | U* (cm/sec) | τ_o (dynes/cm ²) |
|--------|-----|----------------|-----------|---------------|----------------|--------------------------------------|
| Buoy D | 7 | B ₂ | 54.9 | 20.12 | | |
| | | | 42.7 | 21.34 | | |
| | | | 30.5 | 20.73 | | |
| | | | 24.8 | 19.81 | | |
| | | | 21.3 | 19.51 | | |
| | | | 18.3 | 19.20 | | |
| | | | 15.2 | 18.29 | | |
| | | | 12.2 | 17.68 | | |
| | | | 9.1 | 17.07 | 1.19 | 1.42 |
| Buoy D | 8 | B ₂ | 54.9 | 3.05 | | |
| | | | 42.7 | 3.35 | | |
| | | | 30.5 | 3.05 | | |
| | | | 24.8 | 3.05 | | |
| | | | 21.3 | 3.02 | | |
| | | | 18.3 | 3.05 | | |
| | | | 15.2 | 3.02 | | |
| | | | 12.2 | 2.99 | | |
| | | | 9.1 | 2.96 | 0.05 | 0.003 |
| Buoy D | 9 | B ₂ | 54.9 | 14.63 | | |
| | | | 42.7 | 15.54 | | |
| | | | 30.5 | 15.85 | | |
| | | | 24.8 | 16.15 | | |
| | | | 21.3 | 15.54 | | |
| | | | 18.3 | 15.24 | | |
| | | | 15.2 | 14.94 | | |
| | | | 12.2 | 14.33 | | |
| | | | 9.1 | 13.41 | 0.80 | 0.63 |
| Buoy D | 10 | B ₂ | 54.9 | 22.56 | | |
| | | | 42.7 | 23.47 | | |
| | | | 30.5 | 23.77 | | |
| | | | 24.8 | 23.77 | | |
| | | | 21.3 | 23.77 | | |
| | | | 18.3 | 23.47 | | |
| | | | 15.2 | 22.86 | | |
| | | | 12.2 | 22.25 | | |
| | | | 9.1 | 20.73 | 0.859 | 0.73 |

Table B1 (concluded)

| Set | Run | Lp | Y (cm) | U (cm/sec) | u_* (cm/sec) | τ_0 (dynes/cm ²) |
|--------|-----|----------------|-----------|---------------|-------------------|--------------------------------------|
| Buoy D | 11 | B ₂ | 54.9 | 30.48 | | |
| | | | 42.7 | 32.00 | | |
| | | | 30.5 | 32.00 | | |
| | | | 24.8 | 31.39 | | |
| | | | 21.3 | 31.09 | | |
| | | | 18.3 | 30.78 | | |
| | | | 15.2 | 30.48 | | |
| | | | 12.2 | 30.18 | | |
| | | | 9.1 | 29.87 | 0.875 | 0.76 |

APPENDIX C: EXPERIMENTAL RUNS



C2

Figure C1. Buoy D dense bed erosional runs (visual plot)

AD-A057 660

TEXAS A AND M UNIV COLLEGE STATION DEPT OF OCEANOGRAPHY F/G 13/2
FLUME EXPERIMENTS ON SAND, SILT, AND CLAY MIXTURES FROM THE OFF--ETC(U)
JUN 78 A J MOHEREK DACW39-76-C-0115

UNCLASSIFIED

3 of 3

AD
A057 660

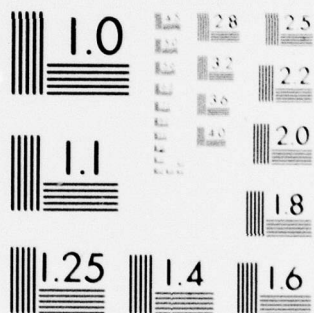
10
11

WEC-TD-D-78-34

ALL

END
DATE
FILMED
9-78

DDC



MICROCOPY RESOLUTION TEST CHART
NATIONAL BUREAU OF STANDARDS-1963-A

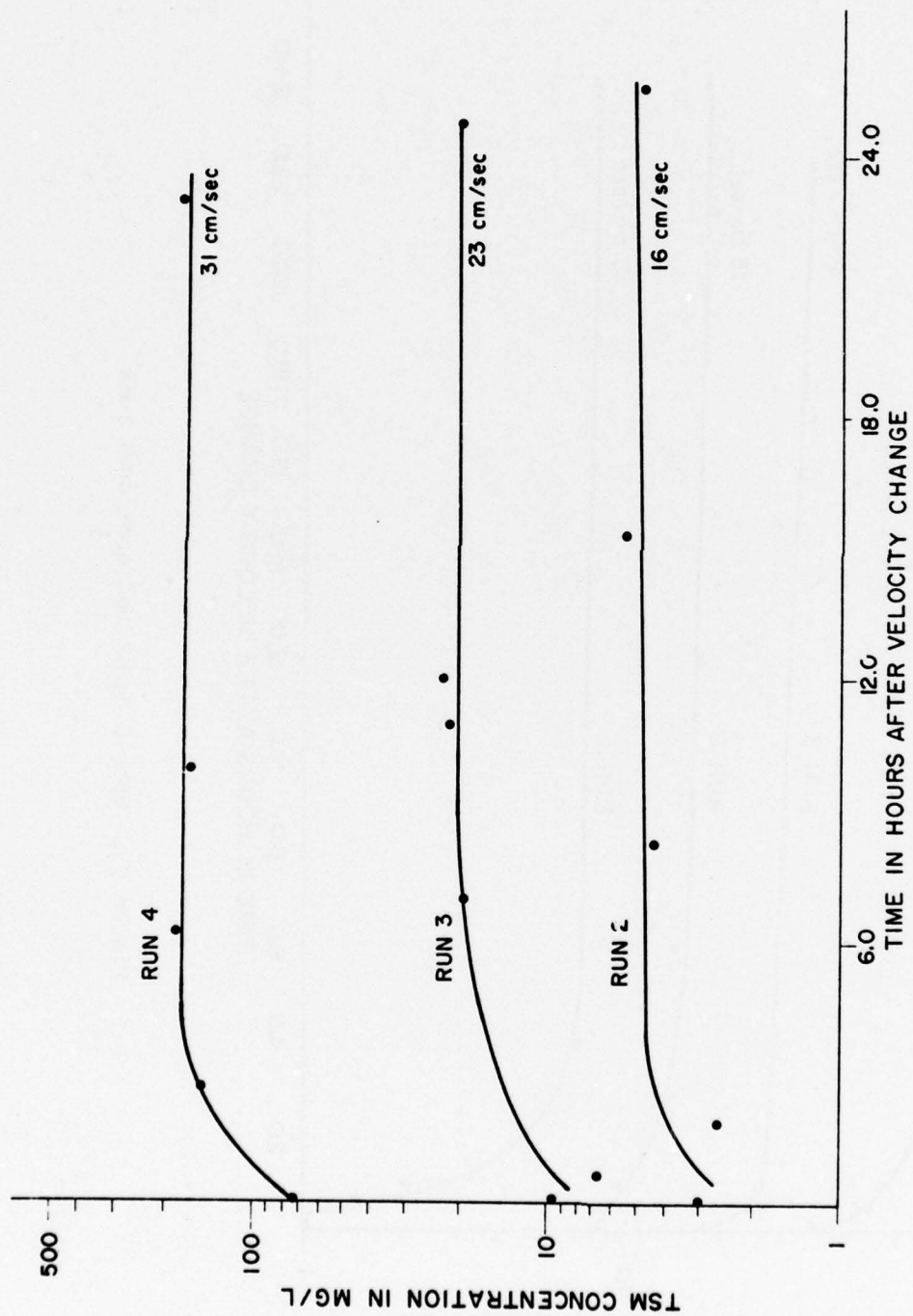
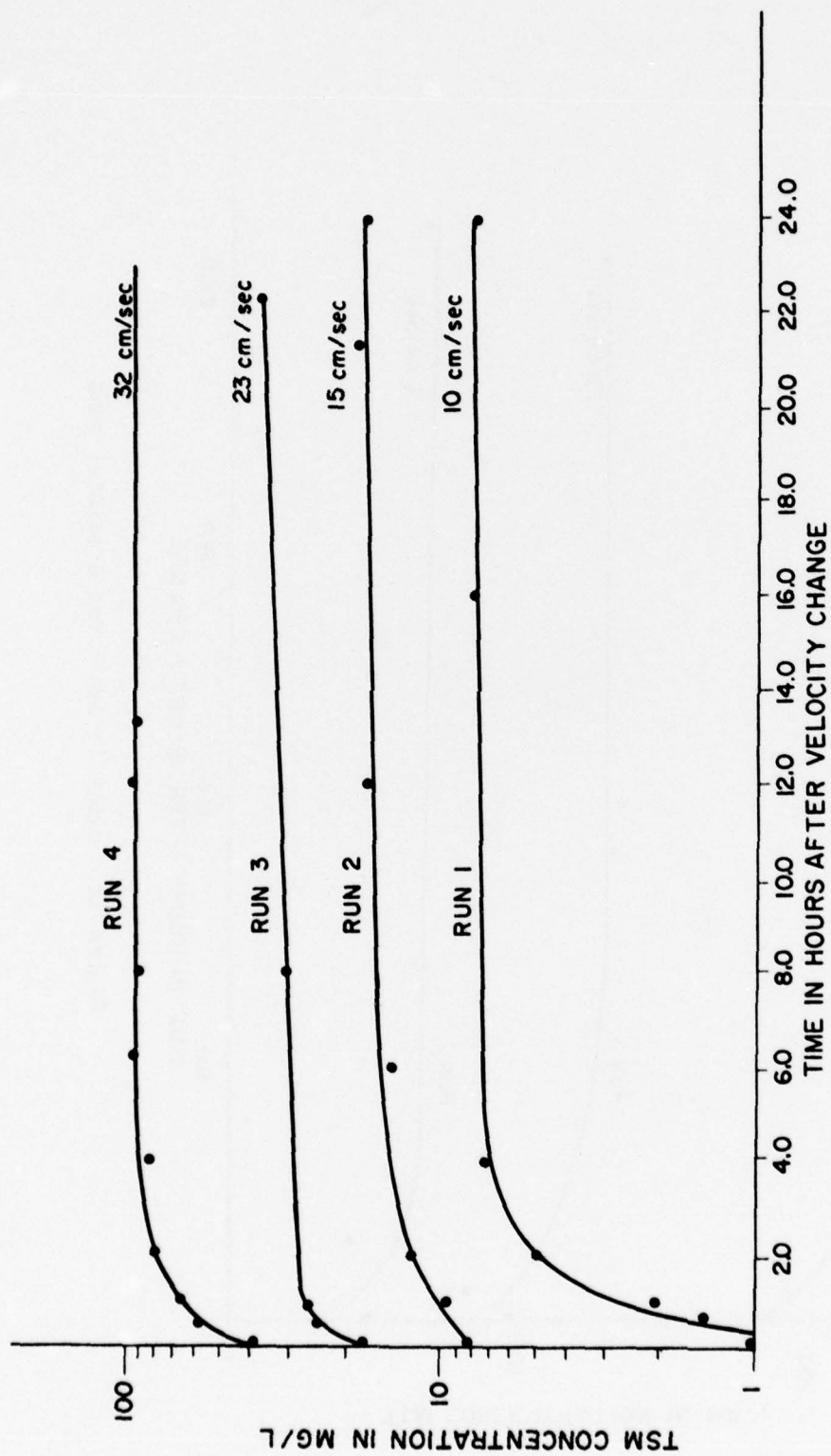


Figure C2. Block 1b dense bed erosional runs



C4

Figure C3. Buoy C dense bed erosional runs

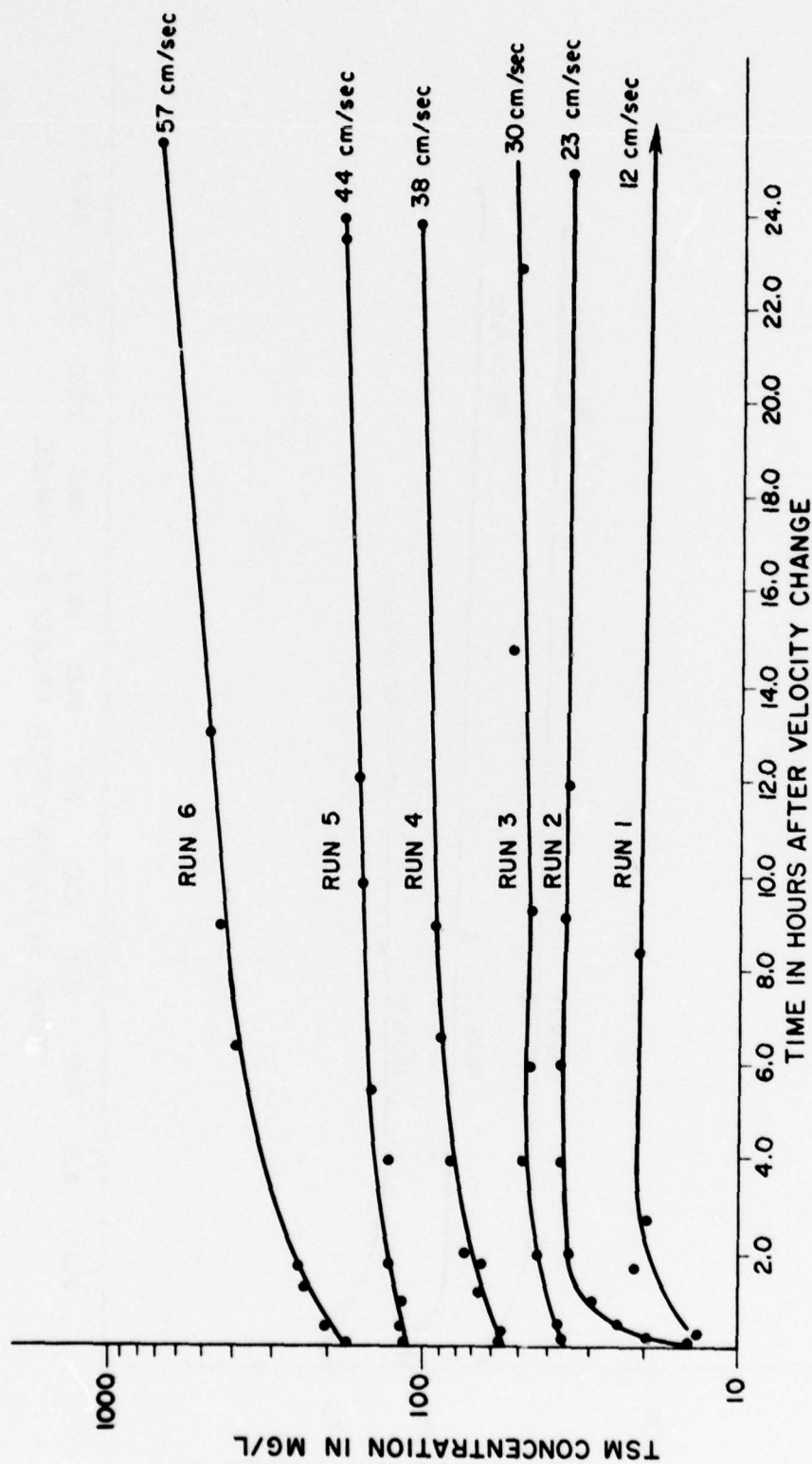


Figure C4 Block 27 dense bed erosional runs

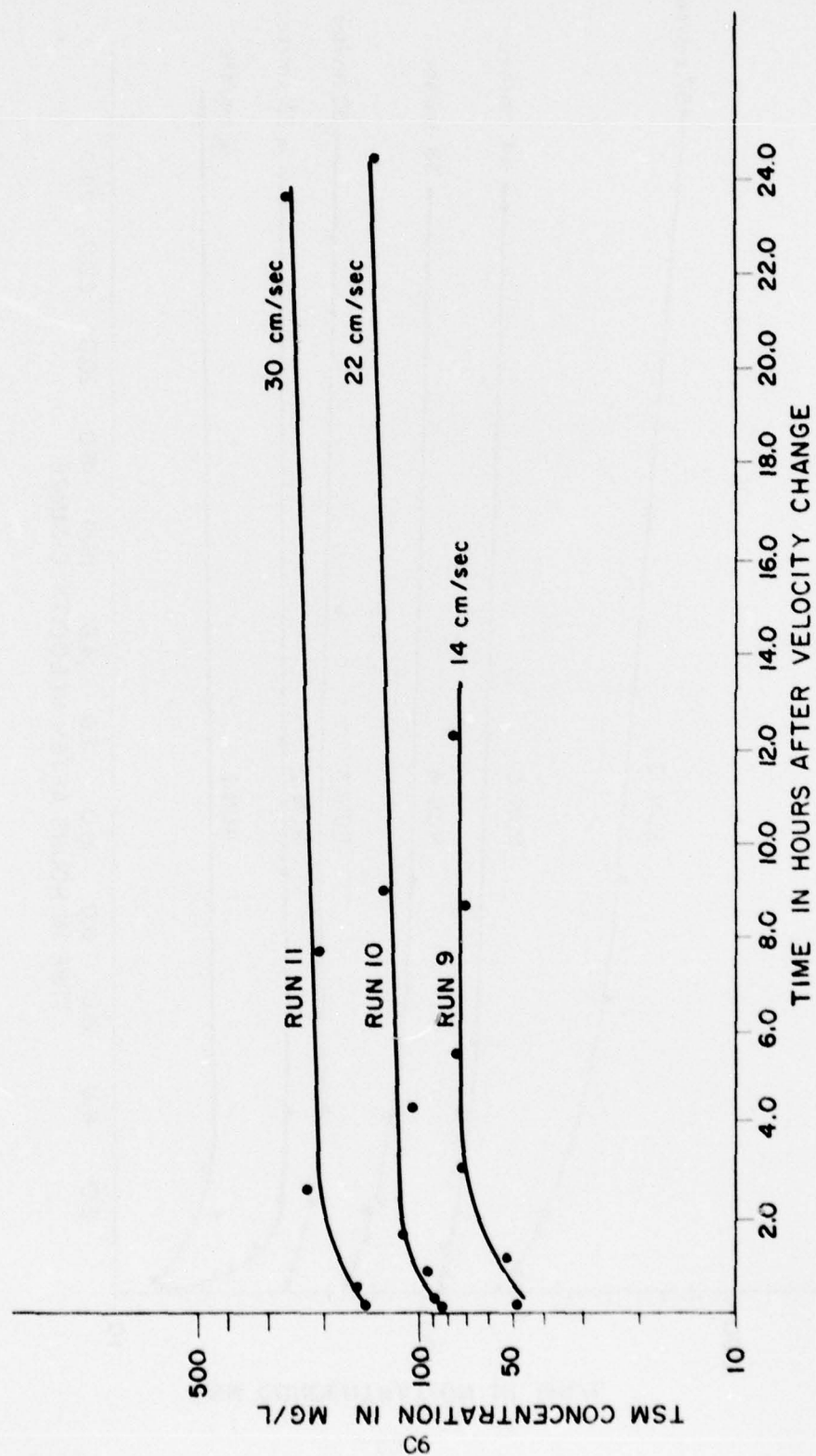


Figure C5. Block 27 flocc bed erosional runs

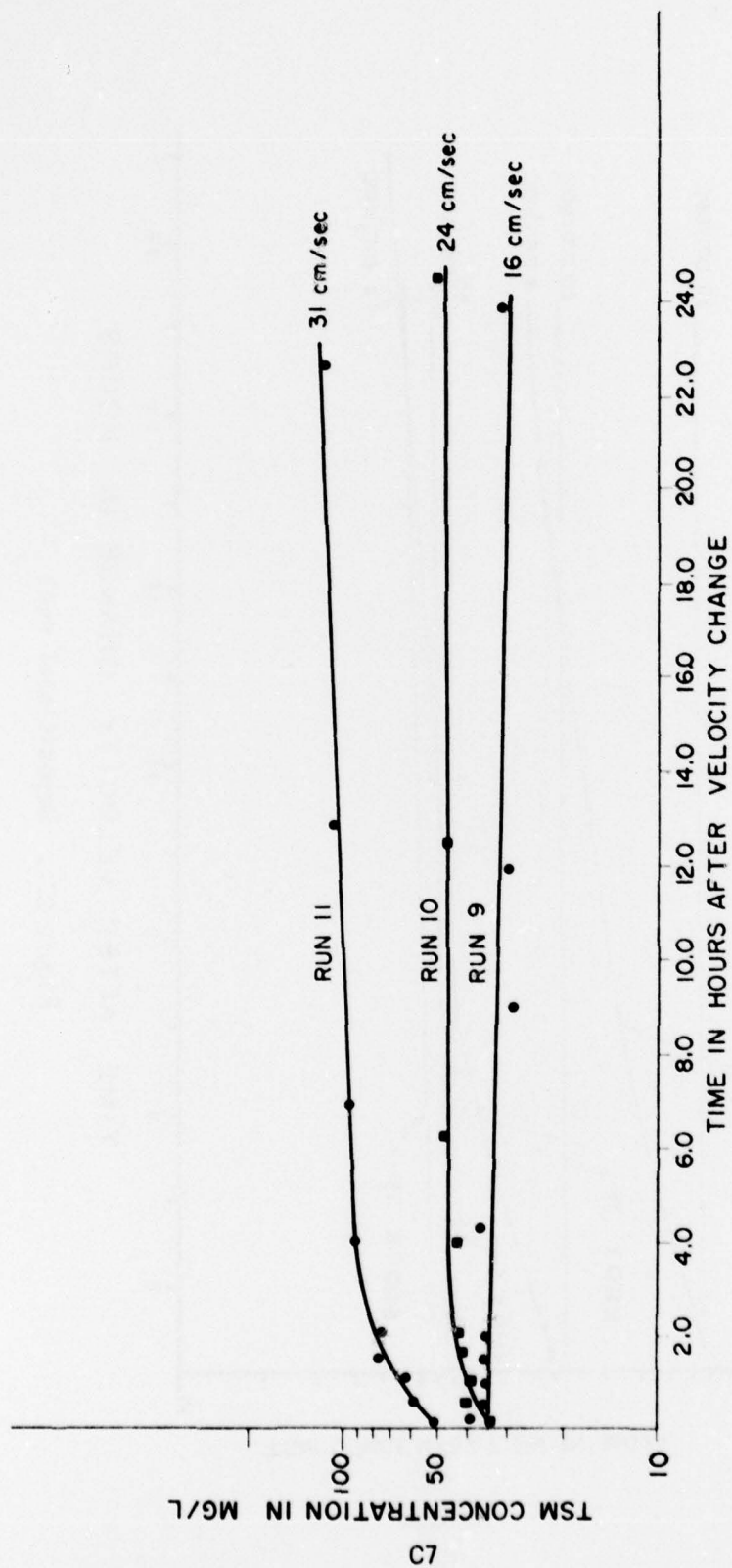


Figure C6. Buoy D floc bed erosional runs

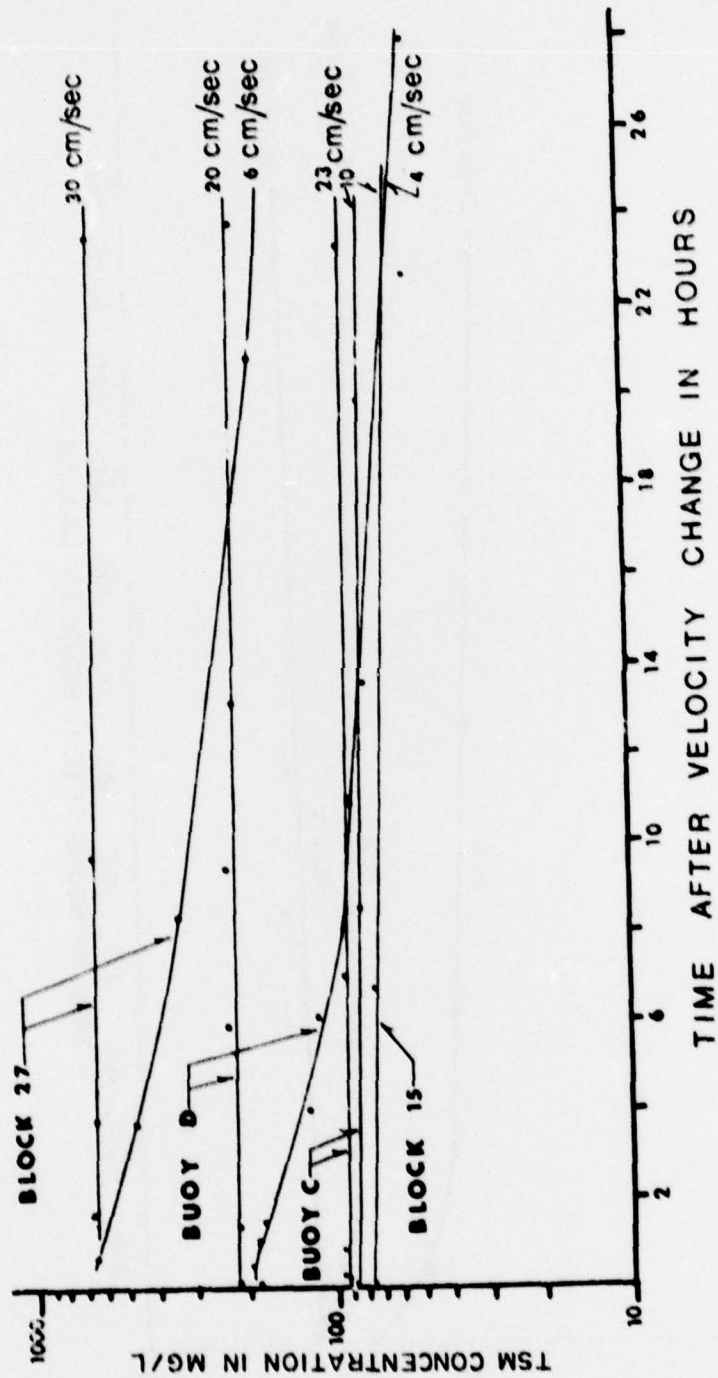


Figure C7 . Depositional runs

APPENDIX D: WASHLOAD GRAIN-SIZE ANALYSES

Table D1

Washload Grain-size Analyses

| Sei | Run No. | Sample No. | T_v^* (hr.) | L_s^{**} | Z^+ (cm) | \bar{U}^{++} (cm/sec) | 16 ϕ | 50 ϕ | 84 ϕ | M_z^\dagger | % Silt | % Clay |
|--------|---------|------------|---------------|------------|------------|-------------------------|-----------|-----------|-----------|---------------|--------|--------|
| Buoy C | 1 | 13 | 20.9 | D2 | 30 | 10 | 7.7 | 8.5 | 9.5 | 8.6 | 20 | 80 |
| | 2 | 16 | 0.5 | D2 | 30 | 15 | 7.6 | 8.8 | 10.1 | 8.8 | 24 | 76 |
| | 3 | 28 | 0.9 | D2 | 30 | 23 | 7.3 | 8.8 | 10.0 | 8.7 | 30 | 70 |
| | 3 | 34 | 22.3 | D2 | 30 | 23 | 8.5 | 9.1 | 10.1 | 9.2 | 5 | 95 |
| | 4 | 46 | 13.3 | E2 | 45 | 31 | 8.5 | 9.5 | 10.4 | 9.4 | 8 | 92 |
| | 4 | 45 | 13.3 | D2 | 30 | 31 | 8.5 | 9.6 | 10.7 | 9.6 | 9 | 91 |
| | 4 | 51 | 71.6 | D2 | 30 | 31 | 8.0 | 8.9 | 9.9 | 8.9 | 16 | 84 |
| | 5 | 57 | 7.05 | D2 | 30 | 23 | 8.1 | 8.8 | 9.7 | 8.9 | 10 | 90 |
| | 5 | 60 | 23.4 | D2 | 30 | 23 | 8.0 | 9.2 | 10.3 | 9.2 | 14 | 86 |
| | 6 | 61 | 0.1 | D2 | 30 | 10 | 8.2 | 8.7 | 9.5 | 8.8 | 13 | 87 |
| | 6 | 63 | 8.5 | D2 | 30 | 10 | 8.1 | 9.1 | 10.3 | 9.2 | 16 | 84 |

* T_v = Time after velocity change.** L_s = Sample location, see Figure 19.+ Z = Water depth of sample.++ \bar{U} = Mean flow speed.† M_z = Graphic mean (from Folk, 1974).

Table D1 (continued)

| Set | Run No. | Sample No. | T _v (hr.) | L _s | Z (cm) | \bar{U} (cm/sec) | 16φ | 50φ | 84φ | M _z | % Silt | % Clay |
|----------|---------|------------|----------------------|----------------|--------|--------------------|-----|-----|------|----------------|--------|--------|
| Block 15 | 3 | 84 | 9.0 | D2 | 30 | 23 | 8.3 | 9.5 | 10.6 | 9.4 | 12 | 88 |
| | 3 | 85 | 9.0 | D2 | 15 | 23 | 7.8 | 8.9 | 10.1 | 8.9 | 20 | 80 |
| | 3 | 86 | 9.0 | D2 | 45 | 23 | 8.3 | 9.4 | 10.5 | 9.4 | 11 | 89 |
| | 4 | 90 | 0.1 | D2 | 30 | 31 | 8.2 | 9.3 | 11.6 | 9.7 | 12 | 88 |
| | 4 | 91 | 2.8 | D2 | 30 | 31 | 6.5 | 8.8 | 10.2 | 8.5 | 30 | 70 |
| | 4 | 92 | 6.3 | D2 | 30 | 31 | 6.7 | 8.9 | 10.2 | 8.6 | 16 | 84 |
| | 4 | 93 | 6.3 | D2 | 15 | 31 | 8.1 | 9.0 | 10.1 | 9.1 | 14 | 86 |
| | 4 | 94 | 6.3 | D2 | 45 | 31 | 8.2 | 9.2 | 10.3 | 9.2 | 12 | 86 |
| | 4 | 95 | 10.0 | D2 | 30 | 31 | 7.1 | 8.3 | 9.4 | 8.3 | 42 | 58 |
| | 4 | 96 | 21.4 | D2 | 30 | 31 | 7.4 | 8.5 | 9.8 | 8.6 | 10 | 90 |
| | 4 | 97 | 23.0 | D2 | 30 | 31 | 7.4 | 8.4 | 9.6 | 8.5 | 8 | 92 |
| | 1 | 21 | 1.0 | D2 | 30 | 16 | 7.3 | 8.4 | 9.5 | 8.4 | 35 | 65 |
| | 1 | 26 | 4.0 | D2 | 15 | 16 | 7.5 | 8.4 | 9.4 | 8.4 | 32 | 68 |
| Buoy D | 1 | 27 | 4.0 | D2 | 30 | 16 | 7.6 | 8.6 | 9.6 | 8.6 | 26 | 74 |
| | 1 | 37 | 4.0 | D2 | 45 | 16 | 5.1 | 5.9 | 8.4 | 6.5 | 77 | 23 |
| | 1 | 41 | 23.9 | D2 | 30 | 16 | 4.5 | 7.7 | 9.2 | 7.1 | 57 | 43 |
| | 2 | 72 | 1.0 | D2 | 30 | 23 | 4.8 | 7.6 | 9.1 | 7.2 | 62 | 38 |
| | 2 | 78 | 6.0 | D2 | 30 | 23 | 4.7 | 8.0 | 9.2 | 7.3 | 50 | 50 |
| | 2 | 83 | 23.0 | D2 | 30 | 23 | 6.4 | 8.3 | 9.6 | 8.1 | 40 | 60 |
| | 3 | 99 | 1.6 | D2 | 15 | 32 | 6.7 | 7.9 | 9.1 | 7.9 | 52 | 48 |
| | 3 | 100 | 1.6 | D2 | 30 | 32 | 5.1 | 8.4 | 9.3 | 7.6 | 36 | 64 |

Table D1 (continued)

| Set | Run No. | Sample No. | T _v (hr.) | L _s | Z (cm) | \bar{U} (cm/sec) | 16 ϕ | 50 ϕ | 84 ϕ | M _z | % Silt | % Clay |
|----------|---------|------------|----------------------|----------------|--------|--------------------|-----------|-----------|-----------|----------------|--------|--------|
| Buoy D | 3 | 101 | 1.6 | D2 | 45 | 32 | 7.0 | 8.3 | 9.3 | 8.2 | 40 | 60 |
| | 3 | 106 | 6.0 | D2 | 30 | 32 | 5.6 | 8.3 | 9.3 | 7.7 | 39 | 61 |
| | 3 | 112 | 23.9 | D2 | 30 | 32 | 5.8 | 8.4 | 9.4 | 7.7 | 40 | 60 |
| | 4 | 130 | 23.7 | D2 | 30 | 39 | 7.6 | 8.4 | 9.3 | 8.4 | 28 | 72 |
| | 5 | 147 | 23.0 | D2 | 30 | 44 | 7.7 | 8.4 | 9.4 | 8.5 | 30 | 70 |
| | 6 | 165 | 24.0 | D2 | 30 | 60 | 7.5 | 8.5 | 9.5 | 8.5 | 33 | 67 |
| | 7 | 180 | 23.9 | D2 | 30 | 20 | 7.4 | 8.2 | 9.3 | 8.3 | 39 | 61 |
| | 8 | 5 | 26.0 | D2 | 30 | 4 | 8.0 | 8.7 | 9.6 | 8.7 | 15 | 85 |
| | 9 | 11 | 2.0 | D2 | 30 | 16 | 7.8 | 8.6 | 9.3 | 8.5 | 24 | 76 |
| | 10 | 195 | 2.0 | D2 | 30 | 24 | 7.7 | 8.7 | 9.4 | 8.6 | 27 | 73 |
| Block 27 | 11 | 206 | 2.0 | D2 | 30 | 31 | 7.6 | 8.6 | 9.6 | 8.6 | 28 | 72 |
| | 1 | 108 | 8.4 | E2 | 30 | 12 | 5.0 | 8.1 | 9.2 | 7.4 | 48 | 52 |
| | 2 | 115 | 1.5 | D2 | 30 | 23 | 6.7 | 8.1 | 9.1 | 7.9 | 47 | 53 |
| | 3 | 128 | 6.0 | E2 | 30 | 30 | 7.2 | 8.1 | 9.0 | 8.1 | 46 | 54 |
| | 4 | 139 | 9.0 | E2 | 30 | 38 | 6.7 | 8.2 | 9.2 | 8.0 | 41 | 59 |
| | 5 | 151 | 5.5 | E2 | 30 | 44 | 7.5 | 8.5 | 9.4 | 8.5 | 30 | 70 |
| | 6 | 162 | 9.0 | E2 | 30 | 57 | 4.0 | 9.7 | 8.7 | 5.8 | 77 | 23 |
| | 7 | 167 | 9.7 | E2 | 30 | 30 | 7.8 | 8.9 | 9.8 | 8.8 | 21 | 79 |

Table D1 (concluded)

| Set | Run No. | Sample No. | T_v (hr.) | L_s | Z (cm) | \bar{U} (cm/sec) | 16 ϕ | 50 ϕ | 84 ϕ | M_z | % Silt | % Clay |
|----------|---------|------------|-------------|-------|----------|--------------------|-----------|-----------|-----------|-------|--------|--------|
| Block 27 | 8 | 171 | 8.3 | E2 | 30 | 6 | 7.8 | 8.8 | 9.8 | 8.8 | 23 | 77 |
| | 9 | 178 | 3.1 | E2 | 30 | 14 | 7.6 | 8.6 | 9.5 | 8.6 | 30 | 70 |
| | 10 | 185 | 0.6 | E2 | 30 | 22 | 7.6 | 8.5 | 9.5 | 8.5 | 30 | 70 |
| | 11 | 8 | 2.6 | E2 | 30 | 30 | 7.8 | 8.8 | 9.7 | 8.8 | 20 | 80 |
| | 11 | 12 | 23.7 | E2 | 30 | 30 | 5.0 | 8.7 | 9.5 | 7.7 | 28 | 72 |

APPENDIX E: REYNOLDS AND FROUDE NUMBER
CALCULATIONS

Equations used for Reynolds (R_e) and Froude (F_r) Number Calculations were:

$$R_e = \frac{UL\rho}{\mu}$$

$$F_r = \frac{U}{(gL)^{1/2}}$$

where, for open channel flow conditions:

$$U =$$

$$L = 61 \text{ cm} = \text{average water depth}$$

$$\rho = 1.022 \text{ g/cm}^3 = \text{density of salt water at } 28^\circ\text{oo and } 25^\circ\text{C}$$

$$\mu = 9.5 \times 10^{-3} \text{ g/sec} \times \text{cm} = \text{dynamic viscosity of salt water at } 28^\circ\text{oo and } 25^\circ\text{C}$$

$$g = 980 \text{ cm/sec}^2 = \text{acceleration due to gravity}$$

and for offshore bottom flow conditions:

$$U = 75 \text{ cm/sec} = \text{maximum recorded bottom current speed (measured } 1.0 \text{ m above bed)}$$

$$L = 300 \text{ cm} = \text{approximate height of bottom currents as evidenced by instantaneous velocity profiles obtained at Buoy C and Buoy D}$$

$$\rho = 1.022 \text{ g/cm}^3$$

$$\mu = 9.5 \times 10^{-3} \text{ g/sec} \times \text{cm}$$

$$g = 980 \text{ cm/sec}^2$$

APPENDIX F: NOTATION

| <u>Symbol</u> | <u>Meaning</u> |
|---------------|--------------------------------------|
| C' | percentage of depositable sediment |
| C_o | coefficient of cohesion |
| C_u | remolded shear strength |
| d | particle diameter |
| d_o | orbital diameter |
| e | void ratio |
| F_r | Froude number |
| g | acceleration due to gravity |
| G | specific gravity |
| h | water depth |
| H | wave height |
| I_p | plasticity index |
| k | wave number |
| L | reference length |
| L_D | deepwater wavelength |
| L_s | sample location |
| L_p | profile location |
| L_w | wave length |
| m | slope |
| M_z | graphic mean |
| R_e | Reynolds number |
| R_h | hydraulic radius or wetted perimeter |
| S | slope of the energy grade line |

| <u>Symbol</u> | <u>Meaning</u> |
|---------------|--|
| SK_I | inclusive graphic skewness |
| t | time |
| T | wave period |
| TSM | total suspended matter |
| T_T | maximum torque |
| T_v | time after velocity change |
| U | horizontal flow speed |
| \bar{U} | mean flow speed |
| U_m | oscillatory bottom velocity |
| \bar{U}_x | horizontal velocity component |
| u_* | friction or shear velocity |
| V_s | solid particle volume |
| V_T | total sediment volume |
| V_v | vold volume |
| W | water content |
| W_L | liquid limit |
| W_p | plastic limit |
| W_s | weight of oven-dried sediment |
| W_{sw} | weight of seawater |
| W_T | total weight of sediment mass |
| Y | elevation above the bed |
| Y_d | bulk density |
| Y_w | specific gravity of distilled water at 4°C |
| Z | water depth |
| Z_o | roughness element = $\Delta = ks/x$ In Equation 13 |

| <u>Symbol</u> | <u>Meaning</u> |
|---------------|--------------------------------------|
| α | constant |
| β | constant |
| γ | unit weight of fluid |
| ϕ_I | Inclusive graphic standard deviation |
| ρ | water density |
| τ_o | bed shear |
| τ_{ocr} | critical bed shear |
| μ | dynamic viscosity |
| ν | kinematic viscosity |
| δ | laminar sublayer |
| θ | rotation angle |

In accordance with letter from DAEN-RDC, DAEN-ASI dated 22 July 1977, Subject: Facsimile Catalog Cards for Laboratory Technical Publications, a facsimile catalog card in Library of Congress MARC format is reproduced below.

Moherrek, Anthony J

Flume experiments on sand, silt, and clay mixtures from the offshore dredged material disposal site, Galveston, Texas / by Anthony J. Moherrek, Department of Oceanography, Texas A&M University, College Station, Tex. Vicksburg, Miss. : U. S. Waterways Experiment Station ; Springfield, Va. : available from National Technical Information Service, 1978.

166, 238 p. : ill. ; 27 cm. (Technical report - U. S. Army Engineer Waterways Experiment Station ; D-78-34)

Prepared for Office, Chief of Engineers, U. S. Army, Washington, D. C., under Contract No. DACW39-76-C-0115 (DMRP Work Unit No. 1B08A)

References: p. 163-166.

1. Dredged material. 2. Dredged material disposal. 3. Flumes. 4. Galveston Offshore Dredged Material Disposal Site. 5. Sediment transport. 6. Waste disposal sites. I. Texas. A&M University, College Station. Dept. of Oceanography. II. United States. Army. Corps of Engineers. III. Series: United States. Waterways Experiment Station, Vicksburg, Miss. Technical report ; D-78-34.
TA7.W34 no.D-78-34